Friction stir form joining of AA 5052-H32 and AA 6061-T6 sheets

A Thesis Submitted in Partial Fulfillment of the Requirements for the Degree of

DOCTOR OF PHILOSOPHY

by

TINU. P. SAJU

(Roll No. 146103019)

Department of Mechanical Engineering

Indian Institute of Technology, Guwahati

Assam – 781039, India

October 2019

Department of Mechanical Engineering
Indian Institute of Technology, Guwahati
Assam-781039, India

CERTIFICATE

It is certified that the work contained in the thesis entitled "**Friction stir form joining of AA 5052-H32 and AA 6061-T6 sheets**" submitted by **Mr. TINU. P. SAJU** to the Indian Institute of Technology Guwahati for the award of the degree of Doctor of Philosophy has been carried out under my supervision in the Department of Mechanical Engineering, Indian Institute of Technology Guwahati. This work has not been submitted elsewhere for the award of any other degree or diploma.

(Dr. R. Ganesh Narayanan)
Associate Professor
Department of Mechanical Engineering
Indian Institute of Technology Guwahati
Assam-781039
India

Dedicated to

my family

Acknowledgement

At foremost, I express my deepest gratitude to my supervisor, Dr. R. Ganesh Narayanan for his invaluable guidance, and immense support throughout my PhD work. His innovative ideas, and guidance in doing systematic and constructive research with a focused mind are remarkable. His professional ethics, well-planned research, focus in smart work and the presence of mind will remain as a source of inspiration for the rest of my life.

I am thankful to my Doctoral Committee members, Prof. P.S. Robi, Prof. Sachin D. Kore, Prof. Konjengbam Darunkumar Singh and Prof. Pankaj Biswas, for their insightful comments and valuable suggestions during the progress of research work. I would like to express my sincere gratitude to Director of the Institute, Prof. Gautam Biswas, Head of Department, Prof. Santosha K. Dwivedy, Prof. Anoop K. Das, Prof. Shrikrishna N. Joshi, Prof. S. Kanagaraj, Prof. Poonam Kumari, Prof. Gavara Madhusudhana, Prof. Ganesh Natarajan, Prof. Manmohan Pandey, Prof. Ravi M. Sankar, Prof. Rajiv Tiwari, Prof. Atanu Banerjee, and all other faculty members of the Department of Mechanical Engineering for their invaluable support.

I am extremely grateful to Prof. Barnik Saha Roy, Mechanical Engineering Department, NIT Agartala, and staffs of MSME tool room and training center, Guwahati for their invaluable help during challenging occasions of my research work. I am thankful to government organizations namely DST-SERB and CSIR for the financial support to attend the foreign conference.

Special thanks to Prof. Sukhomay Pal, Department of Mechanical Engineering, IIT Guwahati, for providing full privilege to utilize the Advanced Materials Science laboratory facilities.

Special thanks to Prof. K. S. R. Krishna Murthy and Prof. Debabrata Chakraborty, Department of Mechanical Engineering, IIT Guwahati for providing facilities in Strength of Materials laboratory in the right time. Special thanks to Prof. Manas Das, Department of Mechanical Engineering, IIT Guwahati for his support during my research work.

Special thanks to Dr. Ashim Malakar, Central Instruments Facility, IIT Guwahati for providing testing facilities. Technical help given by Mr. Karthik Pandian, Mr. Shiv Sahaya Shukla, Mr. Saptarshi Dutta, Mr. Suman and Mr. Tekcham Gishan Singh is memorable.

I thank IIT Guwahati and Department of Mechanical Engineering administration for providing infrastructure. I am grateful to the technical staffs Mr. Mrinal Sharma, Mr. J. Basumatary, Mr. Sanjib Sarma, Mr. Monuranjan Dowarah, Mr. Nabajyoti Dutta, Mr. S. Ahmed, Mr. Nip Borah, Mr. Minesh Medhi and all department office bearers for their help and support through my research work.

I thank Prof. Satheesh Kumar V, Prof. M. Duraiselvam and Prof. V. Anandakrishnan of NIT Tiruchirappalli for the inspiration and motivation. I thank my lab mates Mr. Pritam Kumar Rana, Mr. Arvind Kumar Agarwal, Mr. Sukanta Das, Mr. Nitish Bhardwaj and Mr. Priyabrata Nath for their technical support.

I am very much grateful to Prof. John Thomas, Department of Humanities and Social Sciences, IIT Guwahati and Mrs. Gayathri, Prof. A. Rajesh, Department of Electronics and Electrical Engineering, IIT Guwahati for their constant support in all the ways.

The company of my beloved friends and all keralites of IIT Guwahati made my five years of life enjoyable. Special thanks to Mr. Sajith. S, Mr. Vishnu T. Venugopal, Mr. Arjun Puthussery, Mr. Vasudevan Matampu, Mr. Vimal Kumar and Mr. Thomas T. Daniel, who made my stay at IIT Guwahati comfortable. I would like to thank all members of Guwahati MTC for considering me as a family member. I am very much grateful to my close friends Mr. Sujit Das, Mr. Pranay Sarkar, Mr. Sujoy Tikader, Mr. Amit Raj, Ms. Sarita Bharti, Mr. Vignesh Babu R. of IIT Guwahati for providing joyful memories.

I am very much thankful to my beloved friends of NIT Agartala namely Mr. Tanmoy Medhi, Mr. Uttam A. and Mr. Sudhir Kumar for the technical support during my research work. Working with you all have been an ideal and most rewarding learning experience.

Special thanks to band mates Mrs. Bhaswati Sarma, Ms. Shrutidhara Sarma, Ms. Dikhsita Choudhary, Mr. Devanand Pathak, Mr. Dwijasish Das, Mr. Pradip Das, Mr. Joy Prakash Das and Mr. Sanjay Dutta for supporting me to excel in my passion, thereby doing fruitful research with refreshed mind.

I am thankful to my relatives and family members for their moral support. I would like to recognize my parents Saju P Koshy and K Molikutty, my wife Molu, brother Anu, sister in-law Sherine and baby Aedan for their unlimited love, kindness, patience, and valuable time.

Tinu P Saju

Abstract

Aluminum alloys have emerged as a favorite choice for lightweight sheet metal fabrication, particularly in automobile and aerospace industries. Fusion welding of aluminum alloys is a complex process due to hurdles like high thermal conductivity of the metal and the surface oxide layer formation. Recently developed alternatives such as normal riveting and SPR add extra weight to the total body structure. Therefore, friction stir based solid-state joining processes such as FSSW is a reliable solution for sheet metal fabrication.

The pinhole formation and hook defect severely affect the strength of FSSW joints. Recent developments such as pinless FSSW and refill FSSW are proposed to eliminate these defects to some extent. For pinless FSSW, the pinhole defect is successfully eliminated, but the shear strength and fracture mode of these joints are influenced by the presence of hook defect. Refill FSSW process requires a complex and costly tool holding mechanism, which involves relative movement between the tool and sleeve.

FSF is a friction stir based spot joining process developed for lap joining dissimilar sheet metals such as aluminum and automotive steel. Simultaneous mechanical interlocking and metallurgical bonding is the key aspect of joint formation. The pin hole formation and hook defect of FSSW process are successfully eliminated. However, limited knowledge is available about the application of the process for joining homogenous materials like alloy variants of same metal. The present work investigates the feasibility of FSF process and its modified version for spot joining aluminum alloys such as AA 5052-H32 and AA 6061-T6 sheets of 2 mm thickness each.

The effect of process parameters and geometric features on the formation and strength of these joints are studied through systematic experimentation. Mechanical performance tests such as lap shear test, cross-tension test, peel test and tensile test are conducted to evaluate the fracture load, extension at fracture, modes of failure and formability of FSF samples under various loading conditions. Both macro/ microstructure analyses are performed to identify joint evolution, metal flow pattern, zones within the joint and grain size measurement. Hardness measurement is conducted on the joint cross-section using Vickers indentation method. The quantification of external morphological features affecting the joint strength and aesthetic appearance is also performed. The critical weak zones responsible for the failure of the joints are identified.

The process parameters such as RPM and TPD show significant effect on the mechanical performance of FSF joints. Lap shear fracture load of 6.14 kN obtained at 500 RPM and 7.16 kN obtained at 0.7 mm TPD are better than that of FSW joints and FSSW joints reported in literature. The lower and medium RPMs (500-1500 rpm) and medium TPD level (0.5-0.7 mm) are the best choices for fabricating FSF joints. The formability of FSF samples decrease with increase in TPD, which is directly related to the increase in the size of geometrical inhomogeneity formed in the sample. With change in process parameters, lap shear samples show maximum fracture load, peel test samples show minimum fracture load, while the fracture load of cross-tension samples fall in between.

The optical macrostructure analysis of FSF joint cross-sections revealed the presence of five distinct zones namely SZ, TMAZ, PDZ, HAZ and ASZ. The extreme heat generation at higher RPMs leads to damage of lower sheet and results in deteriorated fracture strength and extensibility. Lower TPDs result in poor mechanical interlocking. Moderate TPDs mark the beginning of metallurgical bonding, which contributes the highest joint strength and extensibility. The strength of FSF joints at higher TPDs is inferior due to the formation of critical weak zone by the upward deformation of the lower sheet.

The hardness of the FSF joints is found to be lesser than that of the parent metals. For the upper sheet, inverted ‘W’-shaped hardness profiles is observed throughout the change in RPM and change in TPD. The joint morphological features are independent of the change in RPM. TPD has significant influence on the pin formation and the geometric features generated in the FSF joint. It is also observed that lower sheet flash formation is negligible and the anvil cavity filling is complete at optimum TPD range of 0.5−0.7 mm.

FSF samples show various failure modes such as pin pull-out, pin shear, partial bond delamination and tear off, whose occurrence are governed by the formation of critical weak zones. The critical weak zone formations occur due to upper sheet thinning, improper bonding, upward deformation of the lower sheet and weak neck of the pin. No systematic correlation between the RPM and failure modes are observed. Medium and higher TPD levels show tear-off failure in most cases because the major part of the strength is contributed by the metallurgical bonding.

For FSF joints in aluminum alloys, the exact rivet like pin interlock is not observed as reported in aluminum alloy-steel sheet combination because the plastic deformation of

the lower sheet has resulted in distortion of the shape of the pre-drilled hole. Severe upward deformation of the lower sheet hinders the material continuity of the upper sheet, leading to failure of the joint. In addition, with the course of plunge of the stir tool, the extruded pin disconnects from the upper sheet due to the closure of the pre-drilled hole. Therefore, the authors propose a modified process namely DFSF, in which the anvil block is altered suitably and the tendency of deformation of the pre-drilled hole is effectively used for mechanical interlocking in addition to the trivial metallurgical bonding.

The effect of process parameters such as TPD and TD, and geometric features such as HD and MH on the joint formation and mechanical performance of DFSF joints is comprehensively studied. Lap shear fracture load of 7.7 kN obtained for DFSF joints is superior than that of FSSW and conventional FSF joints. Increase in TPD beyond 0.5 mm has not yielded significant improvement in the mechanical performance. 14 mm TD is found to be optimum choice for fabricating DFSF joints with acceptable mechanical performance specifically lap shear fracture load of 6.22 kN. Appreciable mechanical performance such as lap shear fracture load about 7 kN, cross-tension fracture load about 3 kN and peel fracture load about 1 kN are obtained at optimum HD range about 3 mm to 3.5 mm with singe hole configuration 1H. The uniaxial tensile test conducted on FSF and DFSF joints revealed that the geometrical inhomogeneity created by the size of the stir spot and frictional heat flux have significant impact on formability of the joint.

The macrostructure analysis revealed that slight increase in TPD yields significant improvement in the mechanical interlocking (collar growth) between the two sheets, irrespective of the occurrence of trivial interface metallurgical bonding. Increase in TD leads to larger frictional contact area and subsequently increased heat flux and extent of plastic deformation of the lower sheet. Samples fabricated at TDs other than 14 mm possess either insufficient mechanical interlocking or insufficient metallurgical bonding. Lower HDs result in closure of the pre-drilled hole and higher HDs decreases the metallurgically bonded area. MHs decreased the mechanical performance due to improper mechanical interlocking and absence of metallurgical bonding. The internal features such as collar length and neck dia. of the pin are appreciable at medium and higher HDs. Farther the holes from the stir spot center in MHs, more imperfect the mechanical interlocking becomes.

The microstructure analysis shows that the region under direct contact with stir tool such as SZ is subjected to dynamic recrystallization, while the HAZ and the PDZ are statically recrystallized. The TMAZ and flash have undergone dynamic recovery under thermal cycle. The PDZ and ASZ are exclusive zones observed in FSF and DFSF joints. HAZ region located closer towards the SZ undergo prolonged heat flux and plastic deformation, which results in annihilated grain growth.

The microstructural changes due to frictional heat flux and plastic deformation has brought about significant hardness reduction in the joint spot than the parent metal hardness. SZ regained the parent metal hardness with the fine grain formation. It is revealed that the extruded upper sheet metal undergoes compression and forging inside the pre-drilled hole in DFSF joints at appropriate TPDs and HDs. The hardness distribution shows identical pattern irrespective of the change in TPD and change in HD. Increase in the SZ size, increase in the volume of upper sheet metal extruded into the pre-drilled hole and change in the mode of joint formation with increase in MH have affected the hardness of the upper sheet.

The growth of external morphological features are significantly influenced by the closure of the pre-drilled hole and prefect extrusion of the upper sheet metal into the pre-drilled hole. Poor interlocking results in severe UB. Increase in geometric features such as HD and MH enables extrusion of more upper sheet metal, consequently the UB is reduced. The upper sheet flash normally shows a free form deformation. The aesthetic appearance of DFSF joints is deteriorated by severe UB and flash size at higher TPD range of 0.7-0.9 mm. At TD of 14 mm, moderate BW and minimum UB are observed.

The failure modes of DFSF samples are different from that of conventional FSSW samples. At higher TPDs, most of the DFSF samples show tear-off failure. Combined failure modes are also recorded due to the presence of more than one active CRs. However, the increase in TD results in poor mechanical interlocking consequently, pin shear failure is common at highest TD of 18 mm. With change in geometric features such as HD and MH, the DFSF samples show random failure modes. It is revealed that the failure of DFSF samples are initiated from critical weak zones such as neck of the pin, top of the pre-drilled hole, upward deformation of lower sheet, stir spot circumference and reference circle circumference.

The pinless stir tool prevents pin hole formation and absence of stir mixing of the two sheets prevents hook formation in DFSF joints. When two sheets are spot joined through friction stirring, joining by metallurgical bonding is a trivial phenomenon as reported in previous literature. However, achievement of simultaneous mechanical interlocking is a new development, which contributes extra joint strength. Therefore, mechanical interlocking is more significant than metallurgical bonding in the present work.

Abbreviations

SPR	Self-Pierce Riveting
FSW	Friction Stir Welding
FSSW	Friction Stir Spot Welding
RPM	Tool Rotational Speed
TPD	Tool Plunge Depth
FSE	Friction Stir Extrusion
FSF	Friction Stir Forming
CFSF	Conventional Friction Stir Forming
DFSF	Dieless Friction Stir Forming
% wt.	Percentage weight
RD	Rolling Direction
USFW	Upper Sheet Flash Width
USFH	Upper Sheet Flash Height
LSFW	Lower Sheet Flash Width
LSFH	Lower Sheet Flash Height
UB	Upward Bulging of upper sheet
SB	Sideward Bulging of upper sheet
FPD	Final Plunge Depth
SST	Stir Spot Thickness
PW	Pin Width
PH	Pin Height
BW	Bond Width
SZ	Stir Zone
PDZ	Plastically Deformed metal flow Zone
TMAZ	Thermo-Mechanically Affected Zone
ASZ	Annular Stir Zine
HAZ	Heat Affected Zone
CR	Critical Region
dia.	Diameter
TD	Tool shoulder Dia.

MH	Multi-Hole configuration
A5	AA 5052-H32
A6	AA 6061-T6

Nomenclature

n	Strain hardening exponent
K	Strength coefficient
R	Plastic strain ratio

Contents

List of figures

List of tables

Chapter 1

Introduction, Literature review, Significance and Objective of work

1.1 Introduction

Metals form a vital and dynamic part of human life. The art of metalworking is believed to be one of the earliest skills known to man. History shows that all man's culture rests on the metals. Basic tools like the hammer, the forge, the anvil and many other appurtenances of the craft were designed thousands of years ago by men whose names are long since forgotten, yet their inventions live on, in many of our most modern pieces of shop floor equipment. So understanding the philosophy of metals and the metalworking is a route to the heart of understanding our past. Our benefits continue to grow from having this material and the ability to work with them.

Knowledge of the sources, production and uses of metals form the central theme in the development of modern engineering for the last couple of centuries. Joining of metals stands at the opening door of opportunity waiting for us to use its advantages to build a stronger, safer and better world in which we live. New techniques for joining metals are evolving day by day. Therefore, better research is needed in this field.

Joining is the process of linking two or more parts together, whereas assembly is the sequence of multiple joining operations involved in the fabrication of a product. Joining and assembly have significant impact on a product's total manufacturing cost and manufacturing time. If their role is discarded, product performance will be badly affected by stress concentrations, by modifying the microstructure and mechanical properties, or by a catastrophic failure. Joining is not just a matter about functionality, cost, and speed of assembly: it also contributes to the character and aesthetic appearance of the products by exposing a certain style and invoking certain sense of quality. Joining of metals can be either conventional or alternative (mostly joining by plastic deformation).

1.1.1 Conventional Joining

Conventional joining processes for materials can be broadly divided into five sub-groups:

- Welding (suitable for most metals and plastics)

- Brazing and soldering (for certain metals)
- Adhesive bonding (for nearly all materials)
- Mechanical fastening (for nearly all materials)
- Joining using form closures (for nearly all materials)

Each sub-group involves a number of methods; all of them share their common principle in the execution stages.

Welding is the process that involves the local heating of the interface region, after proper alignment of mating parts, to form the joint. Most metals and thermoplastics can be easily joined by welding. In fusion welding, the temperature of the weld zone exceeds the material's melting point and forms the joint as the weld solidifies completely. However, with a few exceptions, welding can join only similar materials. Solid-state welding avoids global melting of the weld zone and uses hot deformation and interface diffusion to form the joint instead.

In brazing and soldering, a filler metal in the form of a wire is melted and applied locally to the parts to be joined. Either the mating parts are heated or the filler wire itself is melted and spread over the joint surface area through capillary force. Solidification enables the formation of a strong joint. Soldering is done at a temperature below 450°C, with tin bearing alloys; brazing is done well above this temperature, to join copper alloys such as brass. Brazing and soldering provide best joint strength when eutectic filler compositions are used because they have specific melting point and a two-phase microstructure, giving greater strength. Since the liquid filler delivers an even spreading, these joints are leak proof and provide better neatness. Brazing gains more popularity than welding for metal furniture fabrication and jewellery making sectors. Most often brazed and soldered joints can be dismantled simply by applying sufficient heat, thus advantageous for repairs without crucial damage to the parts.

Adhesion is a complex process involving a combination of physical (e.g., microscopic material inter-locking) and chemical (e.g., Van der Waals forces) aspects. The importance of careful surface preparation, even more than welding, brazing and soldering, such as removing oxide layers thorough cleaning and adding wetting agents, all with extreme control of cleanliness, humidity, temperature, and joint fit-up add further complexity. Applications include lightweight, low volume, high performance products such as aircraft structures, high-end racing bicycles, sports cars etc. Adhesive bonded joints can withstand loading due to shear stress only, as the adhesives are often weak in

tension. Since the set times for adhesives are still slow compared to other joining processes, it can be advantageous to combine adhesive bonding with spot welding or riveting to form hybrid joints that possess sufficient handling strength immediately and achieves full strength in the due course without holding up assembly.

Mechanical fastening can be defined as joining two (or more) parts together by means of a separate component, often mentioned as consumables namely bolts, screws, rivets, nails, staples, tie wraps, cable clamps, stitches etc, whose principle relies on mechanical forces, friction, or form closure to create the joint. Mechanical fastening is a relatively easy and fast joining method which involves no heat input or active chemicals, requires little or no pre-processing. It can be used to join dissimilar materials, and it can be disassembled frequently, making them an exquisite platform for parts requiring periodic maintenance and upgradation. However, they can only be used for local joints, and seals or gaskets are required for making the joint airtight and leak proof.

Form closures are the neatest joining methods, which require neither heat or chemicals, nor any additional materials or components. Form closures are usually employed in plastics and light metals. They allow repeated release and can be very rapidly fabricated. These methods can be split into two categories: form closures based on elastic deformation such as snap fits, clamp fits of parts and those based on plastic deformation such as hemming, staking.

1.1.2 Alternative joining/ Joining by plastic deformation

Lightweight assembly and smart structures are the outcomes of the demand for energy efficient systems and sustainable use of resources. The need for new functional processes for joining parts is increasing day by day because the trend in manufacturing is that, both the number of parts and their complexity are increasing. In addition, the commercial requirements like higher performance, higher productivity and lower cost in assembly operations are getting increasingly focussed. Joining by plastic deformation is a suitable choice in the current engineering scenario.

Plastic deformation is generally applied in manufacturing as a tool for forming operation to refine the shape of metal parts and to control their mechanical properties. However, its application can be extended to join parts having sufficient ductility without the use of an external heat source as needed in fusion welding. Joining by plastic deformation offers advantages such as improved accuracy, better reliability, eco-

friendliness as well as creating dissimilar metal combinations. It has a wide spectrum of applicability and it is successful in eliminating defects caused by conventional joining processes. Joining by plastic deformation relies on the principle of mechanical interlocking and metallurgical bonding to effect the joint formation (Mori et al., 2013).

In joining by mechanical interlocking, interfacial pressure and interlocking enables joint formation without utilizing any thermal energy source. They are usually form-closed joints and force-closed joints. Controlled plastic deformation generates proper pressure and interlocks. On contrary to metallurgical joining processes, the contacting surfaces are not chemically bonded, so the breaking up of oxide films as well as the rise in interfacial temperature are not required to initiate a bond formation at atomic level (Groche et al., 2014). Joining by mechanical interlocking involves processes like SPR, mechanical clinching, hydroforming, electromagnetic forming, incremental forming etc.

In joining by metallurgical bonding, also considered as solid-state welding, the oxide films and contaminants that present at the interface between work pieces are broken up by severe plastic deformation and the virgin metal surfaces, which come into contact, are bonded by the advantage of high interfacial pressure. Interfacial slipping and plastic flow result in internal heating of the work pieces, rising its temperature, thereby accelerating its deformation. Cold welding, friction welding, continuous/ spot FSW are some of the joining techniques, which relies on the principle of metallurgical bonding. In addition, there are certain joining techniques, which relies on simultaneous mechanical interlocking and metallurgical bonding.

According to the geometry of mating parts that come into assembly, the joining by plastic deformation can be broadly classified into following categories. They are joining by plastic deformation for

1. Connecting Tube to tube
2. Connecting tube to sheet
3. Connecting sheet to sheet
4. Producing bimetallic tubes/rods and composite pipes
5. Connecting rod to rod
6. Connecting shaft to ring

Based on the principle underlying the joint formation and the temperature at which the process is executed, the joining processes employed for connecting these mating parts are listed in Table 1.1.

Table 1.1. Classification of joining by plastic deformation processes

Type of connection	**Working temperature → ---------- Joining principle ↓**	**High temperature**	**Room temperature**
Tube to tube	**Mechanical interlocking**	-	Asymmetric plastic instability (Gonçalves et al., 2014) Rotary Swaging (Zhang et al., 2014) Angular joining by hydroforming (Groche and Tibari, 2006) Electromagnetic form joining Incremental form joining (Mohebbi and Akbarzadeh, 2010) Interference fit joining (Mori et al., 2013) Crimping /Swaging (Cho and Song, 2007) Joining by rolling (Mori et al., 2013) Tubular lap joint (Silva et al., 2015)
	Metallurgical bonding	-	Cold extrusion (Wagener and Haats, 1994) FSW (Ahmed and Saha, 2018, Kumar and Kailas, 2008) Hybrid friction diffusion bonding (Haneklaus et al., 2016)
	Both mechanical interlocking and metallurgical bonding	-	-
Tube to sheet	**Mechanical interlocking**	Hot extrusion with a slit mandrel (Kuboki and Murata, 2007)	Compression beading and tube inversion (Alves et al., 2011) Boss forming and upsetting (Alves et al., 2018) Sheet bulk forming (Alves et al., 2017) End curling (Agrawal and Narayanan, 2017) Hydroforming (Groche et al., 2014)
	Metallurgical bonding	Low pressure diffusion bonding	-
	Both mechanical interlocking and metallurgical bonding	-	-
Sheet to sheet	**Mechanical interlocking**	SPR with local conditioning of sheet,	SPR using semi hollow rivet (Xing et al., 2015),

		Dieless clinching (Neugebauer et al., 2008)	SPR using solid rivet (Gerson Meschut et al., 2014), SPR using pipe rivet (Huang et al., 2014) Friction stir blind riveting (Min et al., 2015) Rotating tool and pilot hole mechanism (Nakayama et al., 2014) FSE (Evans et al., 2015) Cold pressing deformation joining (Li et al., 2012) Mechanical clinching (Abe et al., 2014) Hole clinching (Lee et al., 2010) Shear clinching (Gerson Meschut et al., 2014) Hemming (Livatyali et al., 2000) Orthogonal sheet bulk forming (Silva et al., 2018) Bulk compression joining (Pragana et al., 2018) Spinning (Groche et al., 2014) Linear flow splitting (Groche et al., 2017)
	Metallurgical bonding	Bar extrusion (von Senden genannt Haverkamp et al., 2012) Hot roll bonding (Groche et al., 2014)	FSW- continuous and spot (Mishra and Ma, 2005) Cold forge-spot bonding (Miwada et al., 2014) Ultrasonic vibration joining (Nanaumi et al., 2014) Cold roll bonding (Fridlyander et al., 2002) Cold shear welding (Mori et al., 2013) Magnetic pulse welding (Sadot et al., 2009) Explosion welding (Findik, 2011) Laser impact welding (Zhang et al., 2011) Linear friction welding (Bhamji et al., 2010)
	Both mechanical interlocking and metallurgical bonding	-	FSF (Lazarevic et al., 2013) Resistance element welding (G. Meschut et al., 2014) Thermally assisted partial clinching (Huang and Yanagimoto, 2015)
Production of bimetallic tubes / rods and composite pipes	**Mechanical interlocking**	-	Multi billet extrusion for metal-ceramic composite pipes (Chen et al., 2001)
	Metallurgical bonding	Multi billet extrusion for bimetallic pipes (Chen et al., 2001)	Co-extrusion (Krishna et al., 2005)

		Equal channel angular extrusion (Eivani and Taheri, 2007) Backward extrusion (Madej et al., 2015)	Low temperature equal channel angular extrusion (Eslami and Taheri, 2011)
	Both mechanical interlocking and metallurgical bonding	Spiral extrusion (Sapanathan et al., 2013)	High pressure tube twisting (Lapovok et al., 2012)
Shaft to shaft	**Mechanical interlocking**	-	-
	Metallurgical bonding	-	Friction welding (Meshram et al., 2007) Divergent extrusion (Lilleby et al., 2009) Cold butt welding (Stroiman and Mitrukov, 2002)
	Both mechanical interlocking and metallurgical bonding	-	-
Shaft/ tube to ring/flange	**Mechanical interlocking**	-	Lateral extrusion (Dörr et al., 2014) Crimping (Cho and Song, 2007) Expanding with rolling tool (Hagedorn and Weinert, 2004) Hydroforming: normal/ dieless (Groche et al., 2014), (Marré et al., 2010) Electromagnetic forming (Groche et al., 2014) Cold Indentation joining (Kitamura et al., 2012) Knurled interference fit (Kleditzsch et al., 2014)
	Metallurgical bonding	Compound hot forging	Lateral extrusion (Groche et al., 2014) Backward cold extrusion forging (Groche et al., 2014)
	Both mechanical interlocking and metallurgical bonding	Indentation joining (Matsumoto et al., 2008)	-

From the table, it is clear that most of the joining by plastic deformation processes are executed at room temperature. Processes executed at high temperature (between recrystallization temperature and melting point) are also less. Mechanical interlocking is the common mechanism during plastic deformation of mating parts. Furthermore, processes with metallurgical bonding and processes with simultaneous mechanical interlocking and metallurgical bonding are limited.

The research presented in this work is confined to joining of sheet metals (sheet to sheet joining) only. The bulk metal joining is out of the scope of this work.

1.2 Literature review

1.2.1 Sheet to sheet joining

Energy conservation has achieved at most importance in all major engineering fields including automotive and aerospace industries. Improving the fuel efficiency and introducing the body-mass reduction are the major measures to realize energy conservation in automobiles. New lightweight sheet metals are introduced into automobile industry to meet the surging need for body mass reduction, fuel economy and vehicle stability (Cole and Sherman, 1995). Joining similar grades/ dissimilar grades of such sheet metals is a major challenge. High thermal conductivity, high coefficient of thermal expansion and surface oxide layer formation hinder the usage of fusion welding techniques for lightweight sheet metals such as aluminium alloys. Processes using joining by plastic deformation principle such as mechanical clinching and SPR are commercially popular. But, they possess disadvantages like split, lack of mechanical interlocking and neck fracture, due to the severe plastic deformation in the joint zone (Lee et al., 2014). SPR requires double sided accessibility and piercing of the upper sheet, which introduces weak zones that can grow into cracks while loading. Use of mechanical clinching is affected by vibration and poor aesthetic appearance such as downward protrusion of the lower sheet and limited use on the sliding surfaces and visible areas.

In the past decade, solid-state welding techniques have acquired popularity in the manufacturing industry due to its inherent advantages, ease of operation and its ability to emerge as alternative joining technique. Friction stir based joining techniques such as FSW and FSSW are some popular choices. These processes retain the combined beneficial properties of both the parent sheet metals (Haghshenas and Gerlich, 2018) as well as ensure sufficient elastic-plastic response and formability levels for the joints. In the early stages of its development, primary focus was on joining ductile sheet metals like aluminum, magnesium and copper. Later the application of these processes is extended for steel sheets also.

1.2.1.1 Friction stir spot welding

FSW is an eco-friendly solid-state joining process using stir friction heat, invented by TWI, England in 1991(Thomas and Nicholas, 1997). Inspired from the same principle, FSSW process marked its presence in manufacturing industry since 2004 (Gerlich et al., 2006). FSSW process has been using as an alternative to resistance spot welding in the manufacturing industry. The schematic illustration of FSSW process is shown in Fig. 1.1. In this process, the conversion of mechanical energy into thermal energy occurs by frictional stir heating without the application of any external heat source. It involves a rotating stir tool with pin penetrating the desired spot in the sheet metals kept in lap joint configuration. The stir spot undergoes frictional heat flux and plastic deformation by stir mixing of the upper and the lower sheets. The joint formation takes place predominantly by metallurgical bonding at the sheet interface (Yang et al., 2014). The plunge of the stir tool normally extends up to one-half of the thickness of the lower sheet.

Numerous literatures are available for better understanding of the FSSW process and its variants(Sarkar et al., 2015). The joint formation and mechanical performance of FSSW joints are influenced by the process parameters and the tool geometry. The RPM, TPD, tool plunge rate and dwell time are the main process parameters. The tool surface profile and tool pin profile are the important geometric features of the stir tool affecting the formation of the joints. Friction stir processing is also developed to with a view to enhance the material properties and metallurgical characteristics of sheet metal (Guru et al., 2015, Kapoor et al., 2013).

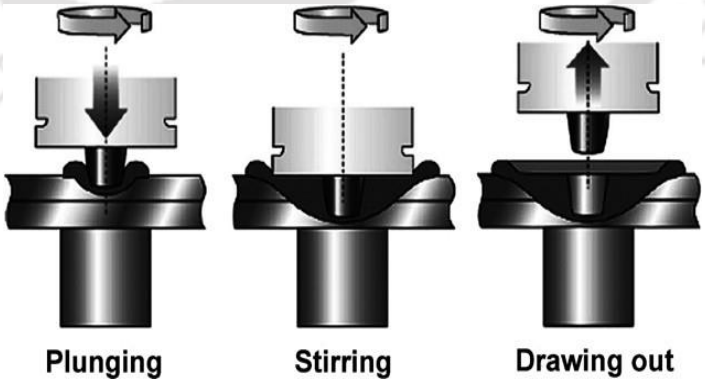

Figure 1.1. Schematic illustration of the FSSW process (with permission from Zhou et al. (2011). Copyright Elsevier)

1.2.1.1.1 Effect of RPM

The effect of RPM, the critical parameter determining the amount of heat generation in FSSW has been widely understood. A study on the effect of process

parameters on lap shear strength of FSSWed AA 6061 sheets of 0.9 mm thickness revealed that RPM is the primary variable affecting the joint strength followed by tool pin profile and dwell time (Garg and Bhattacharya, 2017a). The lap shear strength decreased with increase in RPM. Energy input during FSSW of AA 6061-T6 sheets was investigated by varying RPM and dwell time (Cox et al., 2014b). The energy generated during the spot welding operation was found to have a linear relationship with tensile shear strength. At lower energy levels, above certain threshold value, joints were significantly stronger than those created at higher energy levels. Optimum spot welding energy level for sheets of 2 mm thickness was found to be 4.2 kJ to 6.3 kJ. As reported by Liu et al. (2013) and Arul et al. (2008), the tensile shear strength of FSSW joints in aluminum alloys, namely 2A12-T4 and 6111-T4, increased up to 1000 and 2250 rpms, and then showed a decreasing trend with increase in tool rotational speed up to 1200 and 3000 rpms respectively. The temperature profiles revealed that the maximum temperature attained was low at lower tool rotational speeds like 1500 rpm (573 K) than that at higher tool rotational speeds like 3000 rpm (688 K). Lakshminarayanan et al. (2015) reported that the heat input and processing temperature during FSSW can be controlled by varying the RPM and dwell time. The initial increase and subsequent decrease in tensile shear strength with increase in RPM was mainly due to difference in the size of the annular bond region and the changes in the joint microstructure. The amount of frictional heat generated at SZ increased with increase in RPM of the stir tool (Awang and Mucino, 2010). The lap shear test reported by Rao et al. (2015) showed that weld strength decreased with increase in the RPM during FSSW of magnesium alloy AM60B and aluminium alloy AA 6022-T4. High frictional heat generation caused reduction in the viscosity of the material right under the stir tool, which further resulted in slippage rather than stirring. During FSSW of AA 5182-O aluminium alloy, the increase in RPM led to intense stirring and larger SZ size, but the residual stress at the SZ induced a negative impact on the joint formation, which resulted in poor joint strength at higher RPMs (Bozzi et al., 2010). A three dimensional numerical model of material flow for FSW was developed by Liechty and Webb (2008). From the model, it was estimated that maximum velocity of the weld material was only 9% of the RPM. The model predicted the region of material rotation with the stir tool. Therefore, the RPM affects the lap shear strength, frictional heat input, joint microstructure and residual stress of the joint. Too high RPM has negative impact on FSSW joint strength.

1.2.1.1.2 Effect of TPD

Literature shows that TPD is another process variable, which significantly influences the formation and strength of FSSWed joints. Rao et al. (2015) reported that the lap shear fracture strength of FSSW joints between AA 6022-T4 wrought aluminum alloy and AM60B cast magnesium alloy increased with increase in TPD at 1000 rpm. It was revealed that increase in TPD increased the frictional heat flux and the BW of the joint, which resulted in increase in the joint strength by the interlocking of hard and brittle intermetallic compounds. Increase in the tensile shear fracture load, up to a maximum of 3.07 kN, with increasing TPD was reported during the FSSW of galvanized steel sheets performed by Baek et al. (2010). However, Mitlin et al. (2006) reported that the excessive tool penetration reduced the tensile shear strength of FSSWed AA 6111 aluminum sheets, due to hole formation at the stir spot. Tutar et al. (2014) reported that TPD has the highest influence than dwell time and RPM on the tensile shear failure strength of FSSW samples. Increase in TPD enhanced the stirring of the metals and resulted in wider SZ, HAZ and TMAZ, thereby increasing the shear strength of FSSWed AA 3003-H12 aluminum alloys. Mitlin et al. (2006) reported that TPD had strong influence on the failure mode of FSSWed samples of 6111-T4 aluminum alloy sheets of 1 mm thickness. As the tool shoulder plunged into the upper sheet, the mode of failure was changed from brittle fracture near the pinhole to ductile fracture near the base metal. It was also reported that the tool pin penetration depth has least effect on the lap shear strength of these FSSWed samples. Recrystallized grains formed under the tool shoulder revealed that the frictional heat input contributed by the tool shoulder was much higher than that under the pin. The FSSW of AA 5182-O aluminum alloy sheets performed by Bozzi et al. (2010) revealed that increasing shoulder plunge depth resulted in initial increase and further decrease in tensile shear strength. Too high shoulder plunge depth resulted in the excessive localized thinning of the upper sheet. Yoon et al. (2012) reported that TPD affects the BW. In addition to the influence on tensile shear failure load, TPD has a remarkable influence on surface appearance and macrostructure of FSSWed AA 5454-O aluminum alloy sheets. FSSW of AA 5052−AA 6063 aluminum sheet combination performed by Piccini and Svoboda (2015) revealed that increase in TPD resulted in increase in the peel strength of the joint. In addition, the fracture mechanism changes from interfacial mode to circumferential mode with increase in TPD. Pathak et al. (2013) also reported an increase in the lap shear strength of FSSW samples in AA 5754 aluminum alloy with increasing TPD. During the

FSSW of AA 5052 aluminum alloy to polyethylene terephthalate, it was reported by Yusof et al. (2012) that increase in TPD resulted in tight sticking of polymer to the metal sheet and further resulted in increase in tensile shear strength. Arici and Mert (2008) reported that increase in TPD increased the heat generation and enhanced the plastic deformation of FSSW joints in polypropylene sheets. Therefore, TPD influences the lap shear fracture load, frictional heat flux, BW, stir spot size, joint macrostructure and failure mode of FSSW joints. Excessive plunge depth leads to severe upper sheet damage.

1.2.1.1.3 Effect of tool geometry

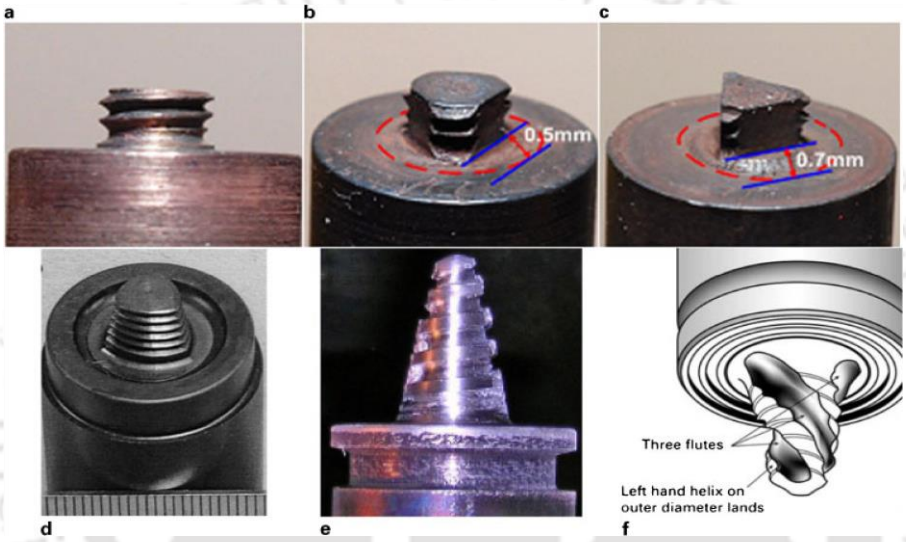

Figure 1.2. Various types of stir tools used in FSSW process (a) Cylindrical threaded, (b) Three flat threaded, (c) Triangular threaded, (d) Trivex, (e) Threaded conical, (f) Triflute tools (with permission from Rai et al. (2011). Copyright Taylor & Francis)

There are numerous literature depicting the effect of tool geometry on the joint formation in FSSW process. Stir tools with various pin profiles are employed in FSSW process as shown in Fig. 1.2. During FSSW of AA 6061 sheets of 0.9 mm thickness, high temperature about 878 K generated with circular pin induced minimum stress at the stir spot (Garg and Bhattacharya, 2017a). The maximum shear fracture strength of the joint was observed with stir tool having square pin. However, square pin and triangular pin were subjected to considerable wear and produced severe damage to the sheets. The effect of triangular pin on joint formation of FSSWed AA 5083 sheets was investigated by Badarinarayan et al. (2009b). Cross-tension strength of welds made with stir tool having triangular pin was twice the strength of spot welds made with stir tool having cylindrical pin. The asymmetric stirring induced by the triangular pin led to hook growth and the crack propagation during fracture was initiated from the hook defect at low loads. FSSW of AA

6061-T4 sheets of 2 mm thickness revealed that the thickness of the upper sheet at the stir spot decreased with increase in pin length for short dwell time and lower RPMs (Tozaki et al., 2007). Increase in the pin length contributed better lap shear strength to the joints, but the cross-tension strength decreased. Pathak et al. (2013) studied the influence of tool pin profile on the lap shear strength of FSSWed AA 5754 sheets under varying TPDs. The stir tools with straight cylindrical pin contributed better strength than that with tapered cylindrical pin. The material flow during FSSW of AZ31 Mg alloy sheets of 1.3 mm and 2 mm were investigated by Yang et al. (2010) using tracer material technique. The intermixing of upper sheet and lower sheet metals take place in the flow transition zone due to the combination of horizontal, vertical and rotational motions of the plasticized metal beneath the tool shoulder. It was revealed that the driving force for the downward motion of the plasticized metal was contributed by the rotating pin of the stir tool. The effect of process parameters such as tool shoulder plunge depth, tool pin geometry and RPM on FSSW of AA 2024-T3 sheets was investigated by Paidar et al. (2014) and Paidar et al. (2015). Pin geometry significantly affected hook formation and SZ shape. During FSSW of 5754-O aluminum alloy sheets of 1.32 mm thickness performed by Badarinarayan et al. (2009a), the axial load for stir tool with triangular pin was smaller than that with cylindrical pin. It was revealed that the pin geometry and tool shoulder profile play significant role in the power consumption during FSSW. However, the SZ formation was not prominent and downward material flow was absent with stir tool having unthreaded triangular pin. Use of stir tool with triangular pin caused drilling effect during the tool plunge, which further led to chipping away of upper sheet as small fragments.

Literature shows that significant improvement in joint strength cannot be obtained under all loading conditions by the usage of pinned stir tool in FSSW. Therefore, the size and features of the stir tool has a significant influence on material mixing, joint strength, extend of bonding in between the faying surfaces, mechanical properties, formation of defects and plastic deformation of the upper and lower sheets. Furthermore, the stir tool with pin results in pinhole formation at the stir spot.

Shen et al. (2013) reported that the pinhole left during FSSW (pin hole defect) limits its widespread applications for commercial purposes. In addition, FSSW joints fabricated with stir tool having pin generates internal hook defect. The hook like structure develops from the lower sheet around the stir mix zone results in upper sheet thinning. Thinning of upper sheet near the pin hole impairs the joint strength. Negative impact of hook defect on the weld strength was also reported by Cao et al. (2016) during FSSW of

AA 6061-T6 sheets of 2 mm thickness. Increase in process parameters such as RPM and TPD resulted in increase in hook height, consequently the weld strength was reduced. The effect of pinned tool geometry on the hook formation and material flow during FSSWed 5754-O aluminum alloy sheets of 1.32 mm thickness was investigated by Badarinarayan et al. (2009a). It was reported that the tool shoulder geometry significantly affected the lap shear strength and hook formation in FSSWed joints. For same plunge depth, samples fabricated with FSSW stir tool having concave shoulder possessed larger upper sheet thickness, therefore obtained better lap shear strength than that with convex shoulder profile and with flat shoulder profile. However, low axial load bearing ability, continuous hook formation and large size SZ were obtained for FSSW tool with concave shoulder profile. Above discussion shows that major drawbacks such as pinhole defect and hook defect hinders the versatility of the FSSW process. These defects act as major hurdles towards achieving high strength joints with FSSW process.

Modifications in the friction stir based spot joining processes are under research with an objective to eliminate the defects and to achieve better joint strength and joint quality. Recent developments such as pinless FSSW (Li et al., 2018) and pinhole refilled FSSW (Chen et al., 2017) can successfully eliminate pinhole defect. The principle of frictional heat generation and further plastic deformation remains same for both the processes.

1.2.1.2 Pinless/ probeless FSSW process

Literature shows that pinhole defect in FSSW process can be successfully eliminated by employing suitable modifications in the stir tool geometry. In an attempt to eliminate pinhole, 0.93 mm thick 6111-T4 aluminum alloy sheets were spot joined with pinless FSSW process (Bakavos et al., 2011), in which a flat faced cylindrical stir tool without pin was employed. High level of grain refinement and plastic zone penetration into the lower sheet were also achieved with the pinless stir tool. AA 6061-T6 aluminum alloy sheets with 2 mm thickness were spot joined using pinless stir tool and a rotating anvil set up (Cox et al., 2014a). Rotating anvil permits joining of thicker sheets, improved mechanical strength and reduced reaction forces on the spot weld set up. Application of rotating anvil increased the joint strength, upto 450 kgf, irrespective of the change in RPM. The pinhole defect was successfully eliminated; but hook defect was retained. Single-spot and multi-spot FSSW of AA 6061-T6 sheets of 0.5 mm thickness was conducted by Garg

and Bhattacharya (2017b) using pinless flat stir tool. Increase in the number of stir spots increased the effective weld width, and consequently, the lap shear strength and cross-tension strength were increased. However, the hook defect was not eliminated and multiple stir spots occupied comparatively larger area. Failure along the circumference of the stir spot was initiated from the hook defect in stir spot. FSSWed butt joints of 6 mm thick AA 6061-T6 aluminum alloys were fabricated with pinless stir tool having an embedded rod by Chiou et al. (2013). The hollow cylindrical tool made of high-speed steel had a provision for holding cylindrical rods of upper sheet metal, considering the fact that coefficient of friction and further heat generation can be improved with self-mated pairs. Failure loads of FSSWed joints fabricated with embedded rods were 1.48 times higher than that of flat pinless tools. FSW of 2A12-T4 aluminum alloy sheet with pinless tools having different groove profile was investigated. Six-groove tool yielded sound joint with 362 MPa strength, reduced flash formation and minimized sheet thinning (Liu et al., 2016). The effect of tool surface features on the material flow during FSSW of AA 6111-T4 aluminum alloy was studied by Reilly et al. (2015) using pinless flat tool and fluted tool. Circumferential material flow was observed in FSSW process with fluted tools. Central region of the stir spot stuck to the tool surface, while a slip region observed towards the outer periphery. Probeless stir tool with involute grooves on the shoulder surface was used for FSSW of AA 2198-T8 aluminum alloy sheets of 1.8 mm thickness by Li et al. (2018). The joints possessed symmetrical basin shape with finely recrystallized SZ structure and severely deformed TMAZ. When the hook angle reached 90°, maximum shear strength was obtained. FSSW of 2 mm thick AA 6061-T4 sheets performed by Tozaki et al. (2010) showed that sound welding can be attained with a probeless tool. They reported that the tensile shear strength of welds made with probeless tool was better than that with probe tool. Similar temperature values were recorded during FSSW with probeless tool and probe tool. Probeless tool attained maximum temperature in shorter time span than probe tool by virtue of its larger shoulder contact surface. Chen et al. (2013) conducted FSSW of 1 mm thick AA 6111-T4 sheets with probeless tool. The hook formation was found to be smaller with shorter welding time (less than 1 second). It was reported that the depth of the deformation zone increased with increase in weld time, which further increased the upward deformation of the lower sheet. Garg and Bhattacharya (2017b) used pinless stir tool to obtain multi-spot friction stir welds between AA 6061-T6 and commercially pure copper sheets. An increase in lap shear strength was observed with increase in the number of stir spots. Li et al. (2018) also conducted probeless FSSW in 2198-T8 aluminum alloy

for eliminating pinhole defect. Therefore, a pinless stir tool can also be employed for FSSW of aluminum alloys to contribute sufficient frictional heat generation and resulting sound joint formation. However, the hook defect affected the shear strength and fracture mode of the joints.

The use of pinless tool in FSSW has eliminated the pinhole defect and improved the joint strength and aesthetic appearance. However, it has four major shortcomings

- Larger plunge depth should be provided as compared to stir tool with pin
- Flash formation is considerable
- Simultaneous elimination of pinhole defect and hook defect was not realized in most cases. So further improvement in joint strength is possible.
- Joint formation by simultaneous mechanical interlocking and metallurgical bonding has not been achieved.

1.2.1.3 Refill FSSW process

Recent literature show that FSSW process can be modified to seal the pinhole generated with stir tool having pin, commonly known as pinhole refilled FSSW or simply refilled FSSW. Stages of refill FSSW process is shown in Fig. 1.3. Refill FSSW of AA 6061-T4 and AA 7075-T6 sheets were conducted by Shen et al. (2018). Samples achieved higher joint strength than that of resistance spot welds due to the increase in effective bonded area. However, metallurgical bonding was not attained at the weld center, when the plunge depth was less than the upper sheet thickness. In addition, minor hook defect was observed at higher TPD. A method for sealing FSSW pinhole using plug insert was proposed by Reimann et al. (2016). The 7.5 mm dia. pinhole left on FSSWed AA 6061-T6 sheets of 4.8 mm thickness was filled with plug insert of same material in subsequent refill FSSW process. In addition to superior aesthetic appearance, the joints possessed high strength with post weld heat treatment and artificial ageing. A two stage refilled FSSW was proposed by Sajed (2016) for removing pinhole defect in FSSW process. A second stage refilling with a pinless stir tool was performed over the pinhole left at the stir spot in the first stage. Strength of FSSW joints in AA 1100 sheets of 2 mm thickness increased with decrease in RPM and increase in pinless TD. Joint strength upto 6.96 kN was obtained at 1000 rpm, 3.8 mm TPD, 6 s dwell time and 14 mm TD. Refill FSSW of AA 5754 and AlSi coated steel showed that the eutectic phase coating on the steel sheet played a key role in dissimilar spot welding (Ding et al., 2017). The high strength joint was attributed to the presence of fine silicon particles, less defects and control of intermetallic formation

at the joint interface. Lap shear strength of the joints increased with increase in TPD. However, in pinhole refilled FSSW process, the superior aesthetic appearance and the advantage of improvement in joint strength are mitigated by longer execution time of the process. Adding a second stage refilling process consumes extra cost and time. Moreover, the process is not successful in eliminating internal hook defect.

A development of a process with simultaneous elimination of pinhole defect and hook defect in a single operation is inevitable is sheet metal joining. Literature shows that simultaneous elimination of pinhole formation and hook defect using two stage FSSW process was proposed by Li et al. (2014). Hook defect developed in the first stage was eliminated by performing FSW over the hook formation with a pinless stir tool. Shallow nugget zone developed in the second stage removed the hook defect, but size of the stir spot nugget was sacrificed with the addition of the second stage FSW.

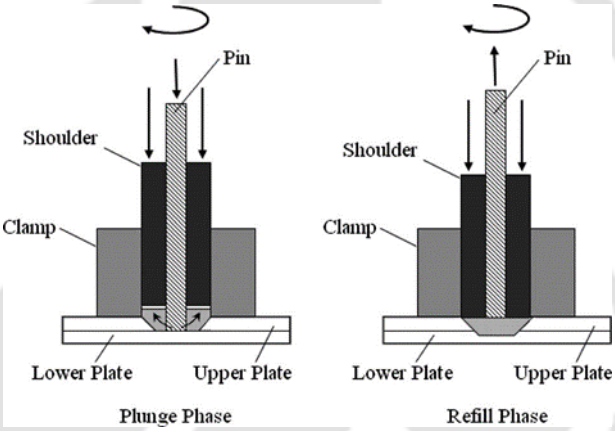

Figure 1.3. Stages of refill FSSW process (with permission from Das et al. (2007). Copyright Springer)

1.2.2 Sheet extrusion

It is obvious that a pinless stir tool can prevent the pinhole formation and at the same time induce sufficient amount of upper sheet stirring. However, the stir mixing of upper and lower sheets should be prevented to eliminate hook defect formation in FSSW. Potential alternatives are developed, in which the sheet metals can also be lap joined by local extrusion forging utilizing the stir friction heat. Several friction stir based processes for joining dissimilar sheet metals such as aluminum alloys and automotive steel fall under the category namely sheet extrusion . FSE and FSF are two such sheet extrusion processes.

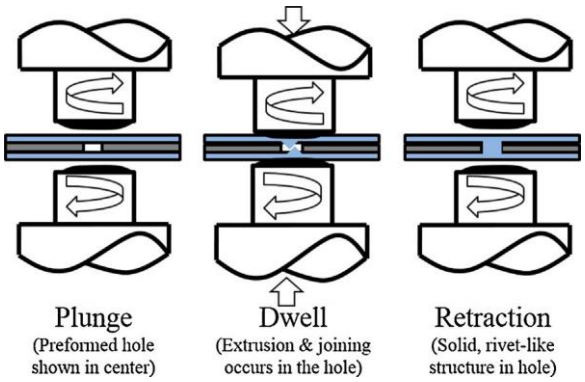

Figure 1.4. Stages of two-sided friction stir riveting by extrusion process (with permission from Evans et al. (2016). Copyright Elsevier)

1.2.2.1 Friction stir extrusion

Sandwich joints of dissimilar sheet metals such as AA 6061-T6 and low carbon steel were fabricated by Evans et al. (2016) using two-sided friction stir riveting by extrusion. Stages of two-sided friction stir riveting by extrusion process is shown in Fig. 1.4. Lap joint configuration of Al/steel/Al was strengthened by simultaneously extruding upper and lower aluminum sheet into a pre-drilled hole in the middle steel sheet using friction stir tool, and further metallurgical bonding at the interface. Fracture strength upto 9.3 kN was obtained for these spot joints. During friction stir riveting by extrusion, it was observed that the strength of the spot joint can be increased by increasing the number of pre-drilled holes in the extrusion zone. MH configurations like two hole and three hole configurations led to 11% and 12 % increase in tensile shear strength respectively, as compared to single hole configuration. Increasing the number of pre-drilled holes and thereby distributing the load between multiple pins is an effective step to improve joint strength. In another attempt of FSE process, a traversing stir tool was used to extrude and interlock aluminum into a pre-made groove in the steel sheet (Evans et al., 2015). Shear strength upto 6 kN was obtained for these joints between AA 6061 sheet and low carbon steel sheet with slit saw groove. The joint quality depends on tool profile and the concern of brittle intermetallic bonding was eliminated.

1.2.2.2 Friction stir forming

A new variant of FSSW namely FSF process is developed for creating lap joints in dissimilar sheet metals such as aluminum and automotive steel. Mechanical interlocking by rivet head formation and interface metallurgical bonding simultaneously strengthens the FSF joints. This solid state joining process is eco-friendly and relatively cheap process

with less added mass, since the need for external consumables such as rivets, bolts and electrodes are eliminated. Thus, the process can be utilized for lightweight sheet metal applications in automobile industry to achieve better fuel efficiency, stability and reduced CO_2 emission.

Stages of an FSF process is shown in Fig. 1.5. FSF process involves the stirred upper sheet metal forged and extruded into an anvil cavity through a pre-drilled hole in the lower sheet. Anvil cavity enables rivet head formation. In addition, the interface of the two samples are metallurgically bonded. The joint formation occurs by simultaneous mechanical interlocking and metallurgical bonding. The formation of a macro size pin and subsequently forming a rivet interlock is one of the inherent and exclusive phenomena happening in the FSF process. The principle/mechanism of joint formation of FSF joints is discussed in detail in subsequent chapters.

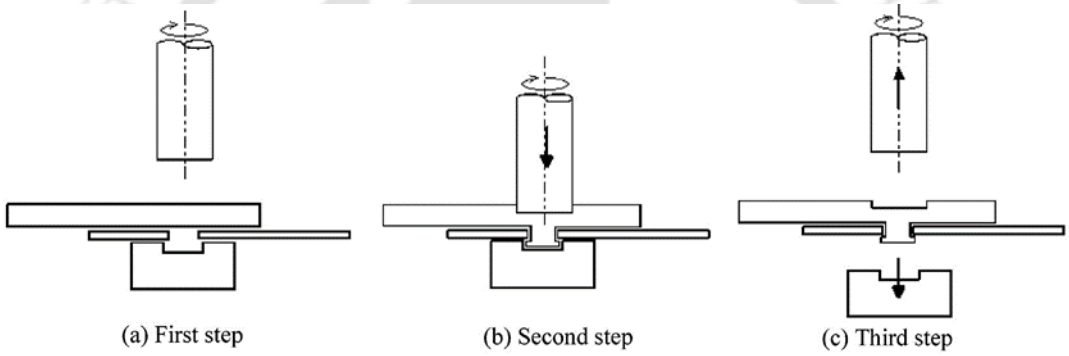

Figure 1.5. Stages of FSF process (with permission from Lazarevic et al. (2013). Copyright Elsevier)

The FSF process is reported in a few literatures. Nishihara and Ito, (2005) conducted initial attempts on FSF process. Lazarevic et al. (2013) performed FSF process for joining aluminum alloys such as AISI 5182 and AA 6014 sheets to zinc coated mild steel. Joint strength upto 5 kN obtained for FSF joints was found to be better than that of SPR in same material combination. Quality joints were obtained with rivet head neck dia. of 3 mm and anvil cavity depth of 0.55 mm. In addition to the formation of a perfect mechanical pin interlocking, braze welding was also formed by the diffusion of zinc from the mild steel coating to upper aluminum alloy sheet. Nishihara and Ito (2005) proposed traversing FSF for cladding S45C steel with AA 6061-T6 aluminum alloy. The process was executed with tool rotational speed of 705 rpm and with traversing speed of 150 mm/ min. The die temperature measurement during FSF showed that a maximum temperature up to 1013 K was recorded. Lazarevic et al. (2015) also reported that TD, TPD and anvil cavity depth have significant influence on joint strength and joint formation in FSF

process. It was revealed that the material extrudes orthogonal to the tool axis and circumferential deformation of the material occurs with rotation of the stir tool. The evolution of the FSF process using microstructure mapping of different stages was also performed. The existence of two different zones namely TMAZ and HAZ were revealed. The geometrical effects of anvil cavity design on the FSF joint formation was also studied. The force and torque measurement during tool plunge in FSF process showed that there is a decline in the force and torque during anvil cavity filling. The completion of anvil cavity filling could be accomplished by the increase in the force and torque values (Ogata and Miller, 2014). Tungsten-copper composite was fabricated by Ahuja et al. (2015) with traversing FSF process using pinless stir tool rotating at 1200 rpm and traverse speed of 100 mm/min. A three-dimensional thermo-mechanical finite element model of FSF process was also developed by Kruger et al. (2017). Accurate prediction of temperature distribution, stress distribution, joint geometry and flash formation were reported. FSF process was also employed for refilling the pin hole in FSSWed joints. Refilling of FSSW stir spot using FSF process was performed by Prakash and Muthukumaran (2011). Second stage refilling of FSSW stir spot fabricated on AA 6061-T6 sheets of 3 mm thickness was performed using a secondary stir tool and die setup. Refilling increased the nugget cross-sectional area and consequently, increased tensile shear strength and joint efficiency were recorded. In another work, refilling of FSSW stir spot using FSF process was also performed by Venukumar et al. (2014). Refilled FSSW joints on AA 6061-T6 sheets of 2 mm thickness possessed better fatigue strength than conventional FSSW joints.

The FSF process possesses similarities with FSSW process although discrete differences can be observed from the intrinsic features of the joint. Unlike FSSW, stirring in an FSF process plasticizes the upper and lower sheet metals other than the mixing of the stirred metal from the upper and lower sheets. Since the filling of the anvil cavity feature in FSF process requires low volume of plasticized metal, the tool indentation required is negligible as compared to the keyhole left by the pin tool in FSSW process. The use of a friction stir tool to obtain mechanical interlocking is an entirely modern concept. To summarize, FSF process differs from FSSW process in the following ways. For FSF process

- Stirring occurs only in the upper sheet metal and stir mixing of the upper and lower sheets is absent.
- A pinless stir tool is sufficient to execute the process

- Pin formation by extrusion of upper sheet requires a pre-drilled hole in the lower sheet

1.2.3 Aluminum alloys

Strict emission control norms, urge for competing fuel efficiency and environmental commitment push vehicle manufacturers to incline towards usage of lightweight sheet metals. Aluminum and magnesium alloys moves forward as alternative to traditional steel sheets in this scenario (Mehta et al., 2004). Interest in the usage of aluminium alloys for vehicle manufacture is steadily increasing due to their lightweight, reasonable strength, acceptable formability and corrosion resistance. More than 80% of the cars made in Europe are manufactured with aluminum. Appreciable mass reduction have been achieved by the use of sheets and press formed parts in aluminium alloys. Automotive manufacturers like *Porsche, Audi, Daimler-Benz, Volvo, Ford* employ deformable aluminium alloys for parts such as doors, radiators and wheel rims. In addition, Al-Mg-Si cast aluminum alloys are used in engine, transmission and suspension (Fridlyander et al., 2002). Replacement of the traditional welded steel variant with modular aluminium structures such as *Audi A8 space-frame* resulted in chassis part weight reduction by 25% and body part weight reduction by 50%. In addition, the body panels and body floor are also fabricated with aluminum. Other than in passenger cars, aluminium alloys can be used in special purpose vehicles such as tractors and haulers to raise the payload and minimise the maintenance cost. Furthermore, aluminium has wide general purpose applications such as body panels of laptops, mobile phones and in kitchen utensils and cabinets.

It is to be noted that aluminum merits over steel with 3X lesser density, better corrosion resistance and high degree of utilization, but the cost of aluminium alloys is 2X higher than that of steel (Jain et al., 2002). However, benefits in organizational, operational, manufacturing and design sectors mitigates the burden of high cost of aluminium alloys. Specifically in the manufacturing sector, recyclability, corrosion resistance and mass production of aluminium alloys can bring noticeable positive result over its higher cost (Das et al., 2007). Secondary requirements of sheet metals such as adhesive bondability, spot weldability and high quality paint finish are added advantages for aluminium alloys (Burger et al., 1995).

Non heat-treatable alloys such as Al-Mn 3XXX series and Al-Mg 5XXX series as well as heat-treatable alloys such as Al-Cu 2XXX series and Al-Mg-Si 6XXX series are preferentially suitable for automotive structural and skin applications. Out of which 5XXX and 6XXX aluminum alloys are commonly used in automotive industries (Burger et al., 1995). Table. 1.2 shows the utilization of 5XXX and 6XXX aluminium alloys in cars. 6XXX is costlier than 5XXX, but 6XXX provide better mechanical properties than 5XXX. The most cost effective approach for body-weight reduction is to use tailor-welded blanks of 5XXX and 6XXX aluminum alloys.

Table 1.2. Utilization of aluminum alloys in cars (Fridlyander et al., 2002)

Aluminum alloy		Purpose
5XXX	AA 5052 AA 5454 AA 5182	• Body parts (Internal) • Frame
6XXX	AA 6009 AA 6016 AA 6111 AA 6061	• Body parts (External body panels) • Frame • Radiator • Fuel tank

6XXX is preferentially used in external body panels due to the ability to harden with partial aging during the paint bake cycle and the absence of Chernov-Leuder lines, subsequently better aesthetic appearance can be obtained. Although less formable, 6XXX achieves high strength after paint bake cycle. 5XXX softens and loses some of its mechanical properties during the paint bake cycle. Rapid work-hardenability, softening and susceptibility to the formation of Chernov-Leuder lines limits its application to internal parts only (Burger et al., 1995, Das et al., 2014). From above discussion, a single aluminium alloy cannot suffice for both structural and skin applications simultaneously. Therefore, a combination of 5XXX and 6XXX aluminium alloys is a viable solution owing to their own specific metallurgical characteristics.

AA 5052-H32 and AA 6061-T6 sheet metals are considered for the present work. AA 5052-H32 is a non heat-treatable Mg based alloy for which grain size dictates the strength of the alloy. Good formability is attributed to high work-hardenability and negligible strain hardening rate (Burger et al., 1995). AA 6061-T6 is a Mg-Si based heat-treatable alloy with better age hardenability. The recrystallized grain structure and crystallographic texture obtained from solution heat treatment provides more or less isotropic mechanical properties. In addition, the strength of AA 6061-T6 alloy has little dependence on grain size (Burger et al., 1995).

Literature shows that AA 5052-H32 and AA 6061-T6 are the commonly used in automotive and aerospace industries. FSW of AA 6061 aluminum alloys, conducted by Das et al. (2014) revealed that the heat input during FSW has significant influence on ultimate tensile strength and fatigue behaviours. High strength 6061 offers better dent resistance. Ilangovan et al. (2015) reported that FSW of AA 6061−AA 5086 aluminum alloys showed defect free SZ with improved hardness. Higher grain boundary fraction and formation of brittle intermetallic phases improved the hardness at the weld zone. Hejazi and Mirsalehi (2016) utilized microhardness mapping to predict the microstructure and mechanical properties of AA 6061 FSWed sheets with mathematical equations. Two-dimensional contour of grain size and three-dimensional mapping of ultimate tensile strength and yield strength were plotted, which showed good agreement with experimental results. Double-sided FSW of AA 6061-T913 alloy was also conducted by Hejazi and Mirsalehi (2016b).

1.3 Significance of the work

It is clear that pinhole formation and hook defect impairs the strength of FSSWed joints. Sheet extrusion processes such as FSF eliminates pin hole formation and hook defect as well as enable joint formation by simultaneous mechanical interlocking and metallurgical bonding. Current literature provides only preliminary investigation on sheet extrusion processes. The potential of sheet extrusion processes can be explored through further research.

1.3.1 Advantages of sheet extrusion over other joining processes

- Joint strength is achieved through simultaneous mechanical interlocking and metallurgical bonding. Only a few processes, both conventional and alternative, are achieving this combined benefit.
- Through heating and forming of one sheet into a prefabricated hole/groove in the second sheet the brittle intermetallic formation could be effectively reduced.
- No need for cutting fluid and fillers, no chip generation and substantial energy input for melting can also be avoided, thereby promising eco-friendly fabrication.
- Does not require any consumables such as rivets, bolts, adhesives etc, thereby presenting excellent weight reduction and cost savings.

- Average lap-shear strength of sheet extrusion processes are higher than commonly used alternatives such as SPR and clinching.
- Ability to join dissimilar materials, like aluminum and automotive steel, which are hard to be joined by conventional joining processes.
- Availability and access to the processes and its inputs are cheap.
- Extensive know how of the related processes such as FSW and FSSW can be effectively used as fundamental information.

1.3.2 Need for further research on sheet extrusion

Extensive investigation on the performance and process parameters are required for thorough understanding of the sheet extrusion processes. Details related to sheet extrusion processes are scarce in literature. Therefore, this knowledge gap can be mitigated by comprehensive research. Only limited knowledge is available about the application of the process for joining homogenous materials like alloy variants of same metal and about metal to non-metal joining. Scope for process automation and new applications such as joining of sheet to structures also exist. These processes can also be further modified for better joining efficiency. In addition, there is scope for combining these processes with other joining processes such as adhesive bonding. Need for joints with multidirectional strength, under different loading conditions imposed by lap shear, cross-tension, peel-off, tensile and fatigue modes, are highly demanding.

In this research, out of various sheet extrusion processes, FSF is chosen as the primary process of interest due to following reasons.

- The comprehensive study on the characteristics and mechanical performance of the FSF joints is scarce in literature. It is essential to understand the effect of process parameters such as RPM, TPD, tool features such as TD and geometric features such as number of pre-drilled holes and HD on the joint quality characteristics of FSF joints. Therefore, a detailed study for finding the effect of critical parameters on FSF process is worth to be conducted.
- The process in initially developed for spot joining dissimilar metals such as aluminium to automotive steel. The viability of the process for fabricating joints in dissimilar alloys of same metal such as aluminum is to be explored because this will open the path for producing multi metal tailor-welded blanks of aluminum

alloys. Therefore, extending the process capability and versatility of FSF process provides ample scope for experimental investigation.

- Furthermore, the research can be extended for seeking modification of the FSF process for its capability enhancement and effectiveness.

Unlike other joining processes, in FSF, joining similar sheet metals is difficult than dissimilar sheet metal joining, since the lower sheet may also get plastically deformed by the time upper sheet attains enough temperature for forging. These challenges are also addressed in the present research.

1.4 Objective of the thesis

The main objective of the thesis is to experimentally investigate the joint strength and joint formation in FSF joints and its variant between dissimilar grade aluminum alloys namely AA 5052-H32 and AA 6061-T6 sheet.

Following sub-objectives are planned to accomplish the same

1. Understanding the influence of process parameters on the formation of FSF joints in dissimilar grade aluminum alloy sheets.
2. Understanding the mechanism of joint formation of FSF joints in dissimilar grade aluminum alloy sheets.
3. Understanding the influence of process parameters on the formation of DFSF joints in dissimilar grade aluminum alloy sheets.
4. Understanding the influence of geometric features on the formation of DFSF joints in dissimilar grade aluminum alloy sheets.

It should be noted that the DFSF process is a modified variant of FSF process, which has been evolved in the course of the present work. More details regarding DFSF process is discussed in subsequent chapters.

1.5 Organization of thesis

The thesis consists of nine chapters, which are organized as follows:

- Chapter 1 provides an introduction, literature review, significance and objective of the thesis

- Chapter 2 investigates the influence of RPM on the mechanical performance, joint macrostructure, hardness, joint morphology and failure modes of FSF joints in dissimilar grade aluminum alloys
- Chapter 3 investigates the influence of TPD on the mechanical performance, joint macrostructure, hardness, joint morphology and failure modes of FSF joints in dissimilar grade aluminum alloys
- Chapter 4 investigates the influence of TPD on the mechanical performance, joint macro/ microstructure, hardness, joint morphology and failure modes of DFSF joints in dissimilar grade aluminum alloys
- Chapter 5 investigates the influence of TD on the mechanical performance, joint macro/ microstructure, hardness, joint morphology and failure modes of DFSF joints in dissimilar grade aluminum alloys
- Chapter 6 investigates the influence of HD on the mechanical performance, joint macro/ microstructure, hardness, joint morphology and failure modes of DFSF joints in dissimilar grade aluminum alloys
- Chapter 7 investigates the influence of MH on the mechanical performance, joint macro/ microstructure, hardness, joint morphology and failure modes of DFSF joints in dissimilar grade aluminum alloys
- Chapter 8 presents some major insights about FSF and DFSF joints
- Chapter 9 presents the conclusions from the thesis work followed by scope of future work and references

Chapter 2

FSF joining of AA 5052-H32 and AA 6061-T6 sheets at varying tool rotational speeds

In this chapter, a comprehensive study on the effect of RPM on the joints formed by FSF process is presented with the help of mechanical performance tests. The joints fabricated with FSF process are characterized by examining the macrostructure, hardness distribution, joint morphology and failure modes.

2.1 Methodology

2.1.1 Principle

The complete process sequence of FSF process is schematically illustrated in Fig. 2.1. The upper sheet and lower sheet are arranged in lap configuration with a pre-drilled hole in the lower sheet (Stage 1). The principle behind FSF process involves a rotating stir tool heats the upper sheet to a plasticized condition by virtue of frictional contact, followed by forging and extruding the plasticized metal through the pre-drilled hole in the lower sheet into an anvil cavity during the tool plunge. The anvil block possesses a hemispherical cavity to realize the mechanical pin interlocking. The plunge of the rotating stir tool onto the surface of the upper sheet generates frictional heat, thereby reducing the flow strength of the upper sheet metal. The heated upper sheet metal is extruded through the pre-drilled hole provided in the lower sheet, which forms the neck of the pin. The deformed metal finally creates a mechanical pin interlock by acquiring the shape of the anvil cavity (Stage 2). Meanwhile, the interface of the two sheets also becomes metallurgically bonded under the frictional heat flux and plastic deformation. Retraction of the rotating tool at this stage completes the joining process (Stage 3). Thus, a lap joint formation started by stir heating is finished by the formation of simultaneous mechanical pin interlocking and metallurgical bonding. Here, the pin interlock acts like a mechanical rivet.

The anvil cavity feature determines the shape of the pinhead, while extruding the plasticized metal. The dia. of the head formed should be greater than the dia. of the pre-drilled hole to ensure proper mechanical interlock. If the dia. of the head is nearly equal to that of the pre-drilled hole, the head formed can be easily pulled out through the hole

resulting in a weak mechanical interlocking. If the anvil cavity size is increased to form a large pinhead, chances are there for the lower sheet to collapse into the anvil cavity while forging. A proper design of stir tool is such that it should generate sufficient and required frictional heat to plasticize the upper sheet metal to facilitate its easier flow into the anvil cavity through the pre-drilled hole. The formation of neck and pinhead, which determine the joint strength is solely dependent on the work piece material, stir tool, anvil cavity design and the process parameters like RPM and TPD. In addition, there is a provision for producing single pin and multi pin configurations.

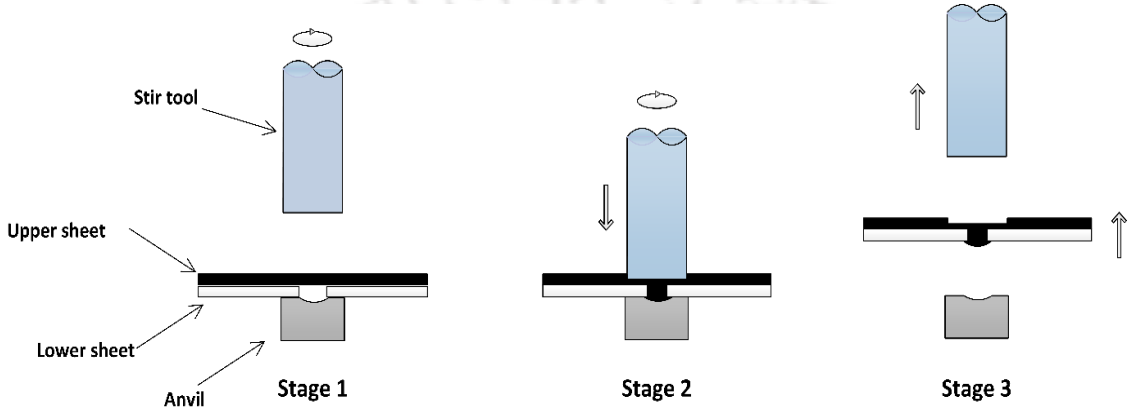

Figure 2.1. Stages of friction stir forming (Not to scale)

2.1.2 FSF experiments

The FSF sample preparation is carried out on an indigenous fixture set up fabricated and mounted on a milling machine (Kirloskar Viking KTM 40) having a wide tool rotational speed range from 45 to 3500 rpm. The basic elements of the experimental set up such as friction stir tool, fixture, anvil and clamps are shown in Fig. 2.2. The custom-made mild steel fixture set up is capable of clamping samples of various dimensions for the mechanical performance tests. The fixture has a provision for holding square blocks of anvil at its diagonal center. The top surface of anvil was machined with a hemispherical cavity by spark EDM process. The details about anvil and stir tool are given in Table 2.1. The anvil cavity size and the stir tool dimensions are selected based on preliminary experimental trials (Lazarevic et al., 2013).

AA 5052-H32 and AA 6061-T6 sheets, each of 2 mm in thickness are used for the experiments. AA 5052-H32 possesses lower tensile yield strength, strength coefficient and hardness than that of AA 6061-T6. Therefore, AA 5052-H32, which is chosen as upper sheet is stir-heated and form joined into the lower sheet, AA 6061-T6. The chemical

composition, determined through EDX analysis (Zeiss Sigma 002−B field emission scanning electron microscope) and the mechanical properties of these alloys obtained through standard procedures are given in Table 2.2 and Table 2.3, respectively. The tensile test is carried out as per ASTM E8 standard (2009) and the plastic strain ratio is evaluated as per ASTM E517 standard (2016). The hardness measurement and grain size measurement were conducted as per ASTM E92 standard (2016) and ASTM E112 standard (2013).

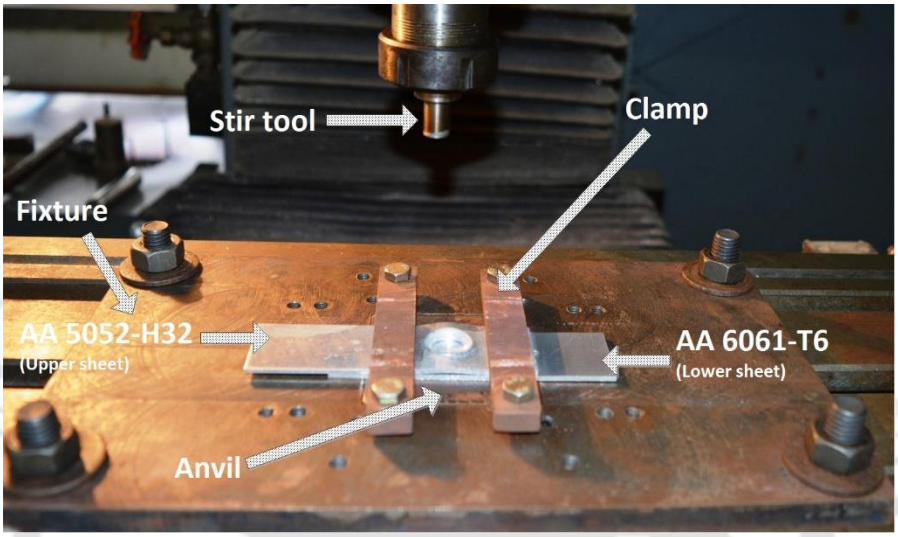

Figure 2.2. FSF experimental set up

Table 2.1. Details of the anvil and FSF tool

Anvil	Material	Mild steel
	Feature	Hemispherical cavity on top surface center
	Cavity dia.	3.5 mm
	Cavity depth	0.55 mm
Tool	Material	H13 tool steel
	Feature	Pinless
	Shoulder dia.	14 mm
	Shoulder length	25 mm

A hole of 3 mm dia. was pre-drilled onto the lower AA 6061 sheet at the desired spot, where the joint is intended. The proper alignment of stir tool center, pre-drilled hole center on lower sheet, and anvil cavity center along a straight line is important for the formation of a sound FSF joint. The axis of an FSF joint lies perpendicular to the plane of the sheets and passes through the center of the stir spot.

The joints are prepared by varying the tool rotational speed from 500 to 3000 rpm at increments of 500 to obtain the effect of tool rotational speed on the mechanical performance and the formation of FSF joints. FSF samples fabricated at lower (500, 1000),

medium (1500, 2000), and higher (2500, 3000) RPMs are subjected to various mechanical tests and joint cross-sectional studies.

Throughout the experiments, the plunge rate, plunge depth, and direction of tool rotation are kept constant at 0.002 mm/s, 1.5 mm and clockwise direction respectively. Dwell time is not employed. Two samples are fabricated per level for all the tests and the average output value is considered. RPM levels are chosen based on experimental trials to ensure that the deformation in the lower sheet is minimum.

Table 2.2. Chemical composition of the parent metals (in % wt.)

Materials	Si	Fe	Cu	Mn	Mg	Cr	Zn	Ti	Al
AA 5052-H32	≤ 0.2	0.1- 0.3	≤ 0.2	0.1-0.2	2.8-4.2	0.2-0.3	≤ 0.3	-	Remaining
AA 6061-T6	0.6-0.9	0.2-0.4	0.2-0.3	≤ 0.1	1.4-1.8	0.1-0.4	≤ 0.2	≤ 0.15	Remaining

Table 2.3. Mechanical properties of the parent metals (along 0º RD)

Mechanical properties	AA 5052-H32	AA 6061-T6
Tensile yield strength (MPa)	155.39±2	225.45±13
Ultimate tensile strength (MPa)	212.705±2	308.40±5
Total elongation (%)	14.82±1	21.44±7
Vickers Micro hardness (HV)	77.4±9	99.8±6
Strain hardening exponent, *n*	0.161±0.002	0.15±0.003
Strength coefficient, *K* (MPa)	355.63±6	489.78±8
Plastic strain ratio, *R*	0.589	0.707
Average grain dia. (μm)	22.5	11.2

2.1.3 Mechanical performance tests

Mechanical performance tests are conducted to evaluate the joint fracture load of the FSF samples under various loading conditions. These tests are carried out on a 100 kN Instron-Dynamic Universal Testing Machine (Model: 8801J4051) for which the extension rate is kept constant at 1 mm/min. The fracture load and extension at fracture of FSF joints are evaluated through lap shear test, cross-tension test and peel test. The formability of the joint is evaluated through uniaxial tensile test. The sample dimensions, prepared as per AWS D8.9M standard (2012), are shown in Fig. 2.3. The metal strips for lap shear test, cross-tension test, peel test and uniaxial tensile test are shear cut from large sheets such that the sheet RD is oriented along the length of the samples.

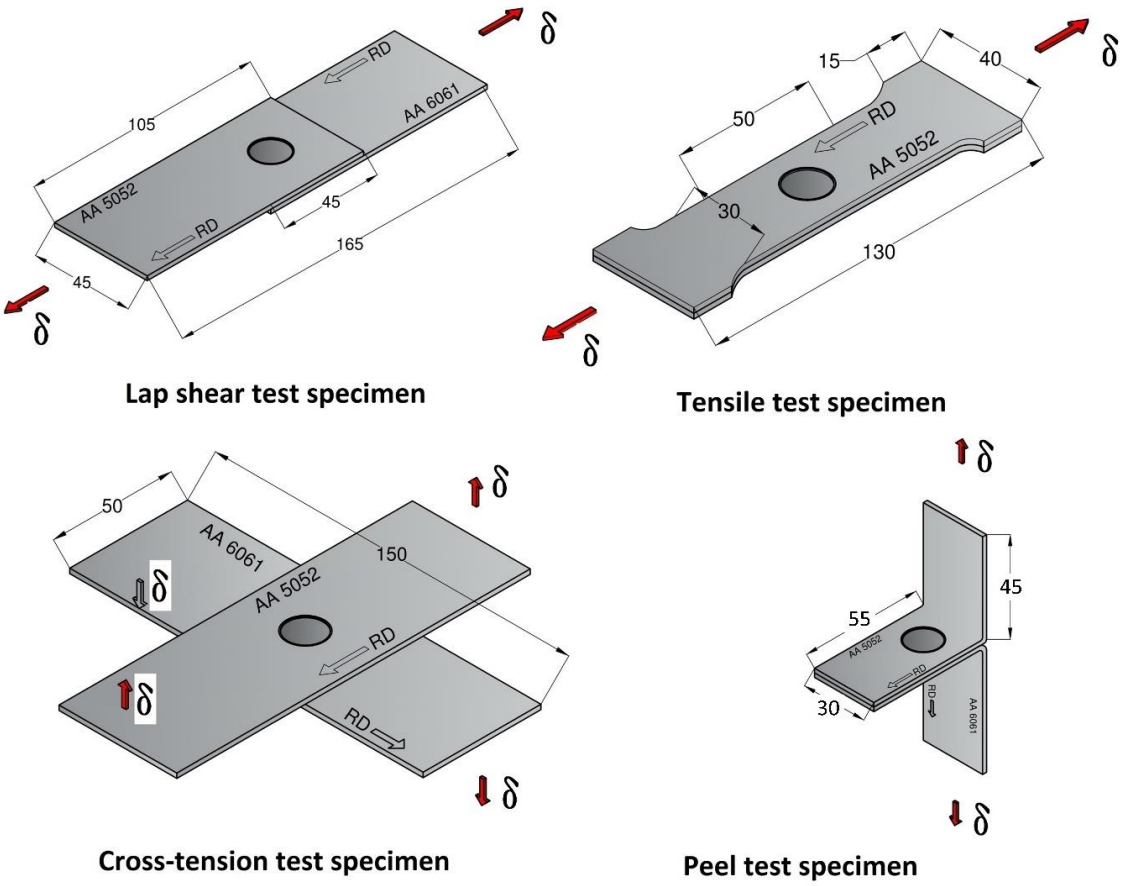

Figure 2.3. Dimensions of the test samples for various mechanical tests (All dimensions are in mm, Not to scale)

Lap shear test is commonly used for evaluating the shear fracture load of a lap joint where tensile load is applied perpendicular to the axis of the FSF joint. Samples are loaded in the grippers of Instron machine with doublers at the grippers in such a way that the tensile load is applied parallel to its length direction. It is ensured that all lap shear samples failed at the joint location only. The overlapped area for lap shear samples is 45X45 mm^2.

Cross-tension test is commonly used for evaluating the fracture load of a lap joint, in which tensile load is applied parallel to the axis of the joint. The upper and lower sheets were aligned to a cross overlapping at the mid-section and joined at its center by FSF process. The samples are loaded in the grippers of Instron machine using custom-made fixtures. The overlapped area for cross-tension samples is 50X50 mm^2.

Peel test is mainly intended to determine the joint fracture load when the sample is subjected to peeling off operation by pulling the two sheets apart by applying tensile load. The resistance against peeling off fracture is evaluated. The upper and lower sheets were aligned to full overlap and joined at its center by FSF process. The ends of the samples are later bent manually, without affecting the joint, to create space for clamping in the grippers

of the testing machine. The samples were loaded in the grippers of Instron machine in such a way that the tensile load is applied parallel to the joint axis.

The above tests are intended to determine the fracture load of the FSF joint under various loading conditions. Depending upon the nature of loading, samples may show multiple strength during each of the mechanical performance tests. Uniaxial tensile test is conducted to evaluate the formability of FSF joints. A tensile specimen with FSF joint at the center of the gauge region is subjected to tensile loading. Unlike above-mentioned strength tests, where the sheet transfers the load to the FSF joint location, in tensile test, the load is simultaneously shared between the FSF joint and the adjoining sheets of the gauge length region, which enables formability of the FSF joint along with extension of the sheets under uniaxial tensile load. The upper sheet (AA 5052-H32) and lower sheet (AA 6061-T6) are initially wire cut to tensile specimens. The cut specimens are overlapped to a single sample and joined at its center by FSF process. The test specimens are aligned with the center line of the grippers of the testing machine to ensure that only axial tensile stress is developed within the gauge length, without any bending stresses.

In all the mechanical performance tests, the load-progression data, fracture load, extension at fracture are recorded. The failure modes are also observed and analyzed.

2.1.4 Macrostructure, hardness measurement and joint morphology analyses

Macrostructure analysis is conducted to identify the various zones present in the joint, the joint evolution, the effectiveness of joint formation, the metal flow pattern, defect formation and the critical weak zones in the joint. Sample preparation for macrostructure analysis is done as per ASTM E407−07 standard (2017). The FSF joints are sectioned perpendicular to the length of the sample to reveal the joint cross-section. The cross-section is initially rough finished with emery paper having grit size ranging up to 2000 and fine finish is obtained by polishing with a velvet cloth treated with isopropyl alcohol based polishing liquid. The polished samples are mild etched with Kellers reagent (190 ml distilled water, 5 mL HNO_3, 3 mL HCl, 2 mL HF) for 20s. Macroscopic images are obtained at 50X magnification using Zeiss Axiocam MR3 microscope (enabled with Axiovision software).

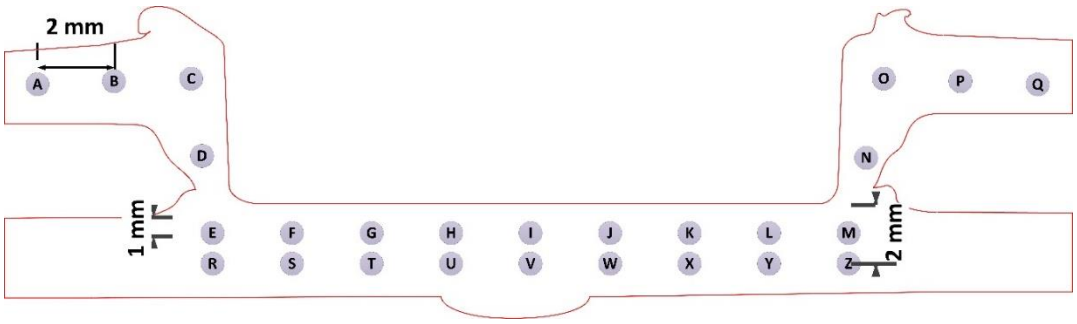

Figure 2.4. Location of hardness measurements along the joint cross-section

Hardness measurement on FSF samples are performed with Vickers indentation method using 500 gf load for 10 s in Buehler MMT3-B Micro Vickers Hardness Tester. Hardness values are taken along the finely polished cross-section of the FSF joints using pyramidal shaped indenter. The location of hardness measurements (A-Q and R-Z) is shown in Fig. 2.4. Array of indentations with 2 mm spacing in between are performed along the joint cross-sections starting from the upper AA5052-H32 strip at one end, through the bonded region up to the other end at a depth of 1 mm from the upper surface (A-Q). Further, at the bonded region one more array of indentation is taken at a 2 mm depth from the upper surface (R-Z) in order to estimate the variation in hardness along the depth of the stir spot.

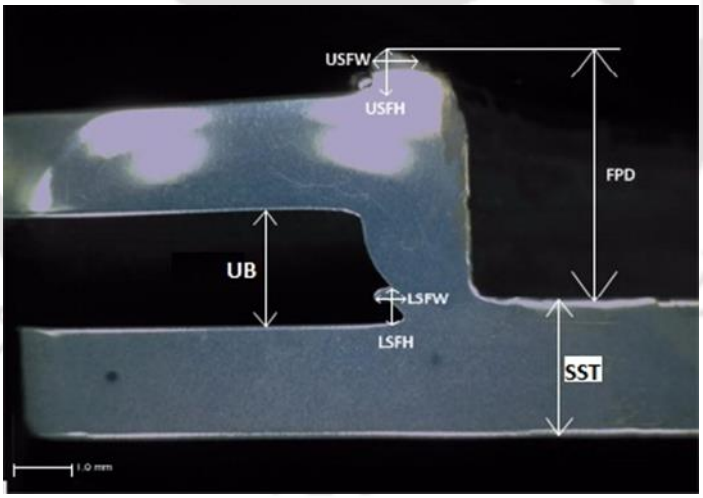

Figure 2.5. Morphological features of the FSF joint cross-section (UB, LSFW, LSFH, USFW, USFH, SST, FPD)

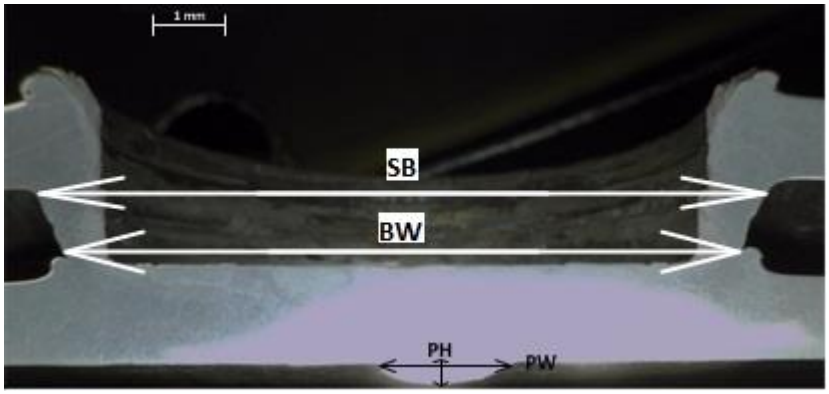

Figure 2.6. Morphological features of the FSF joint cross-section (PW, PH, BW, SB)

Quantifiable information regarding the quality of joint formation is obtained through joint morphology analysis. It involves the quantification of certain external macroscopic joint features and studying the influence of the primary variable such as RPM on its formation. Macro defects can affect the aesthetic appearance of the joint as well as joint features like mechanical pin interlock. Measurable features include macro defects such as USFW, USFH, LSFW, LSFH, UB, SB, FPD, SST and other intrinsic FSF joint features like PW and PH and BW. BW affects the joint strength. The joint features are represented over a typical FSF joint cross-section in Figs. 2.5 and 2.6. The above-mentioned geometrical features are measured using a USB digital microscope (Dinolite Dino Capture 2) at 20X to 30X magnifications.

2.2 Results and discussion

In this section, the effect of RPM on the fracture load obtained through four different mechanical performance tests, evolution of macrostructure, joint morphology and modes of failure are analyzed. Instead of measuring fracture strength, the fracture load is used for comparison (Garg and Bhattacharya, 2017c, Lazarevic et al., 2013) because the exact measurement of bonded area for the samples subjected to mechanical performance tests is impossible, unless the same sample has to be cut along the center for geometric measurement. Since mechanical performance tests are destructive tests, in which the samples are loaded up to failure, calculating the effective bonded area from the damaged sample is ineffective. Nevertheless, distinguishing the bonded and partially bonded region requires microscopic measurements, which is cumbersome.

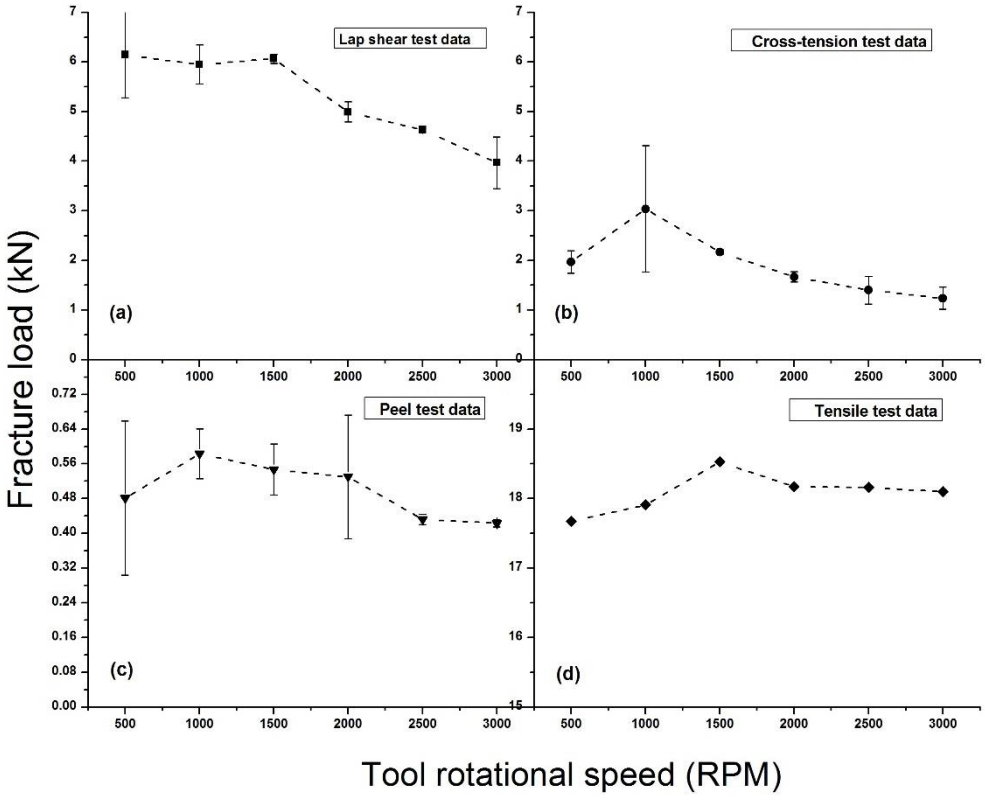

Figure 2.7. Comparison of fracture loads at various RPMs during mechanical tests

2.2.1 Performance during lap shear tests

The average fracture load for lap shear samples is plotted against the RPM in Fig. 2.7a. The fracture load from 500 to 1500 rpms remains almost same at about 6 kN, and it decreases from 1500 to 3000 rpms. A 35% decrease in fracture load is observed when the tool rotational speed is increased from 500 to 3000 rpm. It is found that FSF samples exhibit better lap shear fracture load at lower and medium RPMs. FSF samples at higher RPM exhibits lower lap shear fracture load.

2.2.2 Performance during cross-tension test

The effect of RPM on the fracture load during cross-tension test is shown in Fig. 2.7b. The cross-tension fracture load increases from 500 to 1000 rpm followed by decrease in fracture load up to a minimum at 3000 rpm. A 59% decrease in the cross-tension fracture load is observed when tool rotational speed is increased from 1000 to 3000 rpm.

Similar to lap shear test results, cross-tension samples at high RPMs show lower strength. The main reason for the variation in strength is the influence of frictional heat generation and associated plastic deformation at various RPMs. The extreme heat generation in FSF joints at high rotational speeds like 3000 rpm has created a negative

impact on the joint fracture load. More details are discussed with macrostructure analysis in section 2.2.5.

2.2.3 Performance during peel test

The fracture load for peel test samples is plotted with respect to RPMs in Fig. 2.7c. The peel-off load increases from 500 to 1000 rpm, and then it decreases from 1000 to 3000 rpm. About 27% decrease in the peel fracture load is observed, when the tool rotational speed increases from 1000 to 3000 rpm. However, the variation in peel-off load is within 1 kN, which is insignificant. FSF sample for higher RPM exhibits lower peel fracture load.

FSF samples show appreciable extensibility during lap shear test and cross-tension test of about 0.91 mm and 9.85 mm, respectively. Some of the cross-tension samples show considerable extension because of the peculiar nature of the cross-tension test, where the sample strips undergo bending before the tensile load gets concentrated on the spot joint. Similar to cross-tension test, some of the peel test samples also show higher extensibility, averages about 4.27 mm, due to bending effect of the strip during the peel test.

It is to be noted that for a sample joined at any particular RPM, the fracture load is observed to be highest for lap shear sample, lowest for peel test sample and intermediate for cross-tension sample. In general, it can be concluded that average fracture load during the above tests are found to be better for FSF samples fabricated at lower and medium RPMs. Therefore, lower and medium RPMs are the best choices for fabricating FSF joints between dissimilar grades of aluminum alloys namely AA 5052-H32 and AA 6061-T6 used in the present work.

As mentioned in section 1.2.1.1.1, literature shows that the RPM has similar effect on FSSW process as well, in which weld strength decreased with increase in RPM (Liu et al., 2013, Arul et al., 2008b, H.M. Rao et al., 2015).Therefore, RPM has similar effect on the joint strength in most of the friction stir-based spot joining processes like FSSW and FSF.

Joining of AA 5052-H32 to AA 6061-T6 with FSW and FSSW were already attempted. Table 2.4 shows a comparison of fracture load of these joints with FSF joints of the present work. It is observed that FSF joints possess superior strength over FSW and FSSW joints.

Table 2.4. Comparison of the fracture load of FSF with other joining technologies

Joining technique	Joint form	Test type	Average fracture load	Reference
FSW	Butt joint	Tensile test	5.75 kN* (230 MPa)	(Kumbhar and Bhanumurthy, 2012)
FSW	Butt joint	Tensile test	4.85 kN (180 MPa)	(RajKumar et al., 2014)
FSW	Butt joint	Tensile test	5.93 kN* (237 MPa)	(Park et al., 2010)
FSSW	Lap joint	Lap shear test	4.85 kN	(Jeon et al., 2012)
FSF	Lap joint	Lap shear test	6.14 kN	Present work

* Average fracture load is calculated from average ultimate tensile strength

2.2.4 Performance during tensile test

The effect of RPM on the ultimate load (formability) during tensile test is shown in Fig. 2.7d. The ultimate load remains almost same about 18 kN from 500 to 3000 rpms. Thus, samples joined with FSF process show better formability throughout the RPM range. The average extensibility of tensile samples is 5.48 mm. Literature shows that the formability of FSWed AA 6061-T6 sheets evaluated through limiting dome height tests possessed better formability than unwelded sheets (Ramulu et al., 2013). Tensile test results showed that strength and ductility of AA 5052 sheets joined through friction stir vibration welding is greater than that of corresponding FSW samples (Rahmi and Abbasi, 2016). Therefore, friction stir based joining techniques have the potential to improve the formability of the joining sheets.

2.2.5 Joint macrostructure analysis and its relation with the mechanical performance tests

FSF samples fabricated at lower, medium and higher tool rotational speeds namely 500, 1500 and 3000 rpms respectively, are selected for macrostructure analysis. The complete macrostructure of the joint cross-section, with schematic representation of various zones are shown in Fig. 2.8a-c. In Fig. 2.8a,b, at 500 and 1500 rpms, plastically deformed metal from the upper sheet filled the pre-drilled hole of the lower sheet and further reached the anvil cavity to form a mechanical interlock. Therefore, the approximate pin formation has contributed considerably to the improvement of fracture load of these samples. From Fig. 2.8c, it is observed that at 3000 rpm, because of the excessive

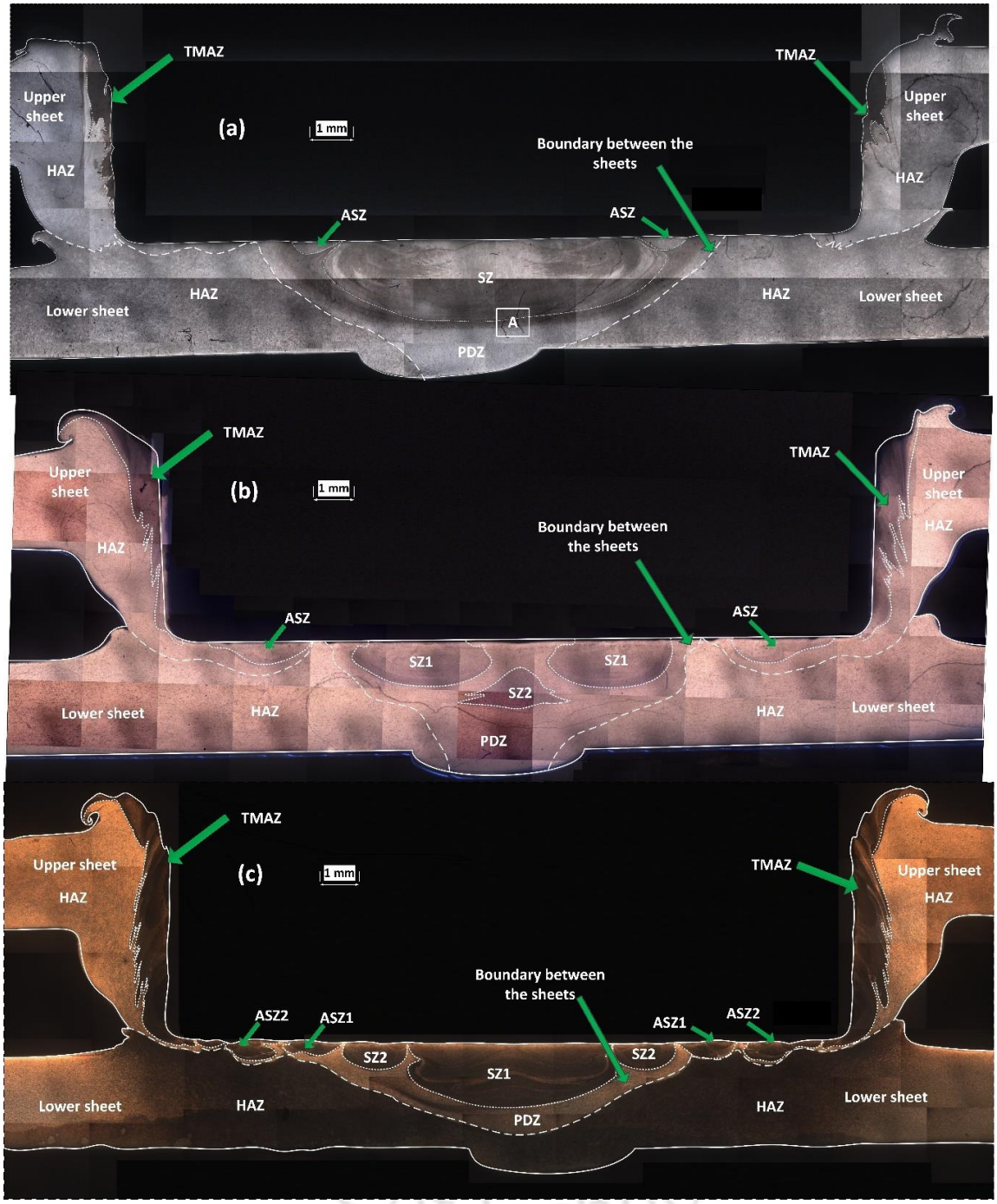

Figure 2.8. Joint macrostructure of FSF samples fabricated at (a) 500 rpm, (b) 1500 rpm and (c) 3000 rpm

deformation of the lower sheet due to extreme frictional heat generation, the anvil cavity is completely filled by the deformed lower sheet metal. Therefore, the plasticized metal from the upper sheet failed to reach the anvil cavity. The pre-drilled hole has undergone closure before the downward metal flow from upper sheet reaches the anvil cavity. Thus, the extreme heat generation at 3000 rpm results in the damage of the pre-drilled hole on the lower sheet and impaired joint formation. This is the reason for poor joint strength of FSF samples fabricated at high RPMs in the mechanical performance tests.

It is observed that in the present work, the heat generation increases with increase in RPM, which further affects the joint formation. The increase in temperature with increase in RPM also deteriorates the strength of other friction stir-based spot joining processes like FSSW. As mentioned in section 1.2.1.1.1, the heat input and processing temperature during FSSW can be controlled by decreasing the RPM and dwell time (Lakshminarayanan et al., 2015, Arul et al., 2008b, Awang and Mucino, 2010, Bozzi et al., 2010).

The influence of RPM on the joint macro features is discussed here. The various zones that can be identified in FSF joints are SZ, PDZ, TMAZ, ASZ and HAZ. Perfect metallurgical bonding is observed at all RPMs. Therefore, no interfacial gaps are visible in the joint cross-section.

At the center of the tool impression where the face of the tool touches the upper sheet, a unique pattern is produced by the stirring of the upper sheet metal. This represents the SZ, which is confined to the upper sheet only. SZ act as the main source of frictional heat generation in the joint spot. It is reported that in FSW, the material mixing patterns and subsequent joint strength are quite different for same material combination, depending upon the position of the stronger base material relative to the advancing side (Park et al., 2010). However, no such issues are there in FSF, since it is free from stir mixing of upper and lower sheet materials.

The ‘onion ring’ pattern commonly seen in FSW and FSSW SZs is clearly observed in FSF joints also (Fig. 2.9d). The SZ is symmetrically distributed about the center of the joint and possesses a shallow ‘U’ shape with maximum depth at the center. This shows that direction of flow and the amount of plastic deformation under the tool varies from center to the periphery of the joint. The width of SZ increases and partitions within the SZ are formed with increase in the RPM as seen from the macroscopic images (Fig. 2.8b,c). At 500 rpm, SZ is unique and no partitions in SZ are visible. At 1500 rpm, SZ is localized and clear separation between the SZs is visible. At this RPM, two distinct SZs, SZ1 and SZ2 are visible. SZ1 is visible near the upper sheet surface and SZ2 is visible just below SZ1, at the center, fully enclosed. At 3000 rpm, localized SZs are distributed over the joint cross-section.

RajKumar et al. (2014) reported that cylindrical threaded pin rendered excellent bondage due to effective stirring and mixing, during FSW of AA5052-AA 6061 aluminum alloys for which a tensile strength of 4.85 kN was obtained. The FSF joints in the present work, on the same material combination, shows a lap shear strength of 6.14 kN wherein

stir mixing of upper and lower sheets is absent. Therefore, stir mixing seen in FSW and FSSW is not only the primary factor for contributing excellent strength in aluminum alloys but also factors like metallurgical bonding and mechanical interlocking as seen in FSF play significant roles.

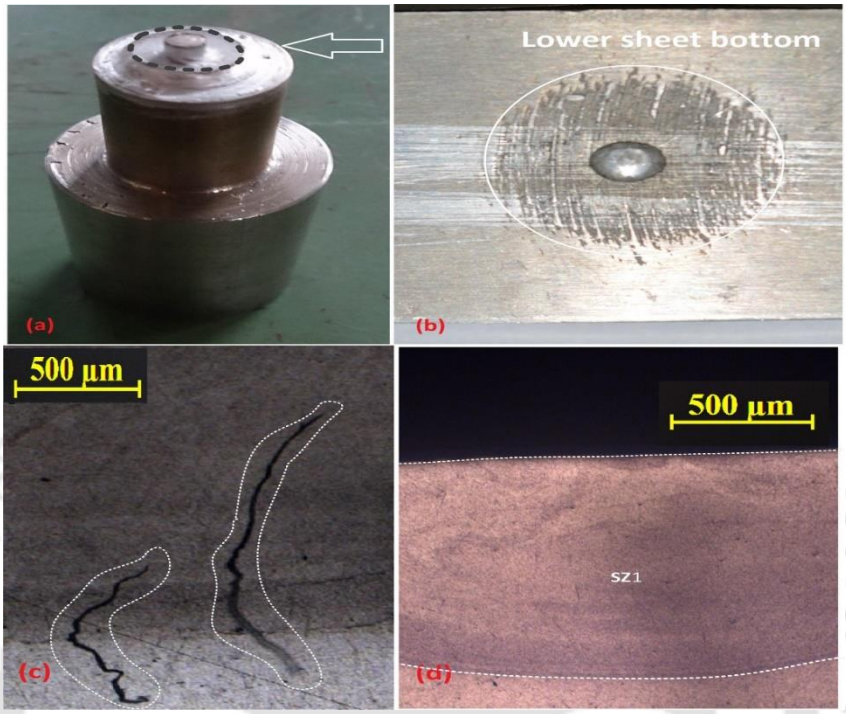

Figure 2.9. (a) Stirred upper sheet metal adhered to FSF tool face, (b) Surface roughness, (c) Cracks over the sample cross-section at location A in Fig. 2.8(a), (d) 'Onion' like pattern on the SZ1 in Fig. 2.8(b)

The PDZ is located just below the SZ, where the stirring of the plasticized upper sheet metal is absent. Here, the metal is forged, and metal flow occurs radially inward into the anvil cavity through the pre-drilled hole due to compressive pressure generated by the downward movement of the stir tool.

The schematic representation of metal flow directions over the joint cross-section of 500, 1500, and 3000 rpm FSF samples is shown in Fig. 2.10a-c. It can be observed that since the stir tool is pinless, the SZ metal just beneath the center point of the stir tool never undergoes stirring due to the zero torque; instead, it flows downward during the tool plunge. The downward flow not only enhances the pin formation but also affects the deformation of the heated lower sheet. The downward flow is prominent only at lower and medium RPMs like 500 and 1500, but absent at 3000 rpm due to closure of the pre-drilled hole.

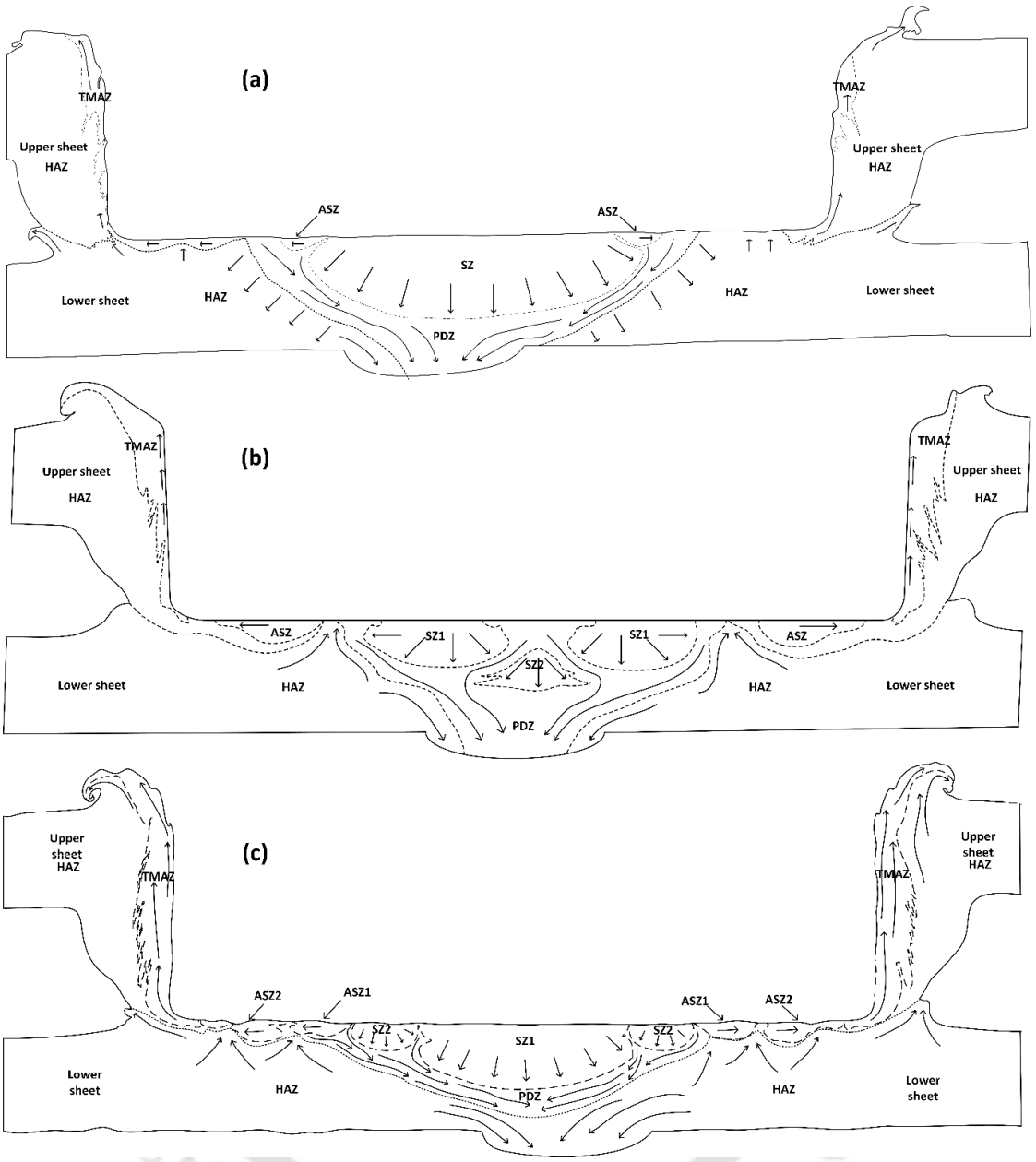

Figure 2.10. Schematic representations of the FSF joint cross-section at (a) 500 rpm, (b) 1500 rpm and (c) 3000 rpm with metal flow directions indicated

The TMAZ is visible on the sidewalls of the stir spot (Fig. 2.8). The frictional contact of lateral surface of the stir tool over the sidewalls of the stir spot also results in the formation of another TMAZ. The width of the TMAZ increases with increase in the RPM (Fig. 2.8a-c). At medium and higher RPMs, the TMAZ generated on the sidewalls of the joint become prominent, which is a consequence of increased frictional heat generation and plastic deformation (Fig. 2.8b,c).

The ASZ is a feature exclusively observed in the macrostructure of FSF joint cross-sections at medium and higher RPMs. These are ring-shaped SZs surrounding the main SZ. These are completely isolated from central SZ and are visible as symmetrical SZ

islands located on both sides of the central SZ in the joint cross-section. The main reasons for the formation of ASZs are the outward radial flow of hot plasticized upper sheet metal due to the downward tool plunge force and the upward deformation of the lower sheet under the influence of heat flux from the SZ. The outward radial flow of the upper sheet metal due to high tool plunge force increases the width of the SZ, which is affected by the upward deformation of the lower sheet. This promotes the separation of a part of the main SZ in the form of ASZ. The ASZ visible at 500 rpm is small-sized and found attached to the central SZ. At 1500 rpm, ASZ is completely isolated from the central SZ, and at 3000 rpm numerous ASZs are visible. Meanwhile, the inward radial flow of the hot plasticized metal promotes the pin formation and increases the depth of SZ.

The region surrounding the above-mentioned zones and the lower sheet together constitutes the HAZ. These regions are not subjected to severe plastic deformation, however frictional heat flux has brought about change in mechanical properties and hardness in the HAZ.

The macrostructure analysis shows that at high RPMs, exact rivet-like pin formation from the upper sheet stirred metal is not practical. Further, the heat flux from the plasticized upper sheet accelerated the deformation of the lower sheet. In addition, the closure of the pre-drilled hole hindered the smooth extrusion of plasticized metal from the upper sheet at higher RPM; thereby mechanical pin interlocking is poorly developed. FSF joint formation is complete only when there is mechanical pin interlocking and metallurgical bonding. At high RPMs, only metallurgical bonding has been generated, but mechanical interlocking is missing. Thus, it can be inferred that high tool rotational speeds like 3000 rpm are not favorable for fabricating FSF joints in similar metal combinations. However, the joints made at 3000 rpm also possess a sound joint appearance even though the required forging of plasticized upper sheet metal through the pre-drilled hole in the lower sheet is absent.

FSF joining trials at 500 rpm failed at certain attempts due to upper sheet failure like sticking of plasticized stirred metal on the face of the pin-less tool as shown in Fig. 2.9a. This is due to higher sticking friction at the tool-upper sheet interface at lower RPMs. Excessive tool vibration was observed for FSF samples fabricated at 3000 rpm. This may be attributed to the slippage at the tool-upper sheet interface at higher RPMs. These vibrations might have influenced the damage of the pre-drilled hole and the poor mechanical performance of FSF joints at high RPMs. No cracks are visible at the outer surface of the upper sheet metal extruded into the anvil cavity in the FSF joints fabricated

during the present work despite such observations were reported, while FSF joints were fabricated between AISI 6014 aluminum alloy and GMW2 mild steel (Ogata and Miller, 2014).

2.2.6 Hardness variation

Fig. 2.11 shows the hardness variation along the upper array (locations A to Q in Fig. 2.4) over the cross-section of the FSF samples fabricated at lower (500 rpm), medium (1500 rpm), and higher (3000 rpm) tool rotational speeds. The hardness of the FSF joint, specifically the upper sheet and lower sheet, is found to be lesser than that of the parent metals. The inverted 'W'-shaped hardness profile typical for a pin tool friction stir process is also observed in all FSF joints for the upper sheet.

Highest hardness is observed at the boundary of the SZ (locations G and K), where the upward deformation of the lower sheet is observed. For all FSF samples, SZ possesses lower hardness and a decrease in the hardness is observed towards SZ center (location I). This asserts the fact that the center of the pinless tool induces downward plunging of the plasticized metal, anvil cavity filling and subsequently enhances the formation of softer region at the center of the SZ. An increase in torque in the radial direction of the pinless tool induces considerable stirring and subsequent formation of stronger region towards the SZ periphery (locations H and J). The lower sheet metal which surrounds the SZ also enhances the SZ hardness.

Beyond the SZ, hardness values decrease towards the outer periphery of the cross-section of FSF samples (locations F to A and L to Q). A decrease in the hardness of about 25 HV than the parent metal hardness is observed at the HAZ of the upper sheet. This shows that considerable heat flux conducted from the SZ has induced some heating effect on the surrounding region of the FSF joint.

It is observed that hardness of the SZ center decreases with increase in the RPM. Maximum and minimum hardness at the SZ center is observed for samples fabricated at 500 rpm and 3000 rpm, respectively. With increase in the RPM, the hardness variation between locations G and H, J and K increases. Maximum variation in the hardness is observed for FSF sample fabricated at 3000 rpm and minimum for FSF sample at 500 rpm. This shows that increase in the RPM has induced considerable stirring and subsequent formation of harder regions at the periphery of the SZ.

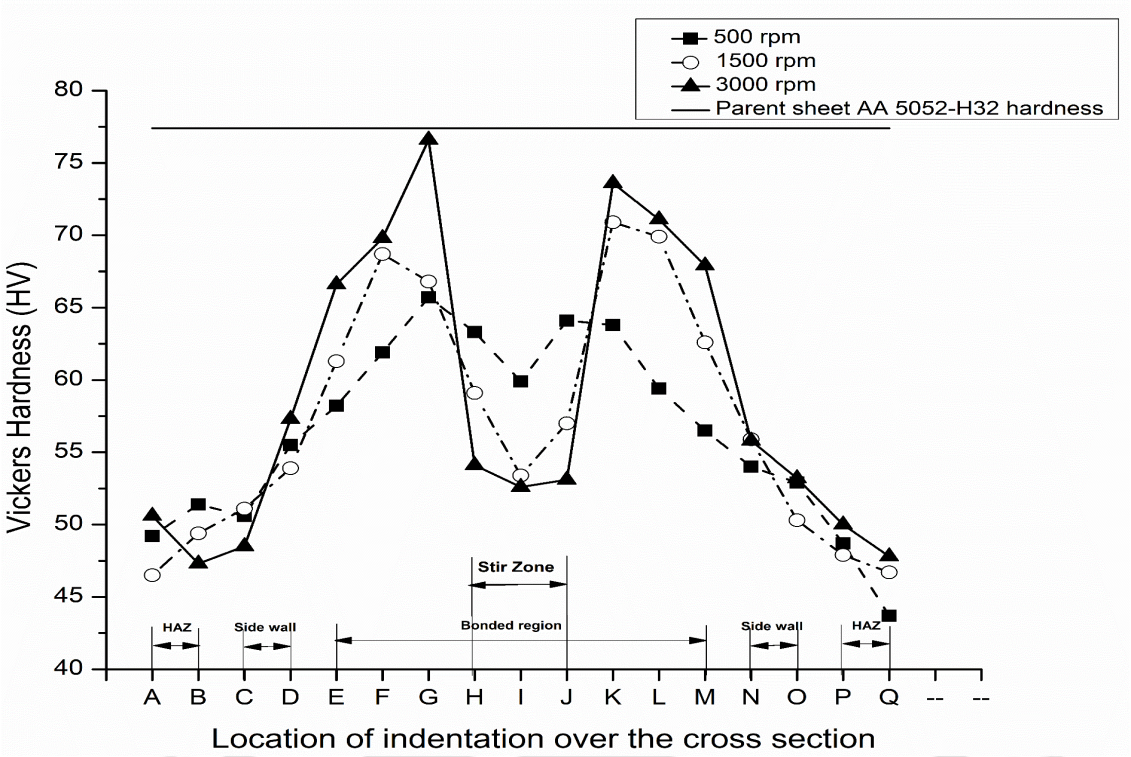

Figure 2.11. Comparison of hardness variation along the joint cross-section fabricated at various RPMs (Typical hardness variation at each measurement location is ±2.56)

The comparison of the hardness over the depth of the cross-section (locations E to M and R to Z of Fig. 2.4) of FSF sample fabricated at 1500 rpm is shown in Fig. 2.12. An inverted 'W'- shaped hardness profile is also observed along the lower array of indentation. The hardness measurements are coinciding at locations over the extruded pin namely I and V. Lower array of indentation possesses hardness values greater than or equal to that of upper array of indentation. Increase in the hardness over the depth of cross-section is also contributed by the compressive deformation of lower sheet under the extreme tool plunge force, though the variation is insignificant.

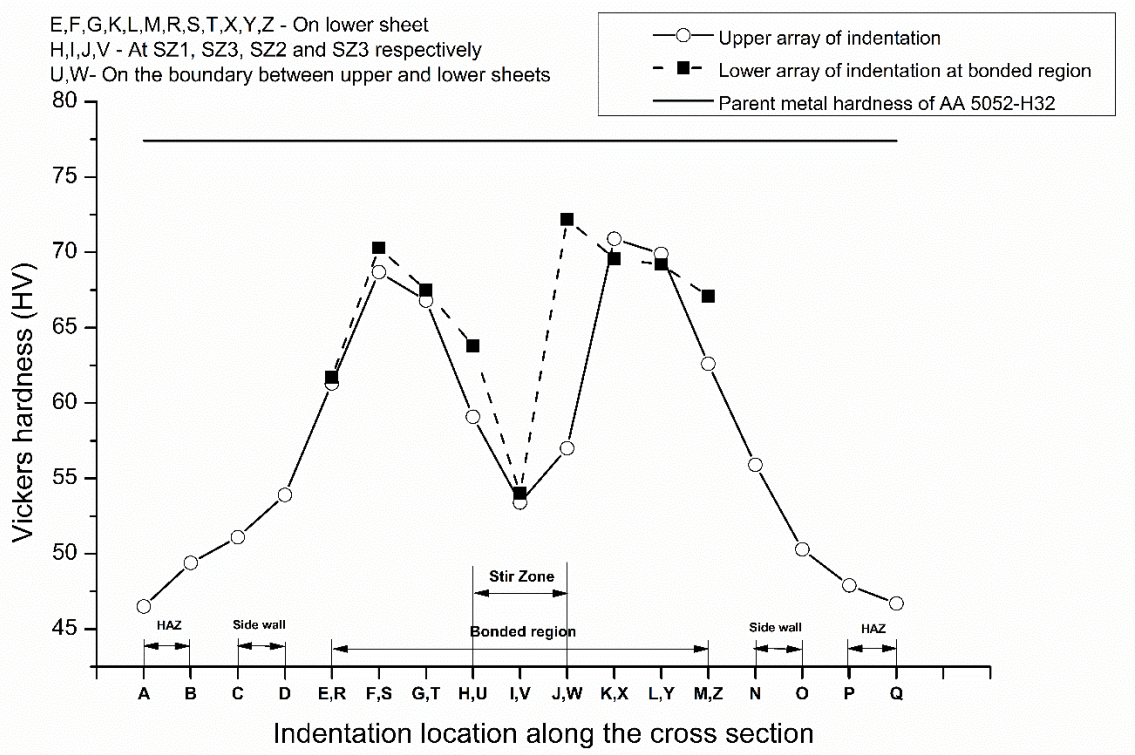

Figure 2.12. Hardness variation along the depth of the joint cross-section of FSF sample fabricated at 1500 rpm (Typical hardness variation at each measurement location is ±2.1)

2.2.7 Joint morphology analysis

The comparison of morphological features (refer to Figs. 2.5 and Fig. 2.6) in the FSF joint cross-section is shown in Table 2.5. It is observed that PW, PH and BW which determine the joint strength, remain almost same for FSF joints when tool rotational speed is varied from 500 rpm to 3000 rpm. Stable PW and PH ensures that the anvil cavity filling during pin formation is complete irrespective of the variation in RPM. This shows that RPM does not have any influence on those external geometric features influencing the strength of the joint.

UB is a distortion defect seen in FSF joints due to the constraining effect of fixture clamps that restrict the expansion of upper sheet in length direction of the sample at higher TPDs. The stirring and axial plunge force might have resulted in excessive upward protrusion of deformed metal along the lateral surface of the tool in the form of UB. UB is minimum in case of 1500 rpm, about 2.13 mm, and maximum in case of 2500 rpm, about 2.65 mm, and at all other RPMs, the UB varies in between. Therefore, the change in UB is insignificant w.r.t the RPM. The reason may be that the constant TPD of 1.5 mm induced almost similar UB throughout the range of RPMs. In addition to UB, SB of upper sheet is also observed for all FSF samples. Maximum and minimum SB of 18.11 and 17.52

mm is recorded for FSF samples fabricated at 2500 and 1000 rpms, respectively. Since the upper sheet can freely bulge in upward and sideward directions within the clamped region, most of the samples show random measurements in bulge values and a trend is not observed with change in RPM.

Table 2.5. Measured values of the morphological features on FSF joint cross-section

RPM	**PW** (mm)	**PH** (mm)	**BW** (mm)	**UB** (mm)	**SB** (mm)	**FPD** (mm)	**USFW** (mm)	**USFH** (mm)	**LSFW** (mm)	**LSFH** (mm)	**SST** (mm)
500	3.55	0.56	16.47	2.16± 0.06	17.85	4.51± 0.13	1.68± 0.17	0.79± 0.01	0.58± 0.04	0.81± 0.014	2.39± 0.14
1000	3.34	0.52	16.0	2.28± 0.13	18.11	5.21± 0.011	1.84± 0.24	0.89±0	0.50± 0.01	0.74±0	2.39± 0.10
1500	3.58	0.53	16.2	2.13± 0.11	17.98	4.62± 0.11	1.26± 0.05	0.77± 0.06	0.44± 0.04	0.79±0	2.23± 0.06
2000	3.19	0.48	16.29	2.37± 0.19	17.67	5.10± 0.03	1.48± 0.2	0.78± 0.09	0.52± 0.05	0.83± 0.043	2.47± 0.14
2500	3.55	0.52	16.12	2.65± 0.25	17.52	5.63± 0.11	1.70± 0.12	0.71± 0.03	0.35±0	0.50± 0.0385	2± 0.09
3000	3.35	0.51	16.29	2.41± 0.08	17.82	5.01± 0	1.43± 0.13	0.75± 0.01	0.21± 0.03	0.60± 0.0335	2.21± 0.09

FPD of the tool creates stir spot on the surface of the upper sheet. Like UB, FPD also remains constant with increase in the RPM. This is because the constant UB and constant TPD consequently control the depth of tool impression on the FSF joint.

Flash is generally a deformation occurs in upper and lower sheets, where the material is free to bulge out in any direction. The comparison of these measurements at various RPMs shows that flash formation is random in nature and the width and height of the flash are not varying much w.r.t RPM.

SST of FSF joints fabricated at various RPMs is also given in Table 2.5. The actual SST is found to be in the range of 2 to 2.39 mm, when 2.5 mm is the expected SST. The difference between the actual and the expected SSTs is negligible. Thus, measured values of above-mentioned morphological features show that their variation is negligible and they are independent of the RPM during FSF joint formation.

2.2.8 Miscellaneous joint features

The following are the miscellaneous joint features generated during the FSF joining of AA 5052-H32 and AA 6061-T6 sheets as observed from the present work.

- A small misalignment between stir tool center and anvil cavity center is visible on the macrostructure of the 500 rpm FSF sample (Fig. 2.8a), where the pin formation is affected by the slight eccentricity of the anvil cavity towards the periphery of the stir tool center. However, the strength of the joint is not impaired.
- Surface roughness is a another feature generated on the bottom of the lower sheet where it is can be clearly distinguished by the presence of a vivid circular roughness area having same dia. as that of the friction stir tool (Fig. 2.9b). These rough markings are generated due to extreme mechanical squeezing and thermal effect of the FSF process on the lower sheet.
- Flash is an undesirable defect that occurs over the upper sheet and lower sheet as a protrusion around the circumference of the stir spot created by the FSF stir tool. Flash seems to have little effect on the joint strength irrespective of its size. However, flash possesses some safety concerns and affects the aesthetic appearance of the joint. The reason behind the formation of lower sheet flash is that the high plunge depth value of 1.5 mm on a 2 mm thick upper sheet have induced some amount of deformation on the lower sheet also, which resulted in the upward bulging of lower sheet, generating flash below the circumference of the stir spot.
- Cracks are visible throughout the cross-section of FSF samples fabricated at low and medium RPMs, even at the SZ, which might be generated due shrinkage of the hot plasticized metal during cooling (Fig. 2.9c).

2.2.9 Modes of failure during mechanical testing

Tear-off, partial bond delamination, and pin pull-out with bond delamination are the three failure modes observed for FSF samples in lap shear, cross-tension and peel tests as shown in Fig. 2.13.

- Tear-off: The upper sheet has undergone tearing off along the circumference of the stir spot leaving the complete bonded region stuck on the lower sheet. This mode of failure happens mainly due to the thinning of the upper sheet near the circumference of stir spot irrespective of the proper pin formation and proper

metallurgical bonding (Fig. 2.13a). The tear off failure mode is identical to the plug fracture mode reported by Tozaki et al. (2010b) in pinless FSSW joints and the shear failure mode in two stage refilled FSSW joints reported by Sajed (2016).

- Partial bond delamination: The bonded region undergoes partial delamination, finally leaving the extruded pin and some bonded region at the stir spot over the lower sheet. This mode of failure is attributed to the poor metallurgical bonding around the circumference of the stir spot even though proper pin formation has occurred (Fig. 2.13b).
- Pin pull-out with bond delamination: The bonded region undergoes complete delamination resulting in the separation of the upper and lower sheets apart. The extruded pin retracts from the pre-drilled hole and remains attached with the upper sheet. Distorted lower sheet hole is also visible in the failed FSF samples. (Fig. 2.13c).

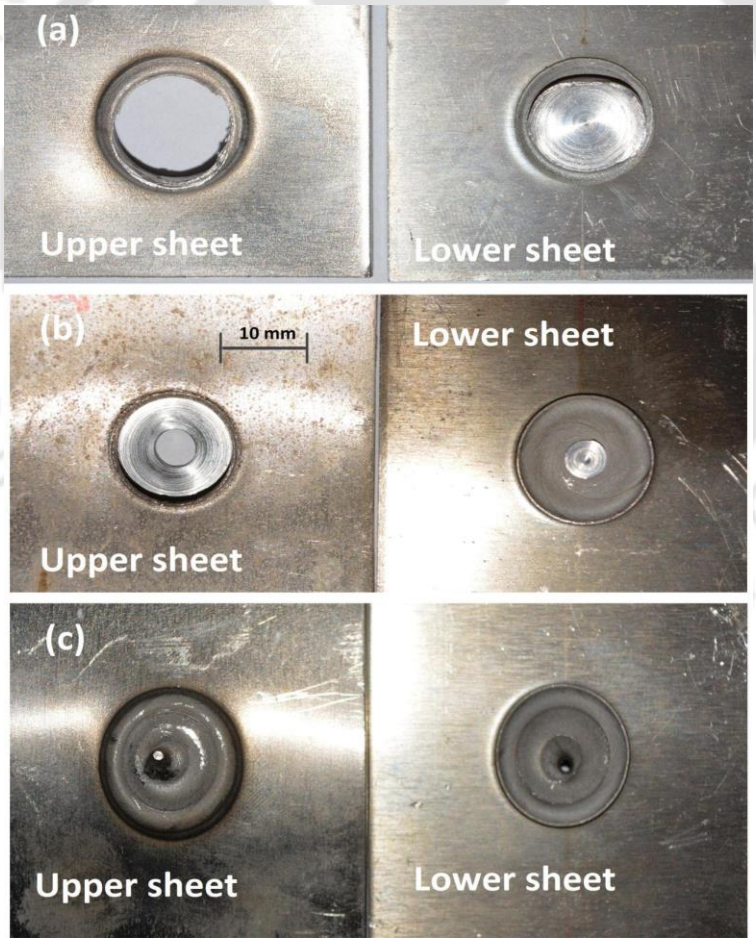

Figure 2.13. Modes of failure (a) Tear-off, (b) Partial bond delamination, (c) Pin pull-out with bond delamination

The main reason behind the failure modes are the weak zone formation at CRs of the FSF joint. Figure 2.14 shows the schematic representation of the critical weak zones

in the cross-section of the FSF joint. The two CRs are (a) the outer circumference of the stir spot in the upper sheet (CR 1) and (b) the distorted lower sheet which protrudes upwards (CR 2). The thinning of the upper sheet near the circumference of the stir spot is mainly responsible for tear-off failure. The upward distortion/ deformation of the lower sheet creates weak zone near the surface of the stir spot, which results in partial bond delamination failure. Poor metallurgical bonding and imperfect pin formation together creates pin pull-out with bond delamination failure.

Jeon et al. (2012) reported that the failure mechanism of AA 5052-AA 6061 FSSW joints under quasi-static shear loads was strongly affected by the stress concentration induced by the hook formation near the SZ. Similarly, failure modes in FSW joints depend on the position of the softer base metal relative to the advancing side (Park et al., 2010). However, the failure of FSF joints initiates from the CRs as mentioned above. This is the reason for FSF joints showing different modes of failure other than that in FSW and FSSW joints.

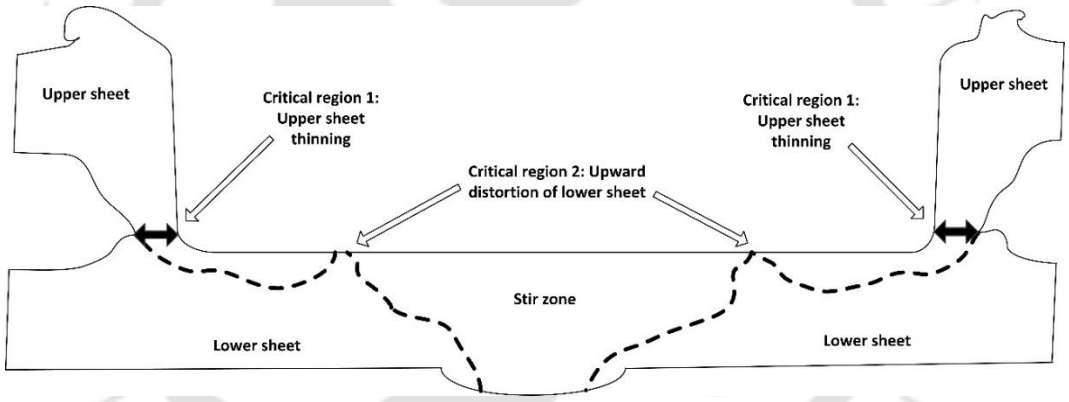

Figure 2.14. Weak zone formation over the cross-section of the FSF sample

Table 2.6 shows the summary of the failure modes of FSF samples at various tool rotational speeds, from 500 to 3000 rpm, subjected to lap shear, cross-tension, and peel tests. Tear-off failure is the most common failure seen in FSF samples, followed by partial bond delamination. Pin pull-out with bond delamination failure occurs in very few cases. It should be noted that FSF samples fabricated at 1500 and 3000 rpms show all the three modes of failure during the mechanical performance testing, while samples fabricated at other RPMs show any two of the three failure modes. Therefore, the modes of failure are random and have no appropriate relation with the RPM. Moreover, the failure modes are random with respect to the two trials at same RPM for a particular test.

Table 2.6. Modes of failure

RPM	Lap shear test		Cross-tension test		Peel test		Tensile test
	Trial 1	Trial 2	Trial 1	Trial 2	Trial 1	Trial 2	

500	Partial bond delamination	Partial bond delamination	Partial bond delamination	Tear-off	Tear-off	Tear-off	Stir spot fracture
1000	Tear-off	Tear-off	Tear-off	Partial bond delamination	Tear-off	Tear-off	Stir spot fracture
1500	Partial bond delamination	Tear-off	Partial bond delamination	Pin pull-out with bond delamination	Partial bond delamination	Tear-off	Stir spot fracture
2000	Tear-off	Tear-off	Pin pull-out with bond delamination	Pin pull-out with bond delamination	Tear-off	Tear-off	Base metal fracture
2500	Tear-off	Tear-off	Partial bond delamination	Partial bond delamination	Partial bond delamination	Tear-off	Base metal fracture
3000	Partial bond delamination	Tear-off	Pin pull-out with bond delamination	Tear-off	Tear-off	Partial bond delamination	Base metal fracture

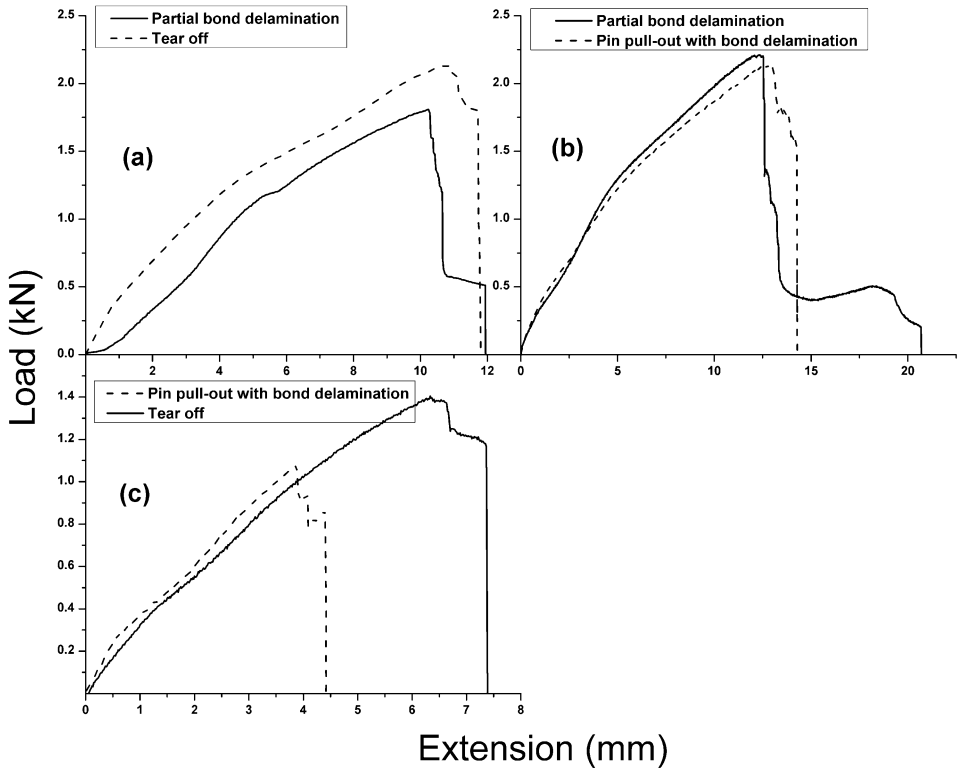

Figure 2.15. Load-progression behavior of cross-tension samples at (a) 500 rpm, (b) 1500 rpm, and (c) 3000 rpm

Fig. 2.15a-c shows the comparison of load-progression behavior during cross-tension test of FSF samples fabricated at 500, 1500, and 3000 rpms for the two different joining trials. From Fig. 2.15a at 500 rpm, it can be seen that for partial bond delamination failure, just after the initiation of fracture, the decrease in the load is gradual till the sample attains full separation between the upper and lower sheets. Therefore, partial bond delamination failure is gradual in nature when compared to tear-off failure although extension acquired after the initiation of fracture remains almost same for both the samples. The gradual failure in partial bond delamination mode is clearly seen in the load-

progression behavior of FSF sample fabricated at 1500 rpm, as shown in Fig. 2.15b. Pin pull-out with bond delamination failure and tear-off failure modes are sudden in nature, which can be seen from the comparison of load-progression behavior of FSF samples fabricated at 3000 rpm, as shown in Fig. 2.15c.

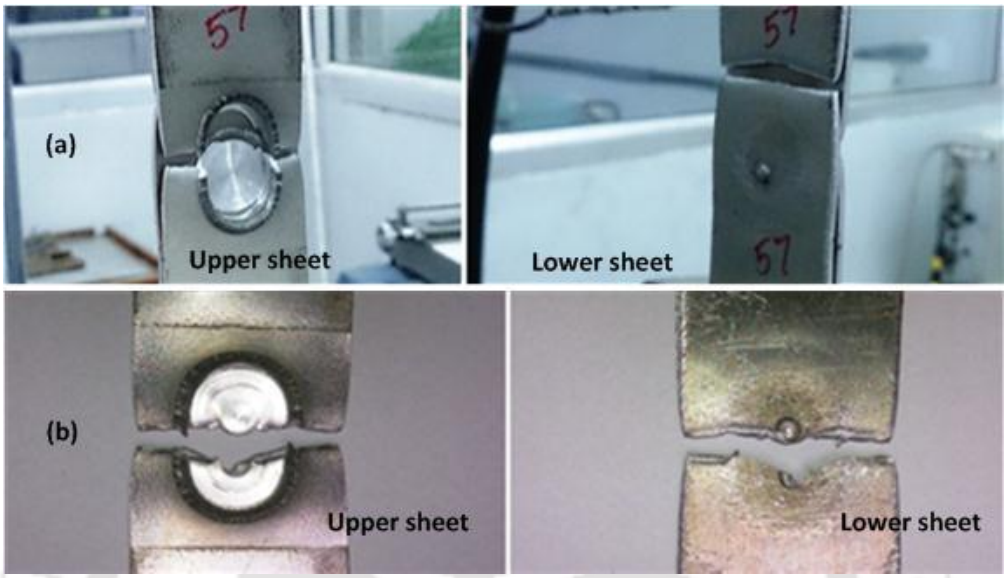

Figure 2.16. Modes of failure in tensile test (a) Base metal fracture (500-1500 rpm); (b) Stir spot fracture (2000-3000 rpm)

The tensile test samples show entirely different modes of failure. Some of the samples show base metal fractures, while others show stir spot fracture. Necking commonly seen in uniaxial tensile test is also observed in these FSF samples.

- Stir spot fracture occurs when failure initiates from within the joint. The sample fails by fracture along a transverse section of the stir spot, the critical geometrical inhomogeneity in the tensile samples (Fig. 2.16a). It can be observed that the load is equally shared by both the sheets in the tensile sample.
- Base metal fracture occurs when the strength of the adjacent sheet region is less than the joint strength. The base metal surrounding the stir spot softens under the frictional heat flux during joint formation. This act as weak zone leading to premature failure at maximum tensile load (Fig. 2.16b). Transverse fracture occurs in the base metal, while the stir spot remains unaffected.

The summary of failure modes during tensile test of FSF samples fabricated at various RPMs is also shown in Table 2.6. It is observed that FSF samples at lower RPM show stir spot fracture and those at higher RPM show base metal fracture. FSF samples fabricated at medium RPMs show both the failure modes.

2.3 Conclusions

Friction stir form joining of AA 5052-H32 and AA 6061-T6 is conducted, and the following conclusions are drawn from the results of the present work.

- FSF can be successfully used to join sheet metals of almost same quality in which obtained lap shear strength of 6.14 kN is better than that of other friction based joining processes like FSW and FSSW. The mechanical performance studies revealed that the fracture load show an increasing trend or nearly same trend, with increase in the tool rotational speed upto 1500 rpm, while a decreasing trend is observed with increase in the tool rotational speed from 1500 to 3000 rpm.
- The extreme heat generation and plastic deformation at higher tool rotational speeds like 3000 rpm deteriorated the fracture strength of FSF samples. Therefore, low and medium tool rotational speeds, from 500 to 1500 rpm, are the best choices for fabricating FSF joints between AA 5052-H32 and AA 6061-T6 sheets.
- Optical macrostructure analysis of the joint cross-sections revealed the presence of five distinct zones namely SZ, TMAZ, PDZ, ASZ and HAZ. It is revealed that the inward radial flow of plasticized metal from the PDZ through the pre-drilled hole in the lower sheet results in the mechanical pin formation.
- Inverted ‘W’-shaped hardness profiles show that the increase in the stirring effect with increase in RPM produces harder regions towards the SZ boundary.
- The joint morphology analysis revealed that the formation of external structural features, which affect the joint strength and aesthetic appearance, are independent of the change in RPM.
- Three modes of failure namely partial bond delamination, tear-off, and pin pull-out with bond delamination are observed during the mechanical performance tests, which are initiated from critical weak zone formation due to upper sheet thinning, improper bonding and imperfect pin formation, and also the upward deformation of lower sheet. The modes of failure are random in nature and they are independent of the change in RPM.

It can be concluded that the RPM has a profound influence on the joint strength and joint formation of FSF samples fabricated on dissimilar grade aluminum alloys. Generally, Al-steel spot joining with FSF process is simpler as the lower steel sheet acts as a rigid body and hence extrusion of Al alloy into the anvil cavity through pre-drilled

hole in the lower sheet is easier. In this context, joining of dissimilar grade aluminum alloys with FSF process attempted in the present work is a valuable contribution.

भारतीय प्रौद्योगिकी संस्थान गुवाहाटी
Indian Institute of Technology Guwahati

Chapter 3

FSF joining of AA 5052-H32 and AA 6061-T6 sheets at varying tool plunge depths

In this chapter, the effect of TPD on the mechanical performance of FSF joints are evaluated through lap shear test, cross-tension test, peel test and uniaxial tensile test. The joint formation is characterized by optical macrostructure analysis. The hardness measurement across the joints formed, the joint morphology and the failure mode analysis are also presented. The optimum tool rotational speed of 500 rpm obtained from the previous chapter and the sheet metal combination employed in the previous chapter for FSF joint fabrication are adopted in present work.

3.1 Methodology

The principle of FSF joint formation is presented in section 2.1.1.

3.1.1 FSF Experiments

FSF sample fabrication is presented in section 2.1.2. The effectiveness of the FSF joint formation is studied by varying the TPD at various levels, with lower levels at 0.2 mm and 0.3 mm, medium levels at 0.5 mm and 0.7 mm and higher levels at 0.9 mm and 1.1 mm. The attempt to fabricate FSF samples at 0.1 mm failed due to the absence of any mechanical pin formation. Therefore, the lowest TPD is set to be 0.2 mm. It is the lowest TPD at which the chance of formation of a sound FSF joint is possible for the present material combination of 2 mm-thick aluminum sheets.

All other process parameters namely plunge rate, tool rotational speed, direction of tool rotation are kept constant at 0.002 mm/s, 500 rpm and clockwise direction, respectively. RPM is selected as per results obtained from chapter 2. Two samples are fabricated per TPD level for all the tests and the average output value is considered.

Details of mechanical performance tests is discussed in section 2.1.3.

3.1.2 Macrostructure, hardness measurement and joint morphology analysis

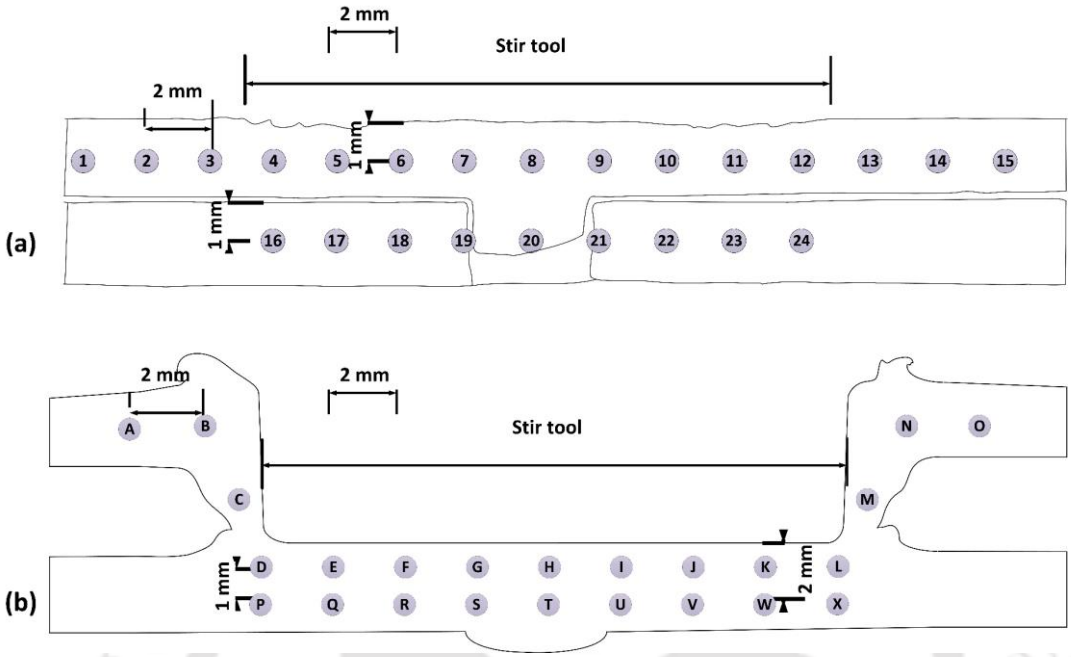

Figure 3.1. Hardness measurement locations along joint cross-sections: (a) Lower TPD (0.2, 0.3 mm) samples; (b) Medium (0.5, 0.7 mm) and higher (0.9, 1.1 mm) TPD samples

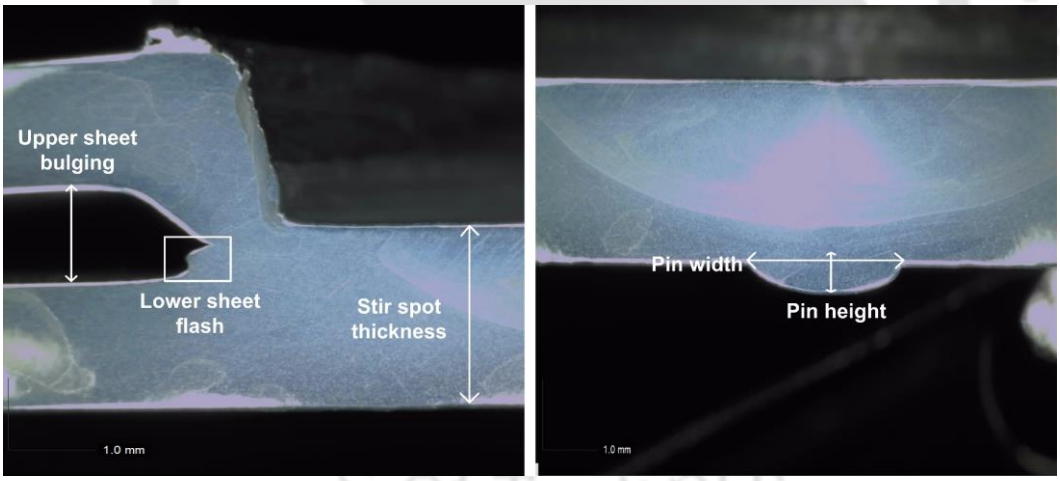

Figure 3.2. Morphological features of joint cross-section

Details of macro structure analysis, hardness measurement and joint morphology analysis are discussed in section 2.1.4. For hardness measurement, the indentations are performed in two arrays. Upper array covers the upper sheet (locations 1-15 in Fig. 3.1a for lower level TPDs and locations A-O in Fig. 3.1b for medium and higher level TPDs). Lower array covers the lower sheet (locations 16-24 in Fig. 3.1a for lower TPDs and locations P-X in Fig. 3.1b for medium and higher TPDs).

The morphological features considered for analysis are macro defects such as LSFW, LSFH, UB, PW, PH and SST. These joint features are represented over typical FSF joint cross-sections, as shown in Fig. 3.2.

3.2 Results and discussion

This section deals with the effect of TPD on the joint fracture load and failure modes of FSF samples obtained through four different mechanical performance tests, macrostructure analysis, hardness measurement and joint morphology analysis.

3.2.1 Mechanical performance tests

Fig. 3.3 shows the effect of TPD on the fracture load (joint strength) obtained from mechanical performance tests. It is observed that there is an optimum TPD range, 0.5-0.7 mm, in which the joint fracture load is maximum. Such maximum fracture load changes slightly with the testing methods. For instance, in lap shear test, the fracture load is maximum at 0.7 mm TPD and it decreases at any TPD, higher and lower than this optimum TPD. There is about 700% increase in lap shear fracture load, when the TPD is increased from 0.2 mm (0.86 kN) to 0.7 mm (7.16 kN). Similarly, in the case of cross-tension test, the optimum fracture load occurs at 0.5 mm TPD. There is about 350% increase in the cross-tension fracture load, when the TPD is increased from 0.2 to 0.5 mm. The change in fracture load is not significant in peel test, though maximum fracture load occurs at 0.3 mm TPD. The variation in peel fracture load is within 1 kN, for the entire TPD range. Sound joint strength is attained at higher TPD range (0.9-1.1 mm) during lap shear test and cross-tension test. However, peel test samples show poor strength at this TPD range, which is not acceptable. At medium TPD range from 0.5 mm to 0.7 mm, the fracture load is optimum during lap shear test and cross-tension test, while peel test samples show fairly better fracture load. Variation in fracture load within the medium TPD range is also observed during these three tests, which is not significant, since the values fall in acceptable range of joint strength.

In uniaxial tensile test, the joint fracture load decreases from 0.3 mm to 1.1 mm TPD. A decrease of 24% within the range is observed, showing the importance of TPD on the forming performance. Such a decrease is directly related to the geometrical heterogeneity developed within the stir spot.

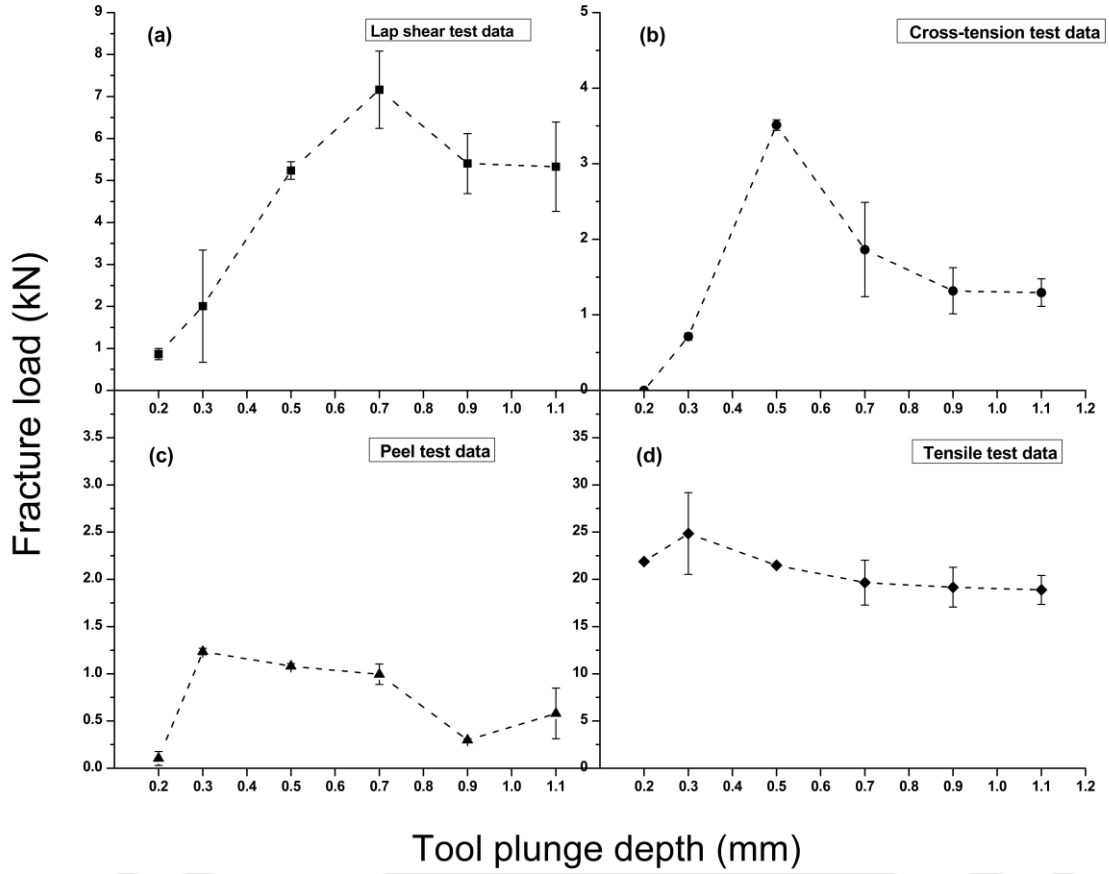

Figure 3.3. Comparison of fracture loads at various TPDs during mechanical tests: (a) Lop shear test data; (b) Cross-tension test data; (c) Peel test data; (d) Tensile test data

FSF samples show appreciable extensibility averaging about 0.54 mm for lap shear test, 6.93 mm for cross-tension test, 4.18 mm for peel test and 3.56 mm for uniaxial tensile test. The fracture load is observed to be the highest during lap shear test and the lowest during peel test. Cross-tension test data falls in between in most of the cases. From the analysis, it can be concluded that the optimum TPD to obtain a strong joint with acceptable extension for AA 5052-H32-AA 6061-T6 combination is in the moderate range of 0.5-0.7 mm. The main reason for the effect of TPD on the joint strength is found to be the pin interlock formation and metallurgical bonding and the same has been explained in section 3.2.2.

Joining of AA 5052-H32 to AA 6061-T6 with FSW and FSSW is already reported in literature. Table 3.1 gives a comparison of fracture load of these joints with FSF joints of the present work. It is observed that FSF joints possess superior fracture load over FSW and FSSW joints.

Table 3.1. Comparison of the fracture load of FSF with other joining technologies

Joining technique	Joint form	Test type	Average fracture load (kN)	Source
FSW	Butt joint	Tensile test	5.75	(Kumbhar and Bhanumurthy, 2012)
FSW	Butt joint	Tensile test	4.85	(RajKumar et al., 2014)
FSW	Butt joint	Tensile test	5.93*	(Park et al., 2010)
FSSW	Lap joint	Lap shear test	4.85	(Jeon et al., 2012)
FSF	Lap joint	Lap shear test	7.16	Present work

*Calculated from average tensile strength in MPa

3.2.2 Joint formation through macrostructure analysis

The FSF joint formation under increasing TPD is explained with the macrostructure analysis. FSF samples fabricated at each of the lower, medium and higher TPDs are selected for macrostructure analysis. The various zones that can be commonly identified in FSF joint cross section are SZ, TMAZ, PDZ and HAZ. The complete macrostructure of the FSF joint cross-section, with schematic representation of various zones and metal flow directions are shown in Fig. 3.4 and Fig. 3.5, respectively.

3.2.2.1 Lower TPDs: 0.2 mm and 0.3 mm

The joint macrostructure and schematic of metal flow in lower TPDs are shown in Fig. 3.4(a-b) and Fig. 3.5(a-b), respectively. At 0.2 mm TPD, the pin formation has just started. The plastically deformed upper sheet has partially filled the pre-drilled hole in the lower sheet, and no mechanical interlocking is established. The anvil cavity is not completely filled with the extruded upper sheet metal, as it is generally required in FSF.

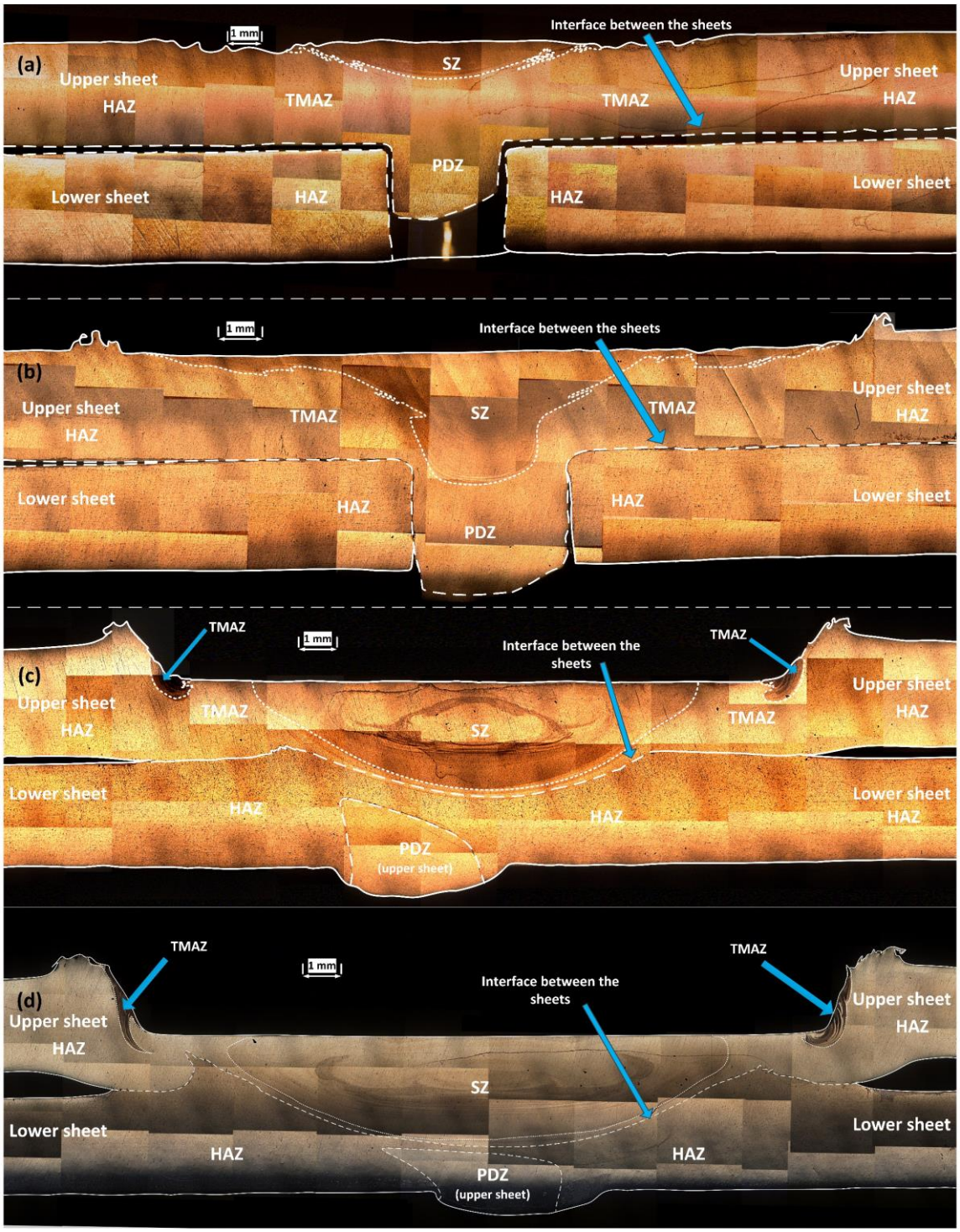

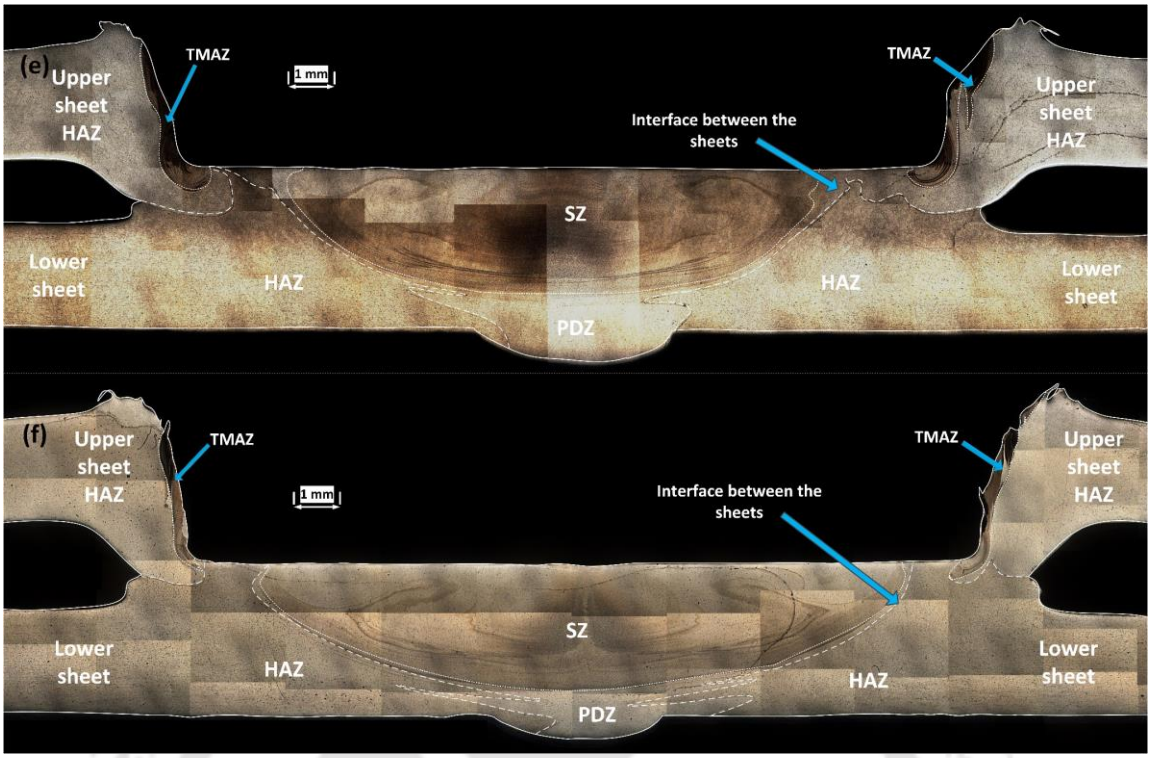

Figure 3.4. Joint macrostructures of FSF samples fabricated at different TPDs: (a) 0.2 mm; (b) 0.3 mm; (c) 0.5 mm; (d) 0.7 mm; (e) 0.9 mm; (f) 1.1 mm

At the end, there is no metallurgical bonding visible at the interface. Since the TPD is insufficient, the SZ size is small and confined to the top of the upper sheet. The flash formation is absent. The partial extrusion of upper sheet in the form of pin has generated a prominent PDZ.

With further increase in TPD to 0.3 mm, the extruded pin has almost reached the bottom of the anvil cavity and filled the pre-drilled hole completely. The SZ size has increased to such an extent that the hole has deformed partially to initiate a mechanical interlocking around the neck of the pin. The upper sheet flash is generated without TMAZ formation.

Since there is no metallurgical bonding between the two sheets, the joint fracture load is lower under these TPDs. The mechanical interlocking has solely contributed to such a lower joint strength.

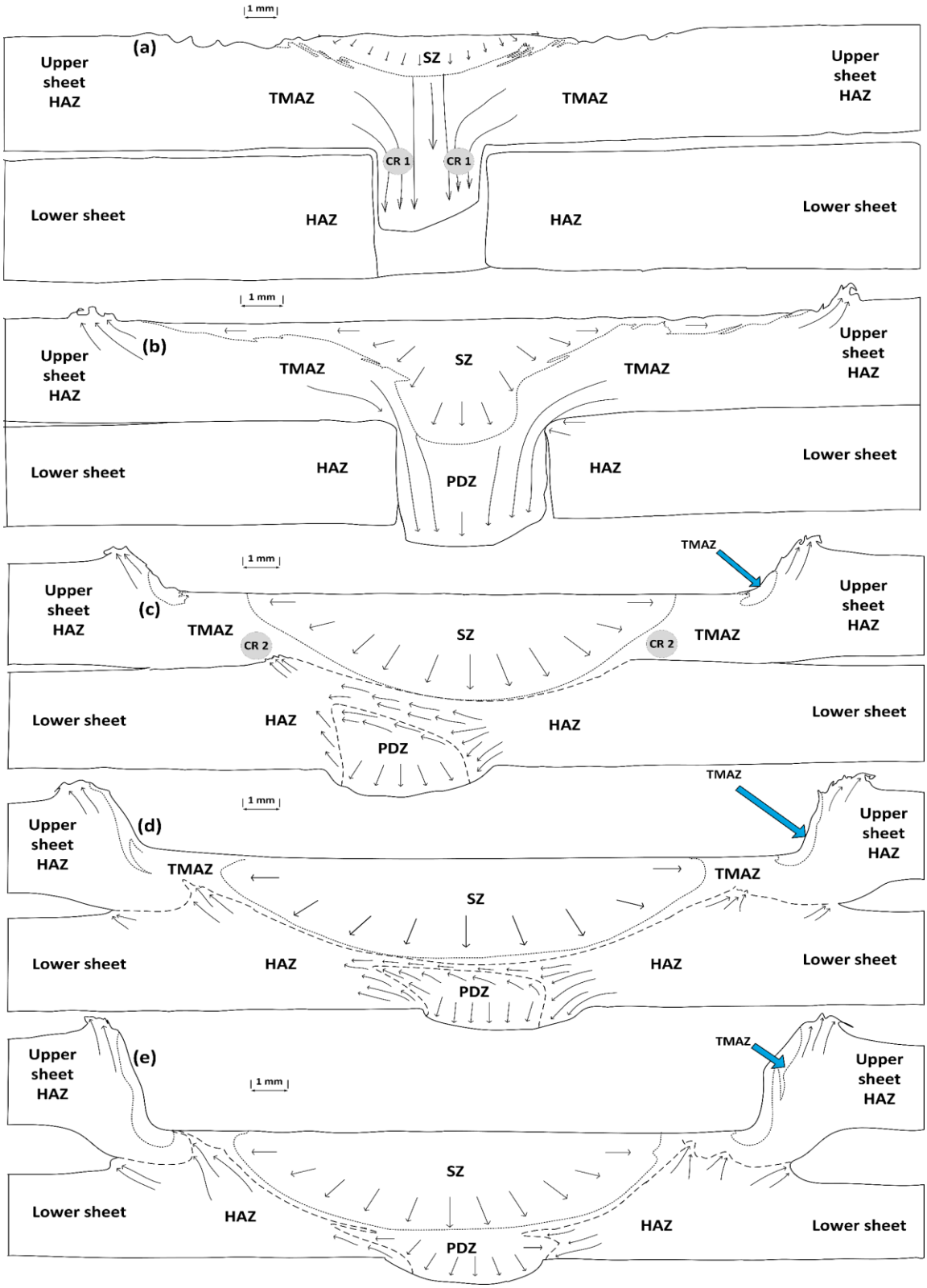

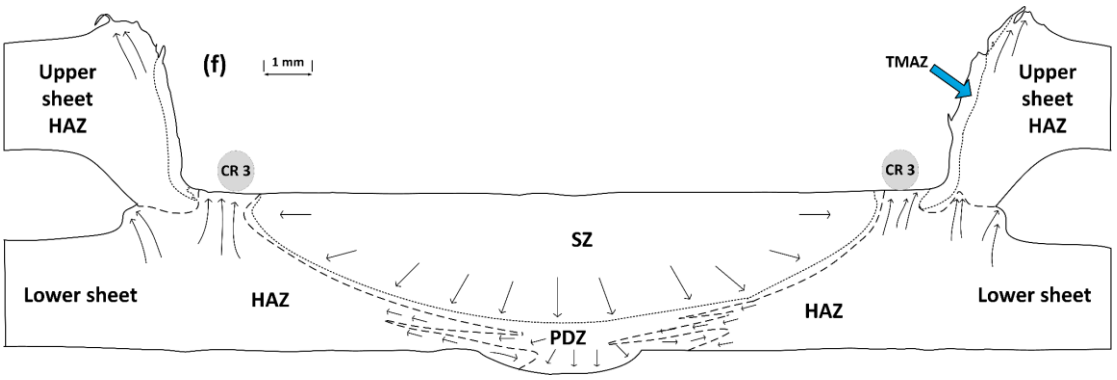

Figure 3.5. Metal flow directions during FSF at different TPDs: (a) 0.2 mm; (b) 0.3 mm; (c) 0.5 mm; (d) 0.7 mm; (e) 0.9 mm; (f) 1.1 mm

3.2.2.2 Moderate TPDs: 0.5 mm and 0.7 mm

Fig. 3.4(c-d) and Fig. 3.5(c-d) show the joint macrostructure and schematic of the metal flow directions for moderate TPDs, respectively. With further increase in TPD to 0.5 mm, the metallurgical bonding has been initiated between the two sheets. The extruded pin also fills the anvil cavity. However, the TPD is severe enough to completely deform the hole and it closes the pin path. Hence, the connection between the pin and the upper sheet is lost during the course of tool plunge. The lower sheet has also deformed and filled the anvil cavity, which is generally not expected in FSF. On the other hand, the SZ and TMAZ size are increased. The upward deformation of lower sheet and UB are seen prominently. The upper sheet flash has increased further. At 0.7 mm TPD, there is nothing new occurring in the joint formation. The disconnected pin has deformed further (Fig. 3.4d and Fig. 3.5d). The SZ, TMAZ, upper sheet flash, UB and upward deformation of the lower sheet have increased further in their size.

It can be observed that direction of tool rotation has an influence on the deformation of the PDZ. The disconnected PDZ has been deviated to the left hand side of the cross section, as seen in Figs. 3.5c and Fig. 3.5d, because of the clockwise direction of rotation of the stir tool along with the downward tool plunge. Under these TPDs, reasonably good joints are fabricated with improved joint strength. Such an improvement is mainly contributed by metallurgical bonding.

3.2.2.3 Higher TPDs: 0.9 mm and 1.1 mm

The joint macrostructure and schematic of metal flow in higher TPD FSF joints are shown in Fig. 3.4(e-f) and Fig. 3.5(e-f), respectively. At higher TPDs of 0.9 and 1.1 mm,

the SZ size is increased further resulting in the remerging of upper sheet to the extruded pin. The metallurgical bonding between the upper and lower sheets exists in these TPDs as well. Like in the moderate TPDs, the TMAZ, UB, upper sheet flash have increased in their size. The lower sheet flash formation is also observed in these higher TPDs. In spite of having a good metallurgical bonding and mechanical interlocking at higher TPDs, the joint fracture load is inferior than that in moderate TPDs. This is because the upward deformation of lower sheet creates a separation between the SZ at center and the sidewalls of the stir spot circumference, thereby creating a material discontinuity 'CR3' at both the ends of SZ (Fig. 3.5f).

Just to summarize, the SZ formation, metallurgical bonding and pin interlocking govern the effect of TPD and joint performance during mechanical testing. The joint performs better at moderate TPDs (0.5 mm and 0.7 mm) because of good metallurgical bonding. At lower TPDs (0.2 and 0.3 mm), the metallurgical bonding and mechanical interlocking are absent, indicating TPDs to be insufficient. At higher TPDs (0.9 and 1.1 mm), the formation of critical weak zones (CR3) deteriorates the performance, in spite of having metallurgical bonding and mechanical interlocking. Table 3.2 describes the evolution of joint formation with change in TPD.

Table 3.2. Summary of evolution of features of FSF joint

Feature	At lower TPD	At medium TPD	At higher TPD
Pin interlock	Visible	Nil	Nil
Metallurgical bonding	Nil	Visible	Visible
SZ	Small-sized	Medium-sized	Large-sized
PDZ	Visible	Disconnected	Reconnected
TMAZ	Nil	Small-sized	Medium-sized
Pin extrudate	Partial pin formation	Disconnected pin	Compressed pin
Upper sheet flash	Small-sized	Medium-sized	Large-sized
Lower sheet flash	Nil	Nil	Small-sized
UB	Nil	Small-sized	Medium-sized
Upward deformation of lower sheet/ upper sheet thinning	Nil	Visible	Severe

An optimum TPD range of 0.5-0.7 mm is suitable to fabricate strong FSF joints between AA 5052-H32 and AA 6061-T6 sheets, as observed from the evolution of joint macrostructure. The same optimum range can be selected from mechanical performance tests like lap shear test and cross-tension test as well. There is a slight deviation in the optimum range of TPD from the peel test. In peel test, the joint fracture load is almost uniform in a larger range of TPD, from 0.3-0.7 mm, making the range flexible.

3.2.3 Hardness variation

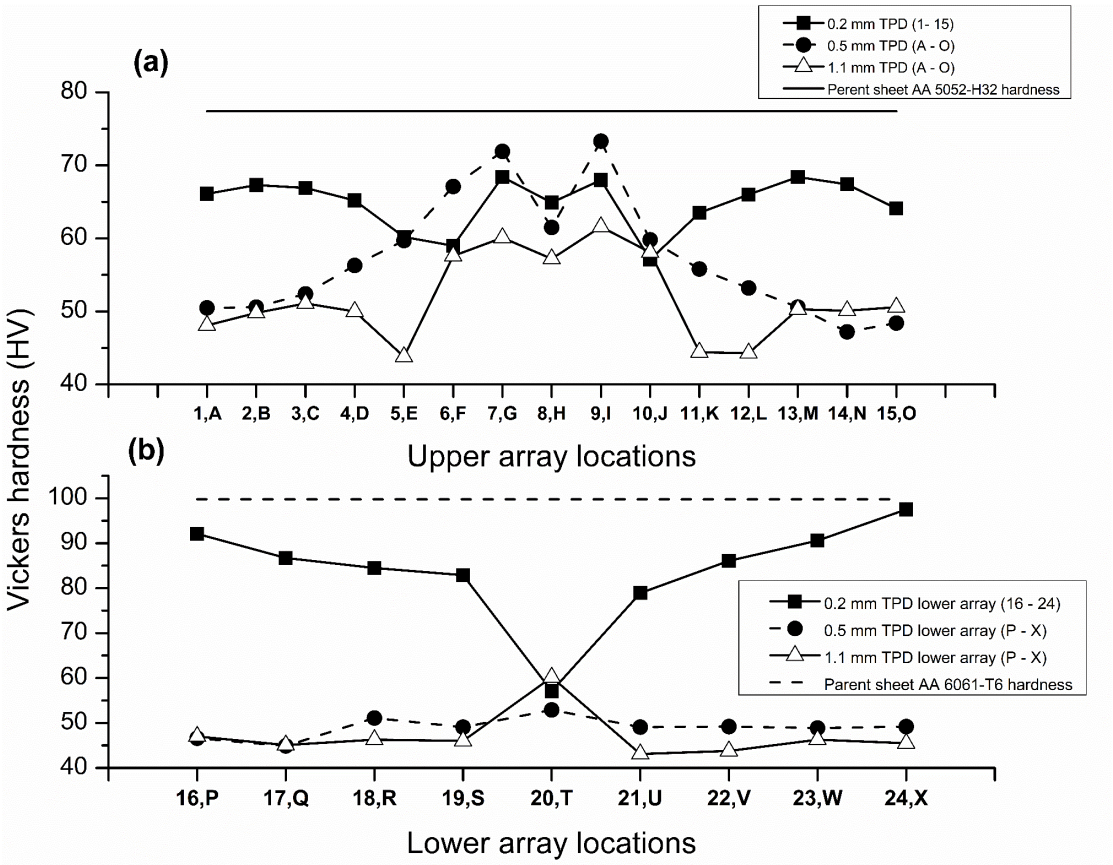

Figure 3.6. Comparison of hardness variation along cross section: (a) Upper array of indentation; (b) Lower array of indentation (Typical hardness variation at each measurement location is ±1.96)

Hardness variation in FSF samples can be analyzed by comparing the hardness profile over the cross-section of selected FSF samples from lower (0.2 mm), medium (0.5 mm) and higher (1.1 mm) TPD levels. It is observed that the hardness of upper array and lower array of indentations are reduced from the parent metal hardness. This due to the effect of frictional heat flux and plastic deformation inducing softening of sheet metals.

Fig. 3.6a shows the comparison of hardness along the upper array of indentation with change in TPD. It can be observed that FSF samples show similar hardness profile at the center of the cross-section, (locations E-K); therefore, the effect of TPD on the formation of SZ is almost similar. SZ possesses minimal hardness at the center and hardness increases towards its periphery. Since the material at the center of the SZ can freely be pushed towards the pre-drilled hole, comparatively softer regions are generated at the center than the surroundings. Moreover, the variation in hardness along the upper array with increase in the TPD is random.

Fig. 3.6b shows the comparison of hardness along the lower array at different TPDs. At 0.2 mm TPD, minimum hardness for the lower array is recorded on the soft extruded pin (at location 20, which is a part of the upper sheet). Higher hardness recorded at other locations shows that these regions are not significantly affected by the low heat flux and mild plastic deformation at lower TPDs. At 0.5 mm TPD, the highest hardness is recorded at the closure of the pre-drilled hole (at location T), which is compressed in between the separated pin extrudate and the upper sheet. Similar hardness profile observed at 1.1 mm TPD shows that the compression of the deformed pin by the downward movement of the tool has resulted in the increase in the hardness at location T. At 0.5 and 1.1 mm TPDs, hardness at all locations of the lower array, other than location T, has reduced considerably from the parent metal hardness due to the influence of frictional heat flux.

In summary, the increase in TPD has significantly affected the hardness along the lower array, while upper array possess identical trend with inverted 'W'-shaped profile. Upper array shows that SZ formation is identical at all TPDs, despite the SZ size is increasing with change in TPD. Lower array shows that the increase in frictional heat flux and associated plastic deformation with increasing TPD has reduced the hardness of the lower sheet.

3.2.4 Joint morphology analysis

The comparison of morphological features in the FSF joint cross-section with change in TPD is described in this section. It is observed that the PW and PH, which determine the anvil cavity filling, remain almost same for FSF joints when the TPD is varied from 0.5 to 1.1 mm (Fig. 3.7a and Fig. 3.7b). Uniform PW and PH ensure that the anvil cavity filling is complete from 0.5 mm TPD onwards. At lower TPD levels, the pin formation is absent, since the extrudate has not reached up to the anvil cavity. This shows that TPD has significant influence on the formation of the external pin interlock.

UB, as explained in section 2.2.7, possesses more or less linearly increasing relationship with change in TPD (Fig. 3.7c). It is minimal at 0.3 mm TPD, about 0.025 mm, and maximum at

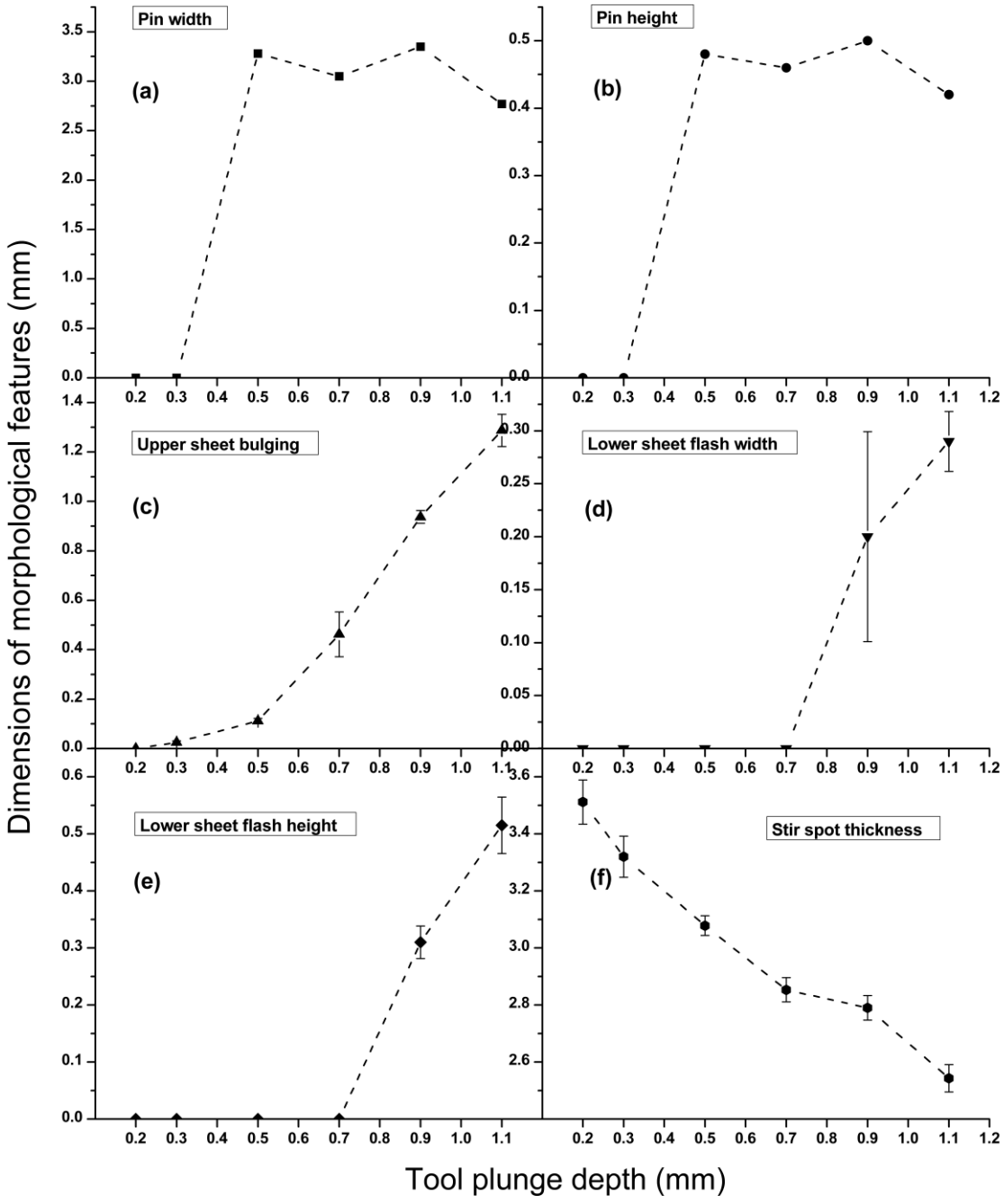

Figure 3.7. Comparison of joint morphological features at various TPDs: (a) PW, (b) PH, (c) UB, (d) LSFW, (e) LSFH, (f) SST

the highest TPD, about 1.28 mm. However, the UB is less in this TPD range, so that its influence on the aesthetic appearance of the FSF joint is not considerable.

Lower sheet flash typically forms when the lower sheet has undergone significant deformation under the heat flux from the SZ and the tool plunge force. It is observed that lower sheet flash has formed only at higher TPDs (0.9-1.1 mm), where the width and height of the flash show an increase in size with increase in the TPD (Fig. 3.7d and Fig. 3.7e). Therefore, it is revealed that the TPD has a direct influence on the deformation of

the lower sheet and further flash formation. The upper sheet flash is not considered in this work because its formation does not directly or indirectly influence the joint formation. From Fig. 3.7f, it is revealed that SST has an inverse relation with TPD. With increase in TPD, the material underneath the tool moves sidewards, resulting in the decrease of SST.

The morphological analysis shows that the variation of the joint morphological features is significant and they are dependent on the TPD during FSF joint formation. At optimum TPDs, namely 0.5 and 0.7 mm, the morphological features such as PW and PH are constant, there is no lower sheet flash formation, and UB and SST are moderate.

3.2.5 Modes of failure during mechanical testing

The following failure modes are observed for FSF samples in lap shear test, cross-tension test, peel test and tensile test, as shown in Fig. 3.8.

- Partial bond delamination: This type of failure mode is explained in section 2.2.9 (Fig. 3.8a).
- Pin shear: Pin undergoes shearing along the neck leaving the broken part inside the pre-drilled hole (Fig. 3.8b). Pin shear occurs for FSF samples, where the extruded pin interlock solely contributes the joint strength, while metallurgical bonding is absent.
- Tear-off: This type of failure mode is explained in section 2.2.9 (Fig. 3.8d).
- Pin pull-out: Pin gets pulled out from the pre-drilled hole due to poor interlocking and due to the absence of metallurgical bonding (Fig. 3.8e).

  Pin pull-out can happen even under no load conditions. This occurs when the pin has not extruded up to the bottom of anvil cavity at lower TPDs.
- Sheet tear: The shearing of the lower sheet can occur from the pre-drilled hole. This occurs commonly when the sheets are peeled apart under pulling load.
- Stir spot fracture: This type of failure mode is explained in section 2.2.9 (Fig. 3.8g).
- Base metal fracture: This type of failure mode is explained in section 2.2.9 (Fig. 3.8h).

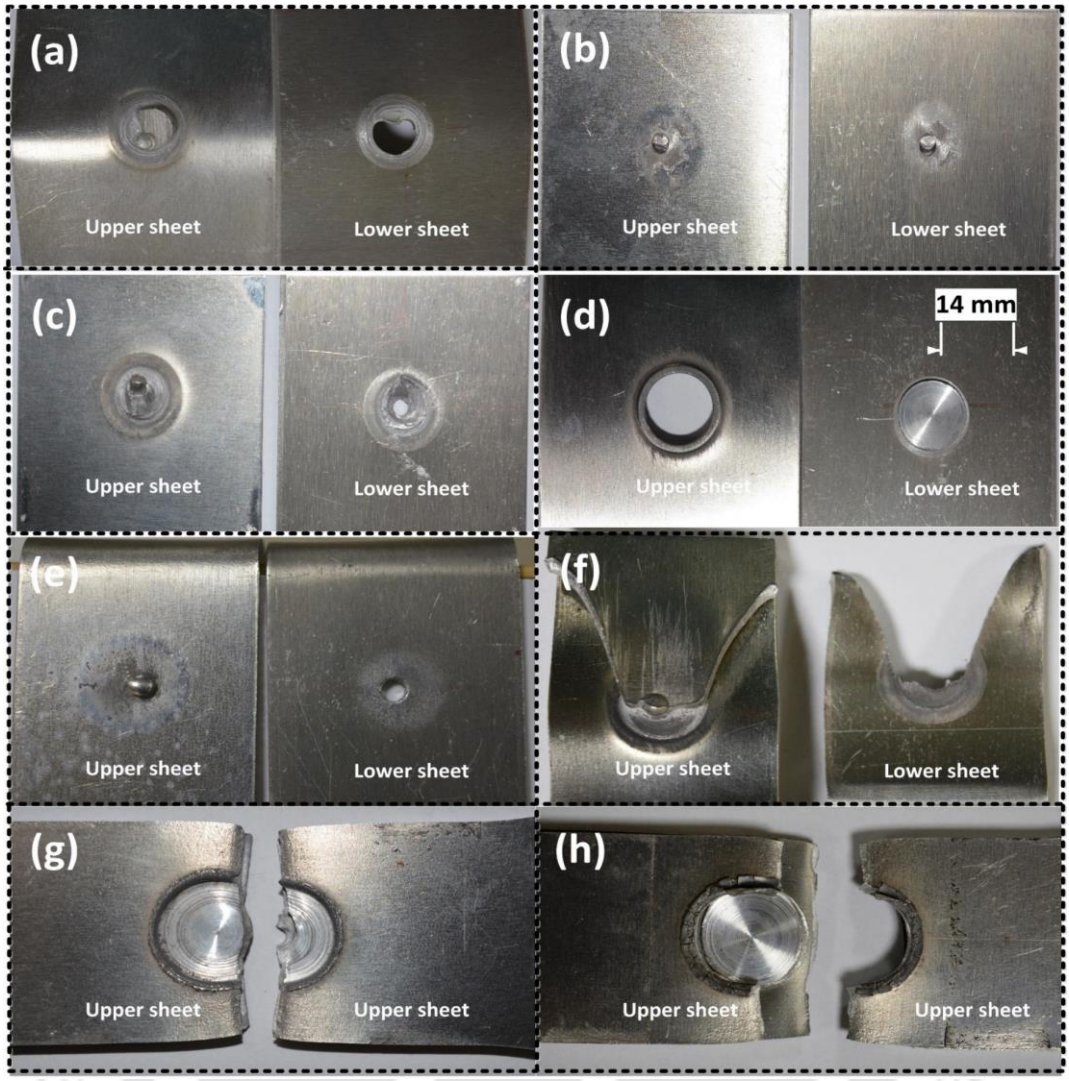

Figure 3.8. Modes of failure during testing of FSF joints: (a) Partial bond delamination; (b) Pin shear; (c) Combined pin shear and bond delamination; (d) Tear-off; (e) Pin pull-out; (f) Combined partial bond delamination and sheet tear; (g) Stir spot fracture; (h) Base metal fracture

Most of the failure modes occur in combined form such as combined pin shear and bond delamination (Fig. 3.8c) as well as combined partial bond delamination and sheet tear (Fig. 3.8f). The main reason behind the failure modes in lap shear, cross-tension and peel tests are the weak zone formation at CRs of the FSF joint. The three CRs are i) the neck of the pin, CR1 (Fig. 3.7a), ii) incomplete/ partial metallurgical bonding, CR2 (Fig. 3.7c) and iii) the upward deformation of the lower sheet, which separates the central SZ from the sidewalls of the stir spot, CR3 (Fig. 3.7f). Sometimes the neck of the pin (CR1) is so weak that shearing can happen along the neck, which leads to pin shear failure. Whenever the metallurgical bonding is incomplete (CR2) around the stir spot circumference, the interfacial delamination initiates from the weakest region, which results in partial bond delamination failure. In some cases, the tool plunge is so severe that the upward deformation of the lower sheet (CR3) creates weak zone near the surface of the

stir spot by upper sheet thinning, which results in tear-off failure. Combined failure modes occur more or less due to the formation of more than one active CRs.

Table 3.3 shows the summary of the failure modes at various TPDs of FSF samples prepared for lap shear, cross-tension, peel and tensile tests. Tear-off is the most common failure mode followed by pin pull-out. It should be noted that FSF samples fabricated at medium and higher TPDs, from 0.7 mm to 1.1 mm, show tear-off failure in most cases because the major part of the strength is contributed by the metallurgical bonding. FSF samples fabricated at lower TPDs, from 0.2 mm to 0.3 mm, show pin pull-out failure. Therefore, the modes of failure have significant relation with the TPD. Moreover, the failure modes are random with respect to the two trials at same TPD level for a particular test, specifically at lower and medium TPDs. The tensile test samples show entirely different modes of failure. Base metal fracture and stir spot fracture occur randomly at medium and higher TPDs.

Table 3.3. Modes of failure

TPD	Lap shear test		Cross-tension test		Peel test		Tensile test	
	Trial 1	Trial 2	Trial 1	Trial 2	Trial 1	Trial 2	Trial 1	Trial 2
0.2	Pin shear	Pin shear	Pin pull- out at no load	Pin pull-out at no load	Pin pull- out at no load	Pin pull- out	Stir spot fracture	Pin pull-out at no load
0.3	Pin shear+ Bond delamination	Pin shear	Pin pull- out	Pin pull-out	Partial bond delamination+ Sheet tear	Partial bond delamination+ Sheet tear	Base metal fracture	Base metal fracture
0.5	Tear-off	Pin shear	Partial bond delamination	Tear-off	Partial bond delamination+ Sheet tear	Tear-off	Base metal fracture	Stir spot fracture
0.7	Tear-off	Tear-off	Tear-off	Tear-off	Tear-off	Tear-off	Base metal fracture	Stir spot fracture
0.9	Tear-off	Tear-off	Tear-off	Tear-off	Tear-off	Tear-off	Base metal fracture	Stir spot fracture
1.1	Tear-off	Tear-off	Tear-off	Tear-off	Tear-off	Tear-off	Base metal fracture	Stir spot fracture

3.3 Conclusions

The following conclusions are obtained from the present work

- FSF joints fabricated on sheet metals of almost same quality delivers lap shear strength of 7.16 kN, which is better than that of other friction stir based joining processes like FSW and FSSW. The mechanical performance tests such as lap shear test and cross-tension test revealed that there is an optimum TPD range (0.5-0.7 mm) at which joint fracture load is maximum. The formability decreases with increase in TPD during uniaxial tensile tests.

- Macrostructure analysis revealed that metallurgical bonding and pin interlocking at different TPDs govern the joint performance during mechanical testing. Low TPDs result in poor mechanical interlocking. Moderate TPDs mark the beginning of metallurgical bonding, which contributes the highest joint fracture load. At higher TPDs, metallurgical bonding and mechanical interlocking contribute the joint strength. Nevertheless, the inferior joint strength of FSF joints at higher TPDs is due to the formation of critical weak zone by the upward deformation of the lower sheet. It is revealed that the extrusion of upper sheet through the pre-drilled hole is not a continuous process.
- Hardness measurement over the cross-section of FSF samples revealed that the effect of TPD on the formation of SZ is almost alike. The frictional heat flux and associated plastic deformation have considerably reduced the hardness of the lower sheet at medium and higher TPDs.
- Joint morphology analysis revealed that TPD has a significant influence on the formation of external features developed on the FSF joints. Lower sheet flash formation is negligible and the anvil cavity filling is complete, at optimum TPD range of 0.5-0.7 mm.
- Failure mode analysis revealed that three CRs, which lead to various failure modes, are the neck of the pin, incomplete metallurgical bonding and upward deformation of the lower sheet. FSF samples fabricated at medium and higher TPDs show tear-off failure and those at lower TPDs show pin pull-out failure. This shows that TPD has a significant influence on the failure modes of FSF samples.

Chapter 4

DFSF joining of AA 5052-H32 and AA 6061-T6 sheets at varying tool plunge depths

In this chapter, a new solid-state spot joining process namely DFSF joining for dissimilar grade aluminum alloy sheets is presented. DFSF process (Indian patent application No: 201741040528) is a modified form of CFSF process discussed in previous chapters. The effect of TPD on the joint strength and joint formation is evaluated through mechanical performance studies, macro/ microstructural analysis, hardness measurement, joint morphology study and failure mode analysis. The optimum tool rotational speed of 500 rpm obtained from chapter 2, the sheet metal combination employed in chapter 2 and optimum TPD of 0.5 mm obtained from chapter 3 are adopted in the present work.

4.1 Introduction

4.1.1 DFSF: A modified form of CFSF process

CFSF joining of aluminum alloys is attempted with a view of achieving joint strength by simultaneous mechanical interlocking and metallurgical bonding, and with an intention to eliminate hook defect and pin hole defect in FSSW process. However, FSF joints have not fulfilled all the above-mentioned requirements due to following reasons.

- The anvil cavity plays a significant role in realizing mechanical interlocking in FSF joints. The mechanical interlock happen due to the formation of a rivet head from the upper sheet metal extruded through the pre-drilled hole. During the plunge of the stir tool, the lower sheet metal also deforms and occupies the anvil cavity in FSF process. Therefore, the upper sheet metal extruded through the pre-drilled hole has not achieved the shape of an exact rivet (Fig. 4.1) in contradiction to that observed for aluminum alloy-steel sheet FSF joints, reported by Lazarevic et al. (2013). Therefore, the quality of mechanical interlocking is poor in FSF process.

  In order to prevent the deformation of the lower sheet, the anvil cavity in FSF process set up is to be avoided. If mechanical interlocking can be realized in some other way and if the anvil cavity can be eliminated, the time required for

extrusion of upper sheet into the anvil cavity will be saved, which ultimately results in shorter joint fabrication time. In addition, this will also reduce the tooling cost.

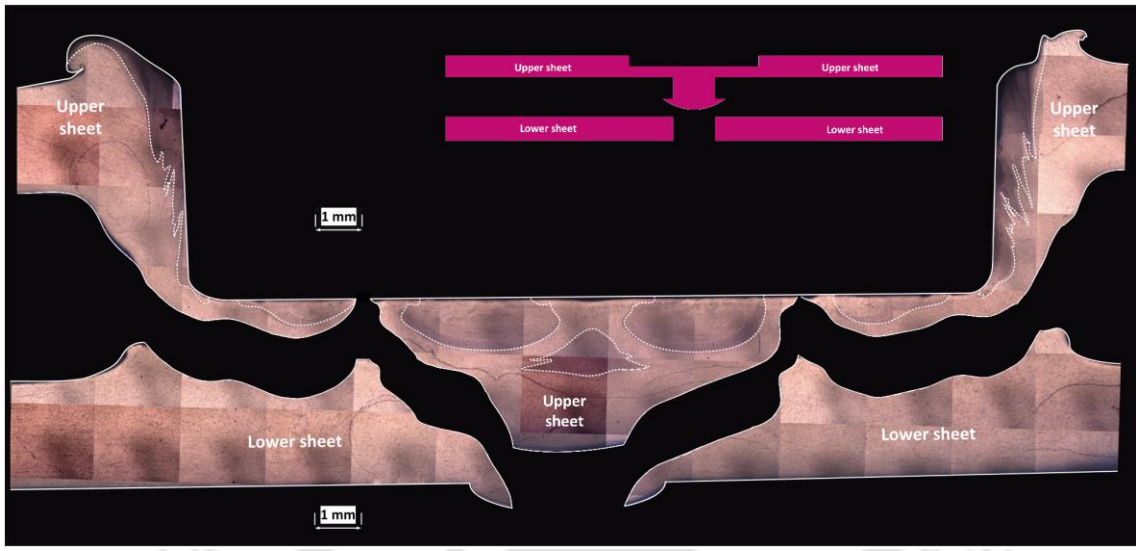

Figure 4.1. The macrostructure of FSF joint fabricated at 1500 RPM with upper sheet and lower sheet separated along the boundary. Inset shows the schematic representation of exact rivet head formation in FSF joints.

- In FSF process, the pin formation occurs by the continuous extrusion of upper sheet metal through the pre-drilled hole during the plunge of the stir tool. However, in chapter 2, the macrostructure analysis shows that with increase in TPD, the extruded pin disconnects from the upper sheet due to closure of the pre-drilled hole (Fig. 3.4c). The upper sheet metal is not able to extrude up to the bottom of the anvil cavity prior to the deformation of the lower sheet. Therefore, the pin extrusion is not continuous in FSF process, which further affects the mechanical interlocking. If the anvil cavity is eliminated, the upper sheet metal will occupy the pre-drilled hole and the deformation of the lower sheet can be purposefully used for mechanical interlocking of the extruded upper sheet metal.
- Other than this, FSF process possesses a disadvantage also. Severe upward deformation of the lower sheet hinders the material continuity of the upper sheet, thereby acting as a critical weak zone, CR3 (Fig. 3.5f) resulting in upper sheet thinning. The upward deformation of lower sheet in FSF process is analogous to hook defect in FSSW process resulting in failure of the joint.

Therefore, from the mechanical performance and joint formation aspects, CFSF process is not the best choice for fabricating spot joints in dissimilar grade alloys sheets of same metal such as aluminum.

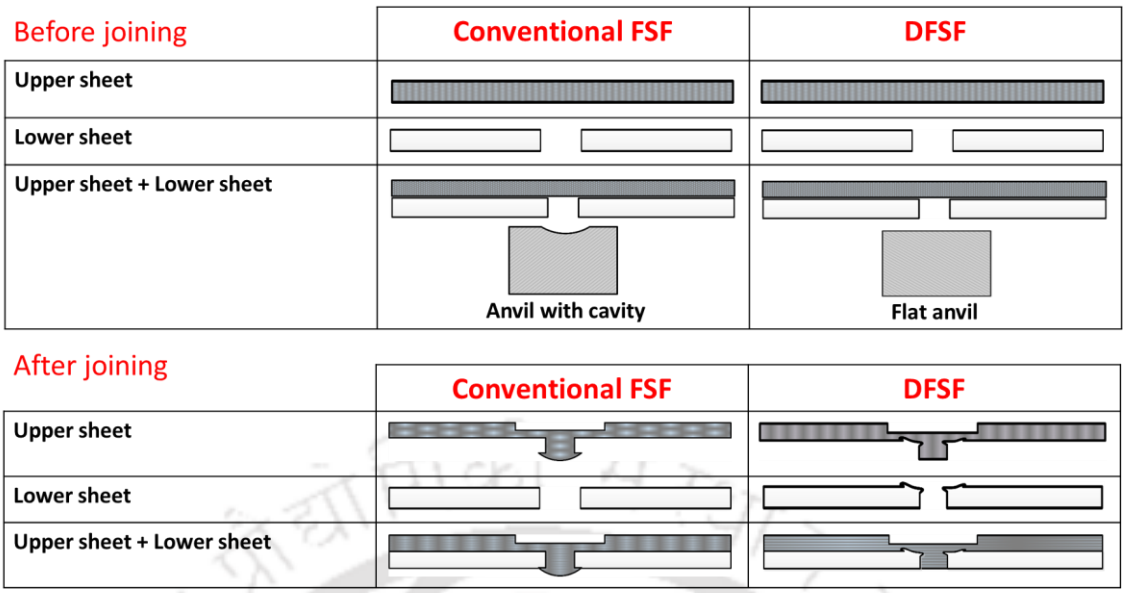

Figure 4.2. Comparison of the transformation of upper sheet and lower sheet in CFSF and DFSF processes

It is to be taken into consideration that the FSF joints in aluminum alloys achieved significant improvement in strength as compared to FSSW joints is same material combination as reported in chapter1 and chapter 2. The major part of the joint strength is contributed by the metallurgical bonding than mechanical interlocking. Therefore, the potential of FSF process for producing high strength joints in aluminum alloys can be further improved, if suitable process modifications can be proposed. The effectiveness of joint formation can be further improved to achieve simultaneous mechanical interlocking and metallurgical bonding. Following factors are to be taken care for achieving above-mentioned aspects.

- The discontinuous extrusion of the upper sheet pin should be prevented by modifying the anvil cavity such that the length of the extruded pin will be reduced.
- The closure of the pre-drilled hole should be avoided and effectively used for mechanical interlocking of the extruded pin.

In this chapter, a new process namely DFSF process has been proposed after incorporating above modifications in the process set up. The anvil block is modified suitably and the tendency of closure of the pre-drilled hole is suitably used for mechanical interlocking by generating inward collar. Moreover, the hook defect and pin hole defect are eliminated as added advantages in the DFSF process. Fig. 4.2 shows the comparison of the transformation of upper sheet and lower sheet in CFSF and DFSF processes, before joining and after joining. The modification is done only in the experimental set up by employing flat anvil block without hemispherical cavity. The fabrication time in DFSF

process is significantly reduced because the joining process can be completed at low TPDs such as 0.5 mm.

4.2 Methodology

4.2.1 Principle

DFSF process comprises a pinless stir tool and a flat backing plate (anvil block) without anvil cavity. The pinless stir tool, with cylindrical shape and flat face, stir the upper sheet metal and generate sufficient frictional heat flux and plastic deformation during the downward plunge. Provisions are provided for clamping the sheets in lap configuration over the backing plate. The process sequence is schematically illustrated in Fig. 4.3. The lower sheet has a pre-drilled hole to realize the extrusion of upper sheet metal. The stir tool, work pieces and clamps are arranged as shown in Stage 1. When the stir tool is rotated and moved downwards, the contact spot at the upper sheet is softened due to frictional heat generated by the stirring action of the tool. Extrusion of the stirred upper sheet metal occurs through the pre-drilled hole in the lower sheet during the downward plunge of the tool. Meanwhile, the lower sheet also receives conducted heat from the stir spot. Further plunge of the stir tool deforms the pre-drilled hole such that neck formation takes place around the extruded upper sheet metal. The neck formation is realized by the growth of an inward collar from the upper part of the pre-drilled hole. Thus, the extruded upper sheet metal is locked in the pre-drilled hole of the lower sheet (Stage 2). The inward collar, which acts as a mechanical interlock prevents the retraction of the upper sheet metal. In addition, the two sheets are also metallurgically bonded at the flat sheet interface below the joint spot. Thus, mechanical interlocking and metallurgical bonding enables the formation of the spot joint in DFSF samples.

The growth of inward collar occurs throughout the circumference of the top of pre-drilled hole in the lower sheet. This enables neck formation in the extruded upper sheet metal, which prevents its retraction from the pre-drilled hole. The inward collar formation from the lower sheet begins only after complete extrusion of the upper sheet pin. Therefore, the pin formation in not interrupted in between the course of DFSF joint formation. The inward collar formation is first of such a kind observed in a friction stir based joint.

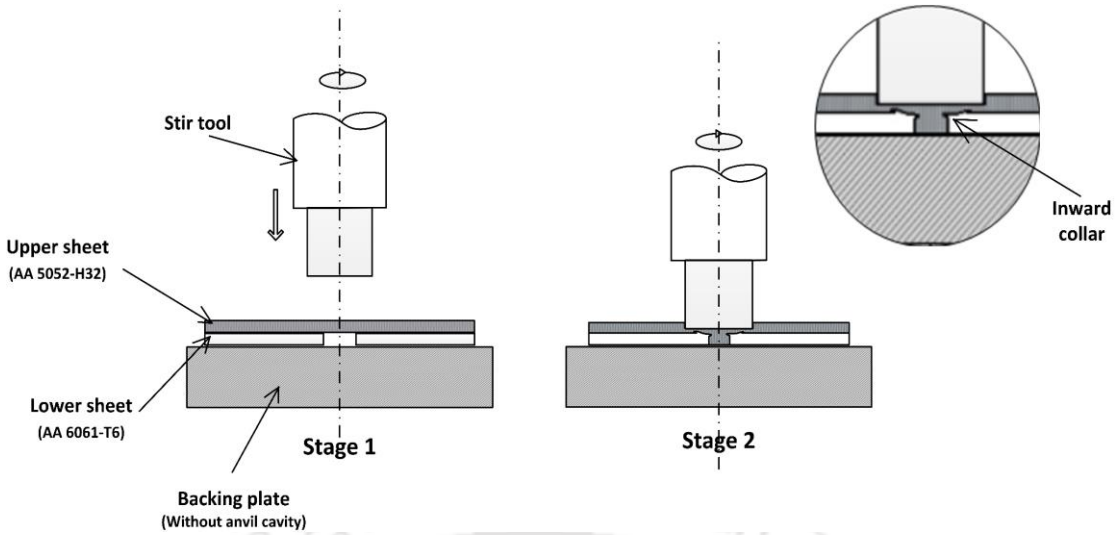

Figure 4.3. DFSF stages (Not to scale)

Unlike other spot joining processes, the pre-drilled hole is deliberately introduced into the lower sheet to accomplish the mechanical interlocking. There is a provision for producing single pin and multi pin configurations using this process, provided the holes are to be drilled into the lower sheet prior to the joining operation. Unlike in CFSF process, this process does not require an cavity in the anvil block to enable rivet head formation. Unlike in FSSW process, the usage of pinless tool in DFSF process prevents the formation of pin hole in the joint spot. The DFSF joint has similar external appearance as that of a pinless FSSW joint, however, the mode of joint formation is different. The joint formation and the strength is governed by the process parameters such as RPM, TPD and the geometric features such as TD and hole configuration.

4.2.2 DFSF Experiments

A mild steel backing plate capable of holding various metal strips of required dimensions is fabricated and the sample preparation is carried out on a milling machine (Kirloskar Viking KTM 40). The stir tool, backing plate and the clamps constitute the basic experimental set up as shown in the Fig. 4.4. The features of the stir tool are given in table 4.1.

The standard properties of the sheet metals are presented in Section 2.1.2. The strength and hardness of AA 6061-T6 sheet is better than that of AA 5052-H32 sheet. Therefore, the former is selected as the lower sheet.

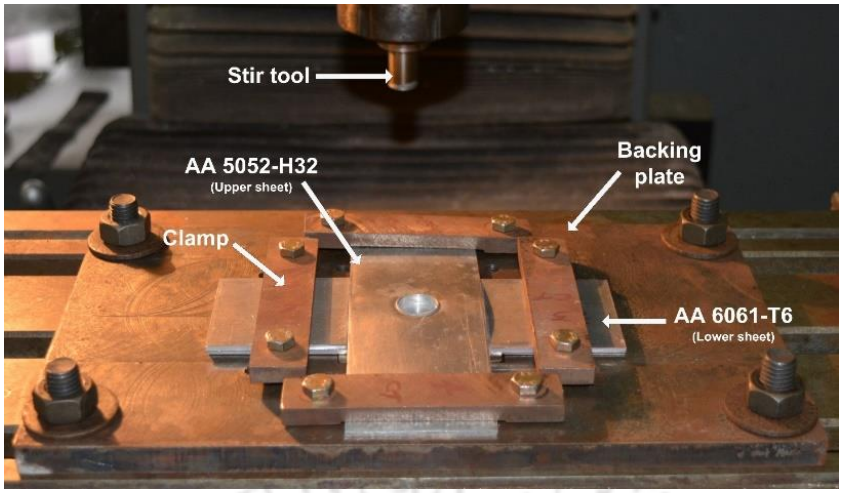

Figure 4.4. Experimental setup for a DFSF process

Table 4.1. Stir tool features

Material	H13 tool steel
Feature	Pinless
Shoulder dia.	14 mm
Shoulder length	25 mm

The pre-drilled HD in the lower sheet is selected as 3 mm, to enable the extrusion of pin with sufficient strength and to prevent the closure of the hole during tool plunge. The stir tool center and pre-drilled hole center are to be aligned along a straight line to enable proper joint formation. The effectiveness of the DFSF joint formation is studied by varying the TPD to multiple levels, with lower levels at 0.25 mm and 0.3 mm, medium levels at 0.35 mm and 0.4 mm, and higher levels at 0.45 mm and 0.5 mm. Trial experiments shows that joint fabrication is not possible with a TPD below 0.25 mm for 2 mm thick aluminum sheets. All other parameters namely plunge rate, tool rotational speed, direction of tool rotation are kept constant at 0.002 mm/s, 500 rpm and clockwise direction respectively, throughout the TPD levels. The values are decided as per previous works and by conducting a few trials before actual experiments. Two samples are fabricated per TPD and the average output is considered for further analyses.

4.2.3 Mechanical performance tests

Details of mechanical performance tests is discussed in section 2.1.3. In addition, lap shear test is conducted on samples joined with CFSF and FSSW processes to compare their fracture load with DFSF samples. A pinless stir tool of 14 mm shoulder dia. with an anvil cavity dia. of 3.5 mm and cavity depth of 0.55 mm are employed for CFSF process. A pre-drilled hole of 3 mm is fabricated in the lower sheet. FSSW process is conducted

with stir tool having pin and with pinless stir tool. A stir tool of 14 mm shoulder dia. with a pin of 4 mm dia. and 1 mm length is used for FSSW with pin. A stir tool of 14 mm dia. having flat face without pin is used for pinless FSSW. All other parameters are kept same as that of DFSF. Previous literature show that, stir tool with 14 mm dia. was also employed in FSSW of aluminum alloys (Paidar et al., 2014). Frictional heat generation and subsequent plastic deformation is the principle underlying all these solid-state spot joining techniques.

4.2.4 Macro/ microstructure, hardness measurement and joint morphology analysis

Details of macrostructure analysis, hardness measurement and joint morphology analysis is discussed in section 2.1.4. For microstructure analysis, the images are obtained using optical microscope (Zeiss Axiocam MR3 make) at 200X magnification. The grain structure, grain size transition and grain size measurement at various zones of interest in the joint are obtained with the line intercept method using Zeiss Axiovision software as per ASTM E-112 standard. Furthermore, the impact of excessive TPDs such as 0.7 mm and 0.9 mm on the joint strength and joint formation is also evaluated through lap shear test and macrostructure analysis.

Indentations for Vickers hardness measurements are performed in two arrays with 2 mm spacing in between the indentations over the sample cross-section. Upper array, locations A to O, covers the upper sheet and lower array, locations P to X, covers the lower sheet, as shown in Fig. 4.5. The lower array also covers the extruded region from the upper sheet. Upper and lower arrays are located at depths 1 mm from the upper surface of upper and lower sheets, respectively.

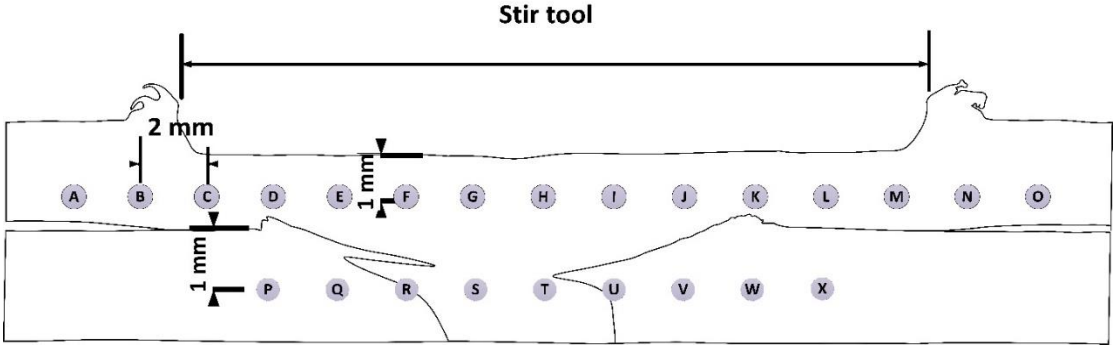

Figure 4.5. Hardness measurement locations along the joint cross-sections (Dimensions not to scale)

Joint morphology analysis involves the quantification of certain external macroscopic joint features whose formation is profoundly influenced by the change in

TPD. The morphological features include defects such as UB, USFW and USFH, and SST. The joint features are shown in Fig. 4.6.

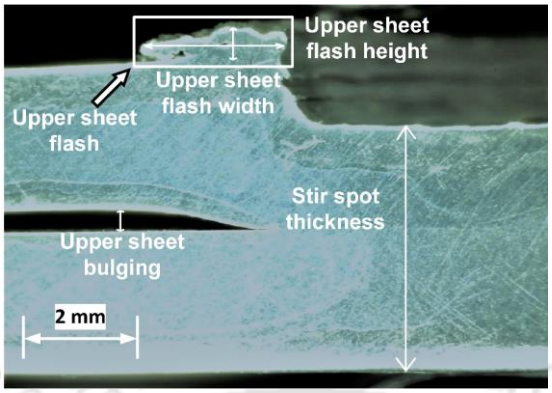

Figure 4.6. Morphological features measured in the DFSF joint cross-section

4.3 Results and Discussion

The effect of TPD on the fracture load and failure modes of DFSF joints are discussed in the following sections. The macrostructure and microstructure analyses, hardness variation and joint morphology analysis are also presented.

4.3.1 Mechanical performance tests

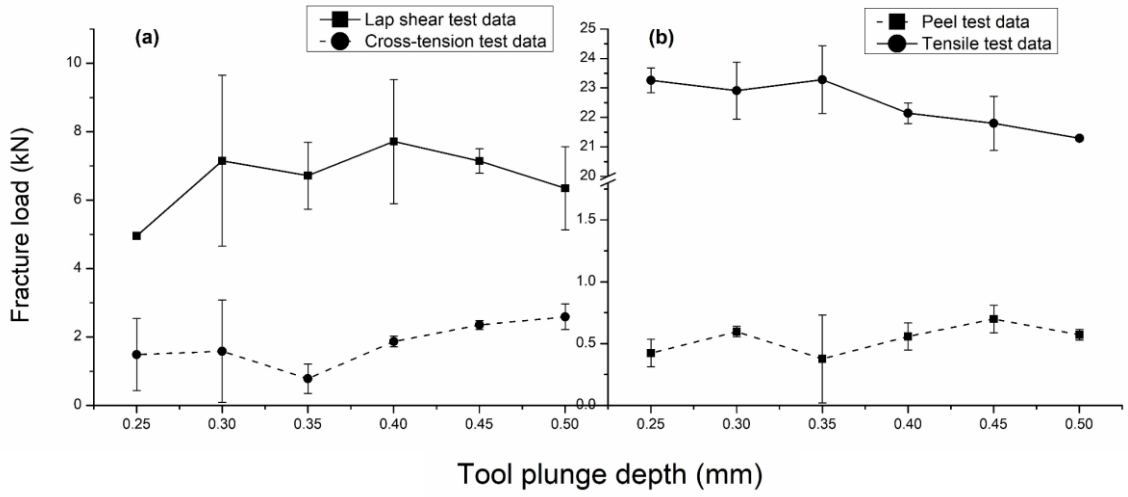

Figure 4.7. Comparison of fracture loads for various TPDs during mechanical performance tests of DFSF samples

Fig. 4.7 shows the effect of TPD on the fracture load obtained from mechanical performance tests. It is observed that the fracture load remains almost same throughout the range of TPDs for lap shear test, cross-tension test and peel test. The variation is within 2 kN. However, the large error bars obtained for TPDs up to 0.4 mm are not reliable because

joint fracture load shows considerable fluctuation from sample to sample with same TPD level.

The DFSF samples show maximum fracture loads (average value) about 7.7 kN at 0.4 mm TPD, 2.5 kN at 0.5 mm TPD and 0.7 kN at 0.45 mm TPD during lap shear test, cross-tension test and peel test, respectively. The mechanical performance is appreciable within this TPD range. At any particular TPD, lap shear strength is observed to be maximum and peel strength to be minimum and cross-tension strength stands in between. The entire TPD range, 0.25 mm to 0.5 mm, is narrow that variation in the fracture load seems to be insignificant for the mechanical performance tests. Therefore, the effect of higher TPDs on the joint fracture load is further evaluated and discussed separately in section 4.3.8. However, the lowest lap shear fracture load obtained at 0.25 mm TPD shows that the chance of formation of a high strength DFSF joint at the lower TPDs is uncertain. DFSF samples shows a decrease in fracture load with increase in TPD during uniaxial tensile test. The geometrical inhomogeneity developed due to reduction in thickness at the stir spot, with increase in TPD, has resulted in slight decrease in the forming load of about 2 kN.

The average extension for lap shear test samples is 0.82 mm and for uniaxial tensile test samples is 3.73 mm respectively for the entire range of TPD. The peculiar nature of cross-tension test and peel test in which bending and unbending of metal strips has contributed some extra amount of extension before failure at certain TPDs. Therefore, the average extension at fracture for cross-tension samples is 8 mm and peel test samples is 5.47 mm respectively. Thus, DFSF samples show considerable extensibility before failure under variable loading conditions generated in the mechanical performance tests.

It can be concluded from the mechanical performance tests that such a small TPD range has no significant influence on the fracture load and extensibility of the DFSF joints. However, stable performance is recorded at higher TPDs such as 0.45 mm and 0.5 mm, when considering acceptable error bars. Therefore, the effect of subsequent higher TPDs are to be evaluated.

4.3.2 Comparison of DFSF joint with CFSF and FSSW joints

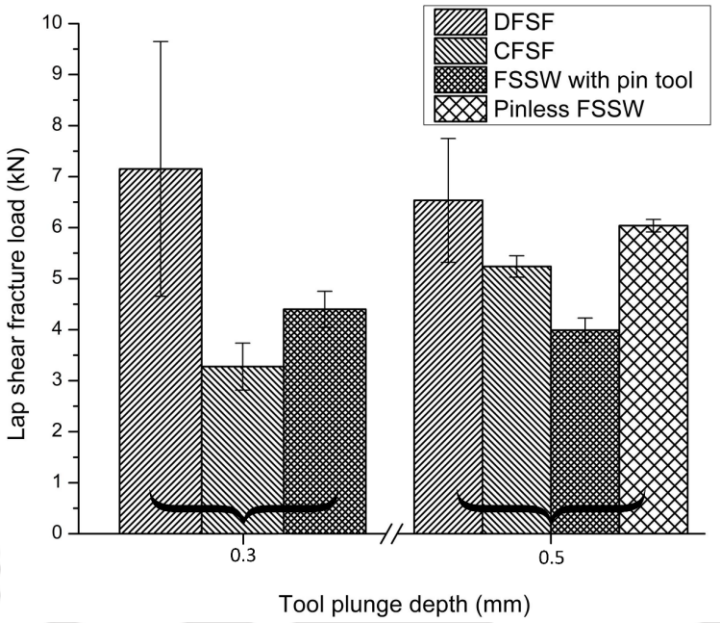

Figure 4.8. Comparison of lap shear fracture load of DFSF samples with CFSF and FSSW samples fabricated in the present work

The joints fabricated with DFSF process are compared with the joints fabricated with CFSF and FSSW processes. The comparison of lap shear fracture load of samples fabricated at 0.3 mm and 0.5 mm TPDs is shown in Fig. 4.8. At lower TPD of 0.3 mm, significant improvement in fracture load is observed for DFSF samples than that of CFSF sample and FSSW sample with stir tool having pin. However, the repeatability is unreliable for DFSF sample at this lower TPD level. It can be observed that at 0.5 mm TPD, the DFSF samples possess lap shear fracture load, which is 25% better than CFSF and 64% better than FSSW samples fabricated with tool having pin. However, 0.5 mm TPD pinless FSSW samples shows better fracture load upto 92% of that of DFSF samples. Therefore, pinless FSSW process and DFSF process can contribute better mechanical performance than that of CFSF and pinned tool FSSW processes.

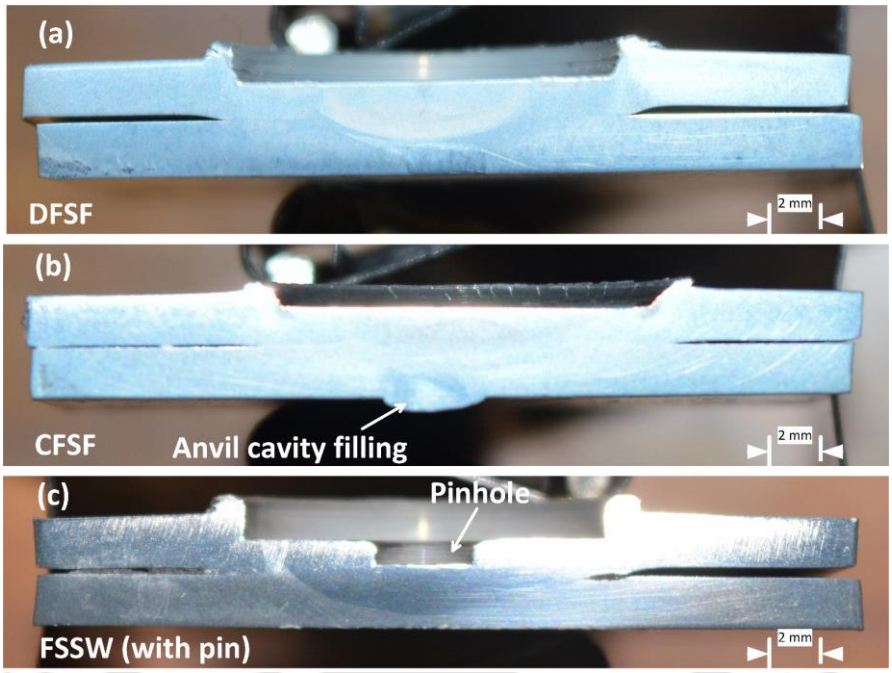

Figure 4.9. Cross sections of (a) DFSF, (b) CFSF and (c) FSSW samples fabricated in the present work at 0.5 mm TPD

The pinhole left by the pinned tool in an FSSW process has a negative impact on the joint strength. Pin hole defect impairs the joint strength by reducing the effective cross sectional area at the stir spot. The hook defect in FSSW process results in thin metal zone formation, which also reduces the joint strength. Literature shows that the increase in the tool pin length results in extensive stirring of upper and lower sheet metals so that the lower sheet tends to lift upwards leading to hook formation and upper sheet thinning (Tozaki et al., 2007). It was reported by Garg and Bhattacharya, 2017c that pinless FSSW samples also possess hook defect formation, which eventually leads to impaired joint strength.

DFSF process relies on the same principles of FSSW process. DFSF process has the advantage of eliminating the pin hole defect and the hook defect. The pinless flat stir tool prevents the pinhole formation. Absence of stir mixing of the two sheets and occurrence of extrusion of upper sheet prevent hook defect formation and subsequently, avoids upper sheet thinning.

The comparison of the cross sections of DFSF, CFSF and FSSW samples is shown in Fig. 4.9. It shows that in addition to the superiority in strength, the aesthetic appearance of DFSF samples is much better than its counterparts. Absence of anvil cavity filling (rivet like head formation), as seen in CFSF, and absence of pinhole formation, as seen in FSSW, result in better physical appearance and improvement of the mechanical performance of DFSF joints in lap shear test. Rivet head formation in CFSF samples restrict its application

to sliding parts. The pinhole left by the pinned tool in FSSW samples deteriorate its shear strength. DFSF joints possess flat base and flat stir spot with no such protruding features, which also differentiate it from samples fabricated by clinching process and SPR. Therefore, DFSF process can be preferred for joining sheet metals, where performance quality and aesthetic appearance matters significantly, for instance the body panels of automobiles. The pinless flat stir tool employed in DFSF process is simpler than that of refill FSSW process (Shen et al., 2018). Complex tool operating mechanism is also not required. Furthermore, drilling a hole in lower sheet for DFSF process is comparatively easier than employing second stage refill FSSW for sealing the pinhole of an FSSW joint (Reimann et al., 2016).

The external appearance of the cross-sections of pinless FSSW joint and DFSF joint are same and the joint strength of pinless FSSW joints is comparable with that of DFSF joints. However, for pinless FSSW joints, the hook defect is not eliminated and the material flow in the through thickness direction is comparatively less (Li et al., 2018). This drawback is solved in DFSF joints by the extrusion of upper sheet through the pre-drilled hole in the lower sheet. It was also reported that the employing pinless tool in FSSW of thicker sheets is ineffective and pinless tool induces severe axial load on the FSSW tool holding set up (Cox et al., 2014a). However, the pinless stir tool is sufficient for DFSF process irrespective of the sheet thickness because intermixing of upper and lower sheets are not required. Literature shows that, similar to DFSF process, mechanical interlocking was also established through complete filling of the extruded aluminum inside the pre-drilled hole in the steel sheet during friction stir riveting process (Evans et al., 2016). The riveted structure acted as an additional clinch or a normal bolting mechanism in these joints.

Joining dissimilar grade alloy sheets of same metal in DFSF process is difficult. In this case, the chance of severe deformation of the lower sheet in the stir spot is higher under chosen conditions. Excessive deformation of the lower sheet may results in pre-drilled hole closure and impaired joint strength. Therefore, unlike FSW and FSSW processes, dwell time is not favorable for DFSF process, and the heat generation as well as the stirring at the joint spot are to be properly controlled. Dwell stage adds extra time after tool plunge so that severe plastic deformation and excessive frictional heat flux can eventually damage the mechanical interlocking and metallurgical bonding. The process can be completed quickly without dwell stage. It is understood that drilling a hole in DFSF

process consumes extra fabrication time and cost. This is compensated by obtaining better joint strength by simultaneous mechanical interlocking and metallurgical bonding.

4.3.3 Joint formation analysis through macrostructure

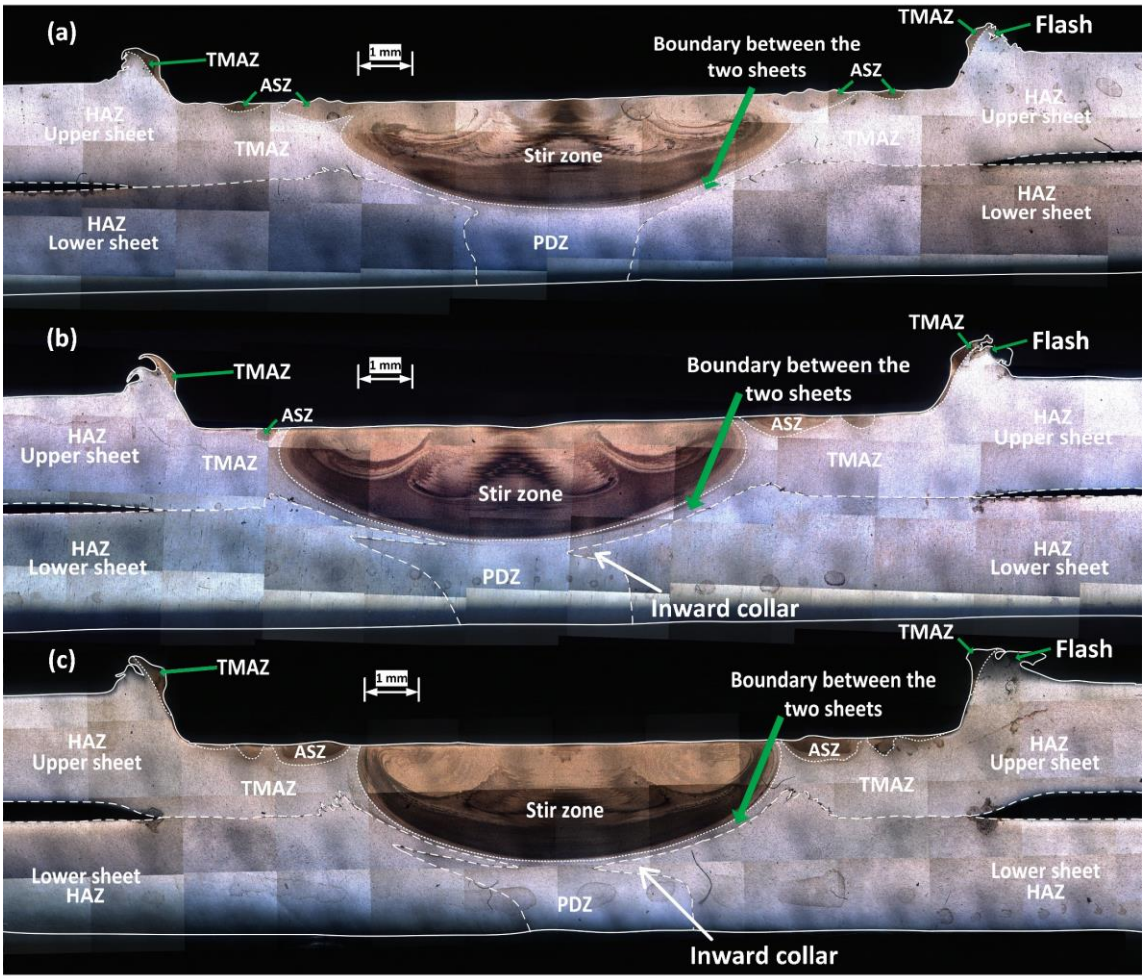

Figure 4.10. Joint macrostructure of DFSF samples fabricated at (a) 0.3 mm (Lower TPD), (b) 0.35 mm (Medium TPD), (c) 0.5 mm (Higher TPD)

The DFSF joint formation under varying TPD range is explained with macro structure analysis, for which samples fabricated at 0.3 mm (lower), 0.35 mm (medium) and 0.5 mm (higher) TPDs are chosen. The complete macrostructure of the DFSF joint cross-section, with schematic representation of various zones and metal flow directions in the joint, are shown in Fig. 4.10 and Fig. 4.11 respectively. The various zones that can be identified in DFSF joint cross-section are SZ, TMAZ, PDZ, ASZ and HAZ. Similar zones (SZ, TMAZ and HAZ) were also identified in FSSW joints (Bakavos et al., 2011) and refill FSSW joints (Ding et al., 2017). However, ASZ and PDZ are identified only in DFSF joints and CFSF joints.

Perfect metallurgical bonding is observed at all TPDs with no interfacial gaps visible at the bonded interface. The SZ is located at the center of the tool impression, where the face of the tool touches the upper sheet and a unique pattern is produced by the stirring of the upper sheet metal. The 'onion ring' pattern commonly seen in FSW and FSSW SZs is clearly observed in DFSF joints also. However, unlike in FSW and FSSW, the SZ is constituted by the upper sheet only. The SZ is symmetric and possesses a shallow 'U' shape with maximum depth at the center. Similar 'basin' shaped SZs was also reported during probeless FSSW process (Li et al., 2018) and refill FSSW process (Ding et al., 2017). Therefore, the amount of work piece deformation under the tool varies from center to the periphery of the joint. The occurrence of radially outward metal flow in the SZ of pinless FSSW samples was reported by Garg and Bhattacharya, 2017a. Similar axisymmetric flow is also observed in the SZ of DFSF samples (Fig. 4.10(a-c)). In other words, the material present at the center of the stir spot flows outward axisymmetrically in a circulating swirl pattern with the downward tool plunge. This flow pattern is represented in the SZ of DFSF samples (Fig. 4.11(a-c)).

The PDZ is located just below the SZ. Here the stirring of the plasticized metal is absent, instead the plasticized metal is forged, and metal flow occurs in radial direction from the stir spot periphery towards the center and subsequently through the pre-drilled hole due to compressive pressure generated by the downward movement of the stir tool. The SZ and the PDZ can be clearly distinguished at all TPDs and both constitute the parts of upper sheet only. It is believed that while the material in the SZ tends to trace circular motion with the stir tool, the material in the PDZ undergoes radially inward motion into the pre-drilled hole.

The TMAZ is visible on the region surrounding the SZ as well as on the sidewalls of the joint as shown in Fig. 4.10(a-c). On the periphery of the SZ where the stirring of the upper sheet metal is absent, the plastic deformation occurs by the plunge of the tool and the frictional heat flux conducted from the SZ. The frictional contact of the lateral surface of the rotating stir tool over the sidewalls of the stir spot at higher RPMs also contribute the formation of TMAZ. This ring shaped region is subjected to plastic deformation under the rubbing contact of the stir tool and frictional heat generated in this region. In addition, the upper sheet flash (also shown in Fig. 4.6) is also visible in the sidewalls of the joint.

The ASZs are ring-shaped stirred regions surrounding the central SZ. These are isolated SZs located on both sides of DFSF joint cross-section. The main reasons for the formation of ASZs are the downward plunge of the stir tool, the extrusion of the upper

sheet towards the pre-drilled hole and the upward deformation of the lower sheet. When the rotating stir tool is plunged, along with the extrusion of the upper sheet, the SZ depth at the center increases towards the pre-drilled hole. Nevertheless, the periphery of the SZ is prevented from expansion by the lower sheet. Consequently, the SZ periphery becomes thinner and a part of the SZ separates in the form of an annular ring. This constitutes the ASZ. Furthermore, the formation of the ASZ is also accelerated by the upward deformation of the lower sheet. Similar ASZs are present in CFSF joints in aluminum alloys, as described in the previous chapters. Upward deformation of lower sheet was also reported during probeless FSSW of aluminum alloys (Li et al., 2018). It was reported that this defect indirectly constrained the width of the SZ in the upper sheet.

The regions of the DFSF joint lying outside the above four zones (but including the lower sheet) constitute the HAZ. Unlike SZ, PDZ, TMAZ and ASZ, the HAZ is not subjected to significant plastic deformation. However, the frictional heat flux has generated considerable changes in both the mechanical properties such as hardness and the metallurgical characteristics.

4.3.3.1 Lower TPDs: 0.25 mm and 0.3 mm

The joint macrostructure and schematic of metal flow directions at lower TPD of 0.3 mm is shown in Fig. 4.10a and Fig. 4.11a. At lower TPDs, the extent of plunge of the stir tool is sufficient to plasticize and extrude the upper sheet metal to completely fill the pre-drilled hole in the lower sheet. A mechanical interlocking is slightly established through the partial deformation of the upper part of the pre-drilled hole. This locks the extruded upper sheet metal inside the hole. However, the exact collar formation is not observed. The partial mechanical interlocking might have resulted in lower lap shear fracture load. ASZ has started separating from the central SZ. The UB beyond the sidewalls is also visible. Similar observation is also expected in 0.25 mm TPD DFSF samples.

4.3.3.2 Moderate TPDs: 0.35 mm and 0.4 mm

The joint macrostructure and schematic of the metal flow directions at moderate TPD of 0.35 mm is shown in Fig. 4.10b and Fig. 4.11b. With further increase in TPD to moderate range, the mechanical interlocking between the two sheets has become more prominent. The PDZ has perfectly locked inside the pre-drilled hole. The collar formation

is complete. An upward deformation of the lower sheet slightly away from the pre-drilled hole due to the plastic deformation is also visible. Similar observation is also expected in 0.4 mm TPD DFSF samples.

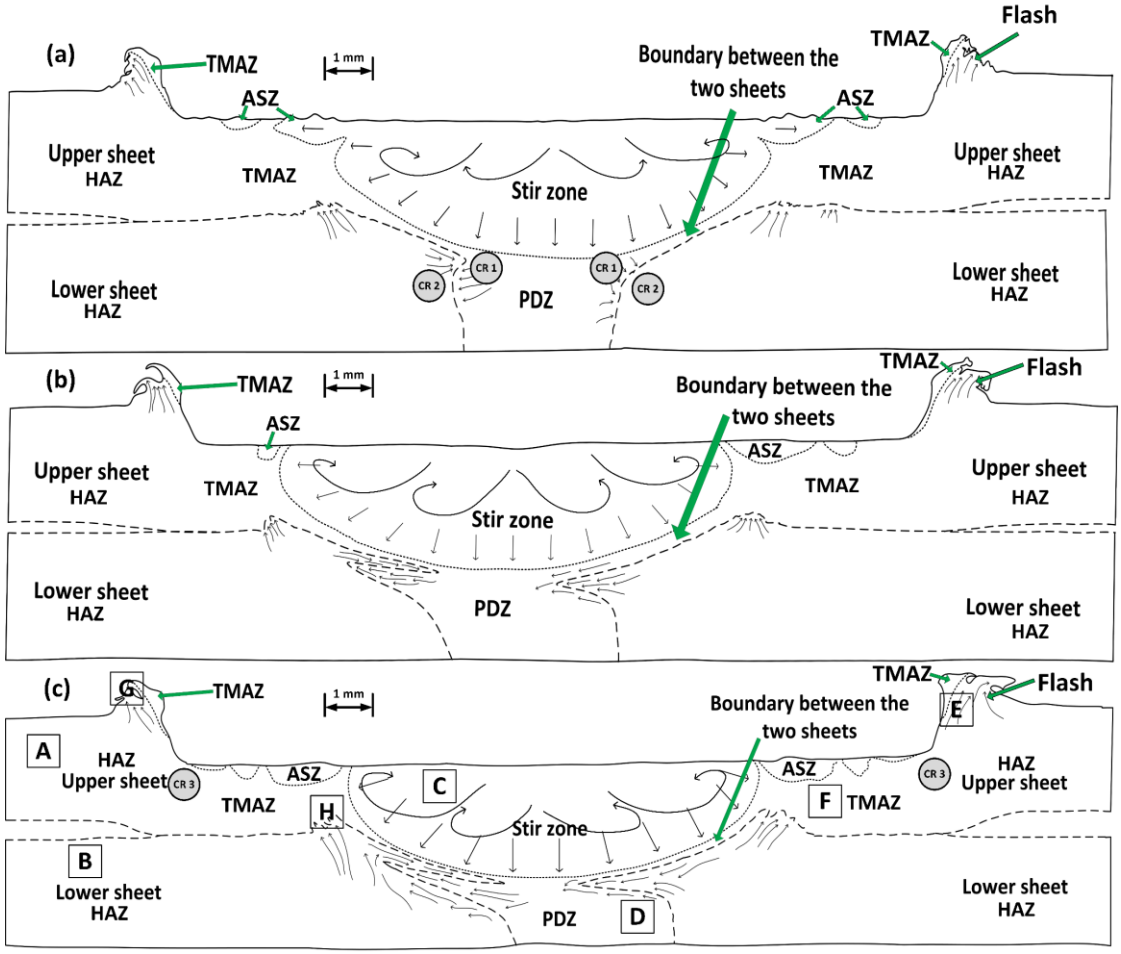

Figure 4.11. Schematic representation of the DFSF joint cross-sections at (a) 0.3 mm, (b) 0.35 mm, (c) 0.5 mm TPDs with metal flow directions indicated

Under moderate TPDs, reasonably good joints are fabricated with improved joint strength. Such an improvement is mainly contributed by the enhancement in mechanical pin interlocking along with sufficient metallurgical bonding.

4.3.3.3 Higher TPDs: 0.45 mm and 0.5 mm

The joint macrostructure and schematic of metal flow directions at higher TPD of 0.5 mm are shown in Fig. 4.10c and Fig. 4.11c. At higher TPDs, the upper part of the pre-drilled hole has further deformed to such an extent that the mechanical interlocking has become perfectly established. Perfect collar formation has been observed. However, further collar growth may result in closure of the pre-drilled hole. ASZ, which is fully separated from the central SZ, can be clearly distinguished. However, a major

improvement in strength is not obtained. Similar observation is also expected in DFSF samples at 0.45 mm TPD.

To summarize, the DFSF joint strength is mainly contributed by mechanical interlocking and metallurgical bonding. The metallurgical bonding is established throughout the entire TPD range, while the mechanical interlocking has become perfect with increase in the TPD. Therefore, a slight change in TPD can contribute a significant improvement in the mechanical interlocking. Medium and higher TPD ranges have resulted in better joint formation. Under chosen operating conditions, an optimum TPD range of 0.35 mm to 0.5 mm is suitable to fabricate a desirable joint made of AA 5052-H32 and AA 6061-T6 sheets as concluded from the evolution of joint macrostructure.

Tool stirring in DFSF process is limited to upper sheet only so that stir mixing of the upper and lower sheets is absent. Therefore, SZ formation has no significant influence on the joint strength, except the fact that stirring induces severe plastic deformation and generation of sufficient heat flux to plasticize and extrude the upper sheet metal through the pre-drilled hole. The size of the SZ remains almost same throughout the entire TPD range. At lower TPDs, a part of the SZ periphery starts to separate from the central SZ as ASZ region. At higher TPDs, the ASZ is completely isolated from the central SZ. In addition, the size of ASZ increases with increase in TPD.

4.3.4 Microstructure characterization

The optical microscopic images of SZ, PDZ, TMAZ, HAZ and flash observed in DFSF joint fabricated at 0.5 mm TPD is shown in Fig. 4.12. The locations from which microscopic images are obtained is shown in Fig. 4.11c with boxes marked with alphabets A to H. The severe plastic deformation and high frictional heat flux lead to recrystallization of grains in and around the SZ of friction stir based joints (Mishra and Ma, 2005). The region under direct contact with the face of the stir tool such as SZ has undergone dynamic recrystallization, while the regions such as HAZ and PDZ have undergone static recrystallization.

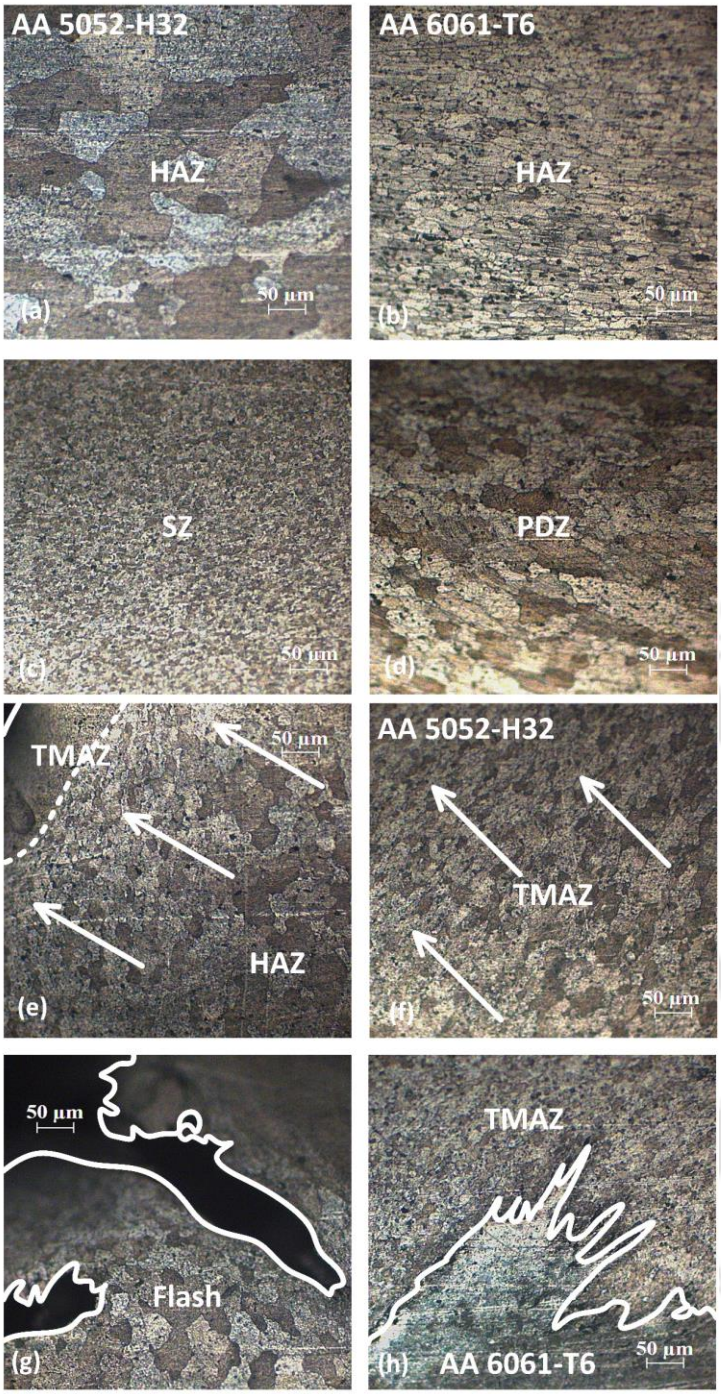

Figure 4.12. Optical microstructure of (a) HAZ of upper sheet, AA 5052-H32 (box A), (b) HAZ of lower sheet, AA 6061-T6 (box B), (c) SZ of the upper sheet (box C), (d) PDZ of the upper sheet (box D), (e) transition from HAZ to TMAZ (box E), (f) Upper sheet flash (box F), (g) Unstirred upper sheet below stir spot (box G) and upward deformation of the lower sheet (box H)

Literature shows that the high stacking-fault energy in aluminum alloys contribute high rate of recovery, therefore, aluminum alloys can easily undergo dynamic recrystallization (Mishra and Ma, 2005). The TMAZ and flash have undergone grain recovery under the frictional heat flux and mild plastic deformation. The bottom of the lower sheet is in contact with the backing plate. Therefore, the heat dissipation in the lower

sheet is faster than that from the upper sheet, consequently the microstructural changes in the upper sheet and the lower sheet are different. Variable grain size is observed in different zones depending upon the heat flux and plastic deformation. Table. 4.2 shows the grain size measurement at various zones and flash in the increasing order.

Table 4.2. Comparison of grain size at various zones and at flash of the DFSF joint

Location	Average grain dia. (μm)
SZ	6.7
TMAZ	18.9
Flash	26.7
HAZ of AA 6061-T6 (lower sheet)	31.8
PDZ	44.9
HAZ of AA 5052-H32 (upper sheet)	75.5

The coarse irregular grains (dia 75.5 μm) observed in the HAZ region of the upper sheet, AA 5052-H32, is bigger than the symmetric grains (dia 31.8 μm) observed in the HAZ region of the lower sheet, AA 6061-T6 (Fig. 4.12(a, b)). It was reported by Mishra and Ma, 2005 that the HAZ region is subjected to thermal cycle without any plastic deformation. As compared to parent sheet grain size (Table 2.3), it is evident that the HAZ grains have undergone static recrystallization and further grain growth due to the frictional heat flux received from the SZ.

Fine equi-axed grains (dia 6.7 μm) are observed in the SZ (Fig. 4.12c). The plastic deformation due to stirring along with frictional heat flux has generated dynamic recrystallization in the SZ. Similar observation was also reported by Garg and Bhattacharya, (2017c), Chiou et al. (2013), Reimann et al. (2016), Mishra and Ma, (2005) and Rana et al. (2018). The fine grain formation in SZ and coarse grain formation in HAZ shows that the annihilation of grain growth is controlled by the extent of plastic deformation. The grain growth in the SZ is arrested by severe plastic deformation due to stirring. However, the HAZ region, which has not undergone any plastic deformation, possesses significant grain growth.

PDZ grains are coarser than SZ grains and TMAZ grains. Irregular coarse grains (dia 44.9 μm) observed in the PDZ region (Fig. 4.12d) are about half the size of the upper sheet HAZ grains. The PDZ region is statically recrystallized with further grain growth under frictional heat flux and moderate plastic deformation by extrusion. However, the PDZ has not undergone severe plastic deformation induced by stirring.

Highly deformed grains (dia 18.9 μm) are also visible in the TMAZ region (Fig. 4.12e), but larger than SZ grains. Change in the grain structure of TMAZ is induced by the

direct contact of the lateral surface of the rotating stir tool on the sidewalls of the stir spot. Plastic deformation and frictional heat flux result in change in grain structure of TMAZ region located outside the SZ. However, that is not sufficient to induce recrystallization (Mishra and Ma, 2005). The frictional heat flux and plastic deformation have brought recovery of the TMAZ grains. Recovered grains were also observed in the TMAZ region during FSW of AA 5083-O aluminum alloys (Sato et al., 2001).

A decrease in the grain size is observed from HAZ towards the TMAZ as pointed by the arrows (Fig. 4.12e). Fig. 4.12f shows the unstirred TMAZ region below the stir spot, where the grain size decreases towards the top of the stir spot, as pointed by the arrows. It shows that the grains become finer towards the SZ. Frictional contact of the flat stir tool face has induced fine grain formation at the tool-upper sheet interface region.

Slightly larger recovered grains (dia 26.7 μm) are observed in the flash formed (Fig. 4.12g). The flash is located a little far from the lateral surface of the stir tool. Stirring is absent in this region, but frictional heat flux and plastic deformation are prominent. The enlarged view of the upward deformation of the lower sheet is shown in Fig. 4.12h. It can be ensured that the hook structure is not formed from this deformed lower sheet. This is because the stir tool has not penetrated much into the lower sheet. Shen et al. (2018) reported similar observation during refill FSSW. Here, the upward deformation of the lower sheet had enabled mechanical interlocking and metallurgical bonding at the sheet interface instead of hook formation.

4.3.5 Hardness variation

Hardness variation in DFSF samples can be analyzed by comparing the hardness profile over the cross-section of selected DFSF samples from lower (0.3 mm), medium (0.35 mm) and higher (0.5 mm) TPDs. The hardness distribution along the upper array and lower array of indentations are shown in Fig. 4.13a,b respectively. Similar hardness distribution is observed in each of the upper and the lower arrays of indentations. Therefore, the change in TPD within the chosen range has little influence on the hardness distribution.

The hardness in the upper array and lower array are reduced from the respective parent metal hardness. As shown in Fig. 4.13a, 29% decrease in hardness is observed along upper array in the TMAZ region (outside the SZ) than the parent metal hardness. Higher hardness is observed from locations G to J inside the SZ along the upper array. This is

because the plunge of the stir tool has resulted in the forging and extrusion of the plasticized metal inside the pre-drilled hole at the center of the DFSF joint. Slight change is observed in the maximum hardness with change in TPD. Identical SZ formation observed at all TPDs can also be reconfirmed by the presence of similar hardness profiles along the upper array.

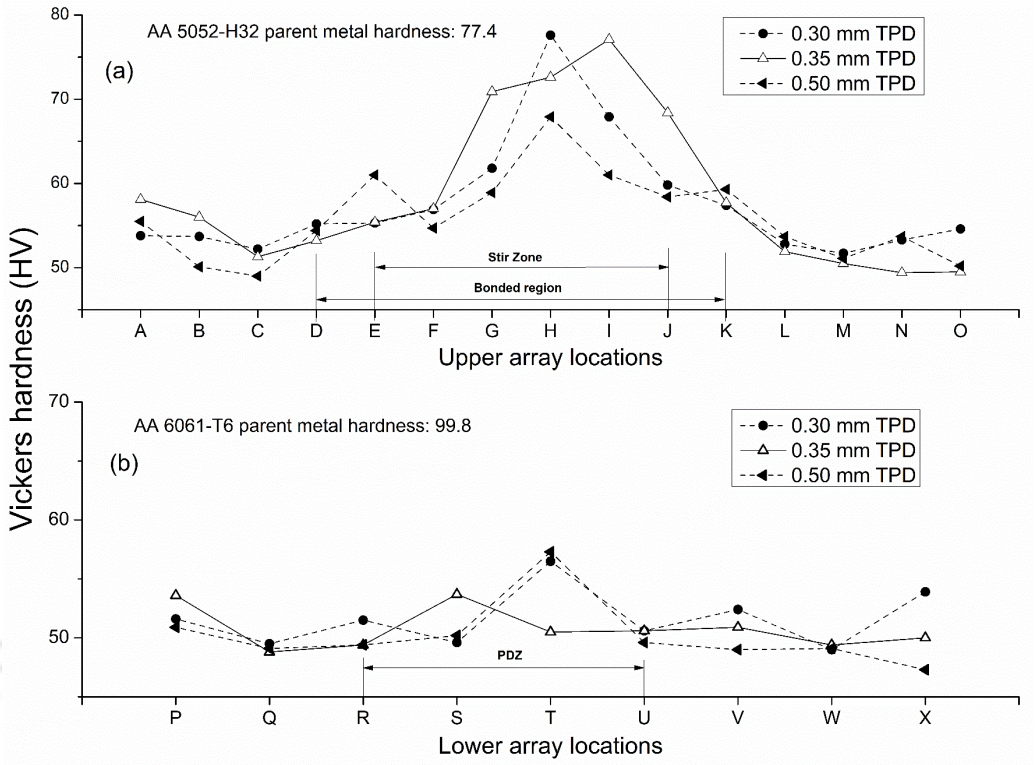

Figure 4.13. Comparison of hardness variation along the DFSF joint cross-sections. (a) Upper array of indentation, (b) Lower array of indentation (Typical hardness variation at each measurement location is ±2.3)

No remarkable change in hardness is observed along the lower array with the change in TPD. However, a 50% reduction in parent metal hardness is observed along the lower array, as shown in Fig. 4.13b, which is attributed to the conducted heat flux and the softening of the lower sheet. Higher hardness recorded at location T shows that the indentation is performed on the upper sheet metal extruded through the pre-drilled hole. Finally, change in TPD has negligible influence on the hardness distribution, specifically in the lower sheet, though significant decrease is observed with respect to the parent metal. Literature shows that the nature of change in hardness in solid solution hardened aluminum alloy (upper sheet) and precipitation hardened aluminum alloy (lower sheet) is different (Mishra and Ma, 2005), which is explained further.

For the upper sheet (AA 5052-H32), the parent metal with coarse grain structure exhibits same hardness as the SZ with fine grains. This can be related to the mechanisms

that govern the hardness of solid solution hardened alloys such as AA 5XXX. Huskins et al. (2010) reported that other than grain structure, many other factors such as dislocation density, solid solution hardening and precipitation hardening play significant role in determining hardness of AA 5XXX alloys. The hardness profile of these alloys is not governed by Hall-Petch relationship, but rather by Orowan mechanism, which explains that the homogenous distribution of particles (such as compounds of aluminum, manganese and iron) as well as the precipitates such as Mn act as obstacles to the dislocation motion, thereby strengthening solid solution hardened aluminum alloys (Mishra and Ma, 2005, Sato et al., 2001 and Huskins et al., 2010). Rana et al. (2018) also reported that dislocation density and fragmentation of second phase particles affected the hardness of the SZ during FSSW of AA 5052-H32. Therefore, it can be inferred that the grain structure alone is not responsible for the hardness variation in the upper sheet.

For the lower sheet (AA 6061-T6), a precipitation hardened aluminum alloy, the softening is created by the coarsening and dissolution of the strengthening precipitates under the influence of frictional heat flux (Mishra and Ma, 2005). A decrease in the hardness in the weld zone for AA 6111-T4 during pinless FSSW was reported by Bakavos et al. (2011). The overall reduction in hardness than that of the parent metal was also observed in the weld zone of FSSWed AA 6061-T6 sheets of 2 mm thickness (Cao et al., 2016). Therefore, the hardness of the lower sheet (AA 6061-T6) is strongly affected by the distribution of precipitates. It was also suggested that the hardness at the weld zone can be recovered by post weld natural aging in these alloys.

The decrease in the hardness around the SZ shows that there is significant softening in the TMAZ region. The softening of the sheet is contributed by grain recovery effect of the frictional heat flux and plastic deformation (Rana et al., 2018, Kesharwani et al., 2015). Coarse grain formation has contributed lower hardness in the HAZ region. Similar observation was also reported during FSSW of AA 5052-H32 aluminum alloys (Rana et al., 2018).

To summarize, the plunge of the stir tool has affected the maximum hardness of the upper array. Since TPD does not influence the hardness distribution (except a few locations) it can be inferred that optimum TPD depends only on the mechanical performance and the joint formation. The grain structure alone is not determining the hardness of the aluminum alloys. The detailed metallurgical studies on the upper and lower sheets are out of the scope of the present research work.

4.3.6 Joint morphology analysis

This section describes the influence of change in TPD on morphological features of the DFSF joints. The morphological features such as UB, SST, USFW and USFH are plotted against the entire TPD range in Fig. 4.14(a-d), respectively.

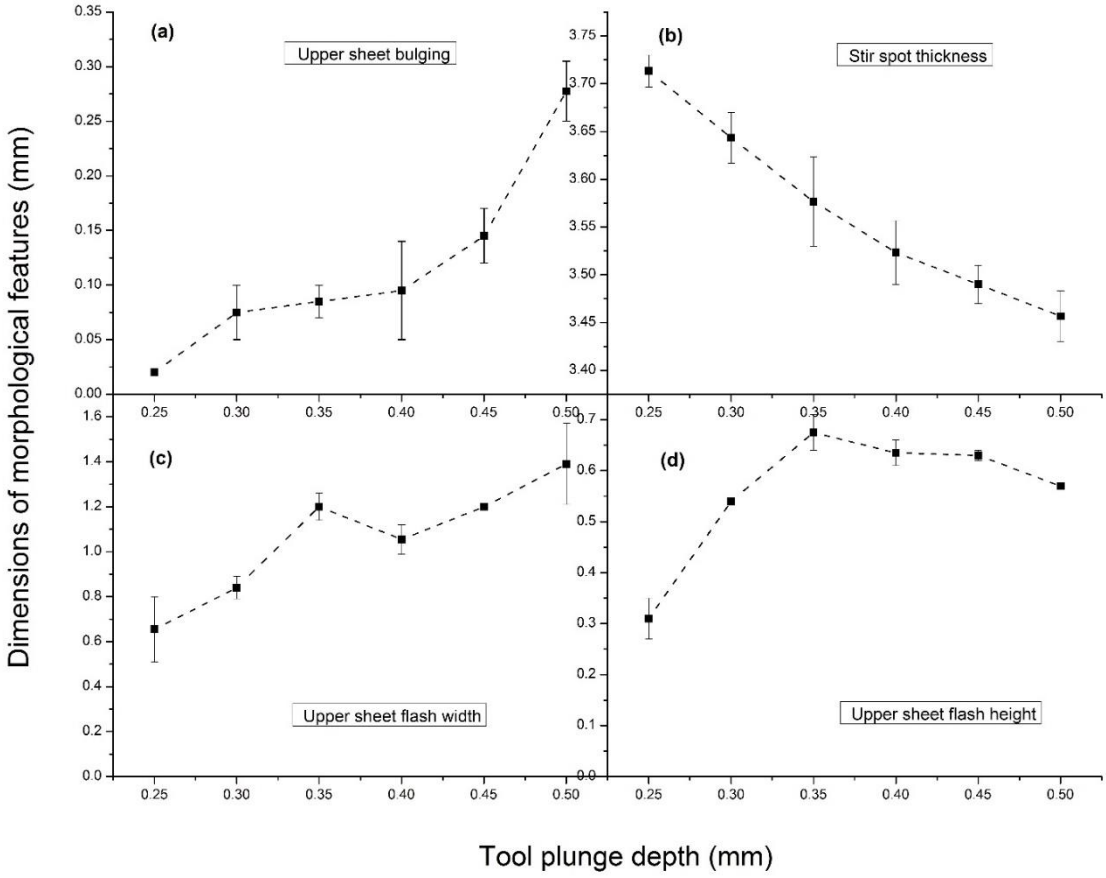

Figure 4.14. Comparison of joint morphological features at various TPDs (a) UB, (b) SST, (c) USFW, and (d) USFH

Whenever the lower sheet pre-drilled hole is completely filled with extruded upper sheet metal, the rest of the plasticized metal tend to displace upwards within the constraint of the clamps, resulting in UB. UB leads to projection of the upper sheet adjacent to the spot joint from its nominal plane, which is undesirable. The interfacial gap created by the bulging of the upper sheet may act as a space for moisture accumulation, corrosive action and further damage of the stir spot. Therefore, UB should be minimized as much as possible. UB increases with increase in TPD. Maximum UB is observed at the highest TPD, as shown in Fig. 4.14a. The value is so small, 0.28 mm, that its impact on the aesthetic appearance of the DFSF joint is negligible. UB is even observed at the lowest TPD, which shows that the pre-drilled hole filling is complete and excess metal is displaced upwards. Fig. 4.14b shows that the SST reduces linearly with increase in the

TPD. Therefore, the plunge of the stir tool results in adequate compression and displacement of material below the tool face.

Flash occurs because of the deformation in the upper sheet, where the material is freely deforming along the circumference of the stir spot due to the downward plunge of the stir tool. In other words, during the plunge of the tool, the outward material flow along the lateral surface of the stir tool leads to flash formation. If flash formation is considerable, it may interfere with the normal working of the product, may arise unnecessary hooking on soft objects, and may act as a source of scratch onto the mating surface. Therefore, flash should be either minimized or removed through post processing operations. Flash width and flash height show more or less increasing trend, but its formation is random in nature as shown in Fig. 4.14c and Fig. 4.14d. It is characterized by USFW of 1.39 mm and USFH of 0.57 mm at 0.5 mm TPD.

The morphology analysis shows that TPD has significant influence in the formation and growth of external features of the DFSF joint. Even at the highest TPD, namely 0.5 mm, the size of the morphological features are considerably smaller such that the aesthetic appearance of the joint is not affected much. Since morphological features are characterized by smaller values, it is believed that they do not have any influence on the joint formation and its mechanical performance. However, the influence of TPD on the evolution of these features are clearly revealed through this study.

4.3.7 Modes of failure during mechanical testing

During mechanical testing, the joints failed by different failure modes. Similar to CFSF samples, failure modes such as pin shear, pin pull-out, partial bond delamination, tear-off and, base metal fracture and stir spot fracture are observed in DFSF samples. The various failure modes are described below.

- Pin shear: This type of failure mode is explained in section 3.2.5 (Fig. 4.15a).
- Pin pull-out: This type of failure mode is explained in section 3.2.5 (Fig. 4.15b). At maximum load, the extruded pins retract from the pre-drilled holes due to the absence of fully developed collars.
- Partial bond delamination: This type of failure mode is explained in section 2.2.9 (Fig. 4.15c).

- Tear-off: This type of failure mode is explained in section 2.2.9 (Fig. 4.15d). Tear off occurs when the stir spot circumference act as the weakest zone at higher tool plunge.
- Base metal fracture: This type of failure mode is explained in section 2.2.9 (Fig. 4.15e).
- Stir spot fracture: This type of failure mode is explained in section 2.2.9 (Fig. 4.15f).

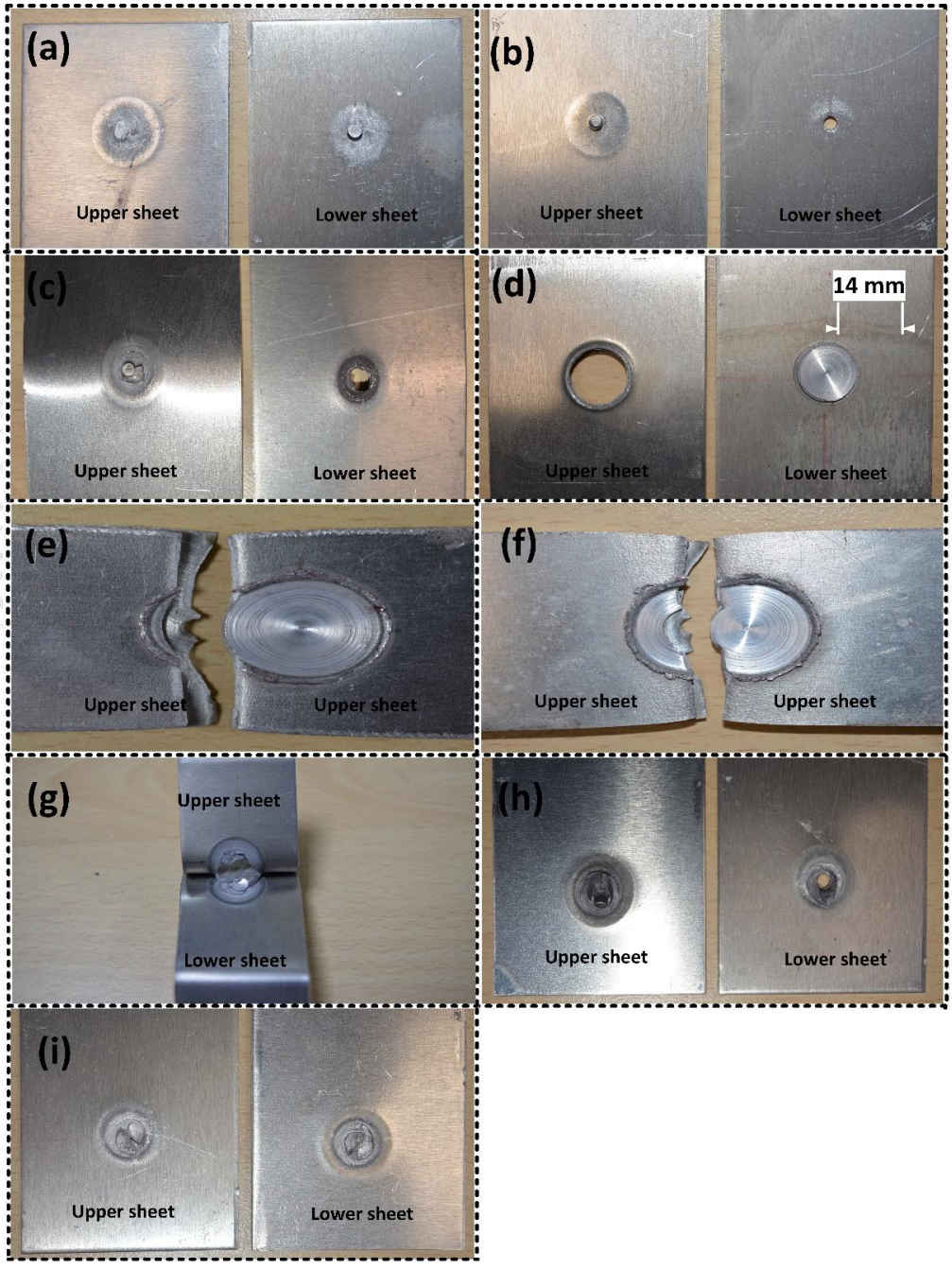

Figure 4.15. Modes of failure. (a) Pin shear, (b) Pin pull-out, (c) Partial bond delamination without pin failure, (d) Tear off, (e) Base metal fracture, (f) Stir spot fracture, (g) Combined bond delamination and

sheet tear, (h) Combined pin pull-out and bond delamination and (i) Combined pin shear and bond delamination

Most of the failure modes occur in combined form namely combined bond delamination and sheet tear (Fig. 4.15g), combined pin pull-out and bond delamination (Fig. 4.15h) and combined pin shear and bond delamination (Fig. 4.15i). The tear-off failure, and combined pin pull-out and bond delamination failure in DFSF samples are analogous to the plug type fracture and nugget debonding failure modes of refill FSSW samples in aluminum alloys (Shen et al., 2013).

Failure of DFSF samples is initiated from CRs, which act as weak zones during mechanical performance tests. The neck of the pin, CR1 (Fig. 4.11a), poor interlock at the top of the pre-drilled hole, CR2 (Fig. 4.11a), and the stir spot circumference, CR3 (Fig. 4.11c) are the three CRs leading to failure of the DFSF samples. When the joint formation happens exclusively by pin interlocking with no metallurgical bonding, CR1 and CR2 act as critical weak zones. CR1 leads to pin shear and CR2 leads to pin pull-out at ultimate load. When the pin interlock and metallurgical bonding, both contribute to joint strength at higher TPDs, tear off occurs by thinning along the stir spot circumference, CR3. Combined failure modes occur more or less due to the formation of more than one active critical weak zones.

Table 4.3. Modes of failure

TPD	Lap shear test		Cross-tension test		Peel test		Tensile test	
	Trial 1	Trial 2	Trial 1	Trial 2	Trial 1	Trial 2	Trial 1	Trial 2
0.25	Pin shear	Pin pull-out + bond delamination	Pin pull-out at no load	Pin pull-out + Bond delamination	Pin pull-out	Pin pull-out + Bond delamination	Stir spot fracture	Base metal fracture
0.3	Pin shear + Bond delamination	Pin shear + Bond delamination	Pin pull-out	Pin pull-out + Bond delamination	Pin pull-out + Bond delamination	Pin shear + Bond delamination	Stir spot fracture	Stir spot fracture
0.35	Pin pull-out + bond delamination	Pin shear + Bond delamination	Pin pull-out + Bond delamination	Pin pull-out	Pin pull-out	Tear-off	Stir spot fracture	Stir spot fracture
0.4	Pin pull-out + bond delamination	Tear-off	Tear-off	Partial bond delamination without pin failure	Pin pull-out + Bond delamination	Pin pull-out + Bond delamination	Stir spot fracture	Stir spot fracture
0.45	Tear-off	Tear-off	Partial bond delamination	Tear-off	Sheet tear + Bond delamination	Pin pull-out + Bond delamination	Stir spot fracture	Stir spot fracture
0.5	Pin shear + Bond delamination	Tear-off	Tear-off	Tear-off	Tear-off	Pin pull-out + Bond delamination	Stir spot fracture	Stir spot fracture

Table 4.3 shows the summary of the failure modes of DFSF samples subjected to various mechanical performance tests. At lower TPD of 0.25 mm, the joint formation is uncertain. Some of the samples show pin pull-out just after the fabrication, while others

exhibit pin shear without metallurgical bonding. Joint strength is contributed by the partial pin interlocking and metallurgical bonding in the rest of the samples. This shows that chance of formation of perfect pin interlocking and complete metallurgical bonding is absent at lower TPDs. At medium TPDs, the samples exhibit pin failure with bond delamination. At higher TPDs, tear off is the common failure mode, wherein the pin formation and metallurgical bonding are perfect. Therefore, the TPD has significant influence on the modes of failure. Moreover, the failure modes are random with respect to trials at same TPD, for any particular test. The tensile test samples show entirely different modes of failure, where stir spot fracture occurs in almost all cases.

4.3.8 Extension of TPD beyond 0.5 mm

From the previous sections, it has been observed that upto a TPD of 0.5 mm, the mechanical interlocking and metallurgical bonding is perfect and appreciable joint strength is obtained. In this section, the effectiveness of DFSF joint formation is further analyzed by increasing the TPD to higher discrete levels such as 0.7 mm and 0.9 mm. The lap shear fracture load, macrostructure and external joint morphology of the DFSF samples are obtained and compared with that of samples fabricated at 0.5 mm TPD. All the samples are fabricated with the same material combination of aluminum alloy sheets.

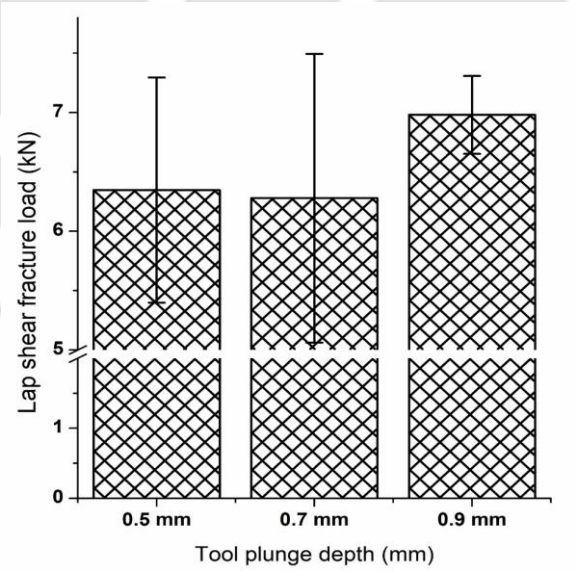

Figure 4.16. Comparison of lap shear fracture load of DFSF samples at 0.5 mm, 0.7 mm and 0.9 mm TPDs

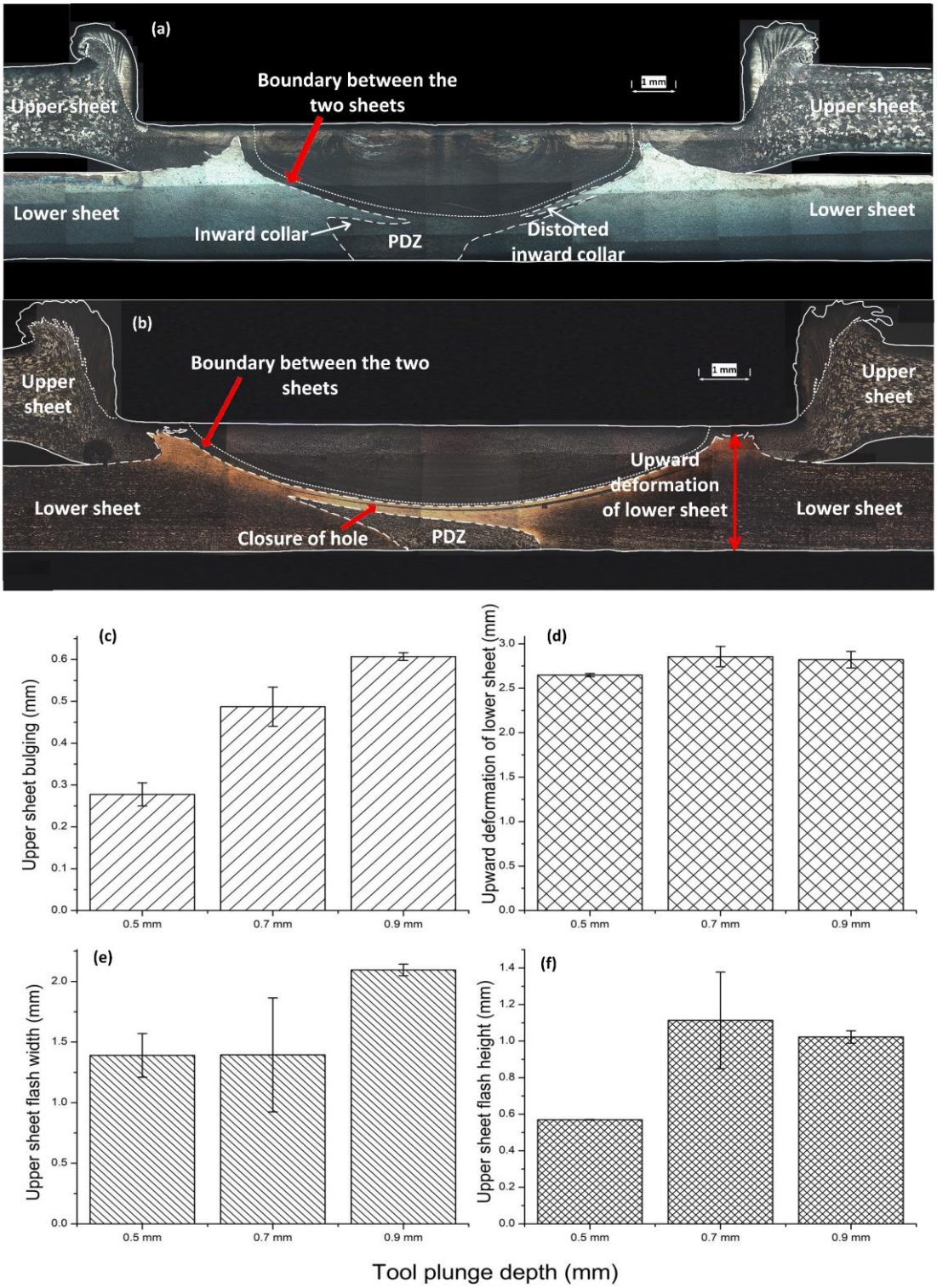

Figure 4.17. Macrostructure of DFSF sample at (a) 0.7 mm TPD, (b) 0.9 mm TPD, comparison of joint morphological features at various TPDs (c) UB, (d) Upward deformation of lower sheet, (e) USFW, and (f) USFH

The comparison of the lap shear fracture load of these samples is shown in Fig. 4.16. Lap shear samples at 0.7 mm TPD shows 0.07 kN lesser strength than that of 0.5 mm TPD samples. Further, the lap shear samples at 0.9 mm TPD shows 0.64 kN higher strength than that of 0.5 mm TPD samples. Therefore, almost similar fracture load is recorded for

all the three samples, which shows that a significant improvement in lap shear fracture load is not observed with increase in TPD beyond 0.5 mm.

The comparison of the macrostructure and joint morphology of DFSF samples at 0.7 mm TPD and 0.9 mm TPD are shown in Fig. 4.17(a-b). The macrostructure analysis shows that considerable change in the joint formation occurs with increase in the TPD. At 0.7 mm TPD, the pre-drilled hole has been slightly damaged and shifted from the center of the stir spot, as shown in Fig. 4.17a. The plunge of the stir tool and its clockwise rotation has created eccentricity in the location of the pre-drilled hole. Unsymmetrical collar formation has also been observed above the PDZ. The right hand side collar is distorted and pushed towards the sidewalls of the pre-drilled hole. An increase in TPD about 0.2 mm (i.e., at 0.9 mm TPD) also yields excessive upward deformation of the lower sheet and severe UB than that of 0.5 mm TPD samples, as shown in Fig. 4.17c and Fig. 4.17d. At 0.9 mm TPD, the pre-drilled hole is completely closed and extruded upper sheet metal namely the PDZ is isolated and deformed towards the one side of the joint (Fig. 4.17b). As shown in Fig. 4.17e and Fig. 4.17f, for 0.7 mm and 0.9 mm TPD DFSF samples, the size of the flash is comparatively larger than that of 0.5 mm TPD DFSF samples.

At higher TPDs such as 0.9 mm, the joint strength is predominantly contributed by the metallurgical bonding. However, the quality of mechanical interlocking is significantly deteriorated beyond 0.7 mm TPD. The aesthetic appearance of the joint is affected by severe UB and flash size as compared to that of 0.5 mm TPD DFSF samples. The joint formation is more or less like forging action due to the excessive tool plunge. The metallurgical bonding between the upper sheet and lower sheet under this forging force has marginally increased the lap shear fracture load (by almost 10%) at 0.9 mm TPD than the lap shear fracture load at 0.5 mm TPD. Therefore, 0.7 mm TPD can be considered as a limit, beyond which the mechanism of joint formation with simultaneous mechanical interlocking and metallurgical bonding cannot be considered effective for the present material combination.

4.4 Conclusions

The following are the conclusions derived from the present work.

- Uniform mechanical performance is obtained during the change in TPD from 0.3 mm to 0.5 mm. Increase in TPD reduced the formability of DFSF samples during

uniaxial tensile test. Increase in TPD beyond 0.5 mm has not yielded significant improvement in the mechanical performance.

- Macrostructure analysis revealed that at lower TPDs, the mechanical interlocking is incomplete and the metallurgical bonding is absent. At medium and higher TPDs, the samples are strengthened by simultaneous mechanical interlocking and metallurgical bonding. Slight increase in TPD results in better mechanical interlocking. Increasing TPD beyond 0.5 mm TPD is not favorable. Considering both the mechanical performance and the macrostructure analysis of DFSF samples, the higher TPD range from 0.45 mm to 0.5 mm can be considered as optimum for the present material combination of aluminum alloys.
- The presence of SZ, TMAZ, ASZ, PDZ and HAZ in the DFSF joint is demonstrated. The SZ formation has no significant influence on the joint strength and it is confined to the upper sheet only. Microstructure analysis shows that the region under direct contact with stir tool such as SZ is subjected to dynamic recrystallization. The PDZ and HAZ have undergone recrystallization and significant grain growth under frictional heat flux conducted from the stir spot. The TMAZ and flash have undergone dynamic recovery under the thermal cycle with grain size about 18.9 µm to 26.7 µm.
- The hardness distribution shows identical pattern irrespective of the change in TPD. The plunge of the stir tool has resulted in forging of the plasticized metal in the pre-drilled hole at the center of the DFSF joint. Hence, higher hardness is observed in the SZ and PDZ of the upper sheet.
- The size external morphological features shows that their impact on aesthetic appearance of the DFSF joint is negligible even at higher TPDs such as 0.5 mm. Severe UB and flash size deteriorated the aesthetic appearance of DFSF joints fabricated at 0.7 mm and 0.9 mm TPDs.
- Incomplete pin formation and absence of metallurgical bonding are revealed for DFSF samples at lower TPDs through failure mode examination. At higher TPDs, most of the samples show tear-off failure. The CRs responsible for the failure modes are located at the neck of the pin, at the top of the pre-drilled hole, and at the stir spot circumference.
- The absence of pin hole defect and hook defect in DFSF joints significantly improved its strength and aesthetic appearance than that of its counterparts. In

addition, the absence of rivet head formation (flat base) in DFSF joints differentiates it from CFSF joints.

Chapter 5

DFSF joining of AA 5052-H32 and AA 6061-T6 sheets at varying tool shoulder diameters

In this chapter, the effect of pinless TD on joint strength and joint formation is evaluated through mechanical performance studies, macro/ microstructural analysis, hardness measurement, joint morphology study and failure mode analysis. The optimum tool rotational speed of 500 rpm obtained from chapter 2, the sheet metal combination employed in chapter 2 and favorable TPD of 0.7 mm obtained from chapter 4 are adopted in the present work.

5.1 Methodology

The principle of DFSF joint formation is presented in section 4.2.1.

5.1.1 DFSF experiments

The details of DFSF sample fabrication is presented in section 4.2.2. Sample fabrication is conducted on FSW machine (3T-FSW unit Model No: WS005 ETA Tech). The standard properties of the upper sheet and the lower sheet are presented in Section 2.1.2. The effect of TD on the DFSF joint formation is studied by varying the dia. of the pinless stir tool, with lower levels at 10 mm and 12 mm, medium level at 14 mm, and higher levels at 16 mm and 18 mm. Minimum lower level TD is set at 10 mm to ensure sufficient plasticization of the upper sheet metal to form simultaneous mechanical interlocking and metallurgical bonding. Tools with dia. above 18 mm are not feasible because the width of the peel test sample is limited to 30 mm. This ensures a minimum amount of upper sheet metal surrounding the stir spot for peel test samples, especially in width direction.

The other parameters namely tool rotational speed, direction of tool rotation, TPD and tool plunge rate were kept constant at 500 rpm, clockwise direction, 0.7 mm and 0.002 mm/s, respectively, throughout the sample fabrication. The values are set as per data available in literature and by conducting a set of preliminary experimental trials. Higher

plunge depth of 0.7 mm is employed in this work to ensure joint formation even with the stir tool having lowest TD 10 mm.

5.1.2 Mechanical performance tests

Details of mechanical performance tests are discussed in section 2.1.3. CFSF and FSSW samples are also fabricated on the same material combination for comparing the lap shear fracture load with that of DFSF samples. For CFSF process, pinless stir tool with shoulder dia. 14 mm and anvil cavity dia. of 3.5 mm and cavity depth of 0.55 mm are employed. A pre-drilled hole of 3 mm dia. is fabricated in the lower sheet. A stir tool of 14 mm shoulder dia. with a pin having 4 mm dia. and 1 mm length is employed for FSSW process. All other parameters used for CFSF and FSSW process are same as that used for DFSF process.

5.1.3 Macro/ microstructure, hardness measurement and joint morphology analysis

Details of macrostructure analysis, hardness measurement and joint morphology analysis are discussed in Section 2.1.4. Details of microstructure analysis is discussed in Section 4.2.4. The microscopic images are obtained at 100X and 200X magnifications.

The hardness measurements are taken on the DFSF sample cross-sections in two arrays of indentations with 2 mm spacing in between the indentations. Upper array and lower array of indentations are shown in Fig. 5.1. The external morphological features such as USFW, USFH, UB, BW and SB are also measured (Fig. 5.2).

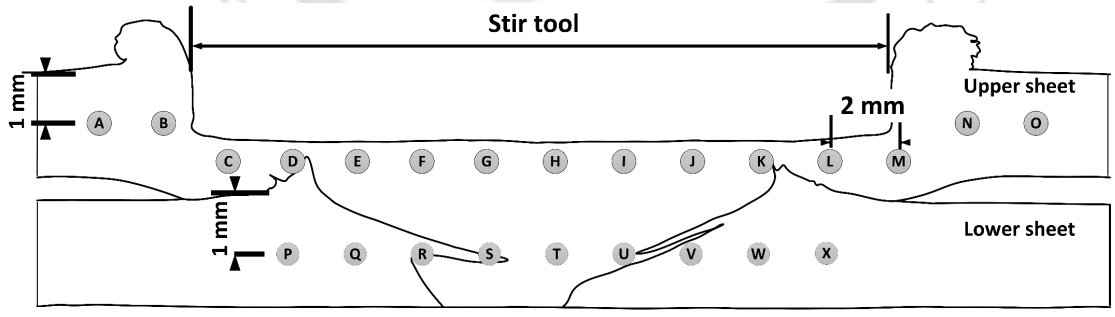

Figure 5.1. Schematic representation of the hardness measurement locations (Dimensions not to scale)

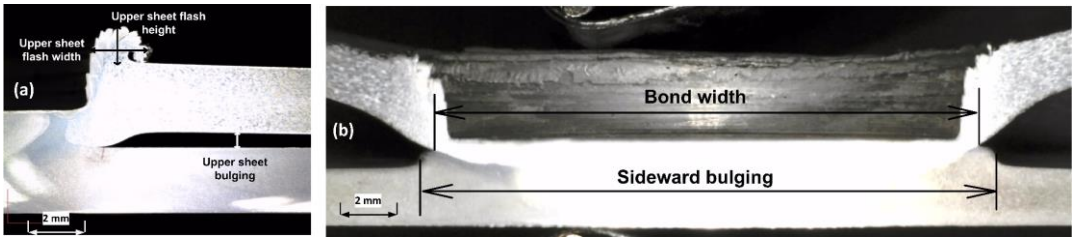

Figure 5.2. Morphological features measured in the DFSF joint cross-section

5.2 Results and Discussion

The results obtained from mechanical performance tests, joint macro/ microstructure analysis, hardness measurement, joint morphology and failure mode analysis are comprehensively discussed in the following subsections.

5.2.1 Mechanical performance tests

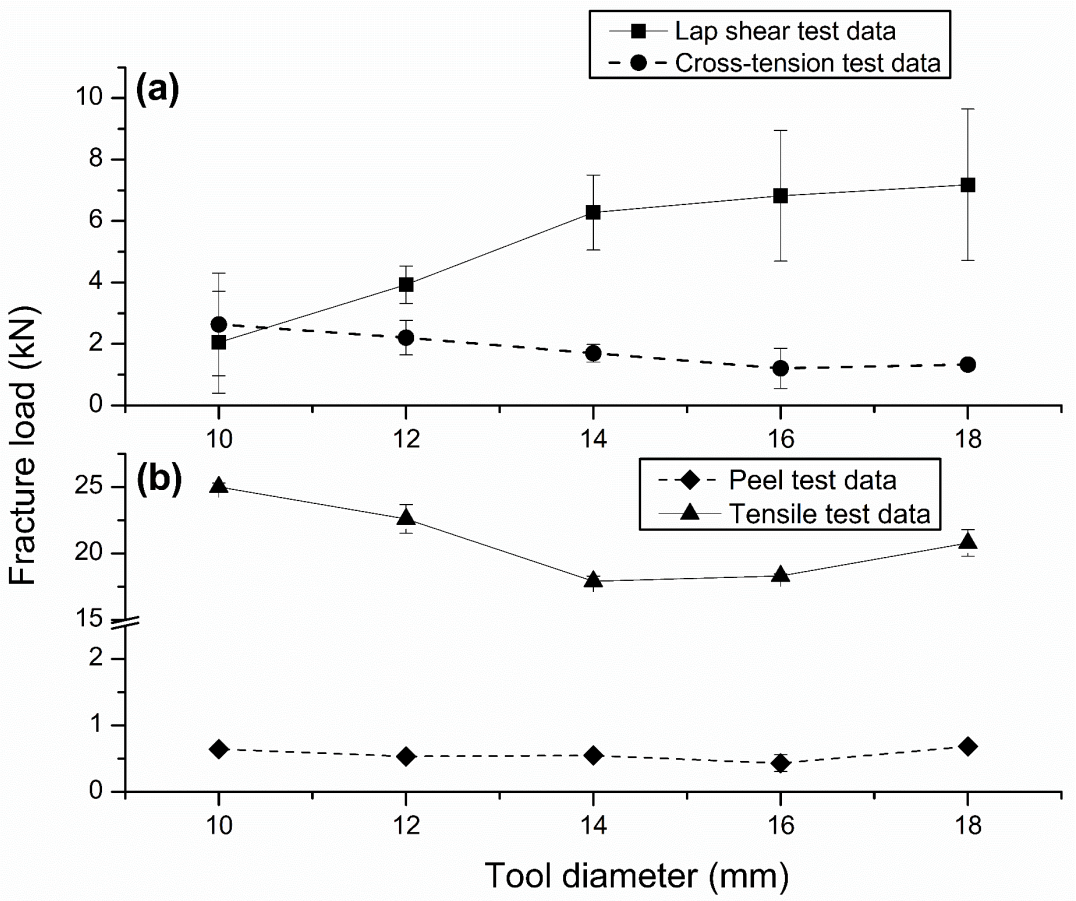

Figure 5.3. Comparison of fracture loads for various TDs during mechanical performance tests of DFSF samples

The effect of TD on the fracture load during mechanical performance tests is shown in Fig. 5.3. It can be observed that TD has a significant influence on the joint strength of DFSF samples subjected to various mechanical performance tests. Lap shear test shows

that 250% increase in the fracture load is obtained as the TD is increased from 10 mm to 18 mm. The cross-tension fracture load recorded a 50% decrease with increase in TD for the same range. The samples with highest lap shear fracture load show lowest cross-tension fracture load and vice versa. The peel test data remain almost same throughout the entire TD range. Uniform peel off resistance of DFSF samples can be explained with the failure mode analysis in section 5.2.7.

It is to be noted that the TD at which maximum fracture load occurs varies from test to test. For samples subjected to loading conditions where shear mode of fracture dominates, medium and higher TDs- 14 mm to 18mm, are suitable for DFSF process. Similarly, for samples subjected to severe cross-tensile loads, lower and medium TDs- 10 mm to 14 mm, are suitable for DFSF process. Lap shear samples at 10 mm to 14 mm TD show acceptable error bar. However, for 16 and 18 mm TDs, the error bar seems to be larger. Larger error bar shows instability in the joint formation and such TDs are not reliable.

From above observations, authors suggest the medium TD of 14 mm as desirable value for DFSF joint fabrication due to following reasons.

- At medium TD of 14 mm, the DFSF samples possess appreciable fracture load in lap shear test, cross-tension test and peel test. Samples show lap shear fracture load of 6.22 kN, which is almost nearer to highest value. Similarly, a moderate cross-tension fracture load of 1.69 kN is obtained at medium TD.
- 200% increase in lap shear fracture load is obtained, when TD is increased from 10 mm to 14 mm. 36% decrease in cross-tension fracture load is observed for the same range. It is also observed that only 14% increase in lap shear fracture load is obtained, when TD is increased from 14 mm to 18 mm. Similarly, 21% decrease in cross-tension fracture load is observed for the same range.

Thus, moderate TD of 14 mm is expected to deliver joints with sufficient mechanical performance for the pair of aluminum alloy sheets chosen. The joints can perform acceptably in both lap shear test and cross-tension test. Therefore, the overall performance of DFSF samples at 14 mm TD is desirable even though the highest fracture load varies from test to test. Moreover, at any particular TD, lap shear test samples show maximum fracture load, peel test samples show minimum fracture load and cross-tension samples show intermediate load.

The lap shear samples exhibit very low extension with an average about 0.637 mm throughout the entire TD range. The main reason for the lower extensibility during lap shear loading may be the higher TPD of 0.7 mm, which has resulted in excessive upward deformation of the lower sheet. More details are provided with the failure mode analysis in section 5.2.7. The average extension at fracture for cross-tension samples and peel test samples are about 6.56 mm and 5.73 mm throughout the entire TD range. These samples have shown significant extensibility due to the peculiar nature of the cross-tension test and the peel test. Here bending and unbending of metal strips have also contributed to the extensibility before failure occurs.

Just to summarize, the range of desirable TDs is dependent on the mode of testing. The lap shear test, cross-tension test and peel test show different range of optimum TD, when fracture load is considered. However, 14 mm TD can be considered for joint fabrication uniformly, with minor loss in mechanical performance.

The DFSF samples show a decrease in tensile fracture load with increase in TD in uniaxial tensile testing. The samples fabricated at lower TDs exhibit smaller stir spot size such that the adjoining gauge length region also bear the tensile load. Increase in TD results in larger geometrical inhomogeneity developed due to large dia. stir spot, which has reduced the fracture load during tensile tests. Average extension for tensile samples is found to be 3 mm. The stir spot along with surrounding gauge length region has also shown appreciable extensibility before failure. It can be summarized from the results of the mechanical performance tests that TD has a significant impact on the load bearing ability of DFSF joints fabricated on AA 5052-H32 and AA6061-T6 material combination.

5.2.2 Fracture load comparison of DFSF, CFSF and FSSW processes

Table 5.1. Comparison of fracture load from lap shear test of samples fabricated with DFSF joining and other joining processes

Joining technique	Average fracture load (kN)
FSSW with pin	5.65
CFSF	6.03
DFSF	6.22

The lap shear fracture load of DFSF samples is compared with that of CFSF and FSSW samples as shown in Table 5.1. To maintain uniformity, all the samples are fabricated on the same material combination, employing same process parameter

conditions. The lap shear fracture load of DFSF samples is 10% better than that of FSSW samples. CFSF and DFSF joints show almost similar fracture load, although marginal improvement is observed for DFSF joints.

5.2.3 Joint formation analysis through macrostructure

The macrostructure of the DFSF samples fabricated at lower, medium and higher TDs are shown in Fig. 5.4(a-e). In addition, the schematic representation of the direction of metal flow is shown with arrows in Fig. 5.5(a-e). The DFSF joints are strengthened by simultaneous mechanical interlocking and metallurgical bonding or either of them. The mechanical interlocking is enabled by the growth of an inward collar (Fig. 5.4b). This prevents the retraction of the extruded upper sheet from the pre-drilled hole. The collar growth occurs by the deformation of the top of the pre-drilled hole.

The frictional heat generation and further plastic deformation under the tool plunge is the mechanism of deformation of the upper sheet. However, the frictional heat flux conducted from the upper sheet and further plastic deformation under the downward tool plunge is the mechanism governing the deformation of the lower sheet. The conducted heat flux is also sufficient to enable metallurgical bonding in between the two sheets, while plastic deformation results in mechanical interlocking.

SZ, PDZ, TMAZ and HAZ can be distinguished in all the joint macrostructures. The SZ, PDZ and TMAZ constitute the parts of upper sheet only, while HAZ appears in upper sheet and lower sheet.

5.2.3.1 Lower TDs (10 mm and 12 mm)

The joint macrostructure and the metal flow directions at lower TDs are shown in Fig. 8(a-b) and Fig. 9(a-b), respectively. The frictional heat generated with 10 mm TD is sufficient to plasticize and extrude the upper sheet metal through the pre-drilled hole in the lower sheet. Nevertheless, pre-drilled hole is not completely occupied and the mechanical interlocking is partially developed (collar formation initiated at one side). The joint is also strengthened by

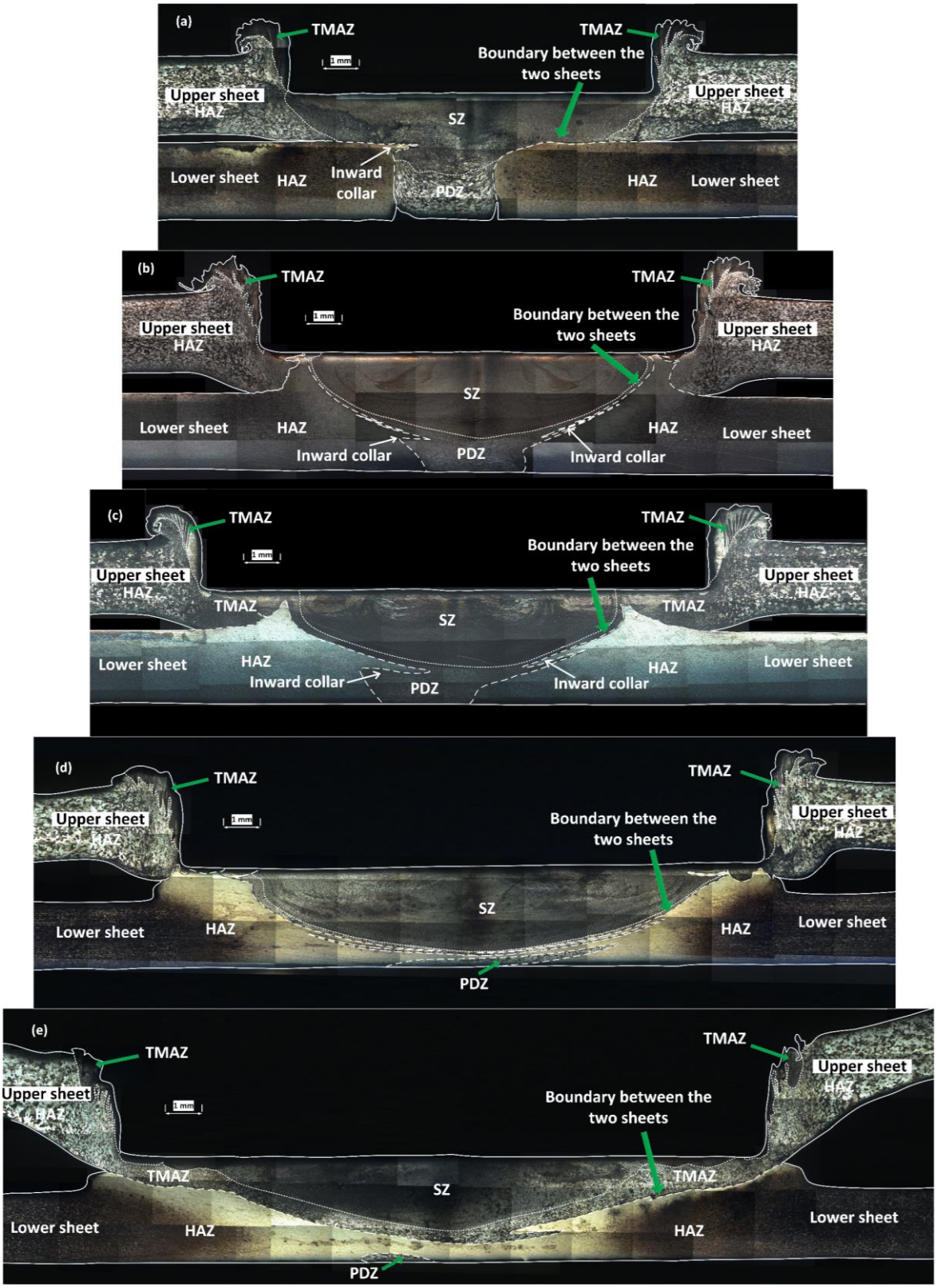

Figure 5.4. Joint macrostructure of DFSF samples fabricated at (a) 10 mm and (b) 12 mm (Lower TDs), (c) 14 mm (Medium TD), (d) 16 mm and (e) 18 mm (Higher TDs)

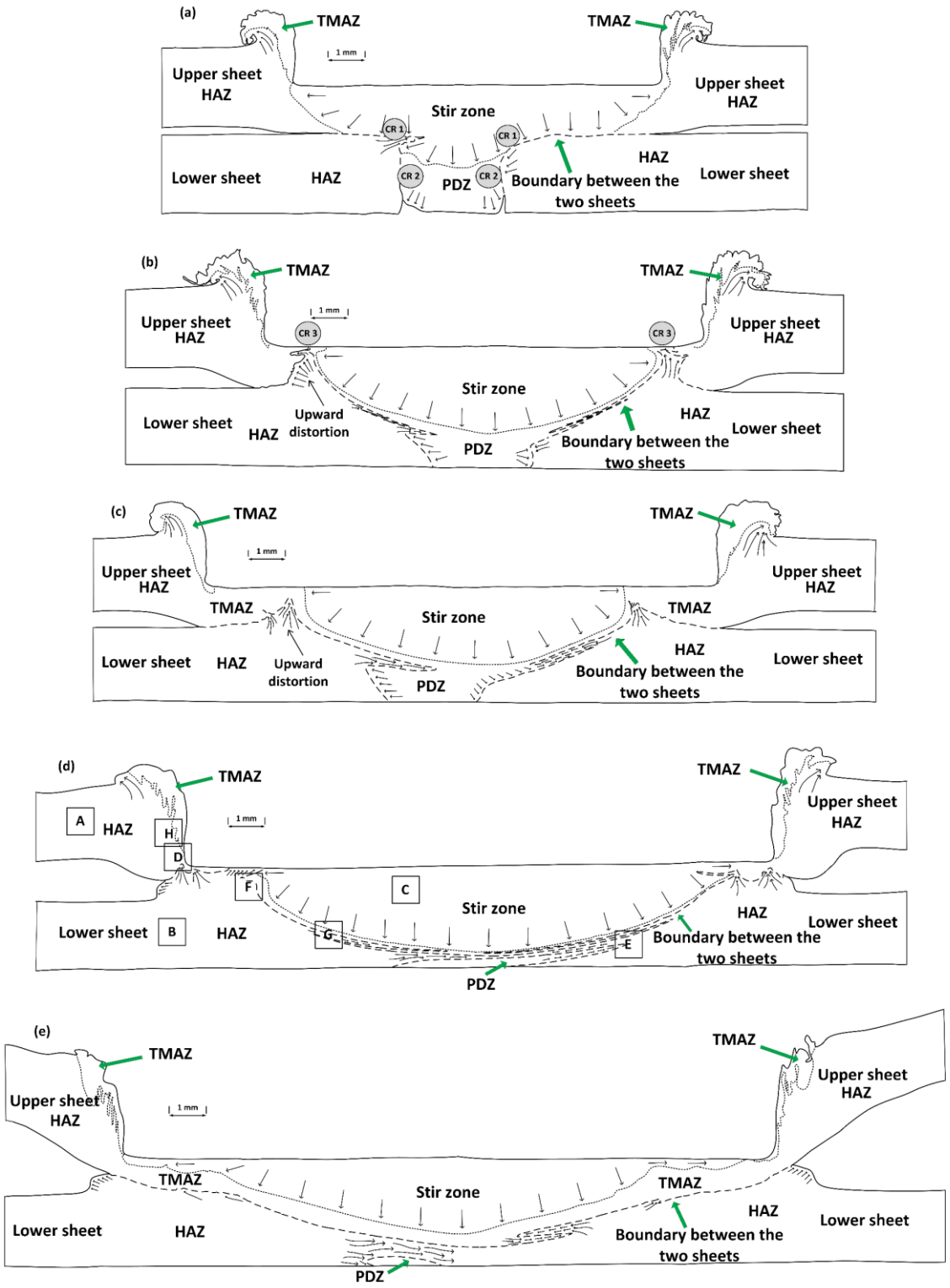

Figure 5.5. Schematic representation of the FSF joint cross-section at (a) 10 mm and (b) 12 mm (Lower TDs), (c) 14 mm (Medium TD), (d) 16 mm and (e) 18 mm (Higher TDs) with metal flow directions indicated

metallurgical bonding at the interface between the two sheets below the stir spot. The pre-drilled hole and the interface between the two sheets remain undeformed. The conducted heat flux and achieved plastic deformation are not sufficient to promote complete mechanical locking of the extruded pin.

At 12 mm TD, better mechanical interlocking and metallurgical bonding can be observed. The extruded pin has been perfectly locked by the deformation of the top of the pre-drilled hole. Collar growth initiates from the top of the pre-drilled hole. Collar formed on the right hand side of the cross-section has been deformed and found attached to the lower sheet. The plunge of the tool has pushed the collar downwards. Slightly reducing the TPD can solve this problem. TD of 12 mm produces sufficient heat flux and deformation to extrude the upper sheet for completely filling the pre-drilled hole.

The strength of the DFSF joints at lower TDs is influenced by the extent of metallurgical bonding at the interface of the two sheets. At lower TDs, the bonded interface between the two sheets is comparatively smaller than that of medium and higher TDs. This has resulted in low lap shear fracture load.

5.2.3.2 Medium TD (14 mm)

The joint macrostructure and schematic of the metal flow directions at medium TD of 14 mm are shown in Fig. 5.4c and Fig. 5.5c, respectively. With further increase in TD to the medium level, the mechanical interlocking has perfectly developed and the extent of metallurgical bonding is increased. The inward collar has grown further. This results in acceptable performance in lap shear test, cross-tension test and peel test. The stir spot size has increased and the deformation of the lower sheet is favorable. However, the plunge of the stir tool has affected the right hand side collar. The right hand side collar is pushed towards the lower sheet, while the left hand side collar remains unaffected. In addition, the TPD of 0.7 mm maintained throughout the TD range has resulted in slight squeezing of the pin inside the pre-drilled hole. Despite above observations, the joint performance is appreciable during mechanical performance test at medium TD.

5.2.3.3 Higher TDs (16 mm and 18 mm)

The joint macrostructure and schematic of metal flow directions at higher TDs are shown in Fig. 5.4(d-e) and Fig. 5.5(d-e) respectively. At higher TDs, the contact area of the stir tool is larger and the joints are subjected to high frictional heat flux and severe plastic deformation. The pre-drilled hole has been severely deformed and resulted in its subsequent closure. The inward collars merge and the hole is completely closed. A part of the extruded metal is isolated from the upper sheet by the closure of pre-drilled hole.

For 16 mm TD DFSF samples, the joint fracture load is solely contributed by the metallurgical bonding and the mechanical pin interlocking (otherwise collar formation) is absent. The lower sheet has undergone severe deformation. For 18 mm TD, the thickness of the closure of the pre-drilled hole has increased further. Significant improvement in the lap shear fracture load is not obtained at higher TDs, while the cross-tension fracture load is decreased probably due to the absence of pin interlocking.

The increase in width of the stir spot with increase in TD is obvious. Despite the fact that frictional heat flux increase with increase in TD, the SZ size remains almost same at lower and medium TDs. At higher TDs, the SZ size has increased due to the closure of the pre-drilled hole and deformation of the lower sheet. Size of the TMAZ on the sidewall remains almost same throughout the entire TD range.

The lower lap shear fracture load recorded at lower TDs shows that joint formation is realized by partial mechanical interlocking and insufficient metallurgical bonding. At higher TDs, significant contribution of the lap shear fracture load is obtained from metallurgical bonding. It can be inferred that with increase in TD, the increase in the lap shear fracture load is contributed by the growth of the metallurgically bonded area. In the case of cross-tension samples, the presence or absence of mechanical interlocking and metallurgical bonding did not change the fracture load significantly. However, with increase in TD, the slight decrease in cross-tension fracture load (maximum 1.4 kN only) may be attributed to poorer mechanical interlocking. Therefore, the strength of the DFSF samples at various loading conditions is a play off between metallurgical bonding and mechanical interlocking, whose presence and absence controls the joint strength. The samples at medium TD are strengthened by simultaneous mechanical interlocking and metallurgical bonding. Therefore, 14 mm TD is suggested as the desirable level to join AA 5052-H32 and AA 6061-T6 sheets of 2 mm thickness. Such a conclusion is acceptable also from macrostructure analysis.

5.2.4 Microstructure characterization

The microstructure of SZ, PDZ, TMAZ and HAZ of DFSF joint fabricated at 16 mm TD is shown in Fig. 5.6. The locations from which microstructure images are captured are represented in Fig. 5.5(d) in boxes marked with alphabets A to H. The comparison of grain size at various zones of the DFSF joint is shown in Table. 5.2.

From Fig. 5.6(a-b), it is observed that HAZ of AA 5052-H32 possesses irregular coarse grains, while HAZ of AA 6061-T6 shows equi-axed smaller grains. These regions are unaffected by the plastic deformation, but undergone static recrystallization and grain growth by conducted heat flux from the SZ. The upper sheet AA 5052-H32 possess larger grains with 31.8 µm size, while the lower sheet of AA 6061-T6 has 13.3 µm grain size. Both are bigger than parent sheet grain size (Table 2.3). SZ and TMAZ grain structures are shown in Fig. 5.6c and Fig. 5.6d respectively. SZ possess very fine, homogenous equi-axed grains of size 11.2 µm. Literature shows that significant grain refinement observed during FSSW of aluminum sheets with pinless tools was attributed to the frictional heating and downward tool plunge (Tozaki et al., 2010). Similarly, in DFSF process, the frictional heat flux and severe plastic deformation due to stirring have resulted in dynamic recrystallization under high tool plunge force in the SZ, which is the same mechanism of microstructure evolution in FSSW of aluminum alloys. The heat generated due to plastic deformation of the upper sheet metal can also contribute to the joint formation and microstructural changes. It was reported that, the contribution of plastic deformation is so small (about 3%) that it can be neglected in case of aluminum alloys. More than 96% of the total heat is generated by the frictional contact between the stir tool and the work piece (Awang and Mucino, 2010).

The recovered grain structure is observed in TMAZ region with grain size about 13.3 µm, which is slightly larger than SZ grains. TMAZ receives comparatively reduced heat flux and undergoes less mechanical deformation than that of the SZ, therefore recrystallization is absent. PDZ possess grains of 22.5 µm size, which is twice as big as SZ grains. This region is not subjected to severe plastic deformation, except the directional extrusion towards the pre-drilled hole. But, heat flux from the SZ and extrusion have influenced the microstructure of PDZ and static recrystallization has occurred. The microstructures of lower sheet-PDZ interface and lower sheet-SZ interface are shown in Fig. 5.6e and Fig. 5.6f, respectively. At 16 mm TD, the pre-drilled hole has been severely deformed and the PDZ is squeezed inside the deformed hole. The lower sheet has deformed through the sides of the SZ and has reached up to the top of the stir spot, showing upward deformation of the lower sheet. SZ-PDZ interface and HAZ-TMAZ interfaces are shown in Fig. 5.6g and Fig. 5.6h, respectively.

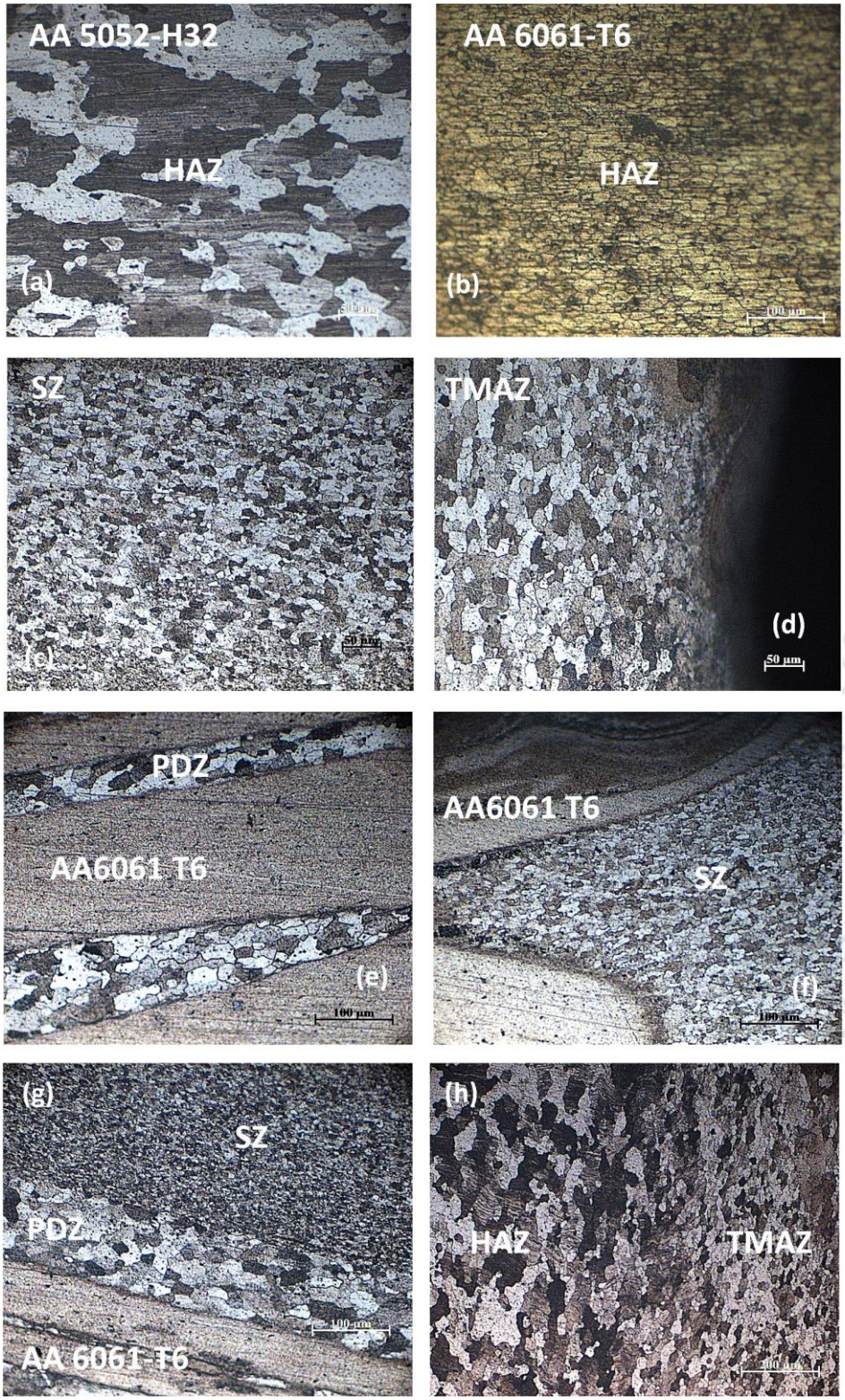

Figure 5.6. Optical microstructure of (a) upper sheet BM at 200X (box A), (b) lower sheet BM at 200X (box B), (c) SZ of the upper sheet at 200X (box C), (d) TMAZ of the upper sheet at 200X (box D), (e) boundaries between PDZ-lower sheet at 200X (box E), (f) boundaries between SZ-lower sheet at 200X (box F), (g) boundaries between SZ-PDZ at 200X (box G), (h) boundaries between BM-TMAZ at 100X (box H) magnifications

Table 5.2. Comparison of grain size at various zones of the DFSF joint

Location	Average grain dia. (μm)
SZ	11.2
TMAZ	13.3
PDZ	22.5
AA 5052-H32 (upper HAZ)	31.8
AA 6061-T6 (lower HAZ)	13.3

A clear distinction in grain structure, fine grain to coarse grain, is visible at the interface between SZ and PDZ. It can be confirmed that the frictional heat flux, plastic deformation due to stirring and downward tool plunge has variable effect on the microstructural evolution of SZ and PDZ. The transition from coarse grains to smaller grains is visible at HAZ-TMAZ interface, which confirms that HAZ region has not been significantly deformed.

Unlike FSSW process, for DFSF process the rotating stir tool is in contact with the upper sheet only and the lower sheet remains mechanically unaffected by tool rotation. In other words, in DFSF process, the stirring is confined to the upper sheet. In contrast, for FSSW process, the pin of the rotating tool initiates stirring and mixing of the upper and lower sheets. Therefore, any combination of ductile dissimilar sheet metals can be joined with the DFSF process, without considering the extent of stirring of upper and lower sheets. It was reported that pinless tool produces insufficient stirring and weak bond formation in FSSWed AA 6061-T4 sheets (Tozaki et al., 2010). The downward material flow was negligible even at TPD of 0.7 mm. For DFSF process at 0.7 mm TPD, the stirring of the pinless flat tool is sufficient for the creation of the spot joints though it can be varied to fabricate better joints.

5.2.5 Hardness variation

The comparison of hardness profiles along the upper array and lower array of DFSF samples are shown in Fig. 5.7(a-b). DFSF samples fabricated at 10 mm TD (lower level), 14 mm TD (medium level) and 16 mm TD (higher level) are selected for hardness measurement. A notable decrease in hardness is observed at the joint cross-section as compared to the parent sheet hardness (from Table 2.3) showing considerable effect of frictional heat flux as well as plastic deformation during stirring and tool plunge.

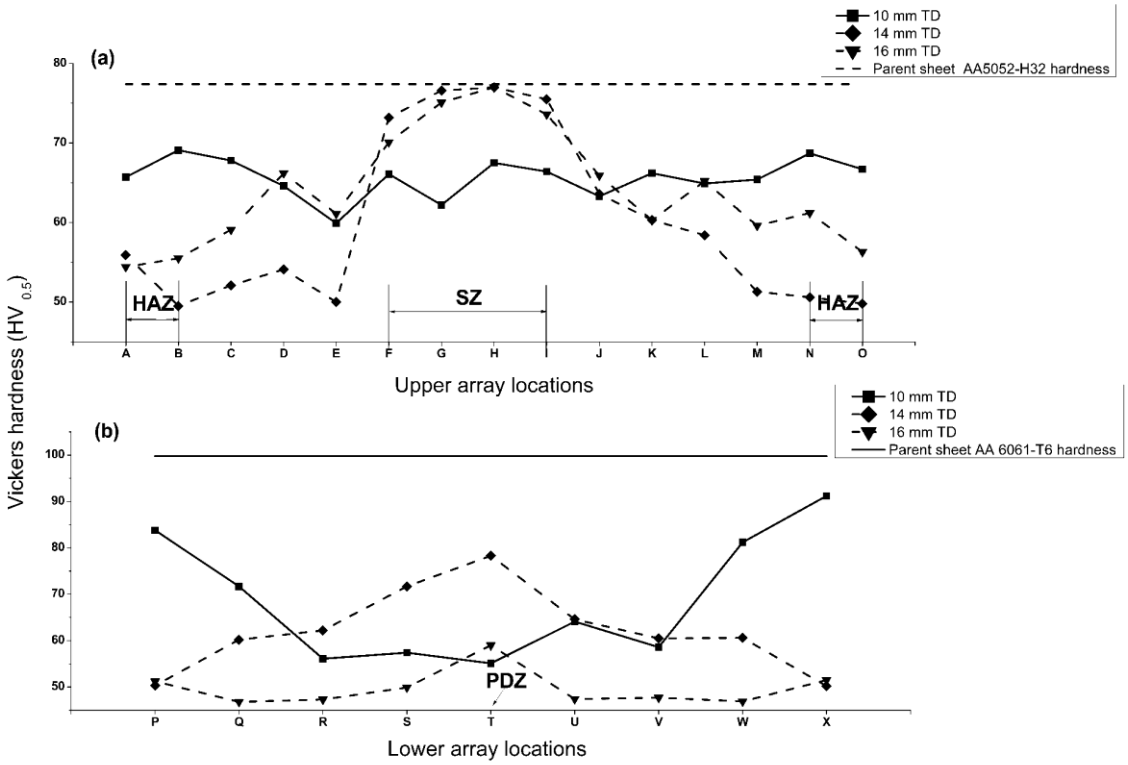

Figure 5.7. Comparison of hardness variation along DFSF joint cross-sections. (a) Upper array of indentation, (b) Lower array of indentation (Hardness deviation at each measurement location: ±1.7) (Refer array location in Fig. 4)

Upper sheet, AA 5052-H32 has undergone severe plastic deformation and microstructural changes under stirring action of the tool. For 10 mm TD, no significant difference in hardness is observed between the HAZ and the SZ. For medium and higher TDs, increase in hardness is seen in SZ as compared to HAZ. Samples at 10 mm TD has not undergone complete filling of pre-drilled hole as shown in Fig. 5.4a. Due to the lack of forging, SZ hardness had not become higher than the HAZ hardness. With increase in TD, samples at medium TD have undergone complete filling of the pre-drilled hole (Fig. 5.4c). Medium TD is sufficient to extrude and forge the upper sheet metal into the pre-drilled hole and further enable mechanical interlocking. Forging at the center has resulted in higher hardness recorded at SZ for medium and higher TD samples than that of lower TD samples. In addition, as evident from the microstructure, dynamic recrystallization has brought fine grain formation in the SZ (Fig. 5.6c) and hardness along locations F to I has increased significantly. A uniform decrease in hardness from the center towards both sides indicate the symmetric DFSF joint formation.

Lower sheet, AA 6061-T6 has undergone significant softening due to the annealing effect of the frictional heat flux. For 10 mm TD, a decrease in the hardness is observed along the lower array locations R to V, under moderate heat flux from the SZ. Hardness

has increased slightly at the center (location T) for 14 mm and 16 mm TD because the extruded upper sheet metal has undergone some amount of compressive deformation or forging and hence strain hardened inside the pre-drilled hole.

The nature of change in hardness of the upper sheet and the lower sheet are different because the upper sheet is solid solution-hardened alloy, while the lower sheet is precipitation-hardened alloy. The SZ with fine grain formation exhibits only the same hardness as the parent metal with coarse grains. Therefore, the hardness of the upper sheet is not only governed by grain structure, but also the dislocation density and its mobility. On the other side, the softening of the lower sheet is contributed by the coarsening and dissolution of strengthening precipitates. More details related to these mechanisms were explained in section 4.3.5 of previous chapter.

It is true that no particular trend of hardness variation is established with change in TD. However, at medium and higher TDs, hardness profiles are identical to some extent.

5.2.6 Joint morphology analysis

Morphological features such as UB, USFW, USFH and BW are influenced by the increase in TD during DFSF joint fabrication. These morphological features are plotted with respect to the TD in Fig. 5.8.

Flash width and flash height show a decreasing trend with increase in TD, as shown in Fig. 5.8a and Fig. 5.8b. This indicates that much of the upper sheet material is used for joint formation including mechanical interlocking and metallurgical bonding with increase in TD. Therefore, the flash size is reduced with increase in TD.

Severe UB is observed at higher TDs as shown in Fig. 5.8c. UB is comparatively less at low and medium TDs. SB (Fig. 5.8d) usually occurs at higher TDs, where the lower sheet undergoes excessive deformation due to the extreme heat flux from the stir spot and the associated pre-drilled hole closure. SB in analogous to lower sheet flash. No SB is observed at low and medium TDs. BW (Fig. 5.8e) shows a proportional increase with increase in TD. It is evident from the fact that the extent of metallurgical bonding increases with the area of contact of the stir tool.

The joint morphology study shows that TD has a significant impact on the generation of external features that result in overall aesthetic appearance of the joint. It should be noted that the UB and SB are less at the TD of 14 mm which was proposed as

the desirable TD as per mechanical performance test results and joint macrostructure characteristics. BW is also appreciable at this medium TD level.

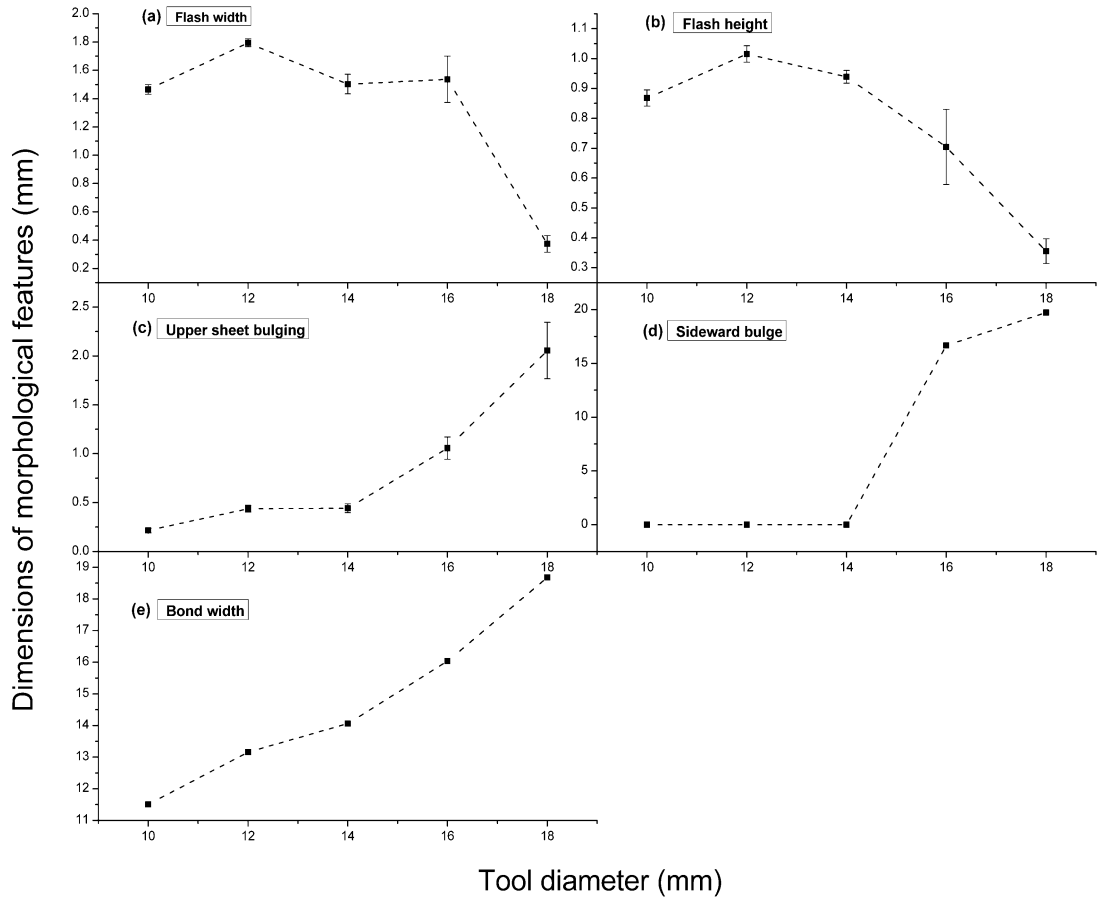

Figure 5.8. Comparison of joint morphological features at various TDs (a) USFW, (b) USFH, (c) UB, (d) SB and (e) BW

5.2.7 Modes of failure during mechanical testing

The following modes of failure are observed during mechanical performance tests of DFSF samples fabricated at various TDs.

- Tear-off: This type of failure mode is explained in section 2.2.9. This is the most common failure mode with change in TD (Fig. 5.9a).
- Partial bond delamination: This type of failure mode is explained in section 2.2.9.
- Pin shear: This type of failure mode is explained in section 3.2.5.
- Pin pull-out: This type of failure mode is explained in section 3.2.5.

  The following modes of failure occurs exclusively for uniaxial tensile test samples.
- Base metal fracture: This type of failure mode is explained in section 2.2.9 (Fig. 5.9d). This is the common failure mode during uniaxial tensile loading.
- Stir spot fracture: This type of failure mode is explained in section 2.2.9 (Fig. 5.9e).

Most of the failure modes occur in combined form such as combined pin shear and bond delamination (Fig. 5.9b) as well as combined pin pull-out and bond delamination (Fig. 5.9c). Three regions are identified, which act as CRs for failure of DFSF samples- (i) neck of the pin, CR1 (Fig. 5.5a), (ii) poor mechanical interlocking, CR2 (Fig. 5.5a) and (iii) upward deformation of the lower sheet, CR3 (Fig. 5.5b). Neck of the pin is subjected to pin shear failure and

Table 5.3. Modes of failure

TD	Lap shear test		Cross-tension test		Peel test		Tensile test	
	Trial 1	**Trial 2**	**Trial 1**	**Trial 2**	**Trial 1**	**Trial 2**	**Trial 1**	**Trial 2**
10	Pin shear + Bond delamination	Pin shear + Bond delamination	Pin pull out + Bond delamination	Pin pull out + Bond delamination	Pin shear + Bond delamination	Pin pull out + Bond delamination	Stir spot fracture	Stir spot fracture
12	Tear-off	Tear-off	Tear-off	Tear-off	Tear-off	Tear-off	Base metal fracture	Base metal fracture
14	Pin shear + Bond delamination	Pin pull out + Bond delamination	Tear-off	Pin pull out + Bond delamination	Tear-off	Tear-off	Base metal fracture	Base metal fracture
16	Tear-off	Tear-off	Tear-off	Tear-off	Tear-off	Tear-off	Base metal fracture	Base metal fracture
18	Pin shear + Bond delamination	Pin shear + Bond delamination	Pin shear + Bond delamination	Pin shear + Bond delamination	Pin shear + Bond delamination	Tear-off	Base metal fracture	Base metal fracture

poor mechanical interlocking leads to pin pull out. Each of these failure modes occur in combination with bond delamination. Upward deformation of the lower sheet results in tear off failure along the circumference of the stir spot as well as bond delamination failure (Fig. 5.4(b-d) and Fig. 5.5(b-d)). The SZ seems to be separated by this deformation from other regions of the upper sheet.

The modes of failure during mechanical performance tests are summarized in Table 5.3. Samples at 10 mm TD show simultaneous bond delamination along with pin shear or pin pull out. Partial mechanical interlocking strengthens these samples along with the metallurgical bonding. For samples fabricated at 12 mm to 16 mm TD, tear off is the most common failure mode for which metallurgical bonding and mechanical interlocking are present. Most of the samples fabricated at 18 mm TD show bond delamination along with pin shear.

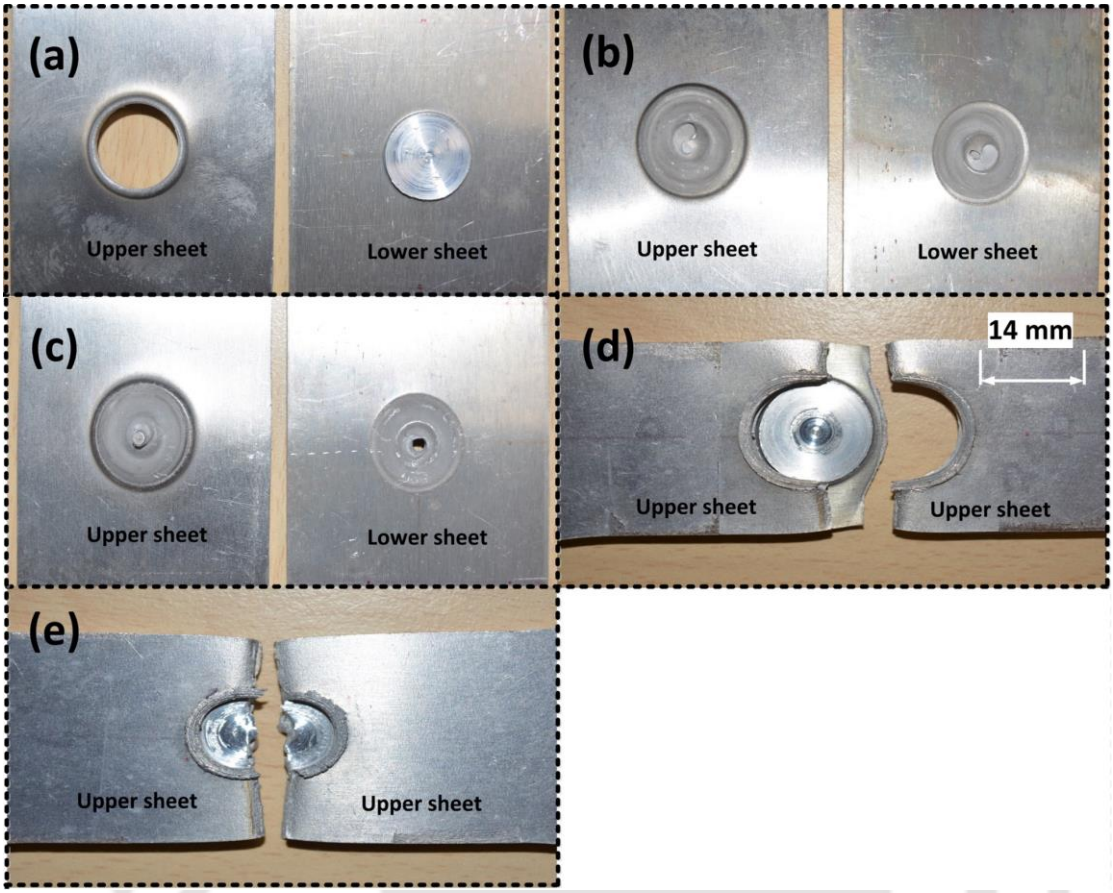

Figure 5.9. Modes of failure. (a) Tear off, (b) Combined pin shear and bond de-lamination, (c) Combined pin pullout and bond delamination, (d) Base metal fracture, (e) Stir spot fracture

It can be observed that the peel test samples commonly show tear-off failure. Samples fabricated at TDs from 12 mm to 18 mm show upward deformation of the lower sheet (Fig. 5.4-5.5). Therefore, upward deformation has uniformly affected the peel off resistance of the samples and peel test fracture load remain almost same throughout the entire TD range. Most of the DFSF samples show base metal fracture under uniaxial tensile testing.

5.3 Conclusions

The effect of TD on the mechanical performance and joint formation of the DFSF joints is comprehensively studied. The following conclusions are made from the results obtained.

- The authors suggest 14 mm TD as the best level to fabricate DFSF joints out of AA 5052-H32 and AA 6061-T6 sheets, but with a slight loss in mechanical performance. Samples fabricated at TDs other than 14 mm possess either insufficient mechanical interlocking or insufficient metallurgical bonding. The

strength of the DFSF samples at various loading conditions is a play off between metallurgical bonding and mechanical interlocking, whose presence and absence governs the joint performance.

- Lap shear fracture load of 6.22 kN obtained for DFSF samples at medium TD (14 mm) is better than that of FSSW and CFSF samples. DFSF joints are free of pin-hole defect, which is commonly found in FSSW joints, and rivet head formation, which is found in CFSF joints.
- Macrostructure analysis shows that increase in TD leads to increase in frictional contact area and subsequently increased heat flux and extent of plastic deformation. This has resulted in closure of the pre-drilled hole and lack of mechanical interlocking at higher TDs.
- The frictional heat flux and plastic deformation generated at the stir spot has induced significant microstructural changes at various zones of the DFSF joints. The SZ exhibits dynamic recrystallization, while the PDZ and HAZ are statically recrystallized.
- Hardness measurements revealed that upper and lower sheets have undergone considerable decrease in hardness with change in TD. With increase in TD, SZ hardness is found to be increasing. TD has a significant influence on the formation of external morphological features. Absence of pinhole and absence of rivet head have improved the aesthetic appearance of the DFSF joints.
- The CRs, which are responsible for the failure of DFSF joints are identified as the neck of the pin, poor mechanical interlocking and upward deformation of the lower sheet. Tear off is the most common failure mode, while samples at highest TD (18 mm) shows pin shear in most of the cases.

Chapter 6

DFSF joining of AA 5052-H32 and AA 6061-T6 sheets at varying pre-drilled hole diameters

In this chapter, the effect of change in pre-drilled HD on the joint strength and joint formation of DFSF joints is evaluated through mechanical performance tests, macro/ micro structure analysis, hardness measurement, joint morphology analysis and failure modes analysis. The optimum tool rotational speed of 500 rpm obtained from chapter 2, the sheet metal combination employed in chapter 2, optimum TPD of 0.5 mm obtained from chapter 4 and optimum TD of 14 mm obtained from chapter 5 are adopted in this work.

6.1 Methodology

The principle of DFSF joint formation is presented in section 4.2.1.

6.1.1 DFSF experiments

The details of DFSF sample fabrication is presented in section 4.2.2. The standard material properties of the upper sheet and the lower sheet are presented in Section 2.1.2. The dia. of the pre-drilled hole, the primary variable of the present work, is varied in three levels, namely lower level at 2.5 mm and 3 mm, medium level at 3.5 mm and 4 mm and higher level at 4.5 mm and 5 mm. Minimum HD is kept at 2.5 mm with an intention to prevent possible closure of the pre-drilled hole. The maximum HD is restricted to 5 mm to keep the metallurgically bonded area unaffected. Rest of the process parameters namely tool rotational speed, TPD, tool plunge rate and direction of tool rotation are kept constant at 500 rpm, 0.5 mm, 0.002 mm/s and clockwise direction respectively considering our experience from the previous experimental trials (Lazarevic et al., 2013).

6.1.2 Mechanical performance tests

Details of mechanical performance tests are discussed in section 2.1.3. In the present work, a comparison of the lap shear fracture load of DFSF samples with that of conventional FSF and FSSW samples, fabricated on the same material combination is presented. DFSF sample fabricated with HD of 3 mm is chosen for comparison. For conventional FSF process, a pre-drilled hole of 3 mm dia. was employed as mentioned in chapter 2. A hemispherical shaped anvil cavity with 0.55 mm depth and 3.5 mm dia. was employed for the rivet head formation. Both pinned FSSWed joints and pinless FSSWed joints were fabricated. For pinned FSSW process, stir tool with a pin of 4 mm dia. and 1 mm length, and shoulder dia. of 14 mm were used (Paidar et al., 2014). For pinless FSSW process, the pinless stir tool used in DFSF process was employed. For uniformity in process execution, all other process parameters were kept same for all the four processes.

6.1.3 Macro/ microstructure, hardness measurement and joint morphology analyses

Details of macrostructure analysis, hardness measurement and joint morphology analysis are discussed in Section 2.1. Details of microstructure analysis is discussed in Section 4.2. The internal joint features such as upward deformation of the lower sheet, neck dia. of the pin and collar length are also considered for measurement.

The hardness measurements were taken on the DFSF sample cross-sections in two arrays of indentations with 2 mm spacing in between the indentations. Upper array and lower array of indentations are shown in Fig. 6.1. The external morphological features such as UB, flash width and flash height were also measured (Fig. 6.2).

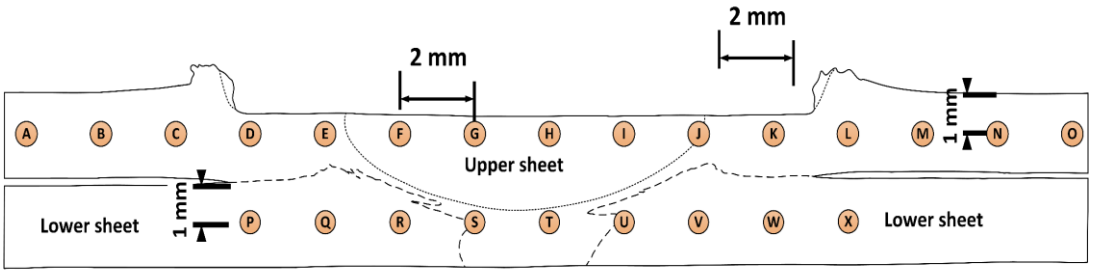

Figure 6.1. Measurement locations of hardness along the joint cross-section (Dimension not to scale)

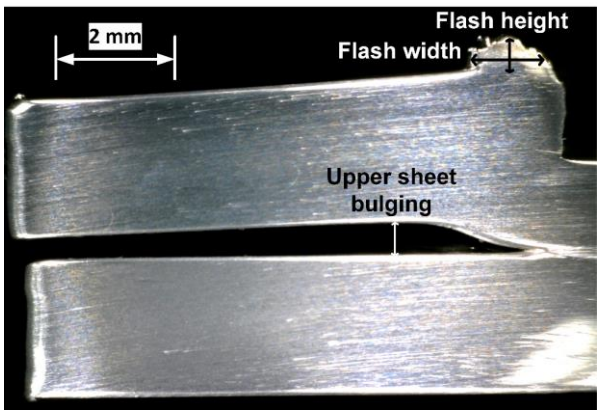

Figure 6.2. External morphological features measured in the DFSF joint cross-section

6.2 Results and Discussion

A comprehensive discussion about the effect of HD on the evolution of joint macrostructure and microstructure, hardness variation, external joint features, mechanical performance and failure modes are presented in the following subsections.

6.2.1 Joint formation analysis through macrostructure

DFSF samples fabricated at various HDs of 2.5 mm, 3.5 mm and 5 mm are selected for macrostructure analysis. In addition, the direction of metal flow during the joint formation are also identified. The macrostructure of the DFSF samples with various zones marked and the schematic representation of the metal flow directions are shown in Fig. 6.3 and Fig. 6.4 respectively. When the upper sheet undergoes plastic deformation and further extrusion due to the stirring action of the tool and the downward tool plunge, the lower sheet undergoes plastic deformation by virtue of the conducted heat flux from the upper sheet and the tool plunge force. The extruded pin forms the central part of the DFSF joint cross-section. It is surrounded by the metallurgically bonded interface between the two sheets.

The various zones in DFSF joint are SZ, PDZ, TMAZ and HAZ. The effect of change in HD over the formation of these zones are discussed below. The upward deformation of the lower sheet, geometric measurements such as neck dia. of the pin and collar length are illustrated in Fig. 6.4c.

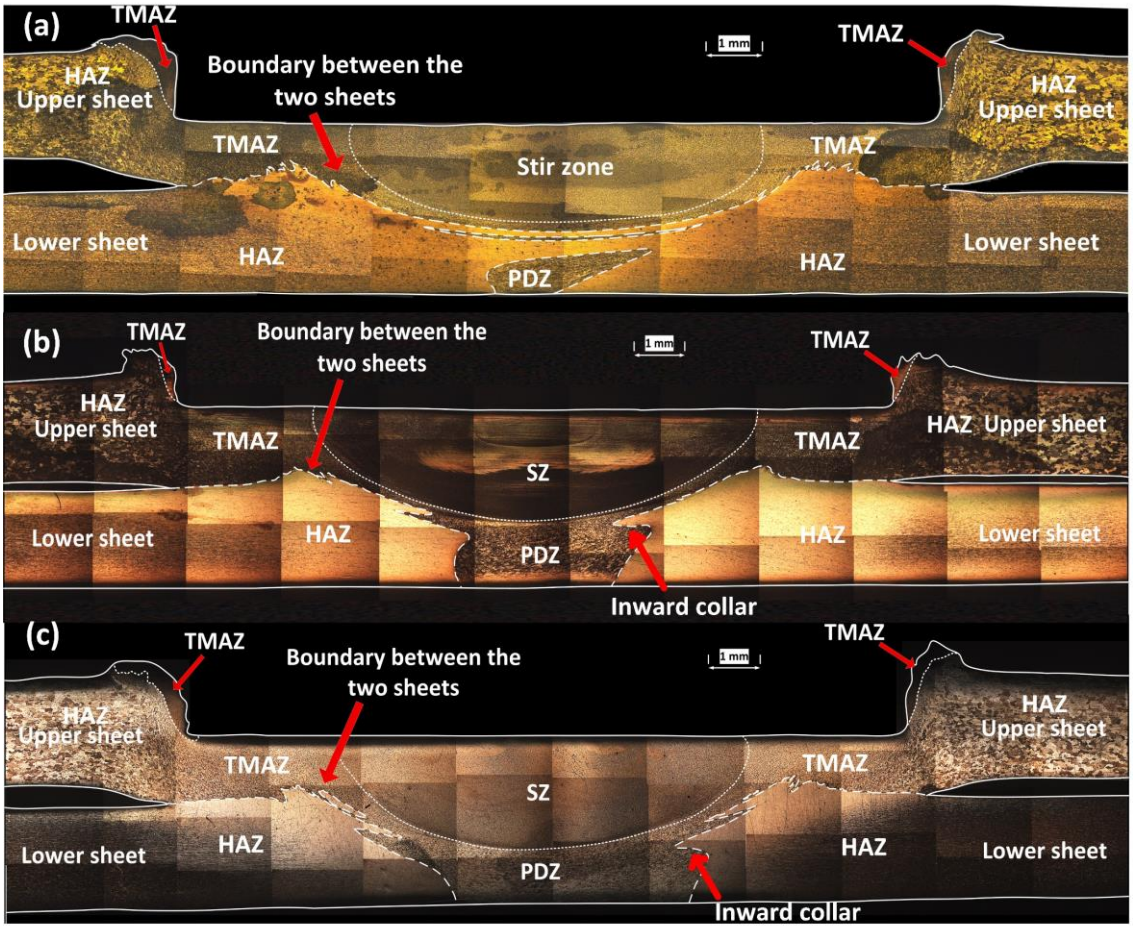

Figure 6.3. Joint macrostructure of DFSF samples fabricated at (a) 2.5 mm (Lower HD), (b) 3.5 mm (Medium HD), (c) 5 mm (Higher HD)

6.2.1.1 Lower HDs (2.5 mm and 3 mm)

At lower HDs, the hole size is so small that chance of closure of the pre-drilled hole is high. The closure of the pre-drilled hole of 2.5 mm dia. is shown in Fig. 6.3a and Fig. 6.4a. The upper sheet metal is partially extruded through the pre-drilled hole. During extrusion, the plastic deformation of the region around the hole has resulted in its closure. Due to this, the extruded upper sheet metal is isolated in the lower sheet. The collar growth and subsequent pin formation is absent at 2.5 mm HD. However, all the DFSF samples with lower HDs are strengthened by metallurgical bonding. With increase in HD, the chance of closure of the hole is comparatively low. The closure of the pre-drilled hole is absent for 3 mm HD as observed in previous chapters. The hook defect formation is not observed even at lower HD levels, however, average upward deformation of lower sheet of about 2.45±0.012 mm is observed at 2.5 mm HD.

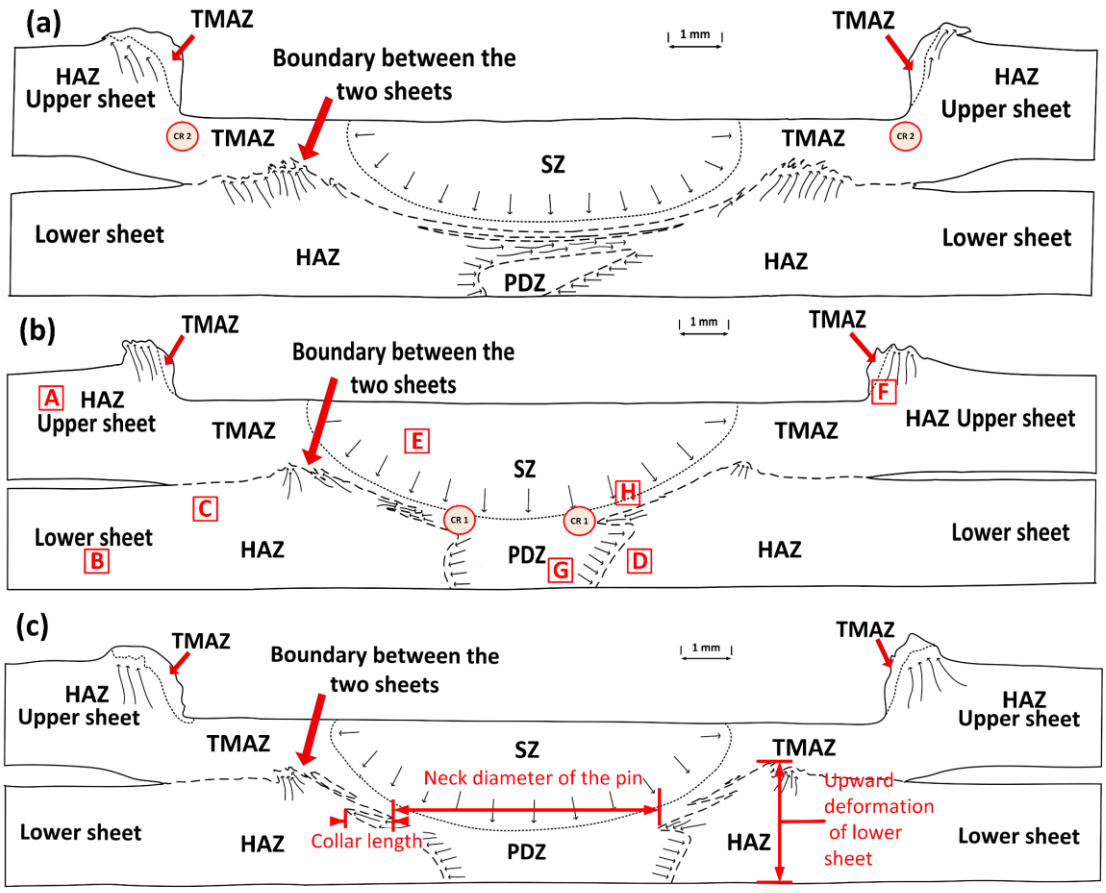

Figure 6.4. Schematic representation of the DFSF joint cross-section at (a) 2.5 mm, (b) 3.5 mm, (c) 5 mm HDs with metal flow directions indicated

6.2.1.2 Medium HDs (3.5 mm and 4 mm)

The chance of closure of the pre-drilled hole is low at medium HDs. At medium HDs such as 3.5 mm, the collar growth is observed in the joint cross-section as shown in Fig. 6.3b and Fig. 6.4b, which interlocks the extruded upper sheet metal. In addition, these joints are also strengthened by metallurgical bonding. Similar observation is seen at 4 mm HD. With increase in HD, the size of the PDZ has increased. Neck dia. of the pin and collar length about 4.15±0.001 mm and 0.83±0.017 mm are obtained, respectively at 3.5 mm HD. Upward deformation of lower sheet is about 2.48±0.004 mm at 3.5 mm HD. However, no hook defect is observed.

6.2.1.3 Higher HDs (4.5 mm and 5 mm)

With increase in HD to higher level such as 5 mm, major improvement in the mechanical interlocking is not observed (Fig. 6.3c and Fig. 6.4c). However, the collar growth is perfect and the samples are metallurgically bonded. The PDZ size is increased

due to larger HD. Neck dia. of the pin is increased to 5.51±0.007 mm at 5 mm HD. A significant improvement in the collar length is not observed. It is about 0.83±0.069 mm at 5 mm HD. The surrounding metallurgically bonded area has been decreased due to larger pin size. Further, upward deformation of the lower sheet remains more or less same as lower and medium HDs. However, the hook defect is absent. Similar situation exists at 4.5 mm HD.

To summarize, HD range from 3 mm to 5 mm can be considered to be optimum from the macrostructure analysis on condition such as the chance of closure of the pre-drilled hole is less. An increase in the neck dia. of the pin is observed with increase in the HD. However, with increase in HD, absence of further collar growth and reduction in metallurgically bonded area results in no further improvement in joint strength. Upward deformation of the lower sheet remains same with increase in HD, which shows that it has not reached up to such severity to act as hook defect in DFSF joints.

For DFSF joints, the SZ size remains almost same throughout the entire HD range and the SZ is confined to the upper sheet only. The SZ has no significant role in joint formation other than generating sufficient heat flux for plastic deformation and extrusion of the upper sheet. Pinless stir tools generate shallow deformation zones (Bakavos et al., 2011). Unlike in FSSW, the stir mixing of upper and lower sheet metals is absent in DFSF joints, which prevents hook defect formation.

6.2.2 Microstructure characterization

Fig. 6.5 shows the microstructures of SZ, PDZ, HAZ and TMAZ at 200X magnification for the DFSF joints fabricated at 3.5 mm HD. The corresponding regions on the macrostructure of DFSF joint is shown in boxes marked with alphabets A to H in Fig. 6.4b. The HAZ is subjected to recrystallization and grain growth under frictional heat flux conducted from the stir spot. The PDZ is subjected to recrystallization and grain growth under frictional heat flux and plastic deformation by extrusion. The SZ has undergone recrystallization due to frictional heat flux and, severe plastic deformation by stirring. TMAZ has undergone grain recovery without recrystallization. Similar recrystallization behaviour of aluminum alloys was also reported during refill FSSW process (Ding et al., 2017). The lower sheet is in contact with the backing plate so that its heat dissipation is faster than that of the upper sheet. This could also contribute to variable microstructural

changes in the upper sheet and the lower sheet. The comparison of grain size of various zones of the DFSF joint is shown in Table. 6.1.

The HAZ of the upper sheet, Fig. 6.5a, possesses coarse grains (with grain dia. of 44.9 µm) than that of the HAZ of the lower sheet (with grain dia. 22.5 µm), Fig. 6.5b. Recrystallization, and grain growth of about 200% is observed in the HAZ of the two sheets, when compared to the corresponding parent sheet grain size (Table 2.3). This is due to frictional heat flux conducted from the stir spot. However, only 41% increase in the grain size is observed in the lower sheet HAZ just under the stir spot as shown in Fig. 6.5c and Fig. 6.5d. These regions have more tendency towards prolonged recrystallization because of its location just under the stir spot. The grain growth in these regions might be arrested by the plastic deformation induced by the plunge of the stir tool.

Fine equi-axed grains are observed in the SZ region (Fig. 6.5e) with grain dia. of about 5.6 µm. The severe plastic deformation due to stirring and frictional heat generation has brought about dynamic recrystallization in the SZ. Similar observation was also reported in conventional FSSW process (Mishra and Ma, 2005). Fine equi-axed grains represent more intensive stirring. Fine grain formation in the SZ and coarse grain formation in the HAZ shows that other than heat flux, the grain growth is controlled by the extent of plastic deformation. Stirring induced plastic deformation arrests the grain growth in the SZ, while HAZ with no plastic deformation possesses larger grains. Transition from HAZ grains to TMAZ grains is shown in Fig. 6.5f. TMAZ grains are also smaller than upper sheet HAZ grains, with grain size of about 18.9 µm. The frictional contact with lateral surface of the rotating stir tool and heat generated highly deformed grains in the TMAZ. Recovered grains without recrystallization is observed in the TMAZ. The strain induced by plastic deformation is insufficient to create recrystallization in the TMAZ. Similar recovered grains were also observed in the TMAZ of FSWed AA 5083-O aluminum alloys (Sato et al., 2001, Ma et al., 2002).

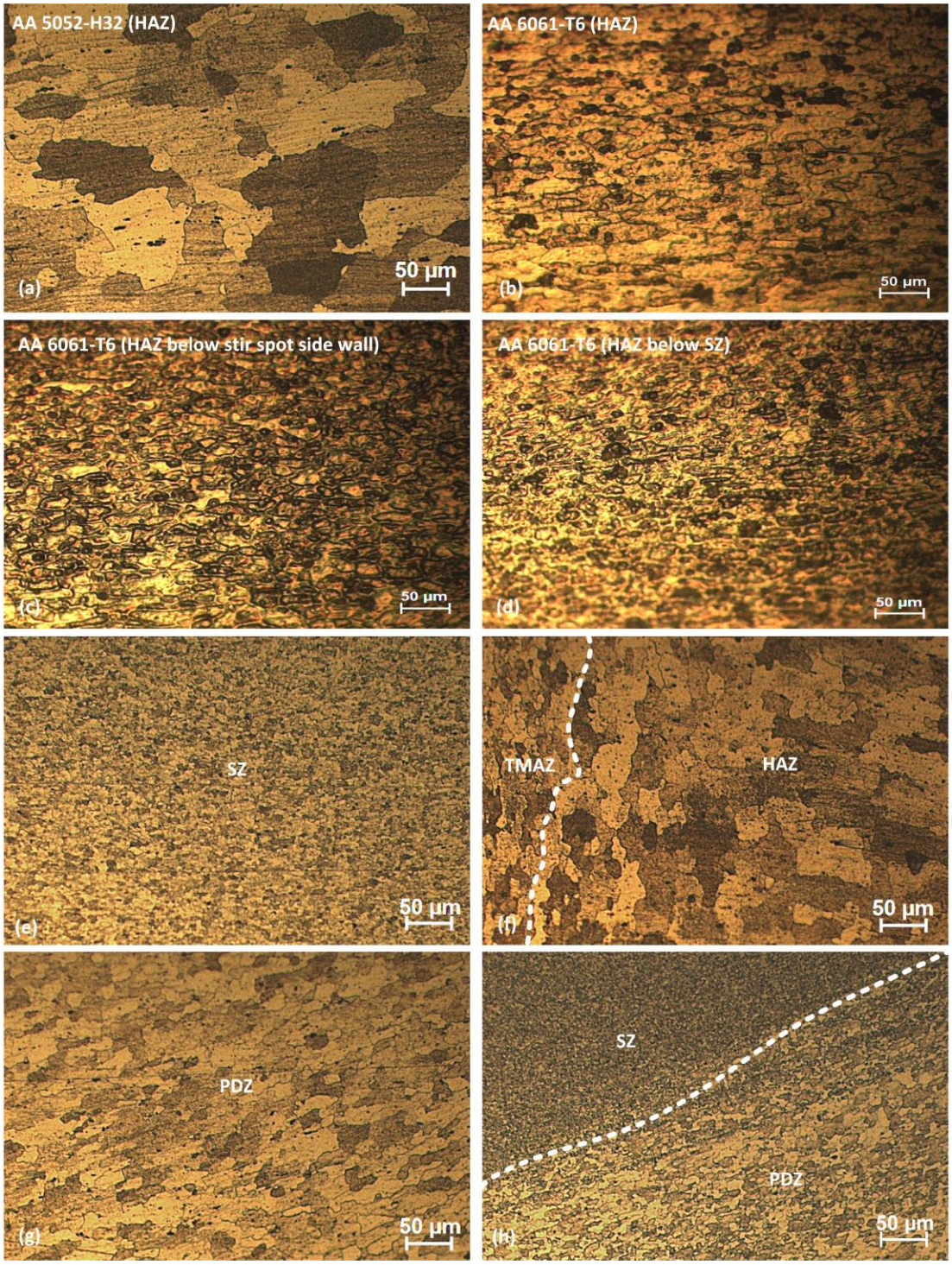

Figure 6.5. Microstructure of (a) AA 5052-H32 HAZ, (b) AA 6061-T6 HAZ, (c) AA 6061-T6 HAZ (below stir spot side wall) , (d) AA 6061-T6 HAZ (below SZ), (e) SZ, (f) TMAZ- HAZ boundary, (g) PDZ and (h) SZ-PDZ boundary at 200X magnification (Regions on which the microstructures were observed are shown with boxes in Fig. 7b)

The PDZ grains are statically recrystallized with further grain growth (having grain dia. of 26.7 µm), whose size is almost comparable with that of the parent sheet metal (Fig. 6.5g). Unlike SZ, the PDZ has not undergone severe plastic deformation due to stirring. However, the frictional heat flux and the directional extrusion towards the pre-drilled hole

during the tool plunge result in static recrystallization and grain growth. The SZ tends to possess circular motion along with the rotating stir tool, while the PDZ undergoes radial inward movement and extrusion into the pre-drilled hole during the tool plunge. Therefore, the extent of grain refinement of these two regions are entirely different. A clear boundary is observed between the grain structures of the two regions as shown in Fig. 6.5h.

Table 6.1. Grain size comparison of the various zones of the DFSF joint

Location	Average grain dia. (μm)
SZ	5.6
AA 6061-T6 HAZ (below stir spot side wall)	15.9
AA 6061-T6 HAZ (below SZ)	15.9
TMAZ	18.9
AA 6061-T6 HAZ (lower sheet)	22.5
PDZ	26.7
AA 5052-H32 HAZ (upper sheet)	44.9

To summarize, the frictional heat flux and plastic deformation has brought about microstructural changes such as recrystallization and grain growth in the DFSF joint. This leads to the distinction of various zones in the cross-section of DFSF joint, which are identical to the zones observed in other friction stir based joining processes.

6.2.3 Hardness variation

Fig. 6.6 shows the hardness variation in DFSF joints along the upper array and lower array locations with change in HD. The hardness variation is not influenced by change in HD because uniform hardness profile is observed in Fig. 6.6a,b.

The upper array of indentations possess an increase in hardness towards the SZ. This is due to strain hardening during extrusion and forging of upper sheet into the pre-drilled hole. However, Kesharwani et al. (2015) reported that the increase in hardness of the SZ is due to fine equi-axed grain formation. The decrease in hardness towards the periphery of the joint is attributed to softening of the HAZ due to recrystallization and grain growth. The lower array of indentations possess uniform hardness. However, the slight increase in hardness at the PDZ occurs due to the forging action of the stir tool. The lower array of indentations are mostly located in the HAZ region of the lower sheet.

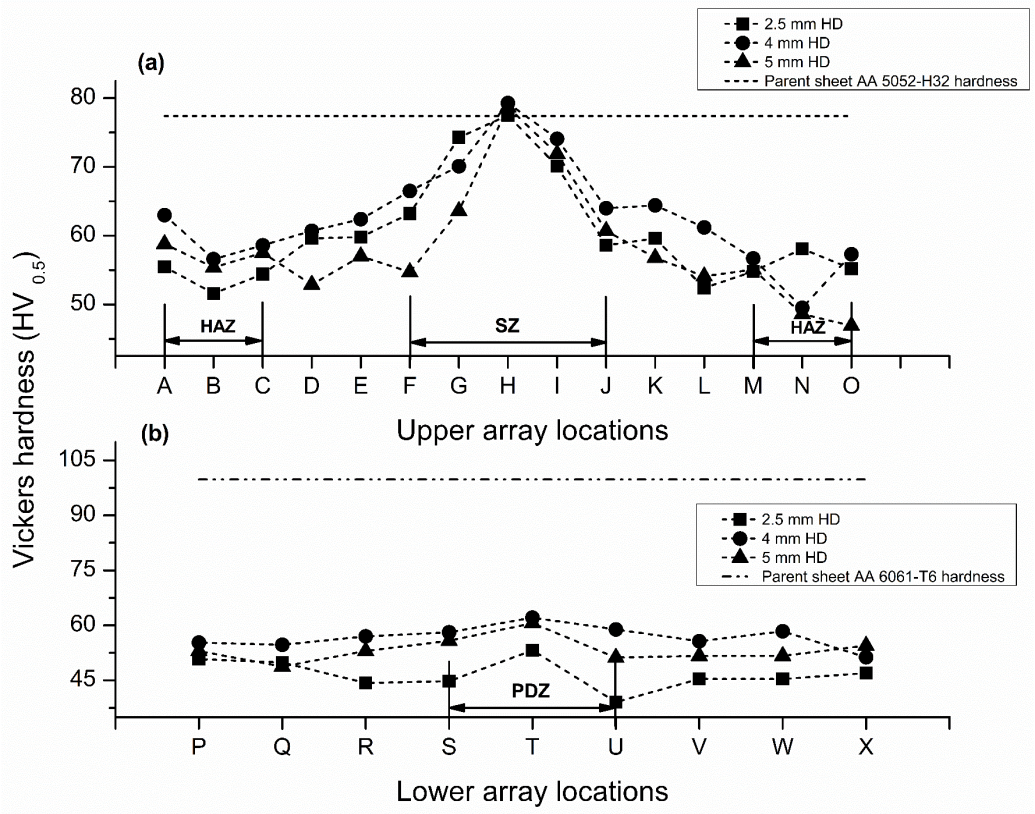

Figure 6.6. Comparison of hardness variation along the DFSF joint cross-sections. (a) Upper array of indentation, (b) Lower array of indentation (Typical hardness variation at each measurement location is ±2.1)

The nature of change in hardness of the upper sheet and the lower sheet are different because the upper sheet, AA 5052-H32 is a solid solution-hardened alloy, while the lower sheet, AA 6061-T6, is a precipitation-hardened alloy. The SZ with fine grain formation exhibits only the same hardness as the parent metal with coarse grain formation. Similarly significant softening of the lower sheet is also observed. The reason behind this phenomena is explained in section 4.3.5 and 5.2.5.

6.2.4 Joint morphology analysis

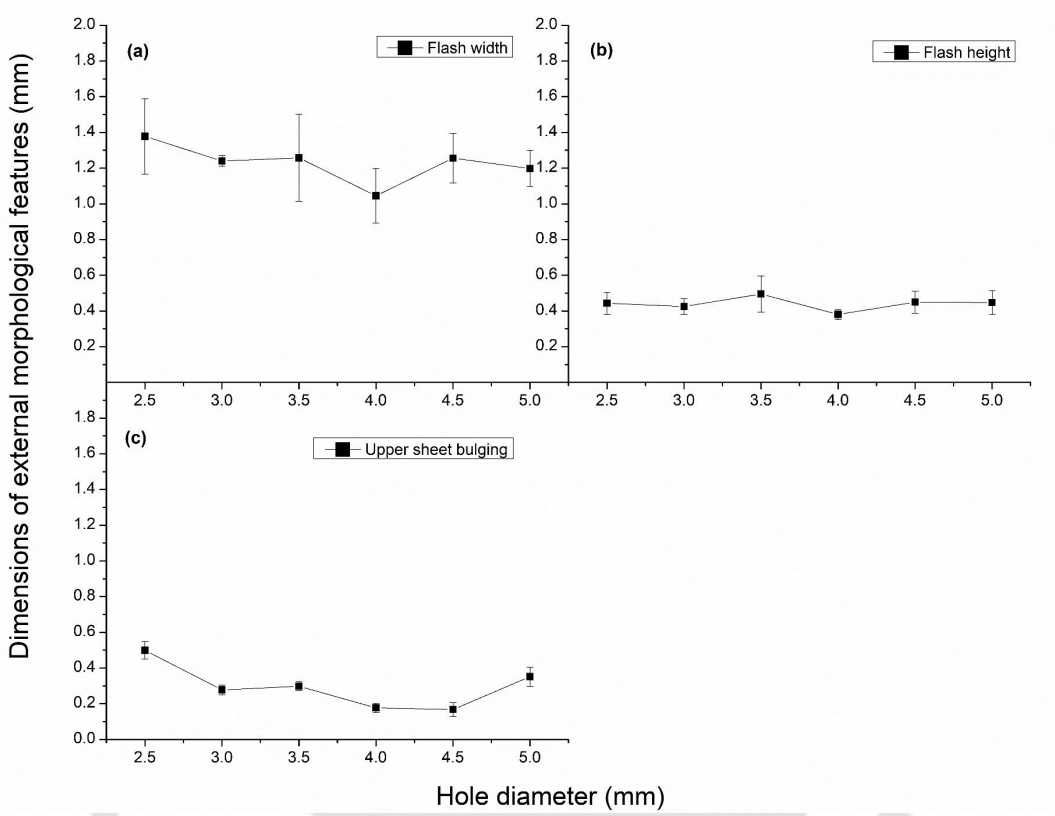

Figure 6.7. Variation of (a) Flash width, (b) Flash height, (c) UB with change in HD

The effect of HD on the size of external morphological features such as flash width, flash height and UB, which affect the aesthetic appearance of DFSF joint is shown in Fig. 6.7. The outward material flow beneath the shoulder of a pinless stir tool leads to weld flash formation (Cox et al., 2014a). Slight decrease in flash width of 1.15 mm is observed when HD increases from 2.5 mm to 5 mm (Fig. 6.7a). However, the flash height remains same throughout the change in HD (Fig. 6.7b). The small reduction in the overall flash size is contributed by the increase in HD. At 2.5 mm HD, the closure of the hole results in outward material flow in DFSF sample. With increase in HD, the plunge of the tool results in extruding more upper sheet material towards the pre-drilled hole, instead of pushing upper sheet material to the periphery of the stir spot as flash.

A decrease in UB is observed between 2.5 mm and 4.5 mm HD (Fig. 6.7c). At lower HDs such as 2.5 mm, due to closure of the pre-drilled hole, the upper sheet is bulged outwards during the plunge of the stir tool. At higher HDs (say at 4.5 mm), there is no closure of the hole and the extension of upper sheet is easy, thereby reducing the UB.

To summarize, with increase in HD to medium and higher levels, the size of the external morphological features, which affect the aesthetic appearance of the joint decreased. The closure of the pre-drilled hole and the extrusion of upper sheet through the pre-drilled hole have opposite effect on the growth of external morphological features. The HD range from 3 mm to 5 mm can be fixed as optimum from the morphology analysis.

6.2.5 Mechanical performance tests

The effect of HD on the fracture load of DFSF samples is shown in Fig. 6.8. The HD at which maximum fracture load obtains varies from test to test. Lap shear samples show almost identical fracture load throughout the HD range. Maximum lap shear fracture load is obtained at 4.5 mm HD and minimum at 4 mm HD. Maximum cross-tensile fracture load is obtained at 2.5 mm HD and minimum at 5 mm HD. For peel test, maximum fracture load is obtained at 3.5 mm HD and minimum at 5 mm HD. However, it is observed that DFSF samples fabricated at 3 mm and 3.5 mm HDs show appreciable overall performance in all the mechanical performance tests. DFSF samples fabricated at 3 mm HD show lap shear fracture load of 7.42 kN (95% of maximum value), cross-tension fracture load of 2.89 kN (83% of maximum value) and peel fracture load of 1.05 kN (90% of the maximum value). Samples fabricated at 3.5 mm HD show lap shear fracture load of 7.18 kN (92% of maximum value), cross-tension fracture load of 3.07 kN (88% of maximum value) and maximum peel fracture load of 1.17 kN. Therefore, 3 mm and 3.5 mm HDs can be chosen as the optimum range for better mechanical performance of the present material combination. At higher HDs like 4.5 mm and 5 mm, samples show minimum fracture load in cross-tension test and peel test. 1.74 kN decrease in cross-tension fracture load (56% decrease) and 0.52 kN decrease in peel fracture load (44% decrease) is recorded, when HD increases from 3.5 mm to 5 mm. For any particular HD, lap shear samples show maximum fracture load, cross-tension samples show intermediate fracture load and peel test samples show minimum fracture load. During friction stir riveting by extrusion, Evans et al. (2016) reported that a strong correlation between joint strength and hole size cannot be established during mechanical performance tests. However, the joint strength of DFSF samples show notable variation with change in HD.

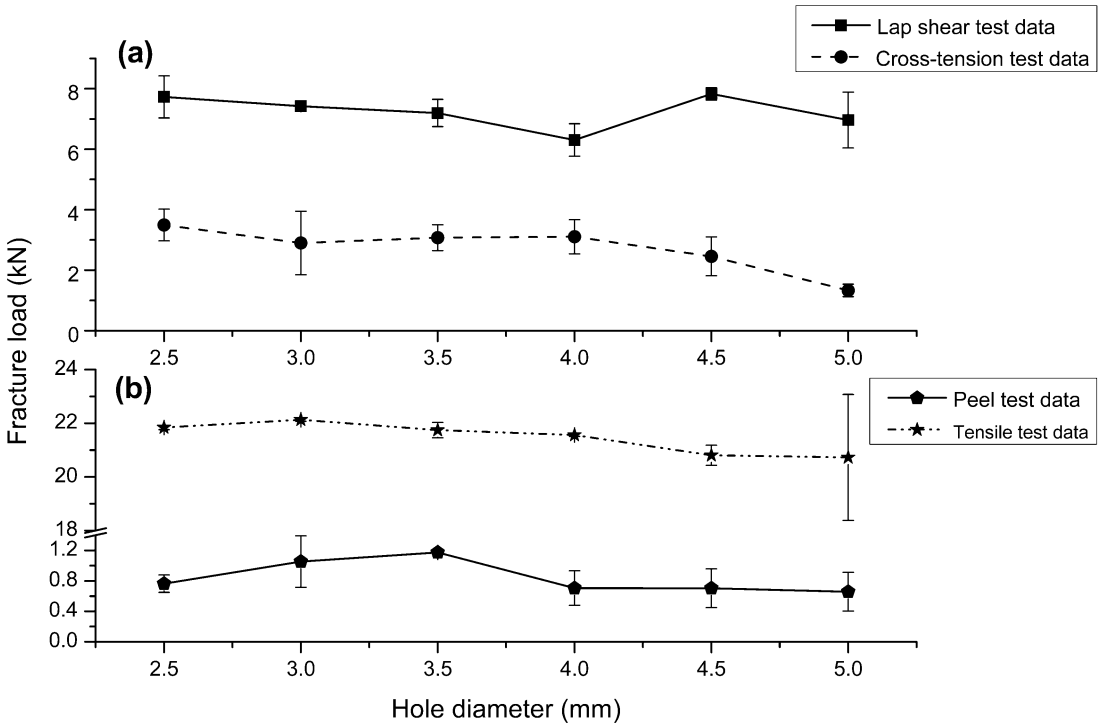

Figure 6.8. Comparison of fracture loads at various HDs during mechanical performance tests of DFSF samples

Sajed (2016) reported that maximum displacement/extensibility can be considered as an indicator of energy absorption before failure of the joint and further accounts to its safety consideration. In DFSF samples, extensibility is about 1 mm for lap shear samples, 13 mm for cross-tension samples and 26 mm for peel test samples. Therefore, the lap shear samples show reasonable extensibility. Extensibility of the cross-tension and peel test samples are considerably large due to the peculiar nature of these tests in which bending and unbending of the metal strips add considerable extension during the tests. DFSF samples show identical fracture load in uniaxial tensile tests. Fracture load of 21.46 kN and average extension about 4.24 mm are recorded throughout the HD range.

To summarize, the HD at which maximum fracture load obtained for each of the mechanical performance test is not unique and it depends on the nature of loading. The effect of HD on the mechanical performance is also significant. However, 3 mm and 3.5 mm HDs can be considered as optimum for the present material combination considering a slight loss in overall mechanical performance.

6.2.6 Modes of failure during mechanical performance tests

Figure 6.9. Modes of failure. (a) Tear-off, (b) Combine pin pull-out and bond delamination, (c) Combined pin shear and bond delamination, (d) Base metal fracture and (e) Stir spot fracture

The failure modes observed during the mechanical performance tests are shown in Fig. 6.9 and summarized in Table. 6.2. The various modes of failure such as tear off, combined pin pull-out and bond delamination, and combined pin shear and bond delamination are observed in DFSF samples.

- Tear-off: This type of failure mode is explained in section 2.2.9 (Fig. 6.9a)
- Bond delamination: This type of failure mode is explained in section 2.2.9.
- Pin shear: This type of failure mode is explained in section 3.2.5.
- Pin pull-out: This type of failure mode is explained in section 3.2.5.

In addition to tear-off failure, most of the failure modes occur in combined form namely such as combined pin pull-out and bond delamination (Fig. 6.9b), as well as

combined pin shear and bond delamination (Fig. 6.9c). Combined pin pull-out and bond delamination is analogous to nugget pull-out observed during friction stir riveting by extrusion (Evans et al., 2016). Combined pin shear and bond delamination was also observed in friction stir riveting by extrusion.

Following failure modes are observed during uniaxial tensile tests.

- Base metal fracture: This type of failure mode is explained in section 2.2.9 (Fig. 6.9d).
- Stir spot fracture: This type of failure mode is explained in section 2.2.9 (Fig. 6.9e).

Two CRs are identified, which are responsible for failure of DFSF samples during mechanical performance tests. They are neck of the pin (CR1), circumference of the stir spot (CR2), as shown in Fig. 6.4a and Fig. 6.4b. Shearing of the pin and pull-out failures are initiated from the neck of the pin, CR1, which act as weakest zone susceptible to failure. Tear off and bond delamination failures originate from the circumference of the stir spot, CR2. At maximum load, the fracture along the circumference of the stir spot leads to tear off failure and bond delamination failure initiates from the partially bonded regions below the circumference of the stir spot.

Table 6.2. Modes of failure.

HD (mm)	Lap shear test		Cross-tension test		Peel test		Tensile test	
	Trial 1	Trial 2	Trial 1	Trial 2	Trial 1	Trial 2	Trial 1	Trial 2
2.5	Pin shear + Bond delamination	Pin pull out + Bond delamination	Tear-off	Pin shear + Bond delamination	Pin pull out + Bond delamination	Pin pull out + Bond delamination	Stir spot fracture	Stir spot fracture
3	Pin shear + Bond delamination	Pin pull out + Bond delamination	Tear-off	Pin shear + Bond delamination	Pin pull out + Bond delamination	Pin pull out + Bond delamination	Base metal fracture	Stir spot fracture
3.5	Pin pull out + Bond delamination	Tear-off	Pin pull out + Bond delamination	Pin pull out + Bond delamination	Pin pull out + Bond delamination	Pin pull out + Bond delamination	Stir spot fracture	Stir spot fracture
4	Pin shear + Bond delamination	Pin shear + Bond delamination	Tear-off	Tear-off	Pin pull out + Bond delamination	Pin shear + Bond delamination	Stir spot fracture	Stir spot fracture
4.5	Pin shear + Bond delamination	Tear-off	Tear-off	Pin shear + Bond delamination	Pin pull out + Bond delamination	Pin shear + Bond delamination	Stir spot fracture	Stir spot fracture
5	Pin pull out + Bond delamination	Pin pull out + Bond delamination	Pin pull out + Bond delamination	Pin pull out + Bond delamination	Pin pull out + Bond delamination	Pin pull out + Bond delamination	Stir spot fracture	Stir spot fracture

The failure modes are random in nature throughout the HD range for various mechanical performance tests. However, combined pin pull-out and bond delamination

failure is the commonly occurring failure mode. This shows that the two CRs are equally active in the DFSF joint. For uniaxial tensile test, the stir spot fracture is commonly observed. The failure of these samples are initiated from the geometrical inhomogeneity created by the stir spot in the gauge length region of the tensile sample.

6.2.7 Comparison between DFSF, CFSF and FSSW processes

Table 6.3 compares the fracture load from lap shear test of samples fabricated by DFSF, CFSF and FSSW with stir tool having pin, and without pin. The lap shear fracture load of DFSF samples is 42% better than that of CFSF samples, 86% better than that of FSSW samples fabricated with a tool having pin and 25% better than pinless FSSW samples. The superior joint strength of DFSF samples is evident from this comparison. Therefore, the extra lap shear strength for DFSF samples is contributed by simultaneous mechanical interlocking and metallurgical bonding.

Table 6.3. Comparison of the lap shear fracture load of DFSF, conventional FSF and FSSW samples.

Joining process	Lap shear fracture load (kN)
DFSF	7.42±0.21
CFSF	5.23±0.21
FSSW with stir tool having pin	3.99±0.23
Pinless FSSW	5.93±0.27

6.2.8 TD-HD ratio for DFSF joints

As mentioned in previous chapter, for DFSF joints, larger TDs are not effective due to severe frictional heat flux and damage of the pre-drilled hole. Smaller TDs will not result in perfect mechanical interlocking and sufficient metallurgical bonding. Smaller HDs result in closure of the pre-drilled hole. Larger HDs result in reduction of metallurgically bonded area. There exist a relation between the TD and HD employed for joint fabrication.

When the TD is varied with constant HD of 3 mm, successful joints are fabricated for TD ranging from 10 mm to 14 mm with single hole configuration. Therefore, the window of sound joint fabrication for these DFSF samples lies in the TD-HD ratio about 3.33 to 4.66. Similarly, when the HD is varied with constant TD of 14 mm, successful joints are fabricated for HD ranging from 3 mm to 5 mm with single hole configuration. Therefore, the window of sound joint fabrication for these DFSF samples lies in the TD-HD ratio about 2.8 to 4.66.

From the above discussion, it can be summarized that the TD-HD ratio for successful DFSF joint fabrication in aluminum alloy sheets of 2 mm thickness should lie in the range of 3.33 to 4.66 for single hole configuration.

6.3 Conclusions

The main aim of the present work is to understand the effect of HD on the mechanical performance and joint formation during DFSF joining. Following conclusions are derived from the present work.

- Macrostructure analysis revealed that for lower HDs like 2.5 mm, the chance of closure of the pre-drilled hole is more. DFSF samples fabricated at HD range from 3-5 mm are strengthened by simultaneous mechanical interlocking and metallurgical bonding. Increase in HD to higher levels such as 5 mm leads to large pin size, but with a corresponding decrease in the metallurgically bonded area. The upward deformation of the lower sheet remains same with increase in HD; however, it has not grown up to severity of hook defect.

- As seen in typical friction stir based spot joints, the SZ, TMAZ and HAZ are identified in DFSF joints also. PDZ is observed exclusively in DFSF joints and in CFSF joints. The frictional heat flux and severe plastic deformation have contributed microstructural changes such as dynamic recrystallization in the SZ, and static recrystallization and further grain growth in HAZ and PDZ. The TMAZ regions possess recovered grains without recrystallization.

- The hardness of the joint spot is independent of change in the HD so that uniform pattern of hardness profiles is observed in the upper array and lower array of indentations. Forging and extrusion of upper sheet metal inside the pre-drilled hole results in higher hardness in the stir spot center.

- From the mechanical performance tests, it is observed that DFSF samples show appreciable fracture load and extensibility throughout the HD range. The uniform formability of DFSF samples irrespective of the change in HD is revealed through uniaxial tensile test. Joint morphology analysis revealed that for HD range of 3 mm to 5 mm, the size of external morphological features such as flash and UB are less.

- Considering the macrostructure analysis, joint morphology analysis and mechanical performance, HD range of 3 mm to 3.5 mm is favorable for joining the present material combination of aluminum alloys with the DFSF process. The DFSF samples show superior lap shear fracture load, about 42% better than conventional FSF samples, 86% better than that of pinned FSSW samples and 25% better than pinless FSSW samples.

- The failure modes of DFSF samples are random in nature during the mechanical performance tests. The neck of the pin and circumference of the stir spot act as critical weak zones initiating the failure of DFSF samples. Stir spot fracture occurs commonly during uniaxial tensile test. The 'TD-HD' ratio for successful DFSF joint fabrication in aluminum alloy sheets namely, AA 5052-H32 and AA 6061-T6 of 2 mm thickness should lie in the range of 3.33 to 4.66.

Chapter 7

DFSF joining of AA 5052-H32 and AA 6061-T6 sheets with multi-hole configurations

In this chapter, the effect of MH on the joint strength and joint formation of DFSF joints in dissimilar grade aluminum alloys are investigated through mechanical performance tests, macro/ micro structure analysis, hardness measurement, joint morphology analysis and failure mode analysis. The optimum tool rotational speed of 500 rpm obtained from chapter 2, the sheet metal combination employed in chapter2, optimum TPD of 0.5 mm obtained from chapter 4, optimum TD of 14 mm obtained from chapter 5 and optimum HD of 3 mm obtained from chapter 6 are adopted in the present work.

7.1 Methodology

The principle of DFSF joint formation is presented in section 4.2.1.

7.1.1 DFSF experiments

The details of DFSF sample fabrication is presented in section 4.2.2. The standard material properties of the upper sheet and the lower sheet are presented in section 2.1.2.

The effectiveness of the DFSF joint formation with change in pre-drilled hole configurations is evaluated by varying the primary variable, the number of holes drilled on the lower sheet. Multiple levels from single hole configuration up to four hole configuration, with the cluster of holes oriented at various angles to the RD of the lower sheet, are considered in the present work (Fig. 7.1). The pre-drilled holes are located around a reference circle, for which dia. about 9 mm is determined from previous literature (Lazarevic et al., 2013). The cluster of holes are located inside the reference circle for all configurations. A diametric line parallel to RD is shown for better understanding of the hole configurations.

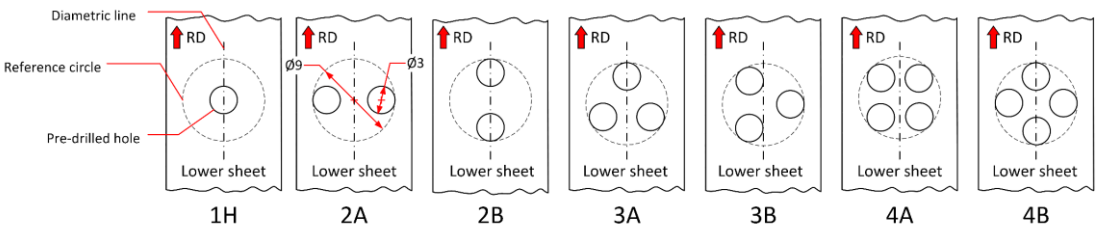

Figure 7.1. Various pre-drilled hole configurations employed in the present work

The various MHs in the lower sheet are

- One hole at the center of the reference circle (designated as '1H' configuration).
- Two hole cluster lying perpendicular to the diametric line (designated as '2A' configuration). The center to center distance between adjacent holes is 6 mm.
- Two hole cluster lying along the diametric line (designated as '2B' configuration). The center to center distance between adjacent holes is 6 mm.
- Three hole cluster having equally spaced three holes, out of which two holes lying along a line perpendicular to RD and one hole lying on the diametric line (designated as '3A' configuration). The center to center distance between adjacent holes is 5.1 mm.
- Three hole cluster having equally spaced three holes, out of which two holes lying along a line parallel to RD (designated as '3B' configuration). The center to center distance between adjacent holes is 5.1 mm.
- Four hole cluster having equally spaced four holes, out of which each pair of holes lying along the lines parallel to RD (designated as '4A' configuration). The center to center distance between adjacent holes is 4.5 mm.
- Four hole cluster having equally spaced four holes, out of which two holes lying along the diametric line (designated as '4B' configuration). The center to center distance between adjacent holes is 4.5 mm.

The hole configurations are prepared in such a way to understand the effect of their relative positions on the load bearing ability of the DFSF joints under various loading conditions. The pre-drilled holes in the cluster are positioned such that the distance between adjacent holes decreases with increase in the hole configuration. Different locations of the pre-drilled holes enable pin extrusion at multiple locations in the stir spot. This could exert variable loads in the mechanical interlocking, which is believed to affect the load bearing ability of the joints. It is ensured that the stir tool center and the geometric center of the hole cluster (i.e. the center of the reference circle) are collinear. Initial experimental trials suggest that multiple holes beyond four numbers is not appropriate with

a stir tool of 14 mm shoulder dia. because the lower sheet undergoes severe decrease in cross-sectional area with increase in the number of holes. This could impair joint strength and joint formation. The rest of the process parameters namely tool rotational speed, TPD, tool plunge rate, direction of tool rotation were kept constant at 500 rpm, 0.5 mm, 0.002 mm/s and clockwise direction respectively, throughout the sample fabrication process.

7.1.2 Mechanical performance tests

Details of mechanical performance tests are discussed in section 2.1.3.

7.1.3 Macro/microstructure, hardness measurement and joint morphology analyses

Details of macrostructure analysis, hardness measurement and joint morphology analysis are discussed in section 2.1.4. Hardness measurements along the joint cross-section are taken in two arrays as explained in section 6.1.3 of chapter 6 (Fig. 6.1 of chapter 6). The external morphological features such as UB, flash width and flash height are also measured (Fig. 6.2 of chapter 6) as explained in section 6.1.3 of chapter 6. Details of microstructure analysis is discussed in section 4.2.4.

7.2 Results and discussion

The effect of MH on the mechanical performance, joint macro/ microstructure, hardness variation of the joint, external joint morphology and failure modes of the DFSF joints are comprehensively discussed in the following subsections.

7.2.1 Mechanical performance tests

The effect of MH on the fracture load of DFSF samples is shown in Fig. 7.2. DFSF samples show different fracture loads under various loading conditions imposed by lap shear test, cross-tension test, peel test and uniaxial tensile test. For all the tests, the maximum shear fracture load is obtained at single hole configuration, 1H. Maximum fracture loads obtained are 7.42 kN, 2.89 kN and 1.05 kN respectively for lap shear test, cross-tension test and peel test.

Gradual decrease of 41% in the lap shear fracture load and 64% in cross-tension fracture load is obtained when the hole configuration changed from 1H to 4B. Significant variation in peel test fracture load and tensile fracture load are not observed with increase

in the number of holes. 1H configuration showed larger fracture load of 22 kN in tensile test. For any particular hole configuration, lap shear fracture load is maximum, peel fracture load is minimum and cross-tension fracture load falls intermediate.

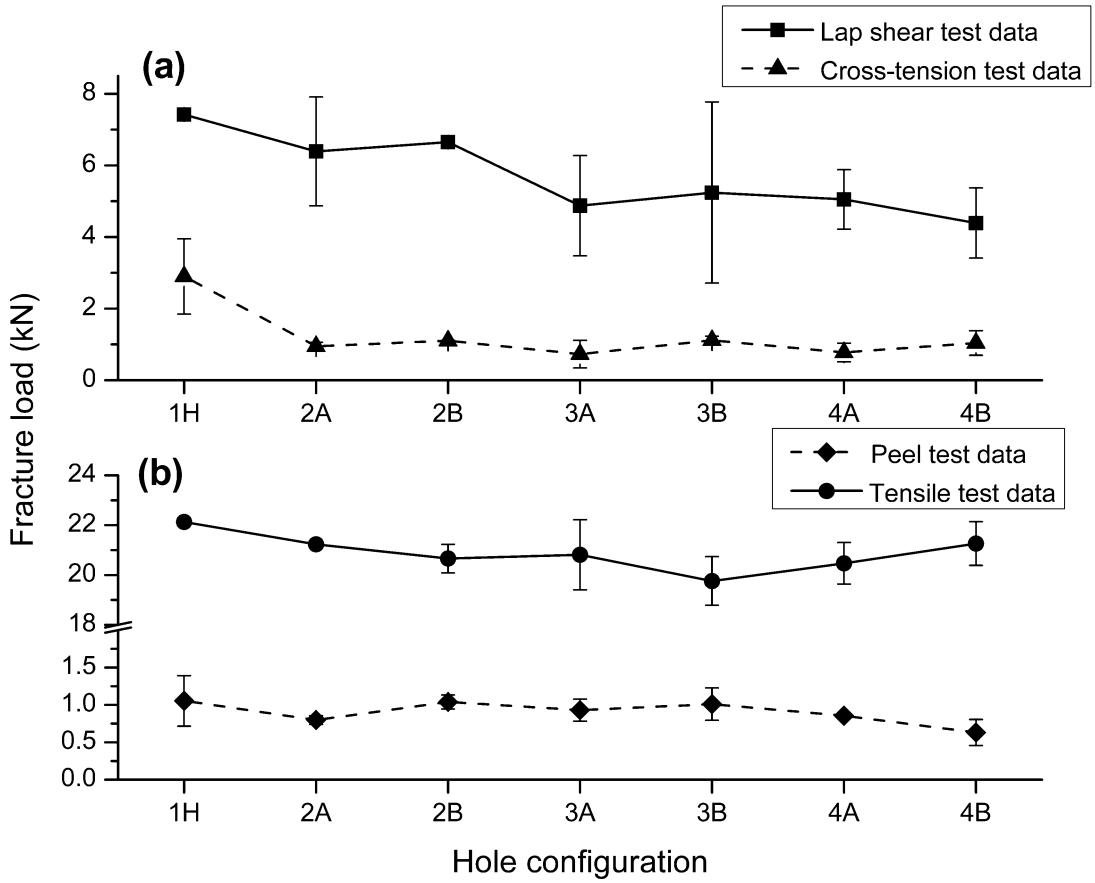

Figure 7.2. Comparison of fracture loads for various hole configurations during mechanical performance tests

On the whole, the MH has significant influence in the lap shear fracture load and the cross-tension fracture load of DFSF samples, while its influence on the fracture load is negligible during the peel test and the uniaxial tensile test. Considerable difference in the fracture load is not observed between two different hole configurations (say 2A and 2B) of the same hole cluster indicating that the joint mechanical performance is independent of the relative location of the holes in the cluster.

The DFSF samples show appreciable extensibility during various mechanical performance tests, which is an essential indicator of energy absorption before failure of the joint. The average extension at fracture for DFSF samples fabricated with single hole configuration are 1.25±0.19 mm, 15.35±3.72 mm, 39.72.60±24.21 mm and 4.22±0.70 mm during lap shear test, cross-tension test, peel test and uniaxial tensile test, respectively. The larger extensibility of cross-tension sample and peel test sample are attributed to the

peculiar nature of these tests in which the bending and unbending of the metal strips add considerable extension before fracture.

To summarize, the increase in number of pre-drilled holes in DFSF joint reduces the performance under lap shear and cross-tension loading conditions. However, such significant change is not seen in peel test and uniaxial tensile test. Even the position of the holes within a hole cluster has insignificant effect on fracture load. From the mechanical performance tests, '1H' hole configuration can be selected as an optimum for fabricating DFSF samples.

7.2.2 Joint formation analysis through macrostructure

Only 1H, 2A, 3A and 4B configurations are selected for joint formation and metal flow pattern analyses through macrostructure. The macrostructures of 2B, 3B and 4A configurations are found to be identical to that of 2A, 3A and 4B configurations respectively because of the identical joint formation, and not considered for analysis. The complete macrostructure of the DFSF samples and the schematic of the metal flow directions are shown in Fig. 7.3 and Fig. 7.4 respectively.

Sectioning (A-A) is done in such a way to cover maximum number of pre-drilled holes (represented by red circles) of each hole configuration. DFSF samples are generally strengthened by simultaneous mechanical interlocking and metallurgical bonding. The plastic deformation in the upper sheet is induced by the stirring action of the tool along with frictional heat flux and the tool plunge. The plastic deformation in the lower sheet is induced by the conducted heat flux and the tool plunge. Perfect metallurgical bonding is observed at the interface of the two sheets with no interfacial gaps. However, a noticeable difference in the macrostructure is observed with increase in the number of pre-drilled holes, (Fig. 7.3(a-d) and Fig. 7.4(a-d)).

The various zones which are identified on the cross-section of DFSF samples are SZ, TMAZ, PDZ, HAZ and ASZ. In traditional FSSW process, the material flow in the through thickness direction of the SZ is controlled by the rotating pin of the stir tool (Sarkar et al., 2016). Literature shows that using stir tools with cylindrical pin having thread profile, the plastic deformation of sheet metal in the through thickness direction can be enhanced (Badarinarayan et al., 2009a). On the contrary in DFSF process, material flow in the through thickness direction is ensured by extrusion of the upper sheet through the

pre-drilled hole. The pinless stir tool also generates swirl pattern of metal flow, which is evident from the unique pattern produced by stirring, Fig. 7.4a and Fig. 7.4b.

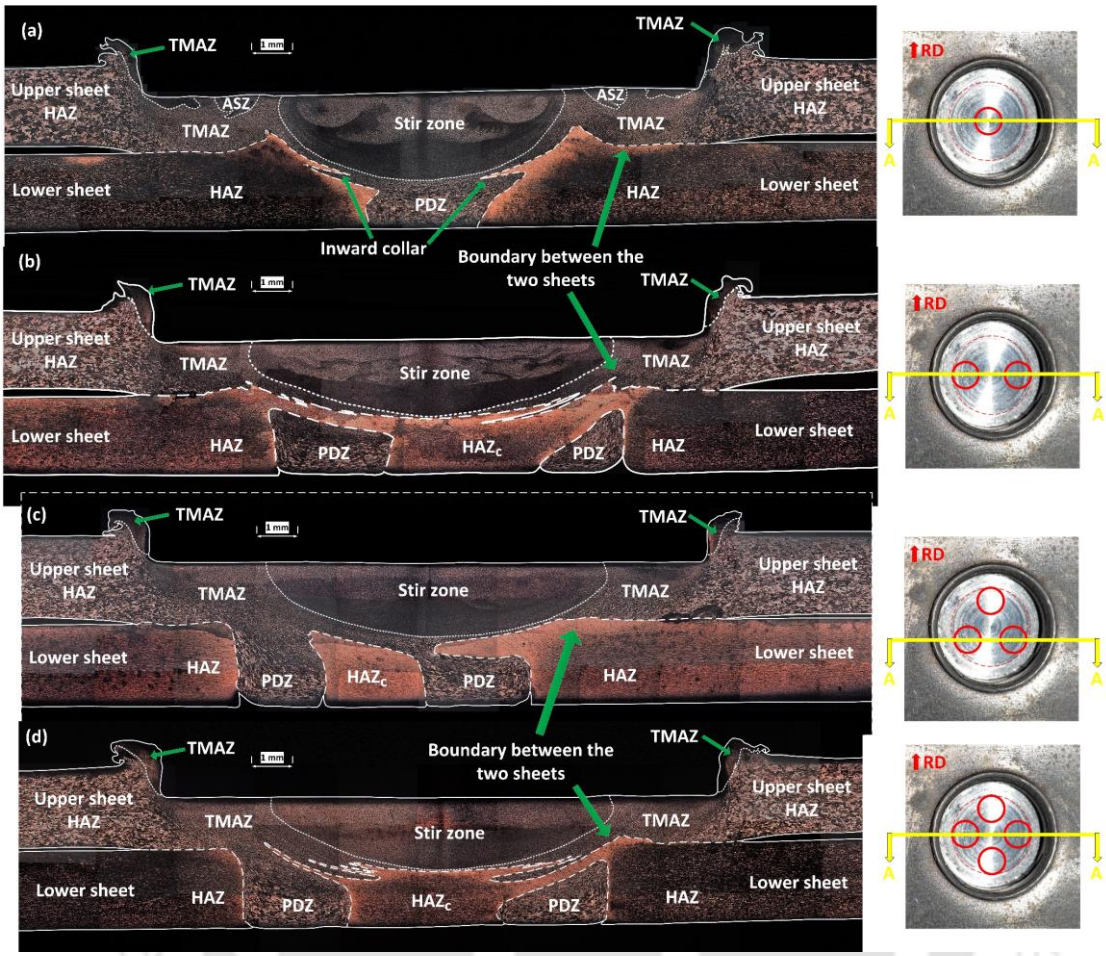

Figure 7.3. Joint macrostructure of DFSF samples fabricated at (a) 1H (single hole configuration), (b) 2A (two hole configuration), (c) 3A (three hole configuration), (d) 4B (four hole configuration). (Section A-A of samples for joint macrostructure is also shown)

7.2.2.1 1H configuration

In this configuration, the mechanical interlocking and metallurgical bonding are perfect (Fig. 7.3a and Fig. 7.4a). More details of single hole configuration is elaborately discussed in the previous chapters.

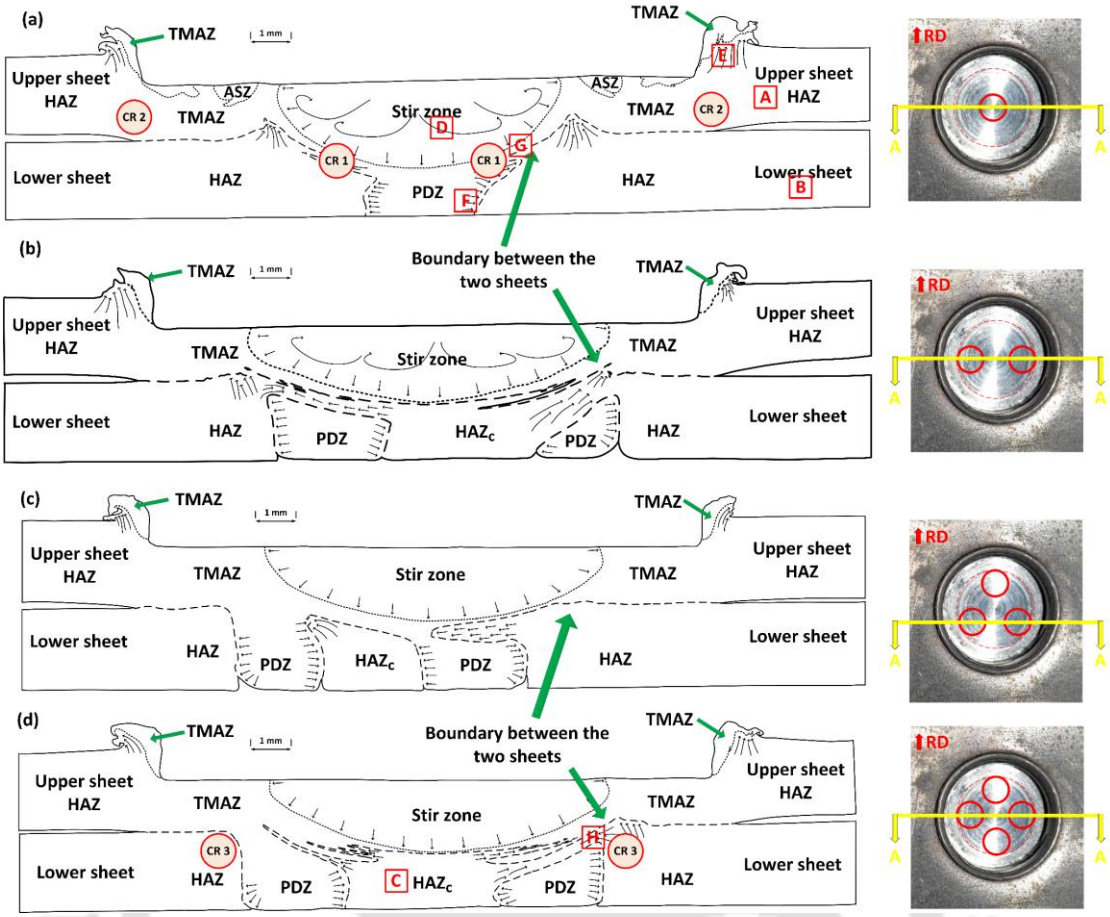

Figure 7.4. Schematic representation of the DFSF joint cross-sections at (a) 1H (single hole configuration), (b) 2A (two hole configuration), (c) 3A (three hole configuration), (d) 4B (four hole configuration), with metal flow directions indicated. (Sectioning of samples for joint macrostructure is also shown)

7.2.2.2 2A and 2B configurations

In these configurations, the holes are located away from the center of the stir spot. Unlike in 1H configuration, the mechanical interlocking is not obtained in this case because of restricted collar growth (Fig. 7.3b and Fig. 7.4b). The extrusion of the upper sheet is incomplete and the pre-drilled holes are partially filled. The deformation of the lower sheet is so severe that that the pre-drilled holes are plastically deformed and closed at its top. Even though the mechanical interlocking is absent, the joint strength is contributed by metallurgical bonding alone. ASZ is absent in these cases because the upward deformation of the lower sheet is not prominent.

7.2.2.3 3A and 3B configurations

The upper sheet metal is partially extruded and the filling of the pre-drilled holes are incomplete (Fig. 6c and Fig. 7c). However, the holes remain open till the end of the

tool plunge. As observed in the joint cross-section, the plastic deformation of the lower sheet results in displacement of the pre-drilled hole on one side. In addition, incomplete collar formation is visible in the pre-drilled hole regions. Hence, the perfect mechanical interlocking is not realized. Similar observation is also believed to occur on the third hole of the hole cluster. Thus, the mechanical interlocking is partially established and the samples are strengthened mainly by metallurgical bonding. ASZ is absent in three hole configuration as well.

7.2.2.4 4A and 4B configurations

In these configurations, the extrusion of the upper sheet into the pre-drilled hole is complete; however, the collar formation is imperfect when compared to 1H configuration. The plastic deformation of the lower sheet has resulted in complete closure of the pre-drilled hole like in 2A, 2B cases. The pre-drilled hole on the left hand side has not undergone closure due to material unavailability (Fig. 7.3d and Fig. 7.4d). Thus, the samples are strengthened by partial mechanical interlocking with minimal chance of collar growth. However, it is noted that the metallurgical bonding is absent in some of the DFSF samples with 4A, 4B configurations. The upward deformation of the lower sheet and the ASZ are absent in this case as well.

The effect of upward deformation of the lower sheet on the formation of ASZ is evident from the macrostructure analysis. For DFSF samples fabricated at 1H configuration, the upward deformation of the lower sheet restricts the width of the SZ resulting in ASZ formation (Fig. 7.3a and Fig. 7.4a). For samples fabricated with MHs such as two hole, three hole and four hole configurations, the upward deformation of the lower sheet is absent so that SZ width is comparatively larger and ASZ formation has not occurred (Fig. 7.3(b-d) and Fig. 7.4(b-d)).

The relation between mechanical performance and hole configuration is summarized as follows;

- 1H configuration is the best choice for DFSF sample fabrication as far as quality of the joint formation is concerned. These samples possess simultaneous mechanical interlocking and metallurgical bonding. Location of the pre-drilled hole at the center of the stir spot favours perfect pin formation and perfect collar growth.

- For MHs, the holes are located farther from the stir spot center; consequently, the chance of collar formation in the pre-drilled hole decreases resulting in imperfect mechanical interlock. The larger lap shear fracture load and cross-tension fracture load for DFSF samples with 1H configuration is thus justified.
- The decrease in lap shear fracture load and cross-tension fracture load with increase in the number of pre-drilled holes is believed due to such imperfect mechanical interlock. Such variation is not evident in peel test and tensile test.

7.2.3 Microstructure characterization

The optical microscopic images of SZ, TMAZ, HAZ and PDZ obtained from DFSF samples fabricated with 1H configuration and 4B configuration are shown in Fig. 7.5. The locations from which the microscopic images obtained are shown in boxes marked with alphabets A to H in Fig. 7.4a and Fig. 7.4d. Table 7.1 shows the comparison of grain size measurement obtained from various zones.

Table 7.1. Comparison of the grain size at various zones of the DFSF joint.

Location	Average grain dia. (μm)
SZ	7.9
AA 6061-T6 HAZ (below SZ)	13.3
AA 6061-T6 HAZ (lower sheet)	22.5
TMAZ	26.7
PDZ	31.8
AA 5052-H32 HAZ (upper sheet)	53.4

Zones such as SZ is subjected to recrystallization induced by the frictional heat flux and the severe plastic deformation. HAZ has been subjected to recrystallization and grain growth under frictional heat flux conducted from the stir spot. Recrystallization and grain growth are also observed in the PDZ region due to frictional heat flux and plastic deformation by extrusion. TMAZ grains have undergone recrystallization and grain growth under the effect of both the frictional heat flux and the plastic deformation induced by the constant rubbing contact of the lateral surface of the stir tool with the side walls of the stir spot. The lower sheet, which is in contact with the backing plate has more frictional heat dissipation by conduction as compared to the upper sheet. Therefore, the microstructural changes in the upper sheet and lower sheet are different.

HAZ of upper sheet and lower sheet possess coarse grain structure. The irregular coarse grains of the HAZ of AA 5052-H32 possess larger grain size (53.4 µm) than symmetric coarse grains of the HAZ of AA 6061-T6 (22.5 µm), as shown in Fig. 8a and Fig. 8b. HAZ_c of the lower sheet located below the SZ possesses grain size of about 13.3 µm (Fig. 8c). Unlike the HAZ region of the lower sheet located outside the stir spot, this region possesses refined grain structure. Significant grain growth is absent in HAZ_c because of its tendency towards prolonged recrystallization. The plastic deformation induced by the plunging stage of the stir tool till the completion of joint formation results in the annihilation of the grain growth in HAZ_c.

SZ in direct contact with the stir tool is dynamically recrystallized. Fine equi-axed grains with grain dia. about 7.9 µm is observed (Fig. 7.5d). Complete dynamic recrystallization in the SZ was also reported during FSSW process (Mitlin et al., 2006, Mishra and Ma, 2005, Rana et al., 2018). The fine grain formation in SZ and the coarse grain formation in HAZ shows that other than heat flux, the grain growth is mainly controlled by the extent of plastic deformation, as reported in section 6.2.2 of chapter 6.

TMAZ possesses highly deformed grains, which has undergone recrystallization and grain growth under the influence of frictional heat flux and plastic deformation (Fig. 7.5e). TMAZ grains of 26.7 µm size are larger than parent sheet metal grains. This shows that grain growth has occurred. Moreover, the extent of grain growth decreases from HAZ towards TMAZ as pointed by arrows in Fig. 7.5e. Literature shows that recovered grains were observed in the TMAZ region during FSW of AA 5083-O aluminum alloys (Sato et al., 2001). Therefore, unlike FSW joints, recrystallization and grain growth can also happen in the TMAZ region of DFSF joints.

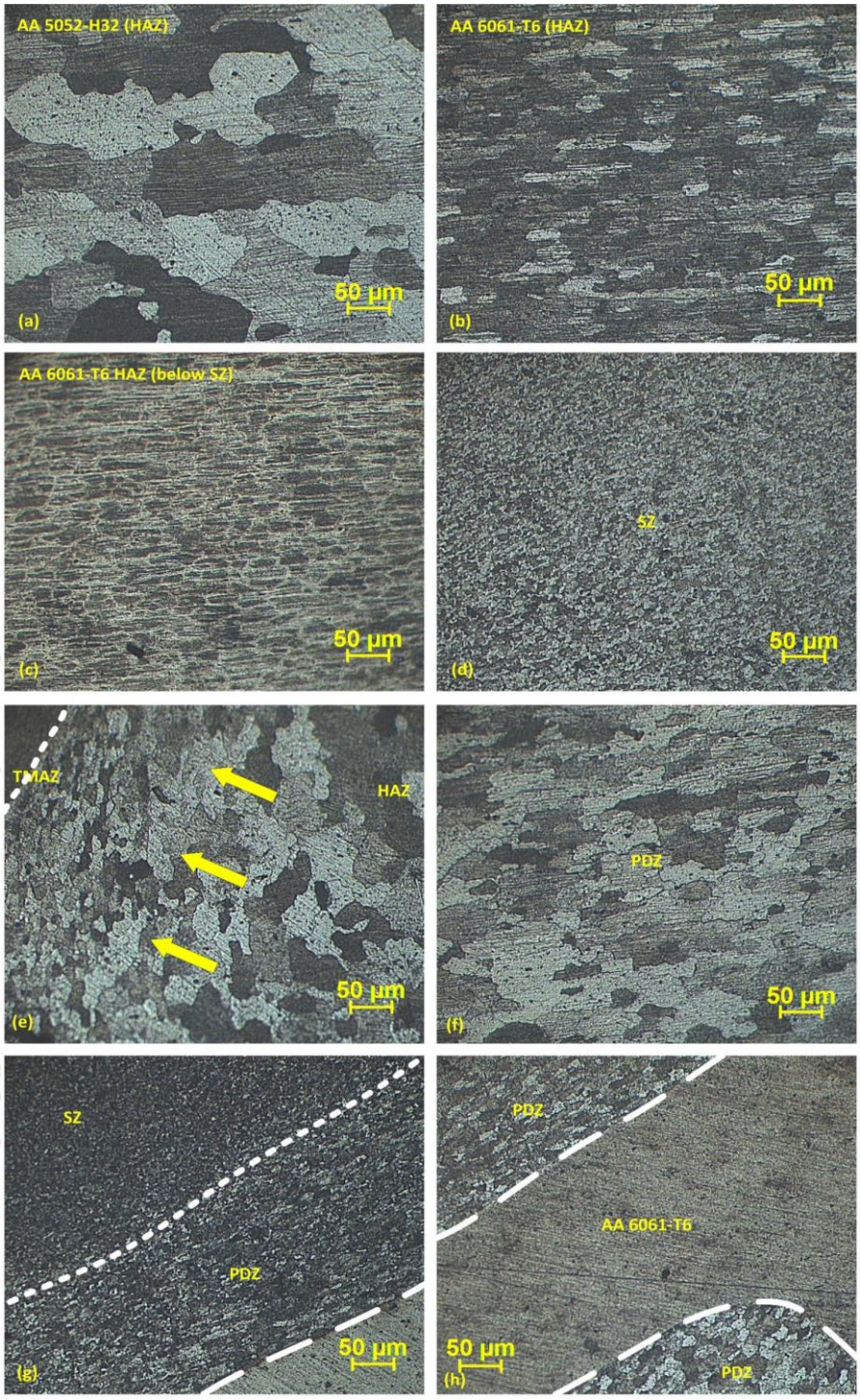

Figure 7.5. Optical microstructure of (a) HAZ of upper sheet, AA 5052-H32 (box A), (b) HAZ of lower sheet, AA 6061-T6 (box B), (c) HAZ of lower sheet below SZ (box C), (d) SZ of the upper sheet (box D), (e) transition from HAZ to TMAZ (box E), (f) PDZ of the upper sheet (box F), (g) SZ-PDZ boundary (box G) and (h) Closure of the pre-drilled hole (box H)

PDZ possess recrystallized grains with further grain growth (Fig. 7.5f). This region has not undergone plastic deformation by stirring, instead plastic deformation occurs by extrusion through pre-drilled hole with the plunge of the stir tool. Recrystallized grains of the PDZ also possesses 41% grain growth (31.8 µm) than that of the parent sheet. PDZ

possesses coarse grains than SZ and TMAZ regions. Clear boundary observed between SZ grains and PDZ grains (Fig. 7.5g) shows that SZ is confined to the upper sheet only and the stir mixing of upper and lower sheets is absent. The closure of the pre-drilled hole and subsequent isolation of a part of the PDZ inside the pre-drilled hole of four hole configuration is shown in Fig. 7.5h.

7.2.4 Hardness distribution

The hardness distribution across the cross-section of samples fabricated at 1H, 2A, 3A and 4B configurations are compared in Fig. 7.6a and Fig. 7.6b. Hardness profile over the upper array of indentations vary significantly with change in the hole configuration. However, considerable variation in hardness is not observed for the lower array. The hardness of the joint spot is lower than parent sheet hardness.

In the HAZ region of the upper array, hardness decrease is observed when compared to the parent sheet. Coarse grain formation has contributed lower hardness in the HAZ. Similar observation was also reported during FSSW of AA 5052-H32 (Rana et al., 2018). Literature shows that during FSSW of AA 5754-O sheets, higher hardness was observed in the SZ than the base metal region due to grain refinement induced by dynamic recrystallization (Badarinarayan et al., 2009a). SZ with higher hardness is also observed for all joint configurations in DFSF joints as shown in Fig. 7.6a. At the center of the stir spot, the number of indentations with higher hardness increases with increase in the number of pre-drilled holes. This can be related to the fact that for MHs, the width of the SZ is more than that of single hole configuration. Higher hardness is observed for four hole configuration than other hole configurations. The volume of upper sheet metal extruded into the pre-drilled holes and the mode of joint formation changes with increase in the number of pre-drilled holes. This might have created abrupt variation in the hardness of adjacent indentations of the four hole configuration. For DFSF joints, the decrease in the hardness in the TMAZ is contributed by the grain growth effect of the frictional heat flux, which in turn generates softening of the sheet metal (Kesharwani et al., 2015, Rana et al., 2018).

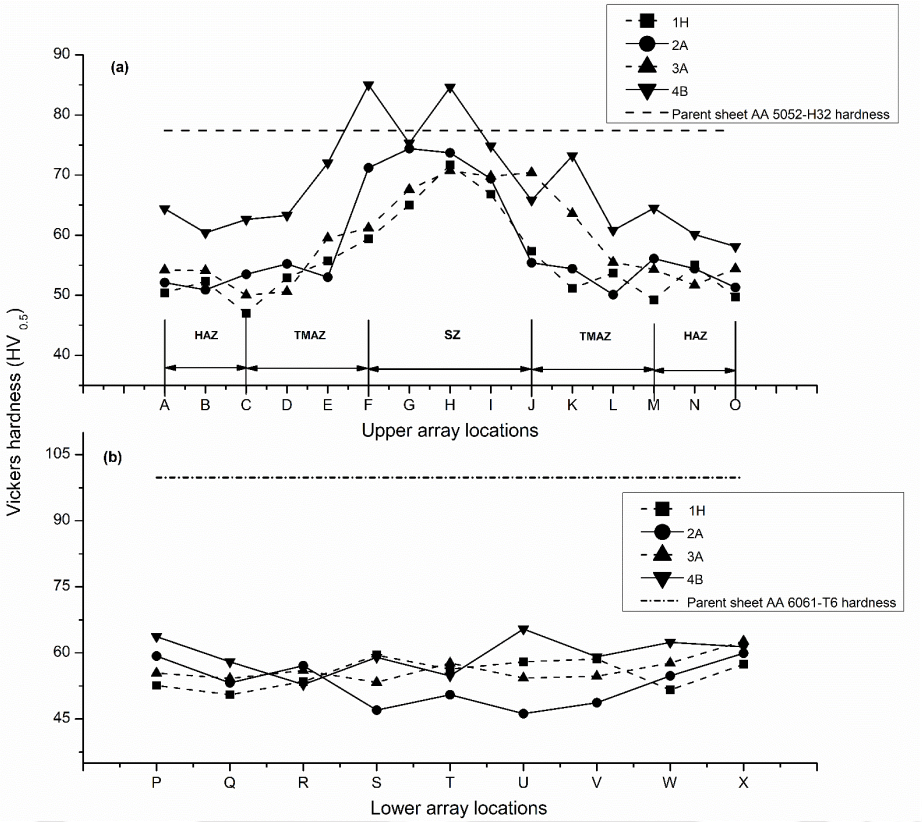

Figure 7.6. Comparison of hardness profiles along the DFSF joint cross-sections. (a) At the upper array, (b) At the lower array (Typical hardness variation at each measurement location is ±1.9)

The hardness along the lower sheet is significantly lower than the parent sheet hardness. Frictional heat flux and plastic deformation brought about softening of the lower sheet. Uniform hardness profiles observed show that change in hole configuration has no significant influence on hardness characteristics in the lower array.

The nature of change in hardness of the upper sheet and the lower sheet are different because the upper sheet is solid solution-hardened alloy, while the lower sheet is precipitation-hardened alloy. The SZ with fine grain formation exhibits only the same hardness as the parent metal with coarse grain formation. Similarly significant softening of the lower sheet is also observed. The reason behind this phenomena is explained in section 4.3.5 and 5.2.5.

7.2.5 Joint morphology analysis

The measurement of external morphological features such as flash width, flash height and UB is performed. The effect of change in hole configurations (1H, 2A, 3A and 4B) on the size of these external morphological features are shown in Fig. 7.7. Considerable variation in the flash height and flash width are not observed with change in

the hole configurations (Fig. 7.7(a-b)). Therefore, the flash formation is random in nature and it has no relationship with the chosen range of hole configurations.

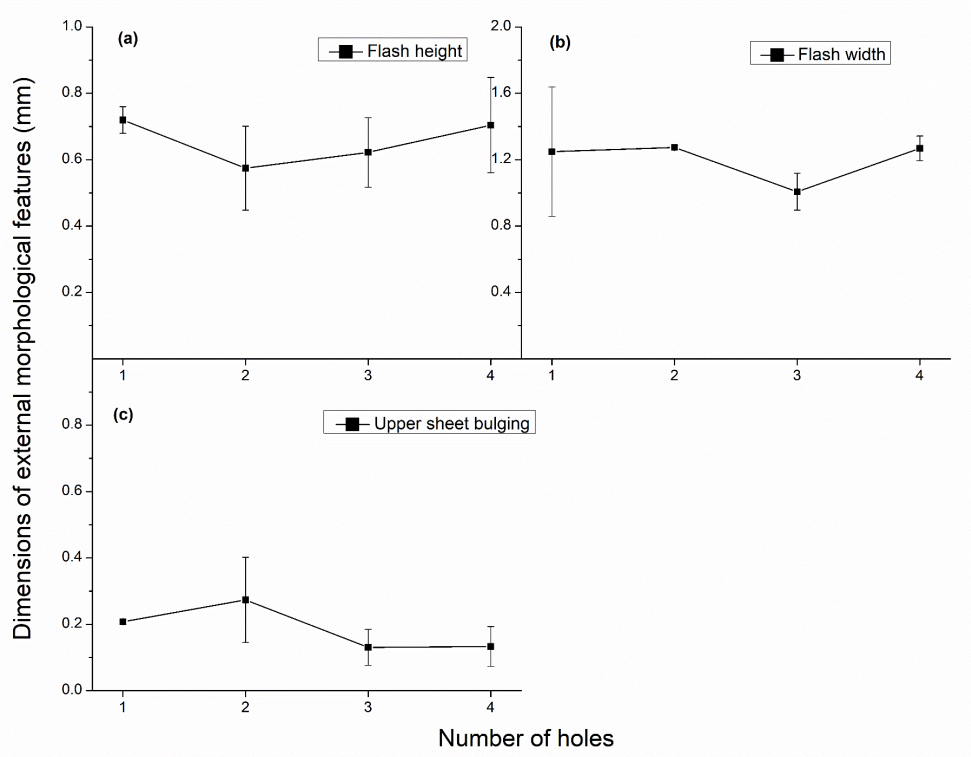

Figure 7.7. Comparison of external morphological features of DFSF samples fabricated at various hole configurations (a) Flash height, (b) Flash width, and (c) UB

During the plunge of the stir tool, bulging of the upper sheet surrounding the stir spot occurs due to following factors such as the resistance offered by lower sheet to the extrusion of upper sheet metal into the pre-drilled hole as well as the constraining effect of the clamps. For two hole configuration, the closure of all the pre-drilled holes lead to severe UB about 0.4 mm (Fig. 7.7c). With increase in the number of pre-drilled holes (3 hole and 4 hole configurations), the UB is comparatively less due to the extrusion of more volume of upper sheet metal into the pre-drilled holes.

It can be summarized that external morphological feature such as UB is more indicative of the quality of joint formation because the closure of the pre-drilled holes has affected the growth of this feature. Flash formation is random in nature and a systematic correlation between flash size and hole configurations does not exist. Furthermore, the growth of these external morphological features affect the aesthetic appearance of the DFSF joint.

7.2.6 Modes of failure during mechanical testing

Figure 7.8. Modes of failure. (a)Pin pull-out, (b) Combined pin pull-out and bond delamination, (c) Pin shear, (d) Combined pin shear and bond delamination, (e) Tear-off, (f) Combined tear-off and pin pull-out, (g) Stir spot fracture and (h) Base metal fracture

The various failure modes observed during mechanical performance tests are pin pull-out, combined pin pull-out and bond delamination, pin shear, combined pin shear and bond delamination, tear-off, combined tear-off and bond delamination. For uniaxial tensile test samples, stir spot fracture and base metal fracture are observed. These failure modes are shown in Fig. 7.8 and summarized in Table. 7.2. The failure modes are discussed further.

- Pin pull-out: This type of failure mode is explained in section 3.2.5 (Fig. 7.8a).
- Pin shear: This type of failure mode is explained in section 3.2.5 (Fig. 7.8c).

- Bond delamination: This type of failure mode is explained in section 2.2.9.
- Tear-off: This type of failure mode is explained in section 2.2.9 (Fig. 7.8e).

Most of the failure modes occur in combined form namely, combined pin pull-out and bond delamination (Fig. 7.8b), combined pin shear and bond delamination (Fig. 7.8d), and combined tear-off and pin pull-out (Fig. 7.8f). Combined tear-off and pin pull-out failure occurs by fracture along the circumference of the reference circle in which the pre-drilled holes are located. For MHs, the reference circle with holes act as a critical geometrical inhomogeneity in the lower sheet. Unlike in tear-off failure mentioned above, the fractured surface is located inside the stir spot circumference, as shown in Fig. 7.8f. The failure is characterized by the presence of pulled-out pins located along the circumference of fractured reference circle.

Following failure modes are observed during uniaxial tensile tests

- Stir spot fracture: This type of failure mode is explained in section 2.2.9 (Fig. 7.8g).
- Base metal fracture: This type of failure mode is explained in section 2.2.9 (Fig. 7.8h).

Table 7.2. Modes of failure of the DFSF joint

Hole configuration	**Lap shear test**		**Cross-tension test**		**Peel test**		**Tensile test**	
	Trial 1	**Trial 2**	**Trial 1**	**Trial 2**	**Trial 1**	**Trial 2**	**Trial 1**	**Trial 2**
1H	Pin shear + Bond delamination	Pin pull-out + Bond delamination	Tear-off	Pin shear + Bond delamination	Pin pull-out + Bond delamination	Pin pull-out + Bond delamination	Base metal fracture	Stir spot fracture
2A	Pin shear + Bond delamination	Tear-off	Tear-off	Pin pull-out + Bond delamination	Tear-off	Tear-off	Stir spot fracture	Stir spot fracture
2B	Tear-off	Pin shear + Bond delamination	Pin pull-out + Bond delamination	Tear-off	Tear-off	Tear-off + Pin pull-out	Stir spot fracture	Stir spot fracture
3A	Tear-off + Pin pull-out	Pin shear + Bond delamination	Tear-off + Pin pull-out	Tear-off + Pin pull-out	Tear-off	Pin pull-out + Bond delamination	Stir spot fracture	Stir spot fracture
3B	Tear-off	Pin shear	Tear-off + Pin pull-out	Tear-off + Pin pull-out	Tear-off	Tear-off	Stir spot fracture	Stir spot fracture
4A	Tear-off	Pin shear + Bond delamination	Tear-off + Pin pull-out	Pin pull-out	Tear-off + Pin pull-out	Tear-off + Pin pull-out	Stir spot fracture	Stir spot fracture
4B	Pin shear	Pin shear + Bond delamination	Tear-off + Pin pull-out	Pin pull-out	Pin pull-out	Pin pull-out	Stir spot fracture	Stir spot fracture

Neck of the pin (CR1), stir spot circumference (CR2) and reference circle circumference (CR3) act as critical weak zones, shown in Fig. 7.4a and Fig. 7.4d, lead to

failure of the DFSF samples. The critical weak zones of failure are located outside the SZ region.

As mentioned in previous chapter, pin shear failure and pin pull-out failure are initiated from the neck of the pin (CR1) as well as tear-off failure and bond delamination failure are initiated from the stir spot circumference (CR2). The reference circle circumference (CR3) with multiple holes is a critical geometrical inhomogeneity in the lower sheet, which act as weak zone for combined tear-off and pin pull-out failure. Rest of the combined failure modes occur by the existence of more than one active critical weak zones in the joint.

During uniaxial tensile tests, stir spot fracture is the common failure mode in MHs. Therefore, the hole cluster in MHs act as a critical geometric inhomogeneity, which leads to failure of the stir spot. Both base metal fracture and stir spot fracture are obtained in 1H configuration. This shows that presence of single hole in the stir spot does not act as a critical weak zone always in the DFSF joint. However, the failure modes are random in nature, and a close correlation between change in hole configurations and the failure modes cannot be established from the mechanical performance tests.

As the number of pre-drilled holes increase, the volume of upper sheet metal extruded into these holes increases, consequently the mode of joint formation is affected. This is more evident in 4A, 4B configurations. In such configurations, the pin shear failure and pin pull-out failure are observed in some of the samples during mechanical performance tests. These failure modes show that these samples are strengthened by mechanical interlocking alone, while the metallurgical bonding is absent.

7.2.7 Comparison between DFSF, CFSF and FSSW processes

DFSF joints with 1H configuration are fabricated on various material combinations of upper and lower sheets using AA 5052-H32 and AA 6061-T6. The lap shear fracture load has been evaluated and compared as shown in Fig. 7.9. For A5A6 combination, AA 5052-H32 and AA 6061-T6 are used as upper and lower sheets respectively. For A5A5 combination, AA 5052-H32 is used as the upper sheet and the lower sheet. For A6A6 combination, AA 6061-T6 is used as the upper sheet and the lower sheet. For A6A5 combination, AA 6061-T6 and AA 5052-H32 are used as upper sheet and lower sheet respectively.

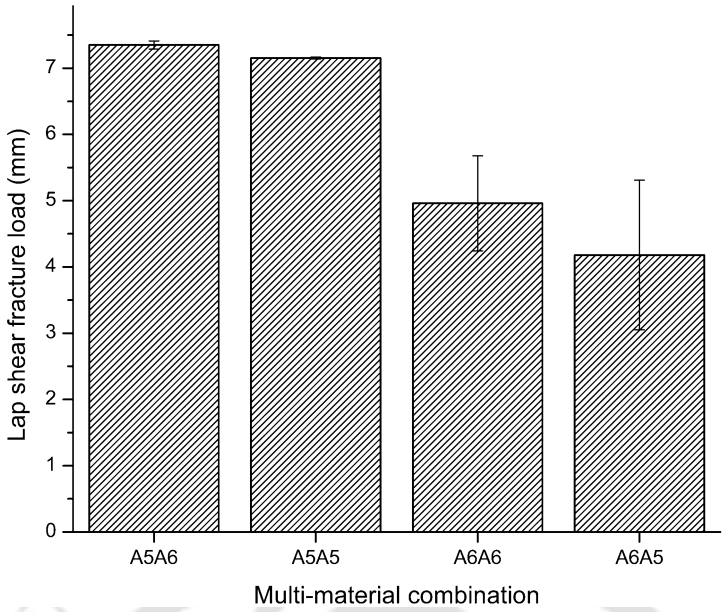

Figure 7.9. Comparison of lap shear fracture load of DFSF samples fabricated with various material combinations

It is observed that the lap shear fracture load changes significantly with the material combination. A5A6 and A5A5 combinations show a larger fracture load of about 7.25 kN, when compared with A6A6 and A6A5 combinations. This indicates that it is better to use softer material, AA 5052-H32, as upper sheet. Among the same material combinations, A5A5 and A6A6, A5A5 shows larger shear fracture load demonstrating the effect of aluminum grades. Hence, other than hole configuration, the material selection and its arrangement also plays a larger role in the joint strength.

7.3 Conclusions

The following conclusions are obtained from the present work.

- From the mechanical performance tests, maximum lap shear fracture load about 7.42 kN and maximum cross-tension fracture load of 2.89 kN are obtained for DFSF samples fabricated with single hole configuration (1H). MHs reduced the mechanical performance of DFSF samples. The relative change in the location of pre-drilled holes within a hole cluster has no significant influence on the mechanical performance.
- Macrostructure analysis revealed that farther the holes from the stir spot center, more imperfect the mechanical interlocking becomes. As the number of pre-drilled holes increases, chance of collar formation into the pre-drilled hole decreases due to lack of material availability in the lower sheet. Extrusion of more upper sheet

metal consequently affected the metallurgical bonding at the interface of the two sheets.

- Frictional heat flux and plastic deformation have brought about recrystallization and further grain growth in the TMAZ region. However, under the influence of frictional heat flux alone, the HAZ possess static recrystallization and grain growth. The grain growth is predominantly controlled by the extent of plastic deformation in the HAZ_c located under the SZ.
- As the number of pre-drilled holes increases, changes such as increase in the width of the SZ, increase in the volume of upper sheet metal extruded into the pre-drilled holes and change in the mode of joint formation affected hardness of the upper sheet such that hardness distribution varies significantly from one another.
- Morphological features namely UB become prominent for DFSF samples with poor mechanical interlocking. The flash size is independent of the change in hole configuration.
- The failure modes are random with change in hole configuration. The neck of the pin, stir spot circumference and reference circle circumference are the critical weak zones initiating failure of DFSF joints. During uniaxial tensile tests, the hole cluster act as a critical geometric inhomogeneity initiating stir spot failure.
- From the results of mechanical performance and macrostructure analysis, single hole configuration can be chosen as the best choice for fabricating DFSF joints. The lap shear fracture load of DFSF joints also depends on material grade and arrangement of materials. Softer sheet metal should be chosen as the upper sheet for better mechanical performance.

Chapter 8

Some major insights about FSF and DFSF joints

This chapter details some of the major observations collectively obtained from previous chapters based on the effect of change in process parameters such as RPM, TPD, TD as well as geometric features such as HD and MH in CFSF and DFSF joints.

8.1 Observations

8.1.1 Lower sheet flash

Lower sheet flash occurs commonly in CFSF joints (section 2.2.8 and section 3.2.4). It is directly related to the TPD more than any other process parameter of CFSF joints. Irrespective of the change in RPM, lower sheet flash is observed for all CFSF joints fabricated at TPD of 1.5 mm. Similarly, when the TPD is varied, lower sheet flash is not observed at lower and medium TPD ranges (0.2-0.7 mm). The lower sheet flash size shows an abrupt growth at higher TPD range of 0.9-1.1 mm (Fig. 3.7).

For DFSF joints, the lower sheet flash is rarely visible. Even at TPD level of 0.7-0.9 mm, the lower sheet flash is absent (Fig. 4.16). However, the higher TD range of 16-18 mm results in considerable lower sheet flash formation due to closure of the pre-drilled hole. Therefore, lower sheet flash in DFSF joints more sensitive towards change in TD than change in TPD.

8.1.2 Hardness distribution

A dip in the hardness at the center of the SZ (location I in Fig. 2.11 and location H in Fig. 3.6a) of the upper sheet is observed. This shows that the SZ center of CFSF joints possess softer region. Even though larger TPDs are employed for CFSF joint fabrication, the extrusion of upper sheet metal through the pre-drilled hole and further anvil cavity filling have not induced significant compression and forging of the upper sheet metal.

However, DFSF joints possess hardness profiles which are different from that of CFSF joints (section 4.3.5 and section 5.2.4), with maximum hardness at the SZ center (location H and location I of Fig. 4.12a and location G and location H of Fig. 5.7a) of the

upper sheet. This is because the plunge of the stir tool has resulted in the forging and extrusion of the plasticized metal inside the pre-drilled hole at the center of the DFSF joint.

The above-mentioned observation can be reconfirmed by the hardness of the extruded pin in lower array of CFSF and DFSF samples. A dip in the hardness is observed over the extruded pin in the lower array (location V of Fig. 2.12) of CFSF joint fabricated at 1500 RPM. Similar observation is also noticed for the softer extruded pin (location 20 of Fig. 3.6b) for 0.2 mm and 0.5 mm TPDs. Therefore, it is clear that the extruded pin in CFSF joints lacks compression and forging. However, for DFSF joints, higher hardness is recorded for the upper sheet metal extruded and forged through the pre-drilled hole (location T of Fig. 4.12b). Similarly, hardness has increased slightly at the center (location T of Fig. 5.7b) of DFSF joints fabricated at 14 mm TD and at various HDs (location T of Fig. 6.6b).

For CFSF joints fabricated at 0.2 mm TPD (Fig 3.7) and for DFSF joints fabricated at 10 mm TD (Fig. 5.7), the hardness profile along the upper array and lower array are not significantly affected by change in the process parameters. Thus frictional heat flux and plastic deformation induced by lower levels of process parameters are comparatively less and have minimal effect on the joint hardness. Incomplete filling of the pre-drilled hole in 0.2 mm TPD during CFSF, and poor mechanical interlocking in 10 mm TD during DFSF are responsible for this. For DFSF joints, the complete extrusion of the upper sheet metal can be confirmed from the hardness profile via higher hardness in the center of SZ (Fig. 4.12 and Fig. 6.6).

8.1.3 UB

For CFSF joints, the morphological feature namely UB is sensitive towards change in TPD than change in RPM. The constant TPD of 1.5 mm induced almost similar large UB throughout the entire range of RPMs (Table 2.5). However, UB possesses more or less linearly increasing relationship with change in TPD (Fig. 3.7).

For DFSF joints, the UB is sensitive towards change in TD than change in TPD. Increase in TD leads to severe UB at higher TD such as 18 mm (Fig. 5.8), while it is negligible even at higher TPD level of 0.5 mm (Fig.4.13). Change in HD and change in MH recorded a decrease in UB.

For CFSF joints fabricated at lower TPD levels (Fig. 3.4(a-b)), the extrusion of the upper sheet metal (the pin formation) is incomplete and consequently the UB is absent. However, for rest of the CFSF and DFSF joints, the UB is present, for which the pin extrusion is visible. This implies that a relation exist between the extrusion stage and the UB. It can be inferred that the UB commences at the stage, when extrusion of the pin is hindered by the closure of the hole (Fig. 3.4(c-d) for CFSF joints and Fig. 5.4 (d-e) for DFSF joints) or when the extrusion of the pin is complete (Fig. 3.4(e-f) for CFSF joints and Fig. 4.9(b-c) for DFSF joints). Thus, the severity of UB can be used as a tool to determine the TPD level at which joint formation is about to complete.

8.1.4 Size of the SZ

SZ size in CFSF joints is directly related to the change in process parameters such as RPM and TPD. The width of the SZ increased and partitions within the SZ are formed with increase in RPM (Fig. 2.8b). Similarly, a steady growth in the size of the SZ is observed with increase in TPD (Fig.3.5).

For DFSF joints, the size of the SZ is independent of the change in TPD (Fig. 4.9) and change in HD (Fig. 6.3). This is mainly the due to upward deformation of lower sheet limiting the SZ size. However, large size SZs are observed at higher TDs (Fig. 5.4) and MHs (Fig. 7.3) due to severe plastic deformation and poor mechanical interlocking. SZ size is related to the mode of joint formation in CFSF and DFSF joints and it depends upon the presence and absence of mechanical interlocking and/ or metallurgical bonding.

8.1.5 Size of TMAZ

The formation of TMAZ in the sidewalls of the joints depends on the extent and duration of frictional heat generation and plastic deformation. For CFSF joints, the size of the TMAZ depends on the change in process parameters such as RPM and TPD. The width of the TMAZ increases with increase in RPM (Fig. 2.8), which is the consequence of increased frictional heat flux and severe plastic deformation. The change in TPD witnesses the formation of TMAZ at medium level and attains considerable size at higher level (Fig. 3.4). Therefore, the time of contact of the stir tool also determines TMAZ size.

For DFSF joints, the formation of TMAZ in the sidewalls is independent of the change in TPD (Fig. 4.9), TD (Fig. 5.4), HD (Fig. 6.3), and MH (Fig. 7.3). This also points

that TPD levels employed in the fabrication of DFSF joints are considerably small enough and sufficient to fabricate successful joints with limited frictional heat input, sufficiently enough plastic deformation as well as minimum fabrication time.

8.1.6 Lower level TPDs in CFSF and DFSF joints

Macrostructure of CFSF and DFSF samples fabricated at 0.3 mm TPD are compared (Fig. 3.4b and Fig. 4.9a respectively). It is observed that for CFSF sample, 0.3 mm TPD is not sufficient to extrude and fill the anvil cavity with upper sheet metal. Therefore, the mechanical interlocking is incomplete and the metallurgical bonding is poor.

However, for DFSF samples, 0.3 mm TPD is sufficient for the complete extrusion of upper sheet metal into the pre-drilled hole and enable partial mechanical interlocking by generation of inward collar. Therefore, lower TPDs yield better joint formation in DFSF joints in comparison with CFSF and FSSW joints.

8.1.7 Upward deformation of the lower sheet

For CFSF and DFSF joints, the upward deformation of the lower sheet is directly related to the TPD level. Upward deformation is severe for CFSF and DFSF joints fabricated at 0.7 mm TPD and beyond (Fig. 3.4(d-f) and Fig. 5.4). The distortion is comparatively less for CFSF and DFSF joints fabricated at 0.5 mm TPD or less (Fig. 3.4(a-c) and Fig 4.9). Severe upward deformation of lower sheet is analogous to hook defect in pinless FSSW joints, which leads to upper sheet thinning. Therefore, the upward deformation of lower sheet, which act as critical weak zone for the failure of CFSF and DFSF samples can be minimized by optimizing the TPD as performed in chapter 3 and chapter 4. Employing optimum TPD of 0.5 mm with change in HD (Fig. 6.3) and change in MH (Fig. 7.3) leads to minimum upward deformation of the lower sheet, as performed in chapter 6 and chapter 7.

8.1.8 Formability of CFSF and DFSF samples

The formability (tensile fracture load) of CFSF and DFSF samples decreases with increase in process parameters such as TPD and TD. This is because the frictional heat generated at the stir spot and the extent of geometrical inhomogeneity created by the size of the stir spot increases with increase in these process parameters. As a result, the base

metal region surrounding the stir spot has undergone significant softening along with increase in the size of the stir spot. Both of these factors lead to decrease in the formability of the samples as well as random occurrence of failure modes such as stir spot fracture and base metal fracture. It is also evident that change in geometric features such a size of the pre-drilled hole (change in HD) and number of pre-drilled holes (change in MH) have not severely affected the formability of DFSF samples and the base metal fracture is rarely occurring due to moderate frictional heat flux.

8.1.9 Significance of various mechanical performance tests

Lap shear test and cross-tension test can be considered as the primary mechanical performance tests for analyzing spot joints because the change in the process parameters and change geometric features have significant influence on the fracture load of CFSF and DFSF samples under shear loading and cross-tensile loading conditions. These tests are more indicative of joint strength than other mechanical performance tests. Uniaxial tensile test presented in this work can be used as an effective tool for evaluating the basic formability.

Peel fracture load remains more or less same throughout the change in process parameters and geometric features. Therefore, peel test can be used only under those applications witnessing such loading conditions.

8.1.10 CRs of CFSF and DFSF joints

The CRs in CFSF and DFSF joints and the reason for their origin are summarized in the following tables

Table 8.1. CRs of CFSF joints

CR of CFSF joints	Reason for origin		Change in process parameter
	Mechanical	Metallurgical	
The stir spot circumference	Upper sheet thinning due to excessive tool plunge	-	RPM
Upward deformation of the lower sheet	Excessive deformation of the lower sheet, Excessive tool plunge	-	RPM, TPD
The neck of the pin	Comparatively smaller cross-sectional area for the pin	Lack of metallurgical bonding	TPD
Incomplete/partial metallurgical bonding	-	Poor interface quality, Vibration of the pinless stir tool	TPD

Table 8.2. CRs of DFSF joints

CR of DFSF joints	Reason for origin		Change in process parameter
	Mechanical	**Metallurgical**	
The neck of the pin	Comparatively smaller cross-sectional area for the pin	Absence of / Incomplete metallurgical bonding	TPD, TD, HD, MH
Poor mechanical interlocking	Improper collar formation	-	TPD, TD
The stir spot circumference	Thinnest part of the stir spot, Absence of other CRs	-	TPD, HD, MH
Upward deformation of the lower sheet	Excessive deformation of the lower sheet, Excessive tool plunge	-	TD
Reference circle circumference	Critical geometrical inhomogeneity in the lower sheet	-	MH

Chapter 9

Conclusions and scope of future work

A detailed study about the applicability of CFSF and DFSF process for spot joining ductile sheet metals of dissimilar grade aluminum alloys is conducted in the thesis work. The effect of process parameters such as RPM and TPD, which significantly influence the joint strength and joint formation of CFSF process is presented in chapter 2 and chapter 3. In chapter 4 and chapter 5, the effect of process parameters such as TPD and TD on the joint strength and joint formation of modified process namely DFSF is discussed. In chapter 6 and chapter 7, the effect of geometric features such as HD and MH on the joint strength and joint formation of DFSF joints are comprehensively presented. Chapter 8 presented some major insights about CFSF and DFSF joints.

9.1 Conclusions

The following conclusions are obtained from the overall thesis work.

9.1.1 Mechanical performance tests

The mechanical performance of both CFSF and DFSF samples are such that lap shear fracture load is maximum, peel test fracture load is minimum and cross-tension fracture load is intermediate throughout the change in process parameters and geometric features. Lap shear test and cross-tension test are more indicative of joint fracture load than other mechanical performance tests.

The extensibility of the CFSF and DFSF samples are appreciable throughout the mechanical performance tests. This accounts to better safety considerations such as significant energy absorption before failure of the joint.

9.1.1.1 CFSF samples

Similar to other friction stir based processes, the higher RPM levels have negative impact on the mechanical performance of CFSF samples. The CFSF samples fabricated at RPM range from 500 to 1500, and medium TPD range from 0.5 mm to 0.7 mm deliver appreciable mechanical performance. A 6.3 kN increase (more than 700% increase) in the

lap shear fracture load and 3.5 kN increase (350% increase) in the cross-tension fracture load are obtained as the TPD is increased from lower range to medium range. The formability of CFSF samples are independent of the change in RPM, but the geometrical inhomogeneity developed due to increase in TPD decreases the formability during uniaxial tensile test.

9.1.1.2 DFSF samples

Larger fluctuation in the fracture loads are detected and only marginal improvement in mechanical performance is obtained for TPD levels and TD levels other than optimum values. A 4.17 kN increase (200% increase) in the lap shear fracture load is obtained as the TD is increased from lower level to medium level of 14 mm. Higher HDs and MHs deliver deteriorated mechanical performance.

The increase in the geometrical inhomogeneity of the stir spot due to increase in process parameters (TPD and TD) decreases the formability of DFSF samples. However, uniform formability is observed with change in geometric features (HD and MH). The change in relative location of holes in any particular hole cluster has not affected the mechanical performance.

9.1.2 Joint macrostructure analysis

The presence of SZ, TMAZ and HAZ, similar to that of other friction stir based spot joints such as FSSW, are identified in both CFSF and DFSF joints. However, the presence of PDZ and ASZ in CFSF and DFSF joints, quite absent in FSSW samples, is revealed through the present work. Unlike in FSSW joints, the SZ has no other role than generating frictional heat flux and confined stirring of the upper sheet metal in CFSF and DFSF joints.

9.1.2.1 CFSF joints

In addition to metallurgical bonding, the CFSF joints are strengthened by approximate rivet interlocking at RPMs ranging from 500 to 2000. The increase in frictional heat generation at higher RPMs results in severe damage of the pre-drilled hole and impaired joint formation. The mechanism of pin formation revealed during change in TPD shows that the pin extrusion is a discontinuous process from TPDs ranging from 0.5 mm to 0.7 mm and the joint strength is mainly obtained from metallurgical bonding alone.

Higher TPDs result in severe upward deformation of the lower sheet, which act as critical weak zone for failure, thereby deteriorating the quality of joint formation.

9.1.2.2 DFSF joints

The absence of stir mixing of the upper and lower sheets as well as minimal upward deformation of lower sheet prevent hook defect. Any combination of ductile dissimilar sheet metals can be joined with the DFSF process without considering the effect of stir mixing. However, the study on MH revealed that ASZ formation is a consequence of upward deformation of the lower sheet.

In addition to trivial metallurgical bonding observed in friction stir based spot joints, the mechanical interlocking realized through inward collar formation is exclusively observed in DFSF joints. Lower TPDs yield better joint formation in DFSF joints in comparison with CFSF and FSSW joints. Slight increase in TPD contributes significant improvement in mechanical interlocking. Lower TDs suffer insufficient metallurgical bonding and higher TDs suffer poor mechanical interlocking. With increase in HD, extrusion of large size pin reduces the surrounding metallurgically bonded area. With increase in MH, the insufficient material availability in between the hole cluster of the lower sheet negatively affects the metallurgical bonding and reduces the chance of perfect mechanical interlocking.

9.1.3 Microstructure characterization

9.1.3.1 CFSF joints

It is expected that the various zones of CFSF joints also possess similar microstructure as that of DFSF joints.

9.1.3.2 DFSF joints

The microstructural changes induced by frictional heat flux and severe plastic deformation on various zones of the DFSF joint revealed that SZ grains are dynamically recrystallized and TMAZ grains exhibits significant recovery without recrystallization, similar to the mechanism of microstructure evolution during FSSW of aluminum alloys. SZ tends to possess circular motion, while PDZ possesses inward radial flow during the course of joint formation. The statically recrystallized grains of HAZ have undergone

further grain growth under the influence of frictional heat flux. The recrystallized grains of PDZ have also undergone grain growth under frictional heat flux and plastic deformation by extrusion. High rate of plastic deformation due to downward tool plunge prolongs recrystallization and arrests the grain growth in the lower sheet HAZ located closer to the stir spot.

9.1.4 Hardness variation

The uniform hardness distribution on both sides of the stir spot axis reveals symmetric joint formation in CFSF and DFSF processes. Except at the SZ region, the hardness of the upper and lower sheets are decreased from parent sheet hardness due to microstructural changes associated with the frictional heat flux and plastic deformation during the joint formation.

9.1.4.1 CFSF joints

An inverted 'W'-shaped hardness profile is observed in the upper sheet of CFSF joints. Increase in variation in the hardness within the SZ with increase in RPM shows that higher levels induce considerable stirring and subsequent formation of harder regions at the SZ periphery. Generally, the extruded pin possesses similar hardness as the SZ center of the upper sheet.

The extruded pin in CFSF joints lacks compression and forging. The beginning of extrusion is marked by the softer region over the extruded pin at lower TPDs. The closure of the pre-drilled hole as well as compression of the deformed pin are marked by harder regions at the center of the pre-drilled hole for medium and higher TPD levels.

9.1.4.2 DFSF joints

The hardness variation in DFSF joints is independent of the change in TPD and change in HD. Higher hardness is recorded for the extruded pin due to the compression and forging through the pre-drilled hole. Lack of forging at lower TD levels is revealed through the hardness measurement. The frictional heat flux and plastic deformation induced by lower levels of process parameters such as TPD and TD are comparatively less and have minimal effect on the joint hardness. Increase in the volume of extruded upper sheet metal, increase in the SZ width and change in the mode of joint formation in MH configurations influenced the hardness profile of the upper sheet. In addition to grain size,

the hardness of the upper sheet, which is a solid solution hardened aluminum alloy, is influenced by the density and mobility of dislocations. Similarly, distribution of precipitates influences the softening of the lower sheet, which is a precipitation hardened alloy.

9.1.5 Joint morphology analysis

9.1.5.1 CFSF joints

The morphological features of CFSF joint are independent of the change in RPM. However, the change in TPD has significant impact. Typically, the size of UB in CFSF joints is two to four times bigger than that of DFSF joints. Formation of lower sheet flash indicates the severity of excessive TPD levels.

9.1.5.2 DFSF joints

Quality of mechanical interlocking determines the growth of external morphological features of DFSF joints. The severity of UB can be controlled by properly choosing the TPD level. The UB and lower sheet flash are more sensitive towards change in TD than change in TPD. BW increases with TD, but it is associated with a corresponding decrease in the mechanical interlocking.

9.1.6 Failure mode analysis

Significant information about the occurrence of mechanical interlocking and/ or metallurgical bonding as well as about the location of critical weak zones in CFSF and DFSF joints are obtained though failure mode examination. Similar failure modes such as tear-off, partial bond delamination and pin pull-out occurring in both CFSF and DFSF samples show that the joint formation is more or less identical. Combined failure modes occur due to the formation of more than one active CRs. The upward deformation of the lower sheet, a critical weak zone, can be minimized by maintaining the TPD level less than or equal to 0.5 mm in CFSF and DFSF joints.

9.1.6.1 CFSF samples

The failure modes are independent of the change in RPM, but dependent on the change in TPD. Tear-off is the most common failure mode with change in these process

parameters. The stir spot circumference, which act as critical weak zone lead to upper sheet thinning and tear-off failure. The upward deformation of the lower sheet, which interrupts the upper sheet continuity also lead to tear-off failure. Incomplete metallurgical bonding act as critical weak zone for partial bond delamination failure. Lower TPDs show pin failure, which is initiated from critical weak zone namely neck of the pin. For uniaxial tensile test, the frictional heat generated at the stir spot and the extent of geometrical inhomogeneity (the stir spot size) increase with increase in the process parameter values. This leads to reduction in joint formability. The change in the mode of failure from stir spot fracture to base metal fracture occurs with increase in RPM.

9.1.6.2 DFSF samples

The neck of the pin, poor interlock at the top of the pre-drilled hole, stir spot circumference and upward deformation of the lower sheet act as critical weak zones initiating failure of DFSF samples. Overall analysis shows that tear-off failure can be considered as the most desirable failure mode because the mechanical interlocking and metallurgical bonding are perfect for these samples. Tear-off is the most common failure mode at optimum ranges, for change in process parameters such as TPD and TD, and change in geometric feature such as MH. Least occurrence of tear-off failure with change in HD shows that there is a proportional decrease in metallurgically bonded area created by bigger dia. holes. Increase in the number of pre-drilled holes in MH act as critical geometrical inhomogeneity in the lower sheet leading to failure of the joints by fracture along the reference circle circumference. Absence of metallurgical bonding in DFSF samples with four hole configuration is revealed through the occurrence of pin shear failure and pin pull-out failure.

With change in TPD, change in HD and change in MH, the stir spot in the gauge length region generally act as critical geometrical inhomogeneity in uniaxial tensile test. Both stir spot fracture and base metal fracture occur commonly with change in TD, which shows that the softening of the base metal under frictional heat flux also increases with increase in TD.

9.1.7 Comparison with other processes

9.1.7.1 FSF process with other commercially available processes

The fracture load of CFSF samples are better than that of samples fabricated with other commercially available joining processes such as FSW and FSSW reported in literature.

9.1.7.2 DFSF process with CFSF and FSSW processes

Considering the mechanical performance, quality of joint formation obtained through macrostructure analysis, morphology analysis and failure mode examination, optimum level of process parameters for DFSF can be fixed as 0.45 mm to 0.5 mm TPD and 14 mm TD, and geometric features can be fixed as 3 mm to 3.5 mm HD and single hole configuration, 1H, for the present material combination of AA 5052-H32 and AA 6061-T6 aluminum alloy sheets of 2 mm thickness.

DFSF samples fabricated at above-mentioned process parameters deliver superior lap shear fracture load about 7.42 kN, which is 42% better than CFSF samples and 86% better than FSSW samples with pin, and 25% better than pinless FSSW samples, provided all the joints are fabricated with identical process parameter values on same material combination.

The superior joint strength of DFSF joints is obtained from simultaneous mechanical interlocking and metallurgical bonding. Pin hole defect and hook defect occurring in FSSW process are successfully eliminated in DFSF process. DFSF joints also possess better aesthetic appearance by eliminating rivet head protrusion in comparison with CFSF joints.

For better mechanical performance of DFSF samples, it is advisable to choose harder sheet metal as the lower sheet. The ‘TD-HD’ ratio for successful DFSF joint fabrication in aluminum alloy sheets of 2 mm thickness should lie in the range of 3.33 to 4.66 for single hole configuration 1H.

9.2 Scope of future work

The present work is a preliminary analysis of the DFSF process. There exist amble scope for future work to enhance the applicability and effectiveness of this process. The following recommendations can be considered for future works in this field.

- The inward collar formation can be further enhanced, through joint strength evaluation and joint formation analysis, if the shape of the pre-drilled hole can be modified suitably. Employing a gradually increasing tapered hole towards the base of lower sheet is worth to be investigated.
- Future investigation can be directed to the usage of modified stir tool appropriately designed to enable refilling of the stir spot as well as achieving minimal flash formation.
- Optimization of process parameters such as tool plunge rate, tool face profiles to minimize fabrication time in DFSF process.
- The mechanism of simultaneous mechanical interlocking and metallurgical bonding can be further enhanced through comprehensive microstructural investigation.
- To minimize the cost of experimentation, alternate investigation techniques such as the finite element analysis of DFSF process can be conducted to develop an efficient model that replicates actual experimental conditions.
- Based on data obtained from the present work, the limits for the process parameters can be set for design of experiment methodology. The process parameters and geometric features, which influence the strength and formation of DFSF joints can be ranked and the individual/ cumulative effect of these parameters can be obtained.

References

Abe, Y., Kato, T., Mori, K.I., Nishino, S., 2014. Mechanical clinching of ultra-high strength steel sheets and strength of joints. J. Mater. Process. Technol. 214, 2112–2118. doi:10.1016/j.jmatprotec.2014.03.003

Agrawal, A.K., Narayanan, R.G., 2017. Joining of a tube to a sheet through end curling. J. Mater. Process. Technol. 246, 291–304. doi:10.1016/j.jmatprotec.2017.03.035

Ahmed, S., Saha, P., 2018. Development and testing of fixtures for friction stir welding of thin aluminium sheets. J. Mater. Process. Technol. 252, 242–248. doi:10.1016/j.jmatprotec.2017.09.034

Ahuja, Y., Ibrahim, R., Paradowska, A., Riley, D., 2015. Friction stir forming to fabricate copper-tungsten composite. J. Mater. Process. Technol. 217, 222–231. doi:10.1016/j.jmatprotec.2014.11.024

Alves, L.M., Afonso, R.M., Silva, C.M.A., Martins, P.A.F., 2018. Joining tubes to sheets by boss forming and upsetting. J. Mater. Process. Technol. 252, 773–781. doi:10.1016/j.jmatprotec.2017.10.047

Alves, L.M., Dias, E.J., Martins, P.A.F., 2011. Joining sheet panels to thin-walled tubular profiles by tube end forming. J. Clean. Prod. 19, 712–719. doi:10.1016/j.jclepro.2010.12.014

Alves, L.M., Gameiro, J., Silva, C.M.A., Martins, P.A.F., 2017. Sheet-bulk forming of tubes for joining applications. J. Mater. Process. Technol. 240, 154–161. doi:10.1016/j.jmatprotec.2016.09.021

Arici, A., Mert, Ş., 2008. Friction stir spot welding of polypropylene. J. Reinf. Plast. Compos. 27, 2001–2004. doi:10.1177/0731684408089134

Arul, S.G., Miller, S.F., Kruger, G.H., Pan, T.-Y., Mallick, P.K., Shih, A. J., 2008. Experimental study of joint performance in spot friction welding of 6111-T4 aluminium alloy. Sci. Technol. Weld. Join. 13, 629–637. doi:10.1179/136217108X363900

Awang, M., Mucino, V.H., 2010. Energy generation during Friction Stir Spot Welding (FSSW) of Al 6061-T6 Plates. Mater. Manuf. Process. 25, 167–174. doi:10.1080/10426910903206758

Badarinarayan, H., Shi, Y., Li, X., Okamoto, K., 2009a. Effect of tool geometry on hook formation and static strength of friction stir spot welded aluminum 5754-O sheets. Int. J. Mach. Tools Manuf. 49, 814–823. doi:10.1016/j.ijmachtools.2009.06.001

Badarinarayan, H., Yang, Q., Zhu, S., 2009b. Effect of tool geometry on static strength of friction stir spot-welded aluminum alloy. Int. J. Mach. Tools Manuf. 49, 142–148. doi:10.1016/j.ijmachtools.2008.09.004

Baek, S.-W., Choi, D.-H., Lee, C.-Y., Ahn, B.-W., Yeon, Y.-M., Song, K., Jung, S.-B., 2010. Microstructure and mechanical properties of friction stir spot welded galvanized steel. Mater. Trans. 51, 1044–1050. doi:10.2320/matertrans.M2009337

Bakavos, D., Chen, Y., Babout, L., Prangnell, P., 2011. Material interactions in a novel pinless tool approach to friction stir spot welding thin aluminum sheet. Metall. Mater. Trans. A 42, 1266–1282. doi:10.1007/s11661-010-0514-x

Bhamji, I., Preuss, M., Threadgill, P.L., Addison, A.C., 2010. Solid state joining of metals by linear friction welding: a literature review. Mater. Sci. Technol. 27, 2–12. doi:10.1179/026708310x520510

Bozzi, S., Helbert-Etter, A.L., Baudin, T., Klosek, V., Kerbiguet, J.G., Criqui, B., 2010. Influence of FSSW parameters on fracture mechanisms of 5182 aluminium welds. J. Mater. Process. Technol. 210, 1429–1435. doi:10.1016/j.jmatprotec.2010.03.022

Burger, A. K. Gupta, P. W. Jeffrey, D. J. Lloyd, 1995. Microstructural control of aluminum sheet used in automotive applications. Mater. Charact. 35, 23–39. doi:10.1016/1044-5803(95)00065-8

Cao, J.Y., Wang, M., Kong, L., Guo, L.J., 2016. Hook formation and mechanical properties of friction spot welding in alloy 6061-T6. J. Mater. Process. Technol. 230, 254–262.

Chen, K., Liu, X., Ni, J., 2017. Keyhole refilled friction stir spot welding of aluminum alloy to advanced high strength steel. J. Mater. Process. Technol. 249, 452–462. doi:10.1016/j.jmatprotec.2017.06.039

Chen, Y.C., Liu, S.F., Bakavos, D., Prangnell, P.B., 2013. The effect of a paint bake treatment on joint performance in friction stir spot welding AA6111-T4 sheet using a pinless tool. Mater. Chem. Phys. 141, 768–775. doi:10.1016/j.matchemphys.2013.05.073

Chen, Z., Ikeda, K., Murakami, T., Takeda, T., 2001. Extrusion behavior of metal-ceramic composite pipes in multi-billet extrusion process. J. Mater. Process. Technol. 114, 154–160. doi:10.1016/S0924-0136(01)00726-9

Chiou, Y.C., Liu, C. Te, Lee, R.T., 2013. A pinless embedded tool used in FSSW and FSW of aluminum alloy. J. Mater. Process. Technol. 213, 1818–1824. doi:10.1016/j.jmatprotec.2013.04.018

Cho, J.R., Song, J.I., 2007. Swaging process of power steering hose: Its finite element analysis considering the stress relaxation. J. Mater. Process. Technol. 187–188, 497–501. doi:10.1016/j.jmatprotec.2006.11.113

Cole, G.S., Sherman, A.M., 1995. Lightweight materials for automotive applications. Mater. Charact. 35, 3–9.

Cox, C.D., Gibson, B.T., Delapp, D.R., Strauss, A.M., Cook, G.E., 2014a. Technical paper A method for double-sided friction stir spot welding. J. Manuf. Process. 16, 241–247.

Cox, C.D., Gibson, B.T., Strauss, A.M., Cook, G.E., 2014b. Energy input during friction stir spot welding J. Manuf. Process. 16, 479–484.

Das, H., Chakraborty, D., Kumar Pal, T., 2014. High-cycle fatigue behavior of friction stir butt welded 6061 aluminium alloy. Trans. Nonferrous Met. Soc. China 24, 648–656. doi:10.1016/S1003-6326(14)63107-1

Das, S.K., Green, J.A., Kaufman, J.G., 2007. The development of recycle-friendly automotive aluminum alloys. JOM 59, 47–51. doi:10.1007/s11837-007-0140-2

Ding, Y., Shen, Z., Gerlich, A.P., 2017. Refill friction stir spot welding of dissimilar aluminum alloy and AlSi coated steel. J. Manuf. Process. 30, 353–360. doi:10.1016/j.jmapro.2017.10.006

Dörr, F., Funk, M., Liewald, M., Binz, H., Köstlmeier, R., 2014. Influence of internal hub profile on joining process of shaft-hubconnection by lateral extrusion. Procedia Eng. 81, 1988–1993. doi:10.1016/j.proeng.2014.10.269

Eivani, A.R., Taheri, A.K., 2007. A new method for producing bimetallic rods. Mater. Lett. 61, 4110–4113. doi:10.1016/j.matlet.2007.01.046

Eslami, P., Taheri, A.K., 2011. An investigation on diffusion bonding of aluminum to copper using equal channel angular extrusion process. Mater. Lett. 65, 1862–1864. doi:10.1016/j.matlet.2011.03.053

Evans, W.T., Cox, C., Gibson, B.T., Strauss, A.M., Cook, G.E., 2016. Two-sided friction stir riveting by extrusion: A process for joining dissimilar materials. J. Manuf. Process. 23, 115–121. doi:10.1016/j.jmapro.2016.06.001

Evans, W.T., Gibson, B.T., Reynolds, J.T., Strauss, A.M., Cook, G.E., 2015. Friction stir extrusion: A new process for joining dissimilar materials. Manuf. Lett. 5, 25–28. doi:10.1016/j.mfglet.2015.07.001

Findik, F., 2011. Recent developments in explosive welding. Mater. Des. 32, 1081–1093. doi:10.1016/j.matdes.2010.10.017

Fridlyander, I.N., Sister, V.G., Grushko, O.E., Berstenev, V. V., Sheveleva, L.M., Ivanova, L.A., 2002. Aluminum alloys: Promising materials in the automotive industry. Met. Sci. Heat Treat. 44, 365–370. doi:10.1023/A:1021901715578

Garg, A., Bhattacharya, A., 2017a. On lap shear strength of friction stir spot welded AA6061 alloy. J. Manuf. Process. 26, 203–215. doi:10.1016/j.jmapro.2017.02.019

Garg, A., Bhattacharya, A., 2017b. Similar and dissimilar joining of AA6061-T6 and copper by single and multi-spot friction stirring. J. Mater. Process. Technol. 250, 330–344. doi:10.1016/j.jmatprotec.2017.07.029

Gerlich, A., Avramovic-Cingara, G., North, T.H., 2006. Stir zone microstructure and strain rate during Al 7075-T6 friction stir spot welding. Metall. Mater. Trans. A 37, 2773–2786. doi:10.1007/BF02586110

Gonçalves, A., Alves, L.M., Martins, P.A.F., 2014. Tube joining by asymmetric plastic instability. J. Mater. Process. Technol. 214, 132–140. doi:10.1016/j.jmatprotec.2013.08.006

Groche, P., Monnerjahn, V., Özel, M., Yu, Y., 2017. Remote joining by plastic deformation in the process of linear flow splitting. J. Mater. Process. Technol. 246, 262–266. doi:10.1016/j.jmatprotec.2017.03.024

Groche, P., Tibari, K., 2006. Fundamentals of angular joining by means of hydroforming. CIRP Ann. - Manuf. Technol. 55, 259–262. doi:10.1016/S0007-8506(07)60411-9

Groche, P., Wohletz, S., Brenneis, M., Pabst, C., Resch, F., 2014. Joining by forming - A review on joint mechanisms, applications and future trends. J. Mater. Process. Technol. 214, 1972–1994. doi:10.1016/j.jmatprotec.2013.12.022

Guru, P.R., Khan MD, F., Panigrahi, S.K., Ram, G.D.J., 2015. Enhancing strength, ductility and machinability of a Al-Si cast alloy by friction stir processing. J. Manuf. Process. 18, 67–74. doi:10.1016/j.jmapro.2015.01.005

Hagedorn, M., Weinert, K., 2004. Manufacturing of composite workpieces with rolling tools. J. Mater. Process. Technol. 153–154, 323–329. doi:10.1016/j.jmatprotec.2004.04.317

Haghshenas, M., Gerlich, A.P., 2018. Joining of automotive sheet materials by friction-based welding methods : A review. Eng. Sci. Technol. an Int. J. 21, 130–148. doi:10.1016/j.jestch.2018.02.008

Haneklaus, N., Cionea, C., Reuven, R., Frazer, D., Hosemann, P., Peterson, P.F., 2016. Hybrid friction diffusion bonding of 316L stainless steel tube-to-tube sheet joints for

coil-wound heat exchangers. J. Mech. Sci. Technol. 30, 4925–4930. doi:10.1007/s12206-016-0832-z

Hejazi, I., Mirsalehi, S.E., 2016a. Mechanical and metallurgical characterization of AA6061 friction stir welded joints using microhardness map. Trans. Nonferrous Met. Soc. China 26, 2313–2319. doi:10.1016/S1003-6326(16)64351-0

Hejazi, I., Mirsalehi, S.E., 2016b. Effect of pin penetration depth on double-sided friction stir welded joints of AA6061-T913 alloy. Trans. Nonferrous Met. Soc. China 26, 676–683. doi:10.1016/S1003-6326(16)64158-4

Huang, Z., Xue, S., Lai, J., Xia, L., Zhan, J., 2014. Self-piercing riveting with inner flange pipe rivet. Procedia Eng. 81, 2042–2047. doi:10.1016/j.proeng.2014.10.278

Huang, Z., Yanagimoto, J., 2015. Dissimilar joining of aluminum alloy and stainless steel thin sheets by thermally assisted plastic deformation. J. Mater. Process. Technol. 225, 393–404. doi:10.1016/j.jmatprotec.2015.06.023

Huskins, E.L., Cao, B., Ramesh, K.T., 2010. Strengthening mechanisms in an Al – Mg alloy 527, 1292–1298. doi:10.1016/j.msea.2009.11.056

Ilangovan, M., Boopathy, S.R., Balasubramanian, V., 2015. Microstructure and tensile properties of friction stir welded dissimilar AA6061-AA5086 aluminium alloy joints. Trans. Nonferrous Met. Soc. China 25, 1080–1090. doi:10.1016/S1003-6326(15)63701-3

Jain, M., Allin, J., Bull, M.J., 2002. Deep drawing characteristics of automotive aluminum alloys. Mater. Sci. Eng. A 256, 69–82. doi:10.1016/s0921-5093(98)00845-4

Jeon, C.-S., Hong, S.-T., Kwon, Y.-J., Cho, H.-H., Han, H.N., 2012. Material properties of friction stir spot welded joints of dissimilar aluminum alloys. Trans. Nonferrous Met. Soc. China 22, 605–613. doi:10.1016/S1003-6326(12)61772-5

Kapoor, R., Kandasamy, K., Mishra, R.S., Baumann, J.A., Grant, G., 2013. Effect of friction stir processing on the tensile and fatigue behavior of a cast A206 alloy. Mater. Sci. Eng. A 561, 159–166. doi:10.1016/j.msea.2012.10.090

Kesharwani, R.K., Panda, S.K., Pal, S.K., Kesharwani, R.K., Panda, S.K., Pal, S.K., 2015. Experimental investigations on formability of aluminum tailor friction stir welded blanks in deep drawing process J. Mater. Eng. Perform. 24, 1038–1049. doi:10.1007/s11665-014-1361-5

Kitamura, K., Hirota, K., Ukai, Y., Matsunaga, K., Osakada, K., 2012. Cold joining of rotor shaft with flange by using plastic deformation. CIRP Ann. - Manuf. Technol. 61, 275–278. doi:10.1016/j.cirp.2012.03.099

Kleditzsch, S., Awiszus, B., Lätzer, M., Leidich, E., 2014. Steel-aluminum knurled interference fits: Joining process and load characteristics. Procedia Eng. 81, 1982–1987. doi:10.1016/j.proeng.2014.10.268

Krishna, B.V., Venugopal, P., Rao, K.P., 2005. Co-extrusion of dissimilar sintered P/M preforms - An explored route to produce bimetallic tubes. Mater. Sci. Eng. A 407, 77–83. doi:10.1016/j.msea.2005.06.025

Kuboki, T., Murata, M., 2007. New extrusion method joining tube and sheet with holed rib. J. Mech. Sci. Technol. 21, 1548–1552. doi:10.1007/BF03177373

Kumar, K., Kailas, S. V., 2008. On the role of axial load and the effect of interface position on the tensile strength of a friction stir welded aluminium alloy. Mater. Des. 29, 791–797. doi:10.1016/j.matdes.2007.01.012

Kumbhar, N.T., Bhanumurthy, K., 2012. Friction Stir Welding of Al 5052 with Al 6061 Alloys. J. Metall. 2012, 1–7. doi:10.1155/2012/303756

Lakshminarayanan, A.K., Annamalai, V.E., Elangovan, K., 2015. Identification of optimum friction stir spot welding process parameters controlling the properties of low carbon automotive steel joints. J. Mater. Res. Technol. 4(3), 262–272. doi:10.1016/j.jmrt.2015.01.001

Lapovok, R., Ng, H.P., Tomus, D., Estrin, Y., 2012. Bimetallic copper-aluminium tube by severe plastic deformation. Scr. Mater. 66, 1081–1084. doi:10.1016/j.scriptamat.2012.03.004

Lazarevic, S., Miller, S.F., Li, J., Carlson, B.E., 2013. Experimental analysis of friction stir forming for dissimilar material joining application. J. Manuf. Process. 15, 616–624. doi:10.1016/j.jmapro.2013.05.004

Lazarevic, S., Ogata, K. A., Miller, S.F., Kruger, G.H., Carlson, B.E., 2015. Formation and Structure of Work Material in the Friction Stir Forming Process. J. Manuf. Sci. Eng. 137, 051018. doi:10.1115/1.4030641

Lazarevic, S., Miller, S., Kruger, G., Niekerk, Theo van, Carlson B, 2017. Finite element analysis of the friction stir forming process. In proceedings of the ASME 2017 12th International Manufacturing Science and Engineering Conference MSEC2017, June 4-8, 2017, Los Angeles, CA, USA, MSEC2017-3019.

Lee, C.J., Kim, J.Y., Lee, S.K., Ko, D.C., Kim, B.M., 2010. Design of mechanical clinching tools for joining of aluminium alloy sheets. Mater. Des. 31, 1854–1861. doi:10.1016/j.matdes.2009.10.064

Lee, C.J., Lee, J.M., Ryu, H.Y., Lee, K.H., Kim, B.M., Ko, D.C., 2014. Design of hole-clinching process for joining of dissimilar materials - Al6061-T4 alloy with DP780 steel, hot-pressed 22MnB5 steel, and carbon fiber reinforced plastic. J. Mater. Process. Technol. 214, 2169–2178. doi:10.1016/j.jmatprotec.2014.03.032

Li, F., Lin, J.F., Sui, X.C., Bian, N., Xu, M. Da, 2012. Cold-pressing deformation characteristics of steel-aluminum sheets joining. Trans. Nonferrous Met. Soc. China 22, 553–559. doi:10.1016/S1003-6326(12)61760-9

Li, W., Li, J., Zhang, Z., Gao, D., Wang, W., Dong, C., 2014. Improving mechanical properties of pinless friction stir spot welded joints by eliminating hook defect. J. Mater. 62, 247–254. doi:10.1016/j.matdes.2014.05.028

Li, W.Y., Chu, Q., Yang, X.W., Shen, J.J., Vairis, A., Wang, W.B., 2018. Microstructure and morphology evolution of probeless friction stir spot welded joints of aluminum alloy. J. Mater. Process. Technol. 252, 69–80. doi:10.1016/j.jmatprotec.2017.09.003

Liechty, B.C., Webb, B.W., 2008. Modeling the frictional boundary condition in friction stir welding. Int. J. Mach. Tools Manuf. 48, 1474–1485. doi:10.1016/j.ijmachtools.2008.04.005

Lilleby, A., Grong, O., Hemmer, H., 2009. Experimental and finite element simulations of cold pressure welding of aluminium by divergent extrusion. Mater. Sci. Eng. A 527, 179–186. doi:10.1016/j.msea.2009.07.051

Liu, H., Zhao, Y., Su, X., Yu, L., Hou, J., 2013. Microstructural characteristics and mechanical properties of friction stir spot welded 2A12-T4 aluminum alloy Adv. Mater. Sci. Eng. 2013, 1–11.

Liu, Z., Cui, H., Ji, S., Xu, M., Meng, X., 2016. Improving joint features and mechanical properties of pinless friction stir welding of Alcald 2A12-T4 aluminum alloy. J. Mater. Sci. Technol. 32, 1372–1377. doi:10.1016/j.jmst.2016.07.003

Livatyali, H., Müderrisoglu, A., Ahmetoglu, M.A., Akgerman, N., Kinzel, G.L., Altan, T., 2000. Improvement of hem quality by optimizing flanging and pre-hemming operations using computer aided die design. J. Mater. Process. Technol. 98, 41–52. doi:10.1016/S0924-0136(99)00304-0

Ma, Z.Y., Mishra, R.S., Mahoney, M.W., 2002. Superplastic deformation behaviour of friction stir processed 7075Al alloy. Acta Mater. 50, 4419–4430. doi:10.1016/S1359-6454(02)00278-1

Madej, L., Tokunaga, T., Matsuura, K., Ohno, M., Pietrzyk, M., 2015. Physical and numerical modelling of backward extrusion of Mg alloy with Al coating. CIRP Ann. - Manuf. Technol. 64, 253–256. doi:10.1016/j.cirp.2015.04.085

Marré, M., Gies, S., Maevus, F., Tekkaya, A.E., 2010. Joining of lightweight frame structures by die-less hydroforming. Int. J. Mater. Form. 3, 1031–1034. doi:10.1007/s12289-010-0946-2

Matsumoto, R., Hanami, S., Ogura, A., Yoshimura, H., Osakada, K., 2008. New plastic joining method using indentation of cold bar to hot forged part. CIRP Ann. - Manuf. Technol. 57, 279–282. doi:10.1016/j.cirp.2008.03.126

Mehta, D.S., Masood, S.H., Song, W.Q., 2004. Investigation of wear properties of magnesium and aluminum alloys for automotive applications. J. Mater. Process. Technol. 155–156, 1526–1531. doi:10.1016/j.jmatprotec.2004.04.247

Meschut, G., Janzen, V., Olfermann, T., 2014. Innovative and highly productive joining technologies for multi-material lightweight car body structures. J. Mater. Eng. Perform. 23, 1515–1523. doi:10.1007/s11665-014-0962-3

Meschut, Gerson, Matzke, M., Hoerhold, R., Olfermann, T., 2014. Hybrid technologies for joining ultra-high-strength boron steels with aluminum alloys for lightweight car body structures. Procedia CIRP 23, 19–23. doi:10.1016/j.procir.2014.10.089

Meshram, S.D., Mohandas, T., Reddy, G.M., 2007. Friction welding of dissimilar pure metals. J. Mater. Process. Technol. 184, 330–337. doi:10.1016/j.jmatprotec.2006.11.123

Min, J., Li, J., Li, Y., Carlson, B.E., Lin, J., Wang, W.M., 2015. Friction stir blind riveting for aluminum alloy sheets. J. Mater. Process. Technol. 215, 20–29. doi:10.1016/j.jmatprotec.2014.08.005

Mishra, R.S., Ma, Z.Y., 2005. Friction stir welding and processing. Mater. Sci. Eng. R Reports 50, 1–78. doi:10.1016/j.mser.2005.07.001

Mitlin, D., Radmilovic, V., Pan, T., Chen, J., Feng, Z., Santella, M.L., 2006. Structure-properties relations in spot friction welded (also known as friction stir spot welded) 6111 aluminum. Mater. Sci. Eng. A 441, 79–96. doi:10.1016/j.msea.2006.06.126

Miwada, Y., Ishiguro, T., Abe, E., Yukawa, N., Ishikawa, T., Suganuma, T., 2014. Cold forge spot-bonding of high tensile strength steel and aluminum alloy sheets. Procedia Eng. 81, 2006–2011. doi:10.1016/j.proeng.2014.10.272

Mohebbi, M.S., Akbarzadeh, A., 2010. A novel spin-bonding process for manufacturing multilayered clad tubes. J. Mater. Process. Technol. 210, 510–517. doi:10.1016/j.jmatprotec.2009.10.014

Mori, K.I., Bay, N., Fratini, L., Micari, F., Tekkaya, A.E., 2013. Joining by plastic deformation. CIRP Ann. - Manuf. Technol. 62, 673–694. doi:10.1016/j.cirp.2013.05.004

Nakayama, N., Ikeda, T., Kobayashi, N., Horita, M., 2014. Joining process for plates using plastic deformation with rotating tool and pilot hole. Procedia Eng. 81, 2048–2055. doi:10.1016/j.proeng.2014.10.279

Nanaumi, G., Mizushima, D., Ohtake, N., 2014. Joining of various kinds of metal plates using ultrasonic vibrations. Procedia Eng. 81, 2111–2116. doi:10.1016/j.proeng.2014.10.294

Neugebauer, R., Kraus, C., Dietrich, S., 2008. Advances in mechanical joining of magnesium. CIRP Ann. - Manuf. Technol. 57, 283–286. doi:10.1016/j.cirp.2008.03.025

Nishihara, T., Ito, A., 2005. Measurement of die temperature during friction stir forming. Weld. World 49, 22–26.

Ogata, K.A., Miller, S.F., Lazarevic, S., 2014. Dissimilar material joint strength and structure for friction stir forming process. Proceedings of the ASME 2014 International Manufacturing Science and Engineering Conference MSEC2014, June 9-13, 2014, Detroit, Michigan, USA, MSEC2014-4044.

Paidar, M., Khodabandeh, A., Najafi, H., Rouh-aghdam, A.S., 2014. Effects of the tool rotational speed and shoulder penetration depth on mechanical properties and failure modes of friction stir spot welds of aluminum 2024-T3 sheets. J. Mech. Sci. Technol. 28, 4893–4898. doi:10.1007/s12206-014-1108-0

Paidar, M., Khodabandeh, A., Sarab, M.L., Taheri, M., 2015. Effect of welding parameters (plunge depths of shoulder, pin geometry, and tool rotational speed) on the failure mode and stir zone characteristics of friction stir spot welded aluminum 2024-T3 sheets. J. Mech. Sci. Technol. 29, 4639–4644. doi:10.1007/s12206-015-1009-x

Park, S.-K., Hong, S.-T., Park, J.-H., Park, K.-Y., Kwon, Y.-J., Son, H.-J., 2010. Effect of material locations on properties of friction stir welding joints of dissimilar aluminium alloys. Sci. Technol. Weld. Join. 15, 331–336. doi:10.1179/136217110X12714217309696

Pathak, N., Bandyopadhyay, K., Sarangi, M., Panda, S.K., 2013. Microstructure and mechanical performance of friction stir spot-welded aluminum-5754 sheets. J. Mater. Eng. Perform. 22, 131–144. doi:10.1007/s11665-012-0244-x

Piccini, J.M., Svoboda, H.G., 2015. Effect of the tool penetration depth in friction stir spot welding (FSSW) of dissimilar aluminum alloys. Procedia Mater. Sci. 8, 868–877. doi:10.1016/j.mspro.2015.04.147

Pragana, J.P.M., Silva, C.M.A., Bragança, I.M.F., Alves, L.M., Martins, P.A.F., 2018. A new joining by forming process to produce lap joints in metal sheets. CIRP Ann. 67, 301–304. doi:10.1016/j.cirp.2018.04.121

Prakash, S.J., Muthukumaran, S., 2011. Refilling probe hole of friction spot joints by friction forming. Mater. Manuf. Process. 26, 1539–1545. doi:10.1080/10426914.2011.551959

Rahmi, M., Abbasi, M., 2016. Friction stir vibration welding process: modified version of friction stir welding process. Int. J. Adv. Manuf. Technol. 90, 141–151. doi:10.1007/s00170-016-9383-9

Rai, R., De, A., Bhadeshia, H.K.D.H., DebRoy, T., 2011. Review: friction stir welding tools. Sci. Technol. Weld. Join. 16, 325–342. doi:10.1179/1362171811Y.0000000023

RajKumar, V., VenkateshKannan, M., Sadeesh, P., Arivazhagan, N., Devendranath Ramkumar, K., 2014. Studies on effect of tool design and welding parameters on the friction stir welding of dissimilar aluminium alloys AA 5052-AA 6061. Procedia Eng. 75, 93–97. doi:10.1016/j.proeng.2013.11.019

Ramulu, P.J., Narayanan, R.G., Kailas, S. V., 2013. Forming limit investigation of friction stir welded sheets: Influence of shoulder diameter and plunge depth. Int. J. Adv. Manuf. Technol. 69, 2757–2772. doi:10.1007/s00170-013-5245-x

Rana, P.K., Narayanan, R.G., Kailas, S. V., 2018. Effect of rotational speed on friction stir spot welding of AA5052-H32/HDPE/AA5052-H32 sandwich sheets. J. Mater. Process. Technol. 252, 511–523. doi:10.1016/j.jmatprotec.2017.10.016

Rao, H.M., Yuan, W., Badarinarayan, H., 2015. Effect of process parameters on mechanical properties of friction stir spot welded magnesium to aluminum alloys. Mater. Des. 66, 235–245. doi:10.1016/j.matdes.2014.10.065

Reilly, A., Shercliff, H., Chen, Y., Prangnell, P., 2015. Modelling and visualisation of material flow in friction stir spot welding. J. Mater. Process. Technol. 225, 473–484. doi:10.1016/j.jmatprotec.2015.06.021

Reimann, M., Gartner, T., Suhuddin, U., Göbel, J., Dos Santos, J.F., 2016. Keyhole closure using friction spot welding in aluminum alloy 6061-T6. J. Mater. Process. Technol. 237, 12–18. doi:10.1016/j.jmatprotec.2016.05.013

Sadot, O., Shribman, V., Frage, N., Ben-Artzy, A., Stern, A., 2009. Wave formation mechanism in magnetic pulse welding. Int. J. Impact Eng. 37, 397–404. doi:10.1016/j.ijimpeng.2009.07.008

Sajed, M., 2016. Parametric study of two-stage refilled friction stir spot welding. J. Manuf. Process. 24, 307–317. doi:10.1016/j.jmapro.2016.09.011

Sapanathan, T., Khoddam, S., Zahiri, S.H., 2013. Spiral extrusion of aluminum/copper composite for future manufacturing of hybrid rods: A study of bond strength and interfacial characteristics. J. Alloys Compd. 571, 85–92. doi:10.1016/j.jallcom.2013.03.210

Sarkar, R., Pal, T.K., Shome, M., 2016. Material flow and intermixing during friction stir spot welding of steel. J. Mater. Process. Technol. 227, 96–109. doi:10.1016/j.jmatprotec.2015.08.006

Sarkar, R., Sengupta, S., Pal, T.K., Shome, M., 2015. Microstructure and Mechanical Properties of Friction Stir Spot-Welded IF/DP Dissimilar Steel Joints. Metall. Mater. Trans. A 46A, 5182–5200. doi:10.1007/s11661-015-3116-9

Sato, Y.S., Park, S.H.C., Kokawa, H., 2001. Microstructural factors governing hardness in friction-stir welds of solid-solution-hardened Al alloys Metall. Mater. Trans. A 32A, 3033–3042.

Shen, Z., Ding, Y., Gopkalo, O., Diak, B., Gerlich, A.P., 2018. Effects of tool design on the microstructure and mechanical properties of refill friction stir spot welding of dissimilar Al alloys. J. Mater. Process. Technol. 252, 751–759. doi:10.1016/j.jmatprotec.2017.10.034

Shen, Z., Yang, X., Zhang, Z., Cui, L., Li, T., 2013. Microstructure and failure mechanisms of refill friction stir spot welded 7075-T6 aluminum alloy joints. Mater Design 44, 476–486. doi:10.1016/j.matdes.2012.08.026

Silva, C.M.A., Bragança, I.M.F., Alves, L.M., Martins, P.A.F., 2018. Two-stage joining of sheets perpendicular to one another by sheet-bulk forming. J. Mater. Process. Technol. 253, 109–120. doi:10.1016/j.jmatprotec.2017.11.006

Silva, C.M.A., Nielsen, C. V., Alves, L.M., Martins, P.A.F., 2015. Environmentally friendly joining of tubes by their ends. J. Clean. Prod. 87, 777–786. doi:10.1016/j.jclepro.2014.09.022

Standard practice for microetching metals and alloys, ASTM E407-07, (2007).

Standard test methods for determining average grain size, ASTM E112-13, (2013).

Standard test method for plastic strain ratio r for sheet metal, ASTM E517, (2016).

Standard test methods for tension testing of metallic materials, ASTM E8/E8M-09, (2009).

Standard test methods for Vickers hardness and Knoop hardness of metallic materials, ASTM E92-16, (2016).

Stroiman, I.M., Mitrukov, G.A., 2002. Cold-welding of aluminium and copper. Weld. Int. 16, 488–490. doi:10.1080/09507110209549564

Test methods for evaluating the resistance spot welding behavior of automotive sheet steel materials, AWS D8.9M, (2012).

Thomas, W., Nicholas, E., 1997. Friction stir welding for the transportation industries. Mater. Des. 18, 269–273. doi:10.1016/S0261-3069(97)00062-9

Tozaki, Y., Uematsu, Y., Tokaji, K., 2010. A newly developed tool without probe for friction stir spot welding and its performance. J. Mater. Process. Technol. 210, 844–851. doi:10.1016/j.jmatprotec.2010.01.015

Tozaki, Y., Uematsu, Y., Tokaji, K., 2007. Effect of tool geometry on microstructure and static strength in friction stir spot welded aluminium alloys. Int. J. Mach. Tools Manuf. 47, 2230–2236. doi:10.1016/j.ijmachtools.2007.07.005

Tutar, M., Aydin, H., Yuce, C., Yavuz, N., Bayram, A., 2014. The optimisation of process parameters for friction stir spot-welded AA3003-H12 aluminium alloy using a Taguchi orthogonal array. Mater. Des. 63, 789–797. doi:10.1016/j.matdes.2014.07.003

Venukumar, S., Muthukumaran, S., Yalagi, S.G., Kailas, S. V., 2014. Failure modes and fatigue behavior of conventional and refilled friction stir spot welds in AA 6061-T6 sheets. Int. J. Fatigue 61, 93–100. doi:10.1016/j.ijfatigue.2013.12.009

Von Senden genannt Haverkamp, H., Engelhardt, M., Grittner, N., Bach, F.-W., Bormann, D., Reimche, W., 2012. Extrusion of hybrid sheet metals. J. Mater. Process. Technol. 212, 1030–1038. doi:10.1016/j.jmatprotec.2011.12.013

Wagener, H.W., Haats, J., 1994. Pressure welding of corrosion resistant metals by cold extrusion. J. Mater. Process. Tech. 45, 275–280. doi:10.1016/0924-0136(94)90352-2

Xing, B., He, X., Wang, Y., Yang, H., Deng, C., 2015. Study of mechanical properties for copper alloy H62 sheets joined by self-piercing riveting and clinching. J. Mater. Process. Technol. 216, 28–36. doi:10.1016/j.jmatprotec.2014.08.030

Yang, Q., Mironov, S., Sato, Y.S., Okamoto, K., 2010. Material flow during friction stir spot welding. Mater. Sci. Eng. A 527, 4389–4398. doi:10.1016/j.msea.2010.03.082

Yang, X.W., Fu, T., Li, W.Y., 2014. Friction Stir Spot Welding: A Review on Joint Macro-and Microstructure, Property, and Process Modelling. Adv. Mater. Sci. Eng. 2014, 1–11.

Yoon, S.O., Kang, M.S., Kwon, Y.J., Hong, S.T., Park, D.H., Lee, K.H., Lim, C.Y., Seo, J.D., 2012. Influences of tool plunge speed and tool plunge depth on friction spot joining of AA5454-O aluminum alloy plates with different thicknesses. Trans. Nonferrous Met. Soc. China 22, 629–633. doi:10.1016/S1003-6326(12)61776-2

Yusof, F., Miyashita, Y., Seo, N., Mutoh, Y., Moshwan, R., 2012. Utilising friction spot joining for dissimilar joint between aluminium alloy (A5052) and polyethylene terephthalate. Sci. Technol. Weld. Join. 17, 544–549. doi:10.1179/136217112x13408696326530

Zhang, Q., Jin, K., Mu, D., 2014. Tube/tube joining technology by using rotary swaging forming method. J. Mater. Process. Technol. 214, 2085–2094. doi:10.1016/j.jmatprotec.2014.02.002

Zhang, Y., Babu, S.S., Prothe, C., Blakely, M., Kwasegroch, J., Laha, M., Daehn, G.S., 2011. Application of high velocity impact welding at varied different length scales. J. Mater. Process. Technol. 211, 944–952. doi:10.1016/j.jmatprotec.2010.01.001

Zhou, G., Xu, X., Zhang, J., Yang, X., Zhang, Z., Zou, B., 2011. Effect of welding parameters on microstructure and mechanical properties of friction stir spot welded 5052 aluminum alloy. Mater. Des. 32, 4461–4470. doi:10.1016/j.matdes.2011.03.058

List of publications

Patent

- Dieless friction stir forming: A new spot joining technology [Indian patent application No: 201741040528-submitted]

Referred journals

- Saju, T.P., Narayanan, R.G., 2019. Dieless friction stir extrusion joining of aluminum alloy sheets with a pinless stir tool at varying tool plunge depths. [Journal of Materials Processing Technology 2020; 276: 116416]
- Saju, T.P., Narayanan, R.G., 2018. Effect of tool plunge depth on joint formation and joint performance of friction stir forming joints made between AA 5052-H32 and AA 6061-T6 sheet metals. Trans. Nonferrous Met. Soc. China 28 (4), 613–628. doi:10.1016/S1003-6326(18)64694-1
- Saju, T.P., Narayanan, R.G., 2017. Friction stir forming of dissimilar grade aluminum alloys: Influence of tool rotational speed on the joint evolution, joint performance, and failure modes. Int. J. Adv. Manuf. Technol. 95 (1–4), 1377–1397. doi:10.1007/s00170-017-1322-x
- Saju, T.P., Narayanan, R.G., Effect of pinless TD on dieless friction stir extrusion joining of AA 5052-H32 and AA 6061-T6 aluminum alloy sheets, J. Mech. Sci. Technol. 33 (8) (2019) 3981–3997.
- Saju, T.P., Narayanan, R.G., 2018. Effect of hole dia. on joint strength and joint formation in Dieless friction stir form joints between dissimilar aluminum alloy sheets, Procedia Manuf. 26, 255–266.

Referred international conferences

- Lap joining of dissimilar grade aluminum alloys by friction stir forming process: A study on the effect of tool plunge depth on shear strength of the joints. Proceedings of the JSME 2017 International Conference on Materials and Processing (ICMP2017), June 4–8, 2017, Los Angeles, CA, USA.
- Effect of tool rotational speed on the mechanical performance of joints fabricated by friction stir forming of dissimilar grade aluminum alloys. Proceedings of 6th International & 27th All India Manufacturing Technology, Design and Research

Conference (AIMTDR-2016), December 16-18, 2016, College of Engineering, Pune, Maharashtra, India, 921–925. ISBN: 978-93-86256-27-0.

- Effect of tool plunge depth on the mechanical performance of joints fabricated by Dieless friction stir form joining of dissimilar grade aluminum alloys. Proceedings of 7th International & 28th All India Manufacturing Technology, Design and Research Conference (AIMTDR-2018), December 13-15, 2018, Anna University, Chennai, India.- *Accepted for publication*